IMPACT MODIFIED NYLON 66-ORGANOCLAY NANOCOMPOSITES

A THESIS SUBMITTED TO
THE GRADUATE SCHOOL OF NATURAL AND APPLIED SCIENCES
OF
MIDDLE EAST TECHNICAL UNIVERSITY

BY

MİRAY MERT

IN PARTIAL FULFILLMENT OF THE REQUIREMENTS
FOR
THE DEGREE OF MASTER OF SCIENCE
IN
POLYMER SCIENCE AND TECHNOLOGY

JANUARY 2007

Approval of the Graduate School of Natural and Applied Sciences

_____

Prof. Dr. Canan Özgen
Director

I certify that this thesis satisfies all the requirements as a thesis for the degree of Master of Science

_____

Assoc. Prof. Dr. Göknur Bayram
Head of Department

This is to certify that we have read this thesis and that in our opinion it is fully adequate, in scope and quality, as a thesis for the degree of Master of Science.

_____

Prof. Dr. Ülkü Yılmazer
Supervisor

Examining Committee Members

Prof. Dr. Erdal Bayramlı (METU, CHEM) _____

Prof. Dr. Ülkü Yılmazer (METU, CHE) _____

Prof. Dr. Teoman Tinçer (METU, CHEM) _____

Assoc. Prof. Dr. Göknur Bayram (METU, CHE) _____

Prof. Dr. Cevdet Kaynak (METU, METE) _____

I hereby declare that all information in this document has been obtained and presented in accordance with academic rules and ethical conduct. I also declare that, as required by these rules and conduct, I have fully cited and referenced all material and results that are not original to this work.

Name, Last name: Miray Mert

Signature:

IMPACT MODIFIED NYLON 66-ORGANOCLAY NANOCOMPOSITES

Mert, Miray
M.S., Department of Polymer Science and Technology
Supervisor: Prof. Dr Ülkü Yılmazer

January 2007, 187 pages

PA 66 nanocomposites and PA 66 blends were prepared using Cloisite® 15A, Cloisite® 25A and Cloisite® 30B as organoclays and Lotader® 2210 (E-BA-MAH), Lotader® AX8840 (E-GMA) and Lotader® AX8900 (E-MA-GMA) as impact modifiers. The effects of the composition, types of the components and the addition order of the nanocomposites on the morphology, mechanical, flow and thermal properties were investigated.

Melt compounding step was carried out twice in a co-rotating twin-screw extruder. This was called as All-S mixing sequence when all the components were melt mixed, simultaneously. The concentration of the elastomer was determined as 5 wt% and the organoclay as 2 wt% to minimize agglomeration of the organoclay and decrease in the mechanical properties. The components which exhibited the best mechanical results and organoclay delamination in All-S mixing sequences were compounded by using different addition orders.

Substantial increases were not observed in the tensile, impact, flexural and hardness test results of the nanocomposites compared to the polymer matrix that was twice extruded. Addition order of the components affected the properties of the nanocomposites and dispersion of the elastomeric domains and the organoclay. The best mechanical test results were obtained for All-S mixing sequence of (PA 66-15A-2210).

The degree of organoclay dispersion is better in Cloisite® 15A and Cloisite® 25A containing nanocomposites than the ones which have Cloisite® 30B. Low melt flow index values aided dispersion of the organoclay whereas the slight changes in the crystallinity did not significantly contribute to the changes in the mechanical properties of the nanocomposites or the blends.

Keywords: Nylon 66; Nanocomposite; Organoclay; Impact modifier; Extrusion.

ÖZ

DARBE DAYANIMI ARTTIRILMIŞ NAYLON 66-ORGANİKKİL NANOKOMPOZİTLERİ

Mert, Miray
Yükseklisans, Polimer Bilimi ve Teknolojisi
Tez Yöneticisi: Prof. Dr Ülkü Yılmazer

Ocak 2007, 187 sayfa

PA 66 nanokompozitleri ve PA 66 karışımları organik kil olarak Cloisite® 15A, Cloisite® 25A ve Cloisite® 30B, darbe iyileştirici olarak Lotader® 2210 (E-BA-MAH), Lotader® AX8840 (E-GMA) ve Lotader® AX8900 (E-MA-GMA) kullanılarak hazırlanmıştır. Komposizyon, bileşen çeşitleri ve nanokompozitlerin ekleme sırasının morfoloji, mekanik, akış ve ısıl özellikleri üzerindeki etkisi araştırılmıştır.

Eriyik bileşimi aşaması vidalarının dönme yönü aynı, çift vidalı ekstruderde iki kez gerçekleştirilmiştir. Bu bütün bileşenler aynı anda eriyik halde karıştırıldığında All-S ekleme sırası olarak adlandırılmıştır. Organik kil yığınlarını ve mekanik özelliklerdeki azalmayı en aza indirmek için elastomer konsantrasyonu kütlece % 5 ve organik kil konsantrasyonu kütlece % 2 olarak belirlenmiştir. All-S ekleme sırasında en iyi mekanik özellikleri ve organik kil dağılımını gösteren bileşenler değişik ekleme sıralarında işleme sokulmuştur.

Nanokompozitlerin çekme, darbe, bükülme ve sertlik testi sonuçlarında iki kere ekstruderde işlem görmüş matrikse oranla fazla bir artış gözlemlenmemiştir. Bileşenlerin ekleme sıraları nanokompozitlerin özelliklerini ve elastomerik faz ve organik kil dağılımını etkilemiştir. En iyi mekanik test sonuçları (PA 66-15A-2210)'un All-S ekleme sırasında elde edilmiştir.

Cloisite® 30B içeren nanokompozitlere nazaran Cloisite® 15A ve Cloisite® 25A içeren nanokompozitlerde organik kil dağılımı daha iyi olmuştur. Düşük eriyik akış endeksi değerlerinin organik kilin dağılımına yardımcı olmasına karşın, kristallenmedeki küçük değişiklikler nanokompozitlerin veya karışımların mekanik özelliklerindeki değişikliklere önemli ölçüde katkıda bulunmamıştır.

Anahtar Kelimeler: Naylon 66; Nanokompozit; Organik kil; Darbe iyileştirici; Ekstrüzyon.

To my family

ACKNOWLEDGEMENTS

I wish to express my deepest gratitude to my supervisor Prof. Dr. Ülkü Yılmazer for his guidance, advice and insight throughout the research. It was a pleasing honor for me to work with him.

I would also like to thank Assoc. Prof. Dr. Göknur Bayram from Department of Chemical Engineering for letting me use the equipments in her laboratory and Prof. Dr. Teoman Tinçer from Department of Chemistry for his permission to use the mechanical testing equipment in his laboratory.

Special thanks go to Cengiz Tan from Department of Metallurgical Engineering for SEM analysis, Necmi Avcı from Department of Metallurgical Engineering for XRD analysis and Mihrican Açıkgöz from Department of Chemical Engineering for DSC analysis.

I would like to express my sincerest thanks to Aylin Güzel, Seda Üngör and Mehmet Ali Orman for their endless friendship, encouragement and support in all the steps of this study. Saniye Gülersönmez and Işıl Işık also deserve a special mention. I am greatly indebted to them for their contributions to my study.

The support of the polymer group including Güralp Özkoç, Sertan Yeşil, Özcan Köysüren and Mert Kılınç is also gratefully acknowledged.

Last, but not the least; I thank each member of my family for their love, encouragement and belief in me.

This study was supported by Tübitak 104M415 and BAP 2006-07-02-00-01.

TABLE OF CONTENTS

LIST OF TABLES

TABLE

LIST OF FIGURES

FIGURE

NOMENCLATURE

a	One of the triclinic PA 66 unit cell parameters, nm
$\bar{A}$	Average area, μm^2
A_0	Undeformed cross-sectional area of the gauge region, mm^2
A_i	Area of a number of domains in SEM analysis, μm^2
b	One of the triclinic PA 66 unit cell parameters, nm
b	Width of beam tested, mm
b_1	Width of the narrow section of tensile test specimen, mm
b_2	Width of overall of tensile test specimen, mm
c	One of the triclinic PA 66 unit cell parameters, nm
d	Depth of beam tested, mm
d	Interlayer spacing, Å
$\bar{d}$	Average domain size, nm
D	Maximum deflection of the centre of the beam, mm
D	Diameter of the screws, mm
E	Young's modulus, MPa
E_B	Modulus of elasticity in bending, MPa
F	Force, N
h	Thickness of tensile test specimen, mm
l_1	Length of the narrow section of tensile test specimen, mm
l_2	Length of overall of tensile test specimen, mm
L	Distance between the grips of tensile test specimen, mm
L	Support span, mm
L	Length of the extruder barrel, mm
L_0	Initial gauge length, mm
ΔL	Change in sample length, mm
m	Slope of the tangent to the initial straight line portion of the load deflection curve, N/mm
n	Degree of diffraction
n_i	Number of domains analyzed in SEM analysis
P	Load at a given point on the load-deflection curve, N
r	Maximum strain in the outer fibers, mm/mm

r_1	Radius of fillet of tensile test specimen, mm
r_2	Outer radius of tensile test specimen, mm
S	Stress in the outer fibers at midspan, MPa
T_g	Glass transition temperature, ℃
T_m	Melting temperature, ℃

Greek Letters

α	Angle of triclinic unit cell of PA 66, °
α	Stable phase of PA 66 crystal structure
β	Angle of triclinic unit cell of PA 66, °
β	Unstable phase of PA 66 crystal structure
ε	Strain, mm/mm
ε_b	Elongation at break, mm
γ	Angle of triclinic unit cell of PA 66, °
λ	Wavelength, nm
σ	Stress, MPa
θ	Diffraction angle, °

Abbreviations

CI-P	Mixing sequence in which melt compounding of the polymer matrix with organoclay-impact modifier combination was carried out in the second step
DIN	Deutches Institut für Normung
DSC	Differential Scanning Calorimetry
E-GMA	Ethylene-Glycidyl Methacrylate
E-MA-GMA	Ethylene-Methyl Acrylate-Glycidyl Methacrylate
E-BA-MAH	Ethylene-Butyl Acrylate-Maleic Anhydride
HDPE	High Density Polyethylene
HT	Hydrogenated Tallow
IEC	International Electrotechnical Commission
IM	Impact Modifier
ISO	International Organization for Standardization
MFI	Melt Flow Index

MMT	Montmorillonite
OMMT	Organic Montmorillonite
PA 6	Polyamide 6
PA 66	Polyamide 66
PC-I	Mixing sequence in which melt compounding of the impact modifier with polymer matrix-organoclay combination was carried out in the second step
PI-C	Mixing sequence in which melt compounding of the organoclay with polymer matrix-impact modifier combination was carried out in the second step
PMMA	Poly (methyl methacrylate)
PS	Polystyrene
PTFE	Polytetrafluoroethylene
SAXS	Small Angle X-ray Scattering
SEBS-g-MA	Styrene-Ethylene/Butylene-Styrene triblock copolymer grafted with Maleic Anhydride
SEM	Scanning Electron Microscopy
T	Tallow
TEM	Transmission Electron Microscopy
TGA	Thermal Gravimetric Analysis
XRD	X-Ray Diffraction
WAXS	Wide Angle X-ray scattering
UHMWPE	Ultrahigh Molecular Weight Polyethylene
UL	Underwriters Laboratories

CHAPTER 1

INTRODUCTION

Composite materials are composed of two or more physically or chemically distinct arranged or distributed phases with an interface in between that separates them. The main advantages of making use of composite materials are their flexible structure that enables carrying combinations of shear and axial forces, simplicity, efficiency due to their high specific properties on a per unit weight basis and savings in materials, energy and longevity of use because of their better creep and fatigue resistance than their monolithic counterparts [1].

Although polymer matrices are preferred in terms of the ease of processing at low temperatures and pressures by simpler processing equipments, their mechanical properties are much lower than metallic and ceramic matrices, thus reinforcement utilization is inevitable. Their main disadvantages are low maximum service temperature, high thermal expansion coefficient that may lead to dimensional instability and sensitivity to UV and moisture. Their low density contradictory to heavy metallic and ceramic composites whose ductility is rather low is a great advantage for the use of polymer matrices [1,2].

The type of the polymer matrix is chosen according to the process type. Thermosetting polymers cannot be reshaped once they are cured and extra energy is required for the curing step. On the contrary, thermoplastics can flow readily under stress at elevated temperatures. They can be reshaped and their toughness is also higher. Yet, their high viscosity makes incorporation of reinforcement, especially continuous fibers, more difficult during processing [3].

Layered silicates that belong to the structural group of 2:1 phyllosilicates are more widely used in polymer nanocomposites. Clay platelets are composed of a 1 nm thick layer made of two tetrahedral sheets of silica fused to an edge shared octahedral sheet of alumina or magnesia. An excess negative charge called as cation exchange capacity is created in the van der Waals gap of clay stacks by

isomorphic substitution of cations, and hydrophilic clay is turned into organophilic by imparting alkylammonium or alkylphosphonium ions within the clay structure replacing the cations like Na^{+} or Ca^{2+} that counterbalance the excess layer charges [4].

Nanocomposites can be synthesized via melt intercalation, in-situ polymerization, solution polymerization and emulsion polymerization. Melt intercalation is a really environmentally sound method since no solvent is involved in the process and it can be performed through the aid of conventional processing techniques. However, residence time, level of shear, selection of polymer grade, organoclay choice and level of reinforcement all play a significant role on the degree of exfoliation. Despite the fact that it is generally easier to disperse the nonpolar clay platelets homogeneously in the polymer matrix by the methods like in-situ polymerization and solution polymerization, the use of conventional methods and elimination of the solvents from the process makes melt intercalation both economically and environmentally benign [5,6].

Polyamide 66 has a polar and polymorphic structure [7]. Therefore, it is expected to have more interaction with the organoclay and the impact modifier functional groups and enhanced mechanical properties relying on its semicrystalline structure. It has been demonstrated that organoclay can be exfoliated in polymer matrix by the combined action of optimum residence times, shear stresses induced both by the screw speed and polymer melt viscosity and increase in clay-polymer interaction [8,9].

The purpose of this study is to prepare PA 66 blends, binary PA 66/organoclay nanocomposites and ternary PA 66/organoclay/impact modifier nanocomposites with Cloisite® 15A, Cloisite® 25A , Cloisite® 30B and Lotader® AX8900 resin (a random terpolymer of ethylene (E), methyl acrylate (MA) and glycidyl methacrylate (GMA)), Lotader® AX8840 resin (a random copolymer of ethylene (E) and glycidyl methacrylate (GMA)), Lotader® 2210 resin (a random terpolymer of ethylene (E), butyl acrylate (BA) and maleic anhydride (MAH)). Copolymers and terpolymers containing functional groups as maleic anhydride, acrylates and glycidyl methacrylate were used as compatibilizers and toughening agents.

Impact modifiers are incorporated into the polymer matrix both for the increase of toughening mechanisms and compatibilization between the polymer and the organoclay as the number of functional groups is increased upon addition of the elastomeric phase. Besides the compatibilization effect, increased viscosity of the polymer also aids homogeneous dispersion of the clay platelets and elastomeric domains within the matrix. At first, all the components were simultaneously fed to the extruder and extruded twice. The polymer melt was injection molded soon after the second extrusion step. All the specimens were conditioned as dry as moulded. The mixing sequences of the ternary nanocomposites that exhibit enhanced mechanical properties and better exfoliation of the clay platelets were varied in the second part of the study.

Mechanical properties of the specimens were evaluated according to the tensile, flexural, impact and hardness test results together with the morphological characterization that was performed by SEM and XRD analysis. In addition to it, crystallinity results obtained by DSC analysis and flow characteristics given by Melt Flow Index analysis were related with the aforementioned test results to explain the prior factors affecting the degree of dispersion in nanocomposite structure as well as improved strength, stiffness and toughness properties.

CHAPTER 2

BACKGROUND

2.1 Composite Structure

Composite is any multiphase material that exhibits a significant proportion of the properties of both constituent phases such that a better combination of properties is obtained. Better property combinations can be acquired by the presence of two or more distinct materials due to the principle of combined action. Constituent phases, their relative amounts and the geometry of the dispersed phase that means the shape of the particles, the particle size, distribution and orientation are the functions of the properties of composites [2]. Both constituents have to be in reasonable proportions so that the composite material properties will be noticeably different from the properties of the constituents [10].

The origin of the distinct discipline of composite materials can be stated as the beginning of 1960s. An extensive research and development effort in composite materials started in 1965s [1]. Plywood and corrugated paper are two examples of the composite term that has been applied to heterophase materials when their dimensions are almost macroscopic [11]. The standard materials have been replaced with composites because of their lighter weight/higher strength alternative. The alternatives they offer are new design flexibilities, improved corrosion and wear resistance and increased fatigue life [12]. By the help of utilizing proper design and manufacturing techniques, some net shaped parts can be produced with composite materials. Several machining operations are eliminated by this feature and thus process time and cost are reduced [13]. The design impact of composites on fighter aircraft, energy and civil construction was surveyed [14] and the possibilities of improvements that can be obtained over conventional materials by making use of composite materials were indicated [15].

Most of the composite materials consist of just two phases, one is termed the matrix, that is continuous and surrounds the other phase, which is often called the dispersed phase [2]. Reinforcement that is the secondary phase enhances or reinforces the mechanical properties of the material. Binding the reinforcement together, acting as a medium for transmitting and distributing the stresses, protecting the reinforcement material from surface damage as a result of mechanical abrasion or chemical environment and separating them to prevent propagation of cracks from one to another are the functions of the matrix phase [10].

2.1.1 Interactions at the Interface in Composites

The interfacial bonding has to be adequate to maximize the stress transmittance from the weak matrix to the reinforcement. Interface is the region through which material parameters such as the concentration of an element, crystal structure, atomic chemistry, elastic modulus, density, coefficient of thermal expansion, etc. differ from one another. The discontinuity across the interface may be sharp or gradual [1]. Failure mechanisms, fracture toughness and stress strain behavior of the material are generally controlled by the interface [16].

Wettability, surface roughness and bonding are the important factors affecting the matrix and reinforcement interface [2].

Wettability is the ability of liquid to spread over a solid surface by covering every part of rough surfaces as well as displacing all the air [10]. The extent of intimate contact possible at the molecular level is also determined by wettability [2]. Surface roughness has a prominent effect on wettability since it can reduce the bonded area and lead to void formation or stress concentrations [10]. Most fibers and reinforcements show some degree of surface roughness [1].

The types of interfacial bonding are mechanical bonding, physical bonding involving weak, secondary, van der Waals forces, dipolar interactions and hydrogen bonding, chemical bonding including bonding by direct reactions in polymer-matrix composite systems, bonding by coupling agents for polymer-fiber

systems, bonding by molecular chain entanglement for polymer-polymer systems and bonding by interdiffusion in ceramic-metallic systems [1].

Mechanical bonding is efficient in load transfer when the force is applied parallel to the interface. In the case of mechanical bonding matrix must fill the pores and surface roughness of the reinforcement. Rugosity or surface roughness are also contributive to bond strength only if the reinforcement surface can be wetted by the liquid matrix. Pure mechanical bonding is not enough in most of the cases since its strength is low compared to chemical bonding at the interface. The same thing is valid for physical bonding. In addition to being retarded by surface contamination and entrapped gases, physical bonding is effective over small distances. That is why they should both operate with the other bonding mechanisms [1].

2.2 Types of Composites

The types of composites include metal-matrix composites, ceramic-matrix composites, carbon-carbon composites and polymer-matrix composites. Properties of nanocomposites are highly affected by the matrix and the reinforcement. Composites find application in a variety of areas including electronics, aerospace and construction.

In metal-matrix composites, the matrix is a ductile metal and they may be utilized at higher service temperatures than their base metal counterparts; with the reinforcement improving specific stiffness, specific strength, abrasion resistance, creep resistance, thermal conductivity and dimensional stability. Higher operating temperatures, non-flammability and greater resistance to degradation by organic fluids are some of their advantages over other composites. Nevertheless, they are much more expensive than their counterparts and their use is somewhat limited [2].

Ceramic-matrix composites are also applicable at high temperatures and severe stresses, especially for components in automobile and aircraft gas turbine engines resulting from their inherent resilience to oxidation and deterioration [2]. However, their properties are restricted by an attractive flaw, an utter lack of

toughness. Therefore, fibers are incorporated in them to preserve the attractive high temperature and environmental strength and prevent a catastrophic failure [1].

Both the reinforcement and the matrix is carbon in carbon-carbon composites. High tensile modulus and tensile strengths that can be observed even at drastically high temperatures up to 2000°C, resistance to creep and relatively large fracture toughness values are among their desirable properties. Their thermal expansion coefficients are low in contrast to the relatively high thermal conductivities and high strengths. The propensity to high temperature oxidation is the major drawback of their use [2].

In terms of the reinforcement material, composite materials are divided into two groups as particle-reinforced and fiber-reinforced composites. Particle-reinforced composite group includes single-layer and multi-layer composites that are composed of laminates (sheet constructions in a specified sequence), hybrids (construction with mixed fibers in a ply or layer by layer) and sandwich panels (structural composites with 2 outer sheets separated by a layer of less dense material) [10]. The strength of a structural composite is relatively high in a number of directions in the two dimensional plane [2].

2.2.1 Polymer-Matrix Composites

Polymer-matrix composites are composed of a resin as the matrix with fibers as the reinforcement medium [2]. These materials are majorly utilized in composite applications in largest quantities, owing to their room temperature properties, ease of fabrication and cost.

The matrix of the composite can either be thermoplastic or thermosetting. Thermoplastics would soften upon heating and then could be made to flow upon application of a stress. When cooled again, their solid or rubbery nature would be reversibly gained. On the other hand, heating causes thermosets undergo a curing reaction; they could be made to flow under stress only once. Further heating of thermosetting materials causes only degradation, not softening or flow [3]. Although thermosets have many advantages over thermoplastics like their

low viscosity, which facilitates the wetting out of the fiber reinforcements, the voids and porosities, thermoset composite processing requires a lengthy cure time and, thus results in lower production rates than thermoplastics [17].

The most widely utilized and least expensive polymer resins are polyesters and vinyl esters. Epoxies have better mechanical properties and better resistance to moisture compared to polyesters and vinyl esters and they are utilized extensively in polymer-matrix composites in aerospace applications, despite the fact that they are more expensive. High temperature thermoplastic resins are especially suitable for use in future aerospace applications; such materials include polyetheretherketone, polyphenylenesulfide and polyetherimide [2].

2.3 Polymer-Layered Silicate Nanocomposites

Nanocomposites are a new class of composites, that contain a particle-filled polymer matrix whose at least one dimension of the dispersed particles is in the nanometer range [18]. The use of layered silicates as a reinforcing phase is one of the most successful ways of designing polymer nanocomposites with a broad range of markedly modified properties among the variety of composites that display unique structure and behavior at the nanometer level, in comparison with classical micrometer scale particulate filled materials [4]. Many polymer nanocomposites based on exfoliated layered silicates have improved properties such as modulus, flammability and barrier properties. Nanocomposites can achieve their optimal properties at relatively low filler content, resulting in lower density, better surface smoothness and transparency, although this is not the case for traditional polymer nanocomposites containing larger particles such as talc or short fibers (glass, carbon, aramid). Exfoliated nature of the layered silicate filler, resulting in very thin particles with large aspect ratios is significant in improving properties at low filler content [18-20].

.

Nanocomposites can be classified according to the number of dimensions in the nanometer range. Isodimensional nanoparticles, such as spherical silica nanoparticles obtained by in-situ sol-gel methods [18,21,22] or by polymerization promoted directly from their surface [18,23] have three dimensions in the order of nanometers. Semiconductor nanoclusters [18,24] also belong to this group. If two

dimensions are in the nanometer scale and the third one is larger than the other two, forming an elongated structure, nanotubes or whiskers are called as, for example, carbon nanotubes [18,25] or cellulose whiskers [18,26,27] which are extensively studied as reinforcing nanofillers yielding materials with exceptional properties. Only one dimension of the third type of nanocomposites is in the nanometer range. In this case, the filler which is in the form of sheets is one to a few nanometers thick while it is hundreds to thousands nanometers long. This type of composites can be named as polymer-layered crystal nanocomposites [18].

2.3.1 Layered Silicates

Layered silicates belong to the structural group of 2:1 phyllosilicates, which is an undergroup of smectites. Natural clay minerals such as montmorillonite, hectorite and saponite and synthetic layered minerals like fluorohectorite, laponite or magadiite belong to this group [4]. Different chemical and physical characteristics such as layer size, stacking perfection, reactivity and Lewis acidity are exhibited by natural and synthetic silicates with variations in the amount, type and the crystallographic origin of the excess layer charge [28]. Their crystal lattice is composed of two-dimensional layers where a central octahedral sheet of alumina or magnesia is fused to two external silica tetrahedron by the tip so that the oxygen ions of the octahedral sheet are also shared by the tetrahedral sheets. The lateral dimensions range from 300 Å to several microns or even larger due to particular silicate, and the layer thickness is around 1 nm. Pristine layered silicates usually contain hydrated Na^+ or K^+ ions and they are only miscible with hydrophilic polymers, such as poly(ethylene oxide) [29,30], or poly(vinyl alcohol) [30,31] in the pristine state. Layered silicates are made miscible with many other polymer matrices by converting hydrophilic silicate surface into an organophilic one and making the intercalation of many engineering polymers possible. It can be accomplished by ion-exchange reactions with cationic surfactants including primary, secondary, tertiary and quaternary alkylammonium or alkylphosphonium cations.

Stacks with a regular van der Walls gap in between them, that are called the interlayer or the gallery, are formed by the regular organization of the layers.

Negative charges are generated by isomorphic substitution within the layers (for example, Al^{3+} replaced by Mg^{2+} or by Fe^{2+} or Mg^{2+} replaced by Li^{+}) and they are counterbalanced by alkali or alkaline earth cations situated in the interlayer [30]. The cations are generally hydrated and the negative charge is quantified as the cation-exchange capacity and it is usually in the range from 80 to 150 meq/100g for smectites [4].

A diverse range of catalytic activity occurs at both the layer edge and to a lesser extent at the planer siloxane surface as a result of the complex crystallographic structure and habit of clay minerals. The fraction of total surface area of an individual layer associated with the edge is 2-4 % for layers with radii between 50 and 25 nm, respectively. Weakly acidic SiOH and strongly acidic bridging hydroxyl groups present at the edge act as Bronsted acid sites. Lewis acid centers can be present at the layer edge because of partially coordinated metal atoms like Al^{3+} or along the siloxane surface from isomorphic substitution of multivalent species, like Fe^{2+} and Fe^{3+} and crystallographic defects within the layer. Single electrons can be accepted by these Lewis acid sites from donor molecules with low ionization potential, coordinate organic radicals and electrons can be abstracted from vinylic polymers [29]. Structure of 2:1 phyllosilicates is shown in Figure 2.1.

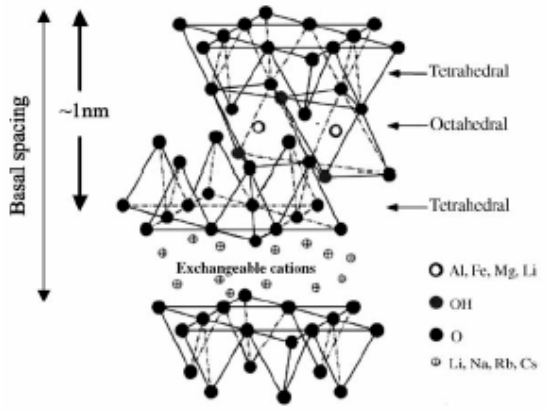

Figure 2.1 Structure of 2:1 phyllosilicates [30].

The surface energy of the inorganic host is lowered by alkylammonium or alkylphosphonium cations in the organosilicates and the wetting characteristics of the polymer matrix are improved resulting in a larger interlayer spacing [30]. Functional groups that can react with the polymer matrix are provided by alkylammonium or alkylphosphonium cations or the polymerization of monomers can be initiated to enhance the strength between the inorganic silicates and the polymer matrix [32,33]. Depending on the charge density of the clay and the onium ion surfactant, different arrangements of the onium ions can be possible. Generally, the longer the surfactant chain length and the higher the charge density of the clay, the further apart the clay layers will be forced because both of these parameters are contributive to the increasing volume occupied by the intergallery surfactant. The position of the onium ions may be parallel to the clay surface as a monolayer, a lateral bilayer, a pseudo-trimolecular layer or an inclined paraffin structure. Large surfactant ions can exhibit lipid bilayer orientations in the clay galleries at very high charge densities [34]. Orientations of alkyl ammonium ions in the galleries of layered silicates with different layer charge densities are shown in Figure 2.2.

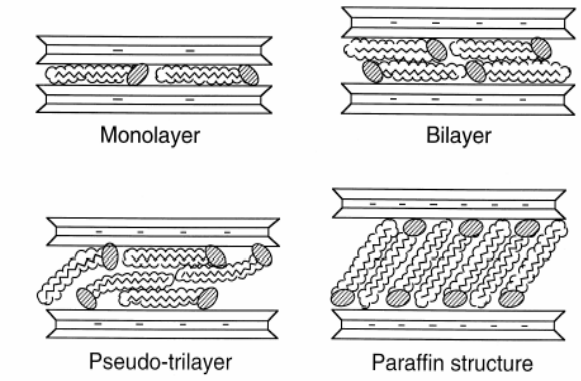

Figure 2.2 Orientations of alkyl ammonium ions in the galleries of layered silicates with different layer charge densities [35].

2.3.2 Nanocomposite Types

It is not always possible to end with a nanocomposite when the organoclay is mixed with a polymer. Unseparated montmorillonite layers are called as tactoids after they are introduced into the polymer [36]. The dispersion of the inorganic compound must be at the nanometer level that is down to elementary clay platelet [4]. The layer thickness of the layered silicates is on the order of 1 nm and they have a very high aspect ratio. (10-10000) Compared to conventional composites, a few weight percent of layered silicates create much higher surface area for polymer-filler interaction [30]. Three types of nanocomposites that are called intercalated, exfoliated and flocculated can be obtained depending on the nature of the components used and the method of preparation [18]. The types of polymer-layered silicate nanocomposites are given in Figure 2.3.

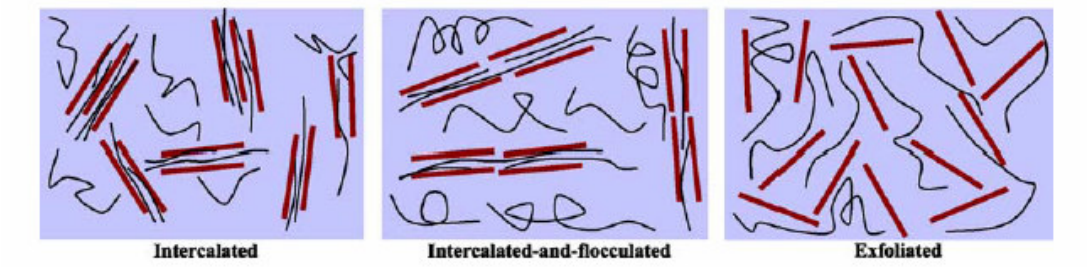

Figure 2.3 Three different types of thermodynamically achievable polymer-layered silicate nanocomposites [37].

If the clay layers are dispersed individually in the host polymer matrix in a delaminated fashion, they are called exfoliated nanocomposites [4]. Clay platelets are separated by 80-100 Å or more [36].

In intercalated nanocomposites polymer chains are intercalated in the gap between the silicate layers while the stacking order is retained [4]. They are normally interlayer by a few molecular layers of polymer. Less than 20-30 Å separations are formed between the platelets, as a small amount of polymer moves into the gallery spacing between the platelets [36].

Flocculated nanocomposites are nearly the same as intercalated nanocomposites. However, silicate layers are sometimes flocculated because of their hydroxylated edge-edge interaction [30].

2.3.3 Nanocomposite Preparation Methods

Various methods have been developed in order to prepare polymer-layered silicate nanocomposites by intercalation of polymer chains in layered silicates. These methods include solution polymerization, in-situ polymerization, melt intercalation and emulsion polymerization [4].

2.3.3.1 Solution Polymerization

Solution polymerization is based on a solvent system in which the polymer or the pre-polymer is soluble and the silicate layers are swellable. The first step is to dissolve the layered silicate in a solvent such as water, chloroform or toluene [30]. Afterwards, it is easy to disperse layered silicates in an adequate solvent, owing to the weak forces that stack the layers together [18]. The solvent within the interlayer of the silicate is displaced upon intercalation of the polymer chains as the polymer and the layered silicate solutions are mixed. The intercalated structure is preserved after the solvent removal [30].

A negative variation occurs in the Gibbs free energy as the polymer is exchanged with the previously intercalated solvent in the gallery. The driving force from the polymer intercalation into layered silicate from solution is the entropy and it is gained by desorption of solvent molecules such that the decreased entropy of the confined intercalated chains is compensated [38].

This method is suitable for the intercalation of polymers with little or no polarity into layered structures and production of thin films with polymer-oriented clay intercalated layers is facilitiated. However, the use of inorganic solvents that is environmentally unfriendly and economically prohibitive is one of the major drawbacks [30]. A schematic illustration of nanocomposite synthesis is given in Figure 2.4.

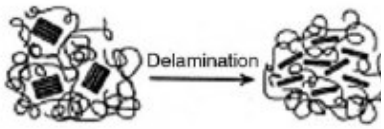

Figure 2.4 Nanocomposite synthesis [39].

2.3.3.2 In-situ Polymerization

In in-situ polymerization, polymer formation can occur between the intercalated sheets of the layered silicate within the liquid monomer or a monomer solution [18]. The diffusion of a suitable initiator or catalyst fixed through cation exchange inside the interlayer before the swelling step can be the initiator of polymerization [30]. Synthesis of nylon 6/clay nanocomposites can be seen in Figure 2.5.

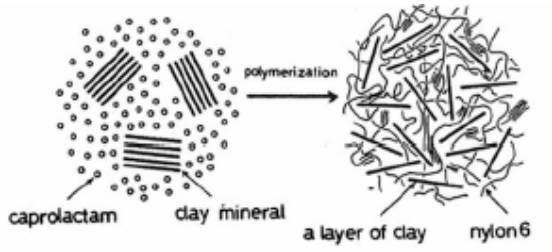

Figure 2.5 Synthesis of nylon 6/clay nanocomposites [40].

2.3.3.3 Melt Intercalation

Melt intercalation method involves diffusion of the polymer chains into the space between the clay and the galleries. Combination of this method with conventional polymer processing techniques decreases the processing time to form the hybrids by breaking up clay particles and increasing sample uniformity. The degree of exfoliation and properties of the final composites are affected by the rheological and thermodynamic character of the material. The filler agglomerates are dispersed when the hydrodynamic separating forces applied by the matrix fluid exceed the cohesive forces. Dispersion degree of the clay particles is

dependent on the matrix viscosity, average shear rate and the mean residence time in the mixing process [8]. The confinement of a polymer melt with nanocomposite formation causes an entropy loss. However, the process is allowed to occur since there is an entropy gain associated with the layer separation, resulting in a net entropy change near to zero. Thus, the outcome of nanocomposite formation by melt intercalation depends primarily on energetic factors, which may be determined from the surface energies of polymer and organically modified layered silicates [30]. Schematic illustration of melt intercalation process is shown in Figure 2.6.

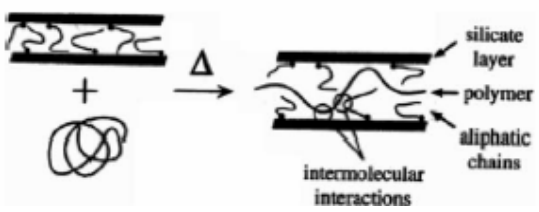

Figure 2.6 Intercalation process between a polymer melt and an organically modified layered silicate [38].

Melt intercalation has many advantages over solution polymerization and in-situ polymerization. It is compatible with the industrial processes and environmentally benign because of the absence of organic solvents. The polymers whose properties are not suitable for in-situ polymerization or solution polymerization can be processed by melt intercalation [30].

2.3.3.4 Emulsion Polymerization

Polymerization in an aqueous medium is an alternative route for polymer-clay nanocomposite preparation considering the high hydrophilic character of sodium montmorillonite. The silicate layers are swollen in process water and the intergallery is made accessible for the polymer so as to improve exfoliation. Potential reduction of the raw materials cost and the increase in thermal stability due to the absence of thermally unstable surfactants make the use of unmodified silicate favorable [41]. Structural analysis confirms intercalation of PMMA and PS

as well as an epoxy system without requiring any ion exchange treatment by this method [42-44].

2.4 Polyamide 66

PA 66 is one of the most famous engineering thermoplastics because of its excellent physical and mechanical properties [45]. Nylon was discovered by Wallace Hume Carothers at the Dupont Company and the introduction of PA 66 as toothbrush filaments by DuPont in 1938 was the first polyamide application [46]. In recent years, the increasing interest in polyamides results from their higher melting points to extend the boundaries of this polymer type to satisfy more stringent high temperature automobile and electronic applications [4].

PA 66 is a semicrystalline polymer that is synthesized by stepwise polymerization between a diacid and a diamine [47]. The first integer of PA 66 represents the number of carbon atoms in the diamine and the second integer belongs to the number of carbon atoms in the dicarboxylic acid [48]. The synthesis reaction is given in Figure 2.7.

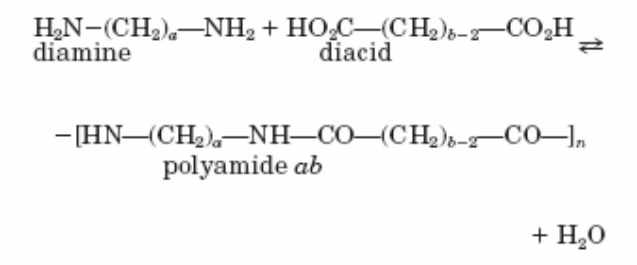

Figure 2.7 Synthesis reaction of diadic polyamides [47].

2.4.1 Crystalline Structure of Polyamide 66

PA 66 has a polymorphic structure and two phase crystallinity arises from the different spatial arrangement in the hydrogen bonding between the oxygen in the carbonyl group of one polyamide molecular chain and the hydrogen attached to the nitrogen in the neighboring polyamide molecular chain. It cannot readily be

drawn to high extensions because of the presence of intermolecular hydrogen bonding. Both crystalline and amorphous phases have hydrogen bonds within their structure and the hydrogen-bonded crystallites behave like quasi-crosslinks during drawing, restricting the achievable drawing ratio and limiting control over polymer microstructure [49].

The crystal structure of PA 66 is composed of triclinic α and β form with one chemical per unit cell [46]. The lower temperature α phase contains chain-folded sheets and is a consequence of the linear hydrogen bonds, imparted by progressive shear of chains, between amide groups in the adjacent chains within the sheet [50]. The molecules are in the fully extended zigzag conformation. The higher temperature β phase is not a distinct phase in the thermodynamic sense and it results in a slight perturbation of α phase [46]. The intersheet shear of chains occurs alternately in *c* direction rather than progressively within pleated sheets of chains joined by hydrogen bonds [50]. Interaxial angles of triclinic structure of PA 66 are unequal and it is of low symmetry [46]. Schematic representation of PA 66 unit cell is shown in Figure 2.8.

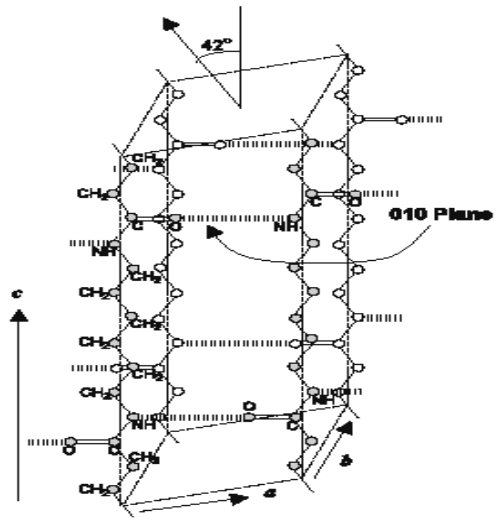

Figure 2.8 Unit cell of PA 66: a triclinic cell with parameters a:0.49 nm, b:0.54 nm, c:1.72 nm and α:48.5, β:77 and γ:63.5 [51].

Ideal unit cell of PA 66 consists of all trans chain conformations hydrogen bonded into sheets (*ac* plane (010) plane) and the intersheet stacking is controlled by van der Waals interaction [51]. The growth axis of crystalline lamellae is in "*a*" direction. The number of H bonds between the two faces of the lamellae determines the thickness, it is about 4x*c* for bulk PA and it is nearly 6 nm for PA 66. The angle between the *c* axis and the direction normal to the chain folded plane is 13°. As a result, the angle between the C=O transition moments and the average angle between the normal to the chain folded plane is equal to 13° [47].

The good balances of properties are improved by the semicrystalline structure. The crystalline regions enhance the stiffness, strength, chemical resistance, creep resistance, temperature stability and electrical properties; while the impact resistance and high elongation are affected by the amorphous region [46].

2.4.2 Properties of Polyamide 66

Toughness, fatigue resistance, low friction, abrasion resistance, resistance to oils and solvents, stability at high temperature, fire resistance, creep resistance, drawability, good appearance and good molding economics are commercially important properties of PA 66. High tensile strength of certain oriented polyamides that is equivalent to that of steel, low density and easy fabricability makes it possible to compete with the metals [46].

More than 60 % of nylon is used in injection molding applications. About 55 % of this use belongs to the transportation industries concerned with automobile production as radiator end tanks, filter housings, connectors, cable ties, switches, handles, seat belt components, air bag containers, pedals, pedal boxes, sun roof surrounds and fuel filler flaps [4]. Textile shuttles of glass reinforced PA 66, handrails of moving stairways, spatula blades, spoons, television tuner parts are some of the other examples of commercial PA 66 uses.

2.4.2.1 Mechanical Properties

PA 66 has moderately high tensile strength, limited modulus, excellent toughness and adhesive properties depending on its semicrystalline structure. It is a very important solution in many applications because of the combination of significant thermal and mechanical properties, high resistance to chemicals, durability to fatigue and abrasion. Despite all these advantages and its high resistance to crack initiation, its crack propagation resistance is rather low. When a crack exists, it breaks easily [46]. Its impact strength is improved by blending it with terpolymers of ethylene and propylene containing carboxylic acid groups [48]. Molecular weight, moisture content, temperature and the presence of additives affect the final mechanical properties. Moisture increase gives a steady increase in impact strength for PA 66, just like the temperature increases, as a result of increasing plastication, although at very low temperatures moisture can embrittle nylon [4].

Generally, PA 66 is notch-sensitive and the unnotched impact strength is dramatically reduced when a notch or flaw is introduced into the material. Sharp angles have to be avoided during the design of different parts. Incorporating impact modifiers in the polymer matrix can considerably reduce the notch sensitivity. Other mechanical properties like strength and stiffness can be remarkably increased through the aid of adding a reinforcing agent to the polymer whereas a sharp decrease is observed in both of them upon the addition of plasticizers that promote ductility, flexibility and impact strength [4].

PA 66 has a low coefficient of friction and melt viscosity. Friction coefficient value is lowered below that of graphite when water is present in the medium. The low melt viscosity is related to many methylene groups between the amide stiffening groups and it may readily be extruded to produce unoriented filaments. Strong fibers of these filaments can be produced by stretching and aligning the chains in a specific direction so that the intermolecular forces are more effective [48].

2.4.2.2 Electrical Properties-Moisture Absorption

Nylons are frequently used in electrical applications especially for the combination of their mechanical, thermal, chemical and electrical properties. Their insulating properties are fairly good at low temperatures and humidities and are generally suitable for low frequency, moderate voltage applications [4].

The water sensitive amide groups of PA 66 are responsible for the good dyebility and diminishing of fair to good non-conductive electrical properties [48]. Moisture absorption is dependent on the degree of crystallinity and the polar amide groups around which water molecules can become oriented. Increasing the length of aliphatic groups in the chain can decrease moisture absorption just like the melting point. Impact strength can be increased by making the polymer more flexible resulting from the plasticizing effect of water absorption related to hydrogen bonding interruption in the amorphous regions [4].

2.4.2.3 UV Degradation-Oxidation-Flammability

It is well documented that nylons are susceptible to air oxidation at elevated temperatures in the dark as well as in the light (200°C) [48]. PA 66 deteriorates in the absence of stabilizers when exposed to UV or oxidation as UV rays make it undergo a free-radical aging process. Oxidation induces the initial formation of a free radical on the carbon alpha of NH group, which reacts to form a peroxy radical with subsequent chain reactions leading to chain scission and yellowing [4].

In terms of flammability, it is self-extinguishing like most of the nylons for a certain period of time and this is achieved by means of giving a certain amount of burning drips [3]. It also has low values of smoke density [46].

2.4.2.4 Thermal Properties

The glass transition temperature of aliphatic polyamides is rather low (40-70°C) and composition does not affect T_g to any great extent [50]. The heat deflection

temperature of PA 66 is about 75°C and it has a linear expansion coefficient of $8*10^{-5}$ cm/cm °C. Its high melting point (about 265°C) is a function of both the strong hydrogen bonding between the chains and the crystal structure. High melting points permit materials to retain significant stiffness above T_g and almost up to the melting point [48]. Despite the fact that PA 66 has good thermal stability, it tends to degrade when held for long periods of time at high temperatures. The adipic acid segment can cyclize, leading to chain scission, the production of cyclopentanone and derivatives and evolution of carbon dioxide and ammonia. Crosslinking occurs and the material turns into an intractable gel along with reduction of molecular weight [4].

2.4.2.5 Chemical Properties

Generally most nylons have excellent resistance to chemicals but they can be made to participate in a variety of reactions. The site of attack may be in the molecule: the end groups, the amide nitrogen, the amide carbonyl, or the hydrocarbon portion depending on the nature of reaction [46]. PA 66 is resistant to aqueous salts, alkalis and nonpolar solvents such as gasoline. However, it is softened by polar solvents such as ethanol and deteriorates in the presence of mineral acids. It is soluble in formic acid, acetic acid, phenols and cresols [48].

2.4.2.6 Optical Properties

Most of the polyamides are opaque in thicknesses over about 2.5 mm and transparent below 0.5 mm. The opacity is due to light scattering at sphereulite boundaries. A further reduction in light transmission can be obtained by increasing crystallinity and the number of sphereulites via use of nucleating agents. However, transparency is enhanced by reducing the rate of crystallization and sphereulitic nature. Quenching the melt during fabrication and by modifying the polymer via copolymerization or plasticization are some of the ways of accomplishing it [4].

2.4.3 Polyamide 66 Nanocomposites

The applications to prepare nanocomposites from thermoplastics that require high melting processing temperatures, and from thermoset resins, which need high cure temperatures are limited by the low thermal stability of alkyl ammonium [52]. Processing temperature affects both the melt rheology and the organoclay surfactant stability. As it is expected, degradation is faster at higher temperatures and in the more oxidative environment [53]. However, the residence time during which the polymer matrix is subjected to high temperatures and thermal stability of the materials are also prominent for decomposition mechanisms. The evolution of decomposition products is more probable for long residence times.

The mean residence time for PA 66 matrix is about a minute in Thermoprism TSE 16 TC twin-screw extruder at 260-280 °C and the mass loss is about 1 wt% for Cloisite® 15A and Cloisite® 25A and 2 wt% for Cloisite® 30B at 280°C for 1-2 minutes as it can be seen from TGA in Appendix D [54]. Therefore, decomposition of the organic modifier does not seem to be profoundly effective on the degree of the organoclay exfoliation in PA 66 nanocomposites in this study.

In all the nanocomposites, a decreasing electrostatic interaction occurs between adjacent montmorillonite layers due to intercalation of the organic surfactant and the enlarged intragallery of the organic montmorillonite providing a good opportunity for macromolecular chains to diffuse into montmorillonite intragalleries during melt compounding [52]. An epoxy resin can also be used in the preparation of nanocomposites, as in co-intercalation clays, to diffuse into the clay galleries to increase the layer distance further in the organophilic environment [55]. However, increasing the basal spacing of the organoclay does not necessarily lead to more exfoliation [56]. Exfoliation is highly dependent on a variety of thermodynamical interactions (polymer-clay, polymer-surfactant, clay-clay), organoclay stability, packing density etc. The cohesive forces between neighboring plates are overcome by organic modification so that polymer intercalation and platelet exfoliation can occur. Thereupon, polar polyamide-polar clay interactions should not be shielded [57]. It is proposed that polyamide-

silicate contacts are more favorable after a sufficient level of platelet separation is achieved to reduce the platelet-platelet interaction [56].

Two key issues that have a direct effect on the degree of exfoliation of the organoclay are melt viscosity of the polymer matrix and thermal degradation of the organic modifier on the clay. The enhancement in mechanical properties can be due to the ionic bonds between the organic polymer and the inorganic silicate since a large number of polyamide molecules are bonded to the silicate layers via the protonated amine chain ends $-NH_3^+$ [8,53,57]. It is observed that there is a strong interaction between the clay layers and polymer chain segments because of forming hydrogen bonds among Si-O, Si-OH, C=O and N-H groups or some ionic interaction because of the tremendous contact between nanoclay layers and PA 66 [58]. The substitution of polar groups such as -OH and -COOH for hydrogens on the ammonium ions is likely to increase the binding energies with the polymer. Although the increase in the volume of the quaternary ammonium salts increases the binding energy between the quaternary ammonium salts and PA 66, organic modifiers with short hydrocarbon chains are found to produce higher binding energies than those with longer ones [59].

Organic montmorillonite is believed to be hydrophobic but some water is still absorbed on the exterior of the aggregates and along the edges of the hydrophilic layer. The water content in organic montmorillonite powder that is released at almost 45°C is about 2 wt% [52]. Weakly bound, physiabsorbed water and free water pockets within the aggregate structure evolve at the lowest temperatures, whereas water within the interlayer and strongly bonded water of hydration (Na^+) evolve at higher temperatures [28]. The decomposition of the organic substance takes place from 200 to 500°C [52]. CO_2 release at 400°C is an indication of the beginning of the oxidation of residual organic within the organic layered silicates that begins shortly after general mass loss via alkenes and alkanes ends and before general dehydroxylation of the aluminasilicate begins. It may also be associated with a small fraction of insoluble metal carbonate impurities [28]. The mass loss from 600 to 700°C is attributed to the dehydroxylation of montmorillonite alumino-silicate [52]. The amount of released CO_2 increases beginning around 600°C and peaking at 800°C. A reaction is

catalyzed between the carbacious residue and the oxygen in the crystal structure of dehydroxylated montmorillonite, yielding CO_2 by the metallic species within the aliminosilicate [28].

It is suggested by Hofmann elimination mechanism that alkyl ammonium ions decompose between 200 and 300°C in order to produce α-olefins and amines [8]. Lewis or Bronsted acid sites in the aluminosilicate have a catalytic effect on the initial stages of decomposition within the organically modified layered silicate. Thus, the proximity of the Lewis base sites and the basic aluminosilicate surface to the intercalated alkyl quaternary ammonium molecule can enhance the Hofmann elimination reaction. Secondary reactions of the initial products like alkyl chain scission, free radical condensation and additions to olefinic group may also occur. The presence of oxygen and metal species in the montmorillonite structure can serve as catalysts and the oxidative cleavage of alkenes may be enabled to produce aldehydes at elevated temperatures [28].

A distinct correlation could not be found between the nanocomposite mechanical properties and the amount of surfactant remaining in the organoclay. A higher level of surfactant degradation does not seem to affect nanocomposite modulus to a great extent; it implies that degradation does not impede the exfoliation process. It may even aid exfoliation to a certain degree since clay surface is made less hydrophobic and the affinity between the polyamide chains and the clay is increased. As the amount of organic modifiers covering the pristine surface of the montmorillonite decreases, the number of polyamide-surfactant interactions is also reduced and the number of polyamide-silicate interactions is increased which results in better platelet exfoliation [9]. It was also determined that increase in residence time or the level of applied shear, a greater exposure of the polymer to surfactant via exfoliation and changes in the extrusion conditions aid degradation for nylon 6-clay nanocomposites [9,60]. Production of volatiles that results from utilization of interlayer decomposition to increase interlayer pressure may be effective in increasing layer separation by gaseous expansion. It is a new paradigm for surfactant design that can enhance exfoliation in melt-processed polymer nanocomposites [28].

2.4.3.1 Impact Modification of Polyamide 66 Nanocomposites

Although the resistance of PA 66 to crack initiation is high, its crack propagation resistance is rather low resulting from the fact that it is a notch-sensitive type of material. Therefore, the impact strength is tried to be improved via blending the polymer matrix with different types of elastomers containing functional groups that can help disperse the clay particles as a result of both increased shear strength and compatibilizing effect.

An elastomeric phase is generally incorporated into the matrix to increase the number of functional groups that can interact with the organoclay surface in order to obtain balanced toughness and stiffness. Organoclay is used as a reinforcing and stiffening agent while elastomeric phase functions as a toughener and compatibilizer [61,62]. Maleic anhydride [61-70] or glycidyl methacrylate containing elastomers can generally be incorporated into polymer matrix for impact modification since the interfacial interaction between polymer, organoclay and impact modifier results in finer dispersion of elastomeric domains and increase in toughness. Lotader® AX8900 resin (E-MA-GMA), Lotader® AX8840 resin (E-GMA) and Lotader® 2210 resin (E-BA-MAH) were used in this study with Cloisite® 15A, Cloisite® 25A and Cloisite® 30B organoclays.

A good balance in the viscosity and melt elasticity ratios of the components at the processing conditions and a certain level of grafting of the dispersed phase that is essential to reduce interfacial tension, to increase the adhesion between the phases and to obtain a finer dispersion and a more stable morphology should be selected to achieve a suitable morphology. An appropriate range of rubber domain size, interdomain distance and uniform distribution of rubber domains, low modulus ratio between the rubber and polyamide bulk phase and high Poisson's ratio with low breaking stress of the dispersed phase are the prerequisites of the increase in toughness values. Viscosity, matrix molecular weight, melt elasticity of the components, shear stresses and rates, the mobility of the interface and surface tension control the final domain size, since a lower tension promotes the stretching of even smaller drops producing a very fine morphology. The coalescence rate of the elastomeric domains decreases

because of the lower tension that is indicative of the chemical reactions forming the interfacial copolymers since the domain size is reduced as a consequence of their immobilizing effect on the interface. The interfacial tension is reduced by the use of compatibilizing agents like maleic anhydride and the adhesion in polyblends is improved [63]. However, the toughening of semicrystalline polymers is considered to be a complex mechanism that includes initial elastic loading of the matrix-rubber blend, internal or external cavitation of the rubber domains, followed by craze initiation and shear bonding of the matrix [71].

The reactions that can take between between the functional groups of the impact modifiers and PA 66 are given in Figures 2.9 and 2.10. At low temperatures (<120°C) formation of the amidic linkages prevail the imidic linkages that may form at higher temperatures in the reactions of anhydride group with PA 66 amine ends. It can obviously be seen from Figure 2.10 that epoxide groups can either be attached to the amine or acid ends of PA 66.

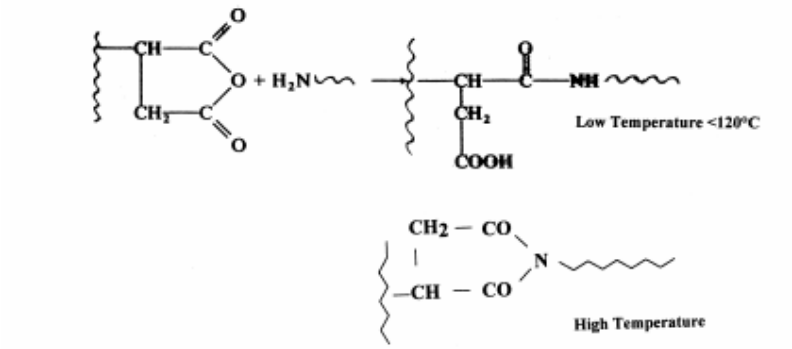

Figure 2.9 Reaction of the amine end group of polyamides with anhydride group [72].

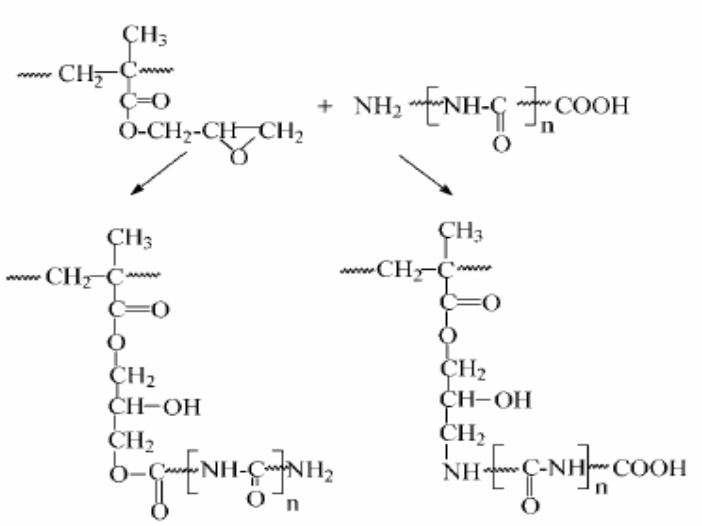

Figure 2.10 Reactions of the epoxide group with acidic and basic groups of polyamides [73].

2.5 Processing Methods

Various types of polymer processing methods like tubular blow molding, fiber spinning and calendering are applied to obtain different products. However, extrusion and injection molding are the two basic processing steps in the polymer industry.

2.5.1 Extrusion

Extrusion is the process by which the material is forced through an opening. Various materials like metals, foodstuffs, ceramics and plastics can be processed by extrusion [74]. Extruder is a versatile machine capable of performing other operations simultaneously with its pumping action. The objective is to produce a homogeneous molten material at a flow rate, pressure and temperature suitable for the next operation in the process line [75].

An extrusion system is composed of three parts: the die, downstream equipment and the extruder. One of its major functions is to compress solid plastic pellets until they melt. It mixes additives such as colorants, lubricants with the plastic

during melting of the polymer. Temperature and viscosity are fixed at a stable value by homogenizing the mixture. Finally, the molten polymer is transmitted to the die section in a viscous state. The viscous melt is reduced to a smaller and different shape including molding, rod, tubing, pipe, sheet, film and wire coating. The extruded polymer is still soft and flexible as it leaves the die. Thus, it is controlled by sizing devices, cooling devices and fixtures to shape it into its final configuration [74].

2.5.1.1 Extruder Types

The main types of extruders include screw extruders, disk extruders and ram extruders. Single screw extruders have one screw that rotates in a stationery extruder barrel. In a single screw extrusion process, pressure is built in a polymer melt so that it can be extruded through a die or injected into a mold. Disk extruders are screwless extruders that make use of some type of disk to transmit the materials. Solids conveying melting, devolatilization, melt conveying and melting are the major factors affecting the shape of the disks. Ram extruders are positive displacement devices that are capable of generating very high pressures. They are preferable in injection molding devices resulting from the ease of discontinuous operation. Polymers that have high melting points like PTFE and UHMWPE can be processed by ram extruders [76].

Twin-screw extruders may have either two co-rotating or counter-rotating screws in the barrel. The screws rotate in the same direction in co-rotating twin-screw extruders while they rotate in the opposite direction in counter-rotating twin-screw extruders. Twin-screw extruders are suitable for processing materials, which are hard to feed because of its positive displacement characteristics in the intermeshing region. Maximum positive displacement is provided by counter-rotating twin-screw extruders which makes them the primary choice for profile extrusion, whereas co-rotating twin-screw extruders are utilized for applications like compounding, mixing, devolatization and chemical reaction because of the complex flow in the intermeshing region, where good mixing and compounding characteristics are required. Good mixing, devolatization properties and good control over residence time are the advantages of twin-screw extruders [77].

The terms ‘intermeshing’ and ‘non-intermeshing’ are used to refer to the closeness of the screws. Non-intermeshing screws are positioned side by side far away from each other. However, it is not the case for fully intermeshing screws that are allowed to rotate without touching each other with a small mechanical clearance between them. The top of one of the screw nests is near the bottom of the other. The screws rotate in opposite direction in the intermeshing region of co-rotating extruders, while the rotation direction of the screws is the same in the intermesh zone in counter-rotating extruders. A self-wiping action is created in co-rotating, intermeshing extruders as the screws rotate. The material is removed from the root of the neighboring screw by the tip of the other screw. The possibility for the material to stay in one spot on the screw is minimized since degradation of the polymer may occur or degraded material may combine with the melt as a contaminant. Counter-rotating intermeshing screws do not create a self-wiping action in the intermesh zone as efficiently as co-rotating screws do. The velocity of the tip of one screw and the root of the other is not significantly different and wiping action is not observed effectively [78]. Typical twin-screw extruder designs are shown in Figure 2.11.

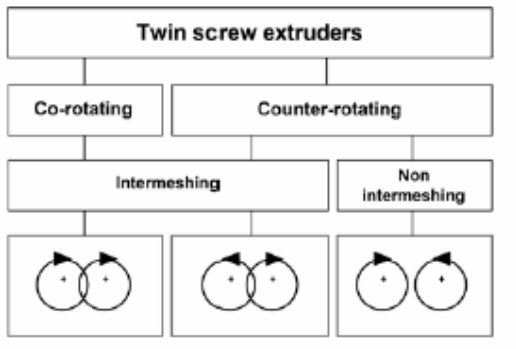

Figure 2.11 Typical twin-screw extruder designs [78].

Drag flow is the operating principle of single screw extruders. The material is transmitted to the end of the extruder by the help of the screws. The polymer is prevented from sticking on the walls of the barrel. While the rotating action of the screws helps the material be pushed down in counter-rotating, fully intermeshing

extruders, both positive displacement and drag flow is effective in co-rotating, fully intermeshing extruders. Some of the positive displacement occurs in the intermesh area as the polymer is dragged along the extruder in the rest of the barrel circumference [78]. Conveying characteristics of extruder can be seen in Figure 2.12.

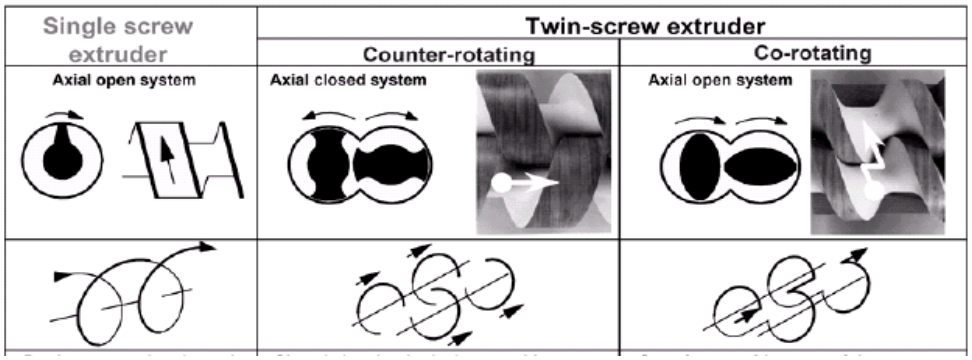

Figure 2.12 Extruder conveying characteristics [78].

2.5.2 Injection Molding

Each step of the injection molding process is carried out in a separate zone of the same apparatus and a cyclic operation is accomplished. The polymer melt from the nozzle of the injection unit flows through the sprue, runner system and gate before entering into the actual mold cavity. A plunger that is also named as ram or piston pushes pellets, which fall from the hopper into the barrel when the plunger is withdrawn into a heated zone. The molten polymer is pushed forward through the nozzle, the sprue bushing, down the runner and past the gate into a cooled cavity. Runner must be large enough to facilitate rapid filling of the cavity but it must not be too large since the time required to freeze the material in the runner can increase. The thermoplastic must be cooled under pressure below T_g and T_m before the opening of the mold followed by part ejection [11].

The molding cycle is composed of three basic steps that are filling, packing and cooling. The pressure rise is slow during the filling cycle. The shrinkage is offset by the maintenance of high pressures at the packing stage and the pressure in

the mold relaxes during the cooling stage. The pressure maintained on the cavity is very high during the cooling stage to minimize shrinkage and shape changes. The total cycle time that is controlled by the cooling stage is dependent on the thickness of the molded piece since the heat transfer through the poorly conductive polymer is the resistance to cooling [75].

The problems that can be met in injection molding are jetting, short shot and thermal degradation. Jetting occurs if the flow progression inside the cavity is not uniform. A short shot is likely to be faced with, in case of decreasing flow rates, because of insufficient process pressures. It is an incomplete part caused by premature solidification inside the cavity [11]. Significant temperature rises of the melt may arise from high viscosity and small flow as it proceeds towards the cavity. Thus, the possibility of thermal degradation is created [75].

Finished articles that range from paper clips to automobile front-end assemblies can be created by injection molding. It is one of the most important polymer flow processes because of its versatility and high industrial output [52].

2.6 Characterization of Nanocomposites

Mechanical, thermal, morphological and rheological (melt flow index) analyses were performed in this study to evaluate the characteristics of PA 66 nanocomposites.

2.6.1 Mechanical Properties

Many materials are subjected to force or loads when in service. The material has to be designed such that the resulting deformation will not be excessive and the possibility of fracture will be low. The mechanical behavior is the relationship between the material's response and deformation to an applied load or force. The load may be tensile, compressive and shear, the magnitude may be constant with time or a fluctuation may be observed continuously. Thus, nature of the applied load and the duration as well as the environmental conditions should be included within the design factors. Strength, hardness, ductility and stiffness are some of the important mechanical properties [2]. Tensile, flexural and impact

tests were carried out and hardness of the specimens was measured in this study.

2.6.1.1 Tensile Test

If a load is static or shows slight variations with time and is applied uniformly over a cross section or surface of a member, the mechanical behavior may be ascertained with a simple stress-strain test [2].

The tensile strength test (ISO 527) [79] is employed on samples of a specified shape, typically a dogbone. It measures the ability of a polymer to withstand pulling stresses. The sample is clamped at one end and pulled at a constant rate of elongation until the centre of specimen fails [48]. The stress-strain behavior of a material is dependent on how precise the test is performed and the physical state of the material such as the material is below or above its T_g [80]. The tensile test for a specimen can be seen in Figure 2.13. Tensile properties are usually measured at rates of strain of 1-100 %/min. At higher rates of strain up to 10^6 %/min - tensile strength and modulus usually increase tremendously, while elongation decreases. Large temperature rises in the specimen complicate the interpretation of these results [80].

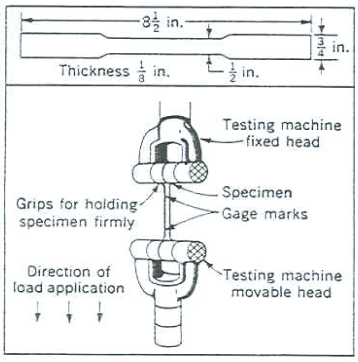

Figure 2.13 Tensile test for a specimen [80].

The length of center section is called the initial gauge length. The force F (N) is measured at the fixed end as a function of elongation. Stress σ (MPa) is plotted

as a function of strain ε (mm/mm), where A_0 (mm^2) represents the original, undeformed cross-sectional area of the gauge region , ΔL (mm) is the change in sample length as a result of the applied force and L_0 is the initial gauge length [48]. The relation between these parameters is indicated in Equations 2.1-2.2.

$$\sigma = F / A_0 \tag{2.1}$$

$$\varepsilon = \Delta L / L_0 \tag{2.2}$$

Recoverable strain or elongation is called elastic strain. Stressed molecules are capable of returning to their original relative locations after release of the applied force. The strain is non-reversible with an end result of permanent deformation, elongation of the test material. Many samples undergo both reversible and irreversible strain [80].

The elastic modulus is the ratio of the applied stress to the strain it produces within the region where the relationship between stress and strain is linear [63] and it can be described in terms of Hooke's law [48]. E is the Young's modulus (MPa), σ is the stress (MPa) and ε is the strain (mm/mm) in Equation 2.3.

$$\sigma = E\varepsilon \tag{2.3}$$

Large values for Young's Modulus indicate that the material is rigid and resistant to elongation and stretching [80].

Stress of ductile materials achieves a maximum value called "yield strength" at a specific strain. As strain increases beyond this point, stress initially decreases. The specimen may fail at the minimum stress that is called the drawing stress or it may undergo orientation hardening because of stretching of the chains in the direction of the load. Rigid polymers exhibit a rapid increase in stress with increasing strain until sample failure whereas the modulus of elastomeric materials is low but elongations to several hundred percent are possible before failure [48]. Typical behaviors of materials under stress are given in Figure 2.14.

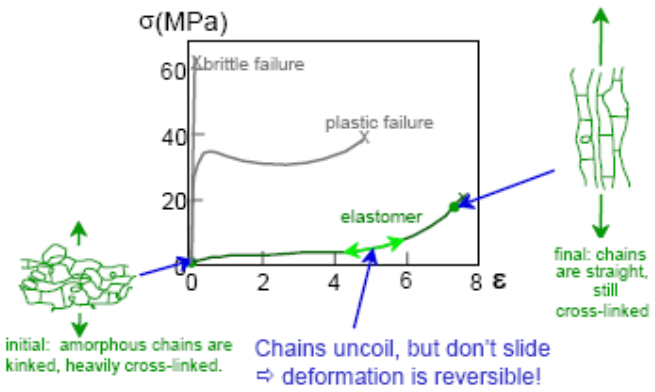

Figure 2.14 Typical behaviors of polymers under stress [81].

2.6.1.2 Impact Test

Impact strength (ISO 179) [82] is a measure of energy needed to break a sample [80]. The test conditions are specified in order to represent those most severe relative to the potential for fracture including deformation at a relatively low temperature, a high strain rate and a triaxial stress state that is introduced by the presence of a notch [2].

Impact strength tests fall within two categories. (1) Falling mass tests that are used to measure the impact strength of solids and films. (2) Pendulum tests. Two standardized tests (Charpy and Izod tests) sometimes also termed as notch toughness were designed and are still used to measure the impact energy. The specimen is positioned at the base of the equipment. A knife edge mounted on the pendulum strikes and the specimen is fractured at the notch, which acts as a point of stress concentration for this high velocity impact blow [80]. The height from which the missile must be dropped to cause failure in half of the specimens is taken as a measure of the toughness of the material [83]. The manner of specimen support is the primary difference between the Charpy and Izod techniques [1]. An unnotched or oppositely notched specimen is employed in the Charpy test [80]. Pictorial description of Charpy and Izod impact tests are given in Figure 2.15.

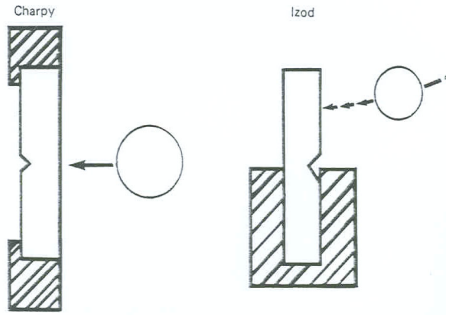

Figure 2.15 Charpy and Izod type pendulum impact tests [80].

2.6.1.3 Flexural Test

Flexural strength (ISO 178) [84] or cross breaking strength measures bending strength of a bar test specimen used as a simple beam [80].

A load is applied at a specified rate in the center of a specimen that is placed on the supports. The loading at failure is called the flexural strength using three or four point bending technique. The top of the surface is placed in a state of compression while the bottom surface is in tension at the point of loading. Stress is calculated from the specimen thickness, the bending moment and the moment of inertia of the cross section [2]. Schematic illustration of flexural strength testing is seen in Figure 2.16.

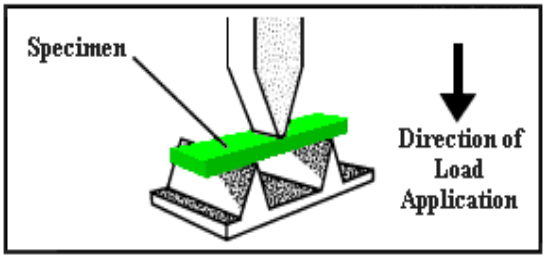

Figure 2.16 Flexural strength testing [85].

The maximum tensile stress is at the bottom of the specimen surface directly below the load application point. Some of the materials do not break at outer fiber strains up to 5 % even after being greatly deflected and the actual strength cannot be calculated [85]. The point at which the load does not increase with an increase in deflection is selected on the load-deflection curve and the flexural yield strength is calculated.

The flexural stress is calculated for any point on the load-deflection curve by Equation 2.4.

$$S = 3PL / 2bd^2 \quad (2.4)$$

S (MPa) is the stress in the outer fibers at midspan, P (N) is the load at a given point on the load deflection curve, L (mm) is the support span, b (mm) is the width of the beam tested and d (mm) is the depth of the beam tested.

The maximum strain occurs in the outer fibers as well as the stress. It is calculated by Equation 2.5.

$$r = 6Dd / L^2 \quad (2.5)$$

r (mm/mm) is the maximum strain in the outer fibers, D (mm) is the maximum deflection of the centre of the beam, L (mm) is the support span and d (mm) is the depth. Increases in both flexural strength and flexural modulus are indications of rigidity like tensile strength and Young's modulus. Flexural modulus is calculated by drawing a tangent to the steepest initial straight line portion of the load deflection curve and calculating the slope. The slope is then substituted into Equation 2.6 to compute the modulus.

$$E_B = L^3m / 4bd^3 \quad (2.6)$$

E_B (MPa) is the modulus of elasticity in bending, L (mm) is the support span, b (mm) is the width of the beam tested, d (mm) is the depth of the beam tested and

m (N/mm) is the slope of the tangent to the initial straight line portion of the load-deflection curve [84].

2.6.1.4 Microindentation Hardness

Microindentation hardness (ISO 868) [86] of a material is determined from the distance a steel ball will penetrate into the material. Scratch and abrasion resistance are the other types of hardness measurement methods especially for coatings and molded objects [11].

It is made use of a spring-loaded, ball tipped indentor in this method so as to eliminate the linear relationship between the stress and the penetration. The measurements can be basically related to compressive modulus, hence stiff materials are expected to be hard and the flexible materials are expected to be soft [11]. Several different scales can be used from possible combinations of various indentors and different loads [2]. The specimen is first placed on a hard, flat and horizontal surface during hardness measurements. The durometer is kept at a predetermined distance from any edge of the specimen and the presser foot is applied to the specimen in a vertical position. It is made sure that sufficient pressure is applied to provide good contact between the presser foot and the specimen. Recommended masses fixed above the operating stands that are utilized for imparting pressure are 1 kg for Type A, B and O durometers, 5 kg for Type C, D and O durometers and 400 g for Type OO durometers [86].

The specimen thickness is advised to be at least ten times the indentation depth while the distance between the centre of one indentation and specimen edge or the distance between the centre of one indentation to the centre of the second one is taken as at least three indentation diameters. The surface of the specimen has to be smooth. It is inevitable to face with an inaccuracy if the specimen is too thin; the indentation is too close to a specimen edge or the indentation points are positioned too closely to each other [86].

2.6.2 Thermal Analysis

Polymers are treated thermally and enthalpy changes associated with heating, annealing, crystallizing are analyzed. Responses of the system to polymerization, degradation and other chemical changes can be obtained. DSC was used for the thermal analysis of PA 66 based nanocomposites in this study.

2.6.2.1 Differential Scanning Calorimetry

DSC in Figure 2.17 is a technique of non-equilibrium calorimetry in which the heat flow into or away from the polymer compared with the heat flow into or away from a reference is measured as a function of temperature and time [48]. The difference in the energy supplied between the sample and the reference is attributed to various thermal events like the glass transition, crystallization and melting. Other processes such as evaporation and chemical reactions can also take place [11].

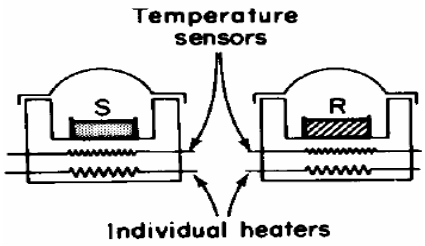

Figure 2.17 Differential scanning calorimetry [87].

The polymer sample is held in an aluminum pan with a crimped-on lid. The reference is mostly an empty reference pan. The temperature change between sample and the reference is detected by separate platinum resistance heaters, which are controlled by the signals from platinum resistance thermometers. The difference in power needed to keep both at the same temperature is amplified and provides information on thermal events [4]. The heating of both the sample and the reference material continues at a constant rate until heat is emitted or consumed by the sample. If the change in the temperature is endothermic, the temperature of the sample will be less than that of the reference. The

temperature of the sample is raised to the reference temperature since a constant temperature has to be maintained for both the reference and the sample. The current required to keep the temperatures constant is recorded and heat of transition, crystallization or melting is measured by calculating the area under the resulting curve [48].

Heat capacity increases at T_g where the temperature of the sample is reduced below its previous level relative to the reference. In contrast to the smooth dip of T_g, a sharper dip is observed at T_m since large amounts of heat are required to melt the crystals at constant temperature. These two thermal events appear on the endothermic side of DSC thermogram shown in Figure 2.18 while crystallization is on the opposite exothermic side because of the heat evolved upon formation of crystals [3].

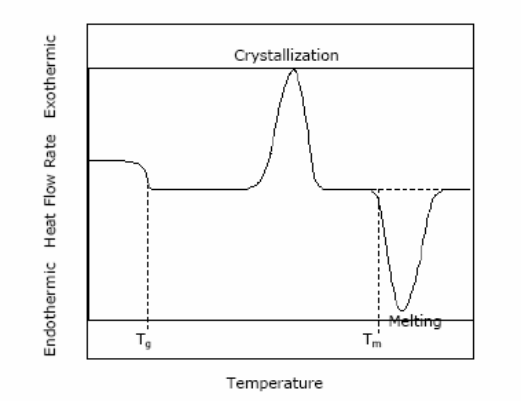

Figure 2.18 DSC thermogram [88].

The sample purity, identity, the heat of transition, the heat of reaction, the phase diagram, the specific heat, the rate of crystallization, melting or reaction and the activation energy can be determined by the help of DSC thermograms [48].

2.6.3 Morphological Analysis

Structural changes in micro and nanosize can be identified by morphological analyses. X-ray and SEM analyses were performed to observe the changes in the polymer matrix in this study.

2.6.3.1 X-Ray Diffraction

Orderly arrangement of atoms or molecules through interaction of electromagnetic radiation to get interference effects with structures comparable in size to the wavelength of the radiation are investigated by X-ray diffraction. The interferences are sharpened in an orderly array or lattice and the radiation is diffracted in a homogeneous fashion [83].

The structural periodicity in the material, the wavelength of the incident ray and diffraction angle are correlated with each other by Bragg's Law [80].

$$n\lambda = 2d\sin\theta \tag{2.7}$$

n refers to the degree of diffraction, λ (Å) is the wavelength, d (Å) is the interlayer spacing and θ (°) is the diffraction angle in Equation 2.7.

A metal target is bombarded with a beam of electrons in a vacuum tube in X-ray production. X-rays pass out through a beryllium or polyester film window in the tube in a well-defined beam. The type of the target material and the applied voltage are effective on the wavelength of the X-rays. The methods of detecting X-rays can be by means of their action on photographic films or a plate, which is convenient for accurate measurements of angles and distances or by a radiation counter and electronic equipment feeding data to a computer if the intensity measurements are required to be measured precisely [83]. Schematic perspective and dimensional relationship of X-ray diffraction of specimens can be seen in Figure 2.19.

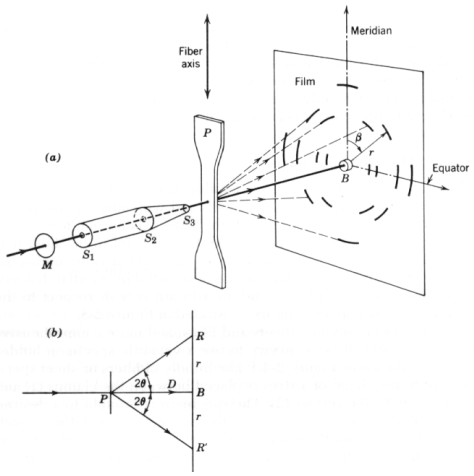

Figure 2.19 X-ray diffraction (a) schematic perspective; (b) dimensional relationship [89].

X-ray diffraction method uses are in accordance with the types of the structures that have to be examined in a specimen. These methods include SAXS and WAXS. The information obtained from scattering at low angles (SAXS) is used for investigation of fibrillar and lamellar structures and detection of cavities, whereas wide angle X-ray scattering (WAXS) detects the changes in crystallinity and orientation by which spatial arrangement of atoms is described [80].

2.6.3.2 Scanning Electron Microscopy

In scanning electron microscopy, a light conducting film is applied by evaporation across the surface of an opaque specimen from which a fine beam of electrons is scanned. Samples are coated with a conducting film as gold, platinum or silver prior to examination under the electron beam, since the surface must be electrically conductive [2]. When the beam hits the specimen, secondary electrons, back-scattered electrons and X-ray photons are emitted and they are collected to form a signal that modulates the intensity of the electron beam in a television tube scanning in synchronism with the microscope beam. The small size is maintained over small distances and images that have a great depth of field with remarkable three-dimensional appearance are obtained. Resolution is on the order of 100 Å in SEM [83].

Fracture surfaces including the final processes of deformation, crack initiation, crack propagation up to fracture, defects which initiate fracture and influence crack path can be detected by SEM. A more detailed vision of ultra-thin replicas from the fracture surfaces can be obtained by transmission electron microscopy (TEM) whose sample preparation is relatively difficult compared to SEM [4]. Etching may be required to extract one of the phases before SEM analysis and diminish the smooth surface vision so as to observe the cavitation, especially in blends.

2.6.4 Rheological Analysis

Flow characteristics of the polymer melt is directly effective on the final properties of the nanocomposites because of the shear strength to which it is subjected in the extruder, as well as the residence time and the thermal effects created due to viscous dissipation. Melt flow index measurements are correlated with the final nanostructure and mechanical properties in this study.

2.6.4.1 Melt Flow Index Test

Melt index which is a measure of flow inversely related to melt viscosity [64] is the mass flow rate of a polymer through a specified capillary under controlled conditions of temperature and pressure [11]. The weight of the extrudate or strand under a specified load at a predetermined temperature and pressure is measured to obtain the melt index values of the polymer melt [83].

Melt flow index apparatus resembles a ram extruder in which a reciprocating piston pushes the material forward through the die. The mode of their operation is discontinuous. The weight located on the capillary of the instrument can vary according to the type of the polymer and the melting temperature (ISO 1133) [90]. The polymers that are sensitive to moisture absorption have to be predried to eliminate the inaccuracies in the melt index values due to bubble formation in the polymer melt.

Melt indexes are generally in the ranges of 0.1 to 50. Although the actual test time can be between 15 s and several minutes, it is expressed as the flow that

would take place in a 10 min period. It is based on the effect of polymer molecular weight on relaxation times, the normal stress effects in extrusion and kinetic energy losses at the entrance and exit of the tubes during Poiseuille flow [11].

2.7 Previous Studies

Yu et al. [91] prepared PA 66 nanocomposites by melt compounding with an organically modified montmorillonite whose ammonium surfactant was about 14 wt% that is a much lower value than the 35-46 wt% surfactant amount in commercial organic montmorillonite powders. They observed exfoliation of the organoclay by TEM analysis and the enhanced mechanical test results. Increases in the tensile strength and Young's modulus led to decreases in ductility and fracture toughness.

Liu et al. [92] used co-intercalation of an epoxy resin and quaternary ammonium into sodium montmorillonite to produce PA 66 nanocomposites via melt compounding. It was reported that the clay was dispersed homogeneously in the polymer matrix as a result of the interaction between the epoxy groups confined in the layers and PA 66 chains. Tensile strength and heat distortion temperature increased dramatically, as well as Izod impact strength. Water absorption was reduced by 40 % upon incorporation of 10 wt% co-intercalation clay into the polymer matrix.

Shen et al. [93] investigated the mechanical properties of PA 66/organoclay nanocomposites prepared by melt compounding in a Brabender twin-screw extruder in terms of nanoindentation technique. Hardness, elastic modulus, storage modulus and creep were gradually improved with increasing clay concentration up to 5 wt%.

Gyoo et al. [94] also used epoxy-modified organoclay to observe its effects on morphology, thermal and mechanical properties of PA 66/clay nanocomposites obtained by melt compounding using a Brabender mixer. According to the evaluated results, the epoxy resin amount was determined be kept at an optimum value, since excess epoxy resin caused a strong interaction between the

hydroxyl end groups of the modifier on the silicate surface and diffusion of PA 66 into silicate layers was limited. Tensile strength, Young's modulus, storage modulus and the crystallization rate increased after introduction of the organoclay into the polymer matrix.

Dasari et al. [95] showed that the microstructure of ternary PA 66/SEBS-g-MA/ organoclay nanocomposites and their mechanical properties were tremendously affected by the mixing sequence. It was demonstrated that location of the organoclay greatly influences the impact strength. Mixing PA 66 with the organoclay first and blending with SEBS-g-MA in the next step gave the best impact strength results since most of the organoclay was found to be in the polymer matrix.

Dasari et al. [61] found out that addition of clay does not accelerate the crystallization process although SEBS-g-MA compatibilizer acts as a nucleating agent. When the organoclay was situated in SEBS-g-MA phase, cavitation ability of the elastomer was retarded despite the increases in flexural strength. Extruding the polymer matrix containing elastomer more than once also had a negative effect on the toughness of the nanocomposites. The mechanical test results were supported by TEM, SEM, X-ray and elastomeric domain size analysis.

Qin et al. [96] compared the flammability and thermal stability of PA 66/MMT microcomposite with PA 66/OMMT nanocomposite obtained by melt compounding. Addition of MMT decreased the heat release rate of PA 66 matrix. The reason of PA 66 matrix ignition that was accelerated with MMT addition was related with the catalytic decomposition effect of MMT in isothermal oxidation experiments. The silicate layers were found to have a barrier effect that retards flammability and nanocomposites were more thermally stable compared to microcomposites.

Mehrabzadeh et al. [97] prepared PA 66/clay, HDPE/clay and HDPE/PA 66/clay nanocomposites by melt mixing in a twin-screw co-rotating extruder. They revealed that compatibility of the clay modifier with the polymer matrix, mixing and kneading elements and higher residence times in twin-screw extrusion aid

intercalation or exfoliation. Clay seemed to have no effect on crystallinity apart from acting as a nucleating agent.

Yu et al. [52] showed that the clay is not exfoliated randomly in PA 66 matrix, but is oriented along the injection molding direction in the specimen. Melt compounding method was utilized. They proposed that MMT with more thermally stable surfactants has to be produced to increase the onset decomposition temperatures of alkyl ammonium pretreated MMT.

Chavarria et al. [53] compared PA 6 nanocomposites with PA 66 nanocomposites prepared by melt processing in a twin-screw extruder and stated that PA 6 nanocomposites have superior mechanical properties, lower average particle length, thickness and aspect ratio that is indicative of a better exfoliated structure in comparison with PA 66 nanocomposites.

Vlasveld et al. [20] made a comparison between the temperature dependence of modulus, yield stress and ductility of nanocomposites based on high and low molecular weight PA 6 and PA 66 produced via melt blending. It was reported that high processing temperatures do not seem to encounter a problem for PA 66 nanocomposite production for which modulus and yield stress were found to be slightly higher. Molecular weight of the polymer was concluded to be chosen according to the required mechanical properties and processing conditions.

Liu et al. [98] found using in-situ X-ray diffraction that the crystalline phase transition temperature is lower for PA 66 nanocomposites prepared by melt compounding in a co-rotating twin-screw extruder and it was attributed to γ crystalline phase induced by the silicate layers. Crystal structure of PA 66 matrix was changed upon addition of silicate layers and its phase transition behavior was affected.

Zhang et al. [99] and Kang et al. [50] investigated the effect of organoclay on the crystallinity of PA 66 nanocomposites produced by melt blending and declared that size of the sphereulites decreases upon addition of the organoclay since clay has a nucleation effect on the polymer matrix.

Tanaka et al. [59] predicted the binding energy for PA 66/clay nanocomposites by molecular modeling and showed that the binding energy between a clay platelet and PA 66 decreases as the volume of the adsorbed quaternary ammonium salt increases. It was vice versa for the binding energy of PA 66 and quaternary ammonium salt. Presence of polar groups like -OH and -COOH on ammonium ions seemed to increase the binding energies with PA 66.

Hedicke et al. [100] compared the crystallization behavior of PA 6 and PA 66 nanocomposites. Compounding was carried out in a twin-screw extruder. Organoclay was not fully dispersed in PA 66 matrix whose crystal structure change was not affected by the presence of the organoclay in contrast to PA 6 nanocomposites in which the organoclay exhibited fully exfoliated behavior.

Lu et al. [51] studied the influence of thermal processing on the perfection of crystals in PA 66 and PA 66 nanocomposites which were melt mixed and extruded in a co-rotating twin-screw extruder. Nanoclay seemed to have two overwhelming effects on PA 66 crystallization. One of them was the nucleation effect that increases the crystallization rate and the second one was the constrained motion of the chains hindering refinement of crystal structures.

Karayannididis et al. [71] investigated rubber toughening of glass fiber reinforced PA 66 with functionalized block copolymer SEBS-g-MA. Blending was performed in a single screw extruder. Incorporation of SEBS-g-MA in PA 66 matrix increased the resistance to crack propagation and hence toughness. Toughening was influenced by the size of cavitation and the extent of reaction.

Nair et al. [101] reported that toughening in silicate clay composites processed by melt blending can be improved by better dispersion of clay and a stronger clay/matrix interface at low clay loadings. In both nanoscale and multiscale nanocomposites, clay reinforcements were found to have an important role in the overall fracture behavior by influencing inelastic deformation in the crack tip region.

Gonzáles et al. [67] modified PA 66 nanocomposites with PA 6 by melt mixing to obtain exfoliated nanocomposites. PA 6 had a mediating role in dispersing the clay platelets. High yield stress and elastic modulus results were associated with exfoliation of the organoclay. Ductility decreased as the amount of the organoclay content increased.

Tomova et al. [102] indicated that end group configuration is important for the interfacial adhesion and morphology formation in binary polyamide/elastomer blends and in ternary PA 6/PA 66/maleated elastomer blends obtained by melt mixing in a Brabender single screw extruder. The domain size of elastomeric phase was found to be 1 μm for PA 6, whereas it was 4-7 μm for PA 66. It was attributed to difunctionality of PA 66 that enables it to react twice per chain with the maleated elastomer.

CHAPTER 3

EXPERIMENTAL

3.1 Materials

3.1.1 Polymer Matrix

Polyamide 66 was purchased from Polyone Company, Istanbul-Turkey and it was supplied in the form of pellets in 25 kg polyethylene bags. The trade name of the product is Bergamid A65. Properties of Bergamid A65 are given in Table 3.1.

Table 3.1 Properties of PA 66 matrix (Bergamid A65) [103].

Properties	Standards	Unit	Test Conditions	Values	
Physical				**d.a.m***	**Cond.****
Water Absorption	ISO 62	%	23°C	8.5	-
Density	ISO 1183	g/cm^3	23°C	1.13	-
Moisture Absorption	ISO 62	%	23°C, 50 % relative humidity	2.8	-
Mechanical				**d.a.m***	**Cond.****
Tensile Strength	ISO 527-1/2	MPa	23°C, 50 mm/min	80	60
Tensile Strain at Yield	ISO 527-1/2	%	23°C, 50 mm/min	4.5	25
Tensile Strain at Break	ISO 527-1/2	%	23°C, 50 mm/min	22	> 50
Tensile Modulus	ISO 527-1/2	MPa	23°C, 1 mm/min	3200	1600
Flexural Strength	ISO 178	MPa	23°C	140	70
Charpy Notched Impact Strength	ISO 179/1eA	kJ/m^2	23°C	6	25
			-30°C	4	-
Izod Notched Impact Strength	ISO 180/1A	kJ/m^2	23°C	6	-
			-30°C	6	-

Table 3.1 Properties of PA 66 matrix (Bergamid A65) [103]. (Cont'd)

Properties	Standards	Unit	Test Conditions	Values	
Thermal				**d.a.m***	**Cond.****
Melting Temperature	ISO 3146	°C	10 K/min	261	-
Heat Deflection Temperature	ISO 75-1/2	°C	0.45 MPa	220	-
			1.8 MPa	80	-
Coefficient of Linear Expansion	DIN 53752	E-4/K	normal	0.85	-
			perpendicular	0.82	-
Electrical				**d.a.m***	**Cond.****
Surface Resistivity	IEC 93	Ohm	-	10^{13}	10^{10}
Volume Resistivity	IEC 93	Ohm.cm	-	10^{15}	10^{12}
Dielectric Strength	IEC 243-1	kV/mm	-	120	80
Flammability				**d.a.m***	**Cond.****
	UL 94	-	0.8 mm	V-2	-
		-	1.6 mm	V-2	-

***d.a.m** : Dry as moulded ** **Cond.** : Conditioned according to ISO 1110

PA 66 specimens were immediately stored in polyethylene bags and kept in desiccator for 24 hours prior to testing in this study, since PA 66 is very sensitive to moisture uptake that profoundly influences the properties of the material and is one of the major drawbacks of its use.

3.1.2 Organoclays

Three types of organoclays named as Cloisite® 15A, Cloisite® 25A and Cloisite® 30B treated with different organic modifiers were purchased from Southern Clay Products, Texas-USA. They are natural off-white montmorillonites modified with quaternary ammonium salts and used as additives for improving various physical properties like reinforcement, heat distortion temperature and barrier effects.

3.1.2.1 Cloisite® 15A

Organic modifier of Cloisite® 15A contains dimethyl, dihydrogenated tallow, quaternary ammonium cation with chloride anion where hydrogenated tallow is predominantly composed of chains with 18 carbons (~65 %), to a lesser degree chains with 16 carbons (~30 %) and 14 carbons (~5 %). Chemical structure of the organic modifier and physical properties of Cloisite® 15A are given in Figure 3.1 and Table 3.2, respectively.

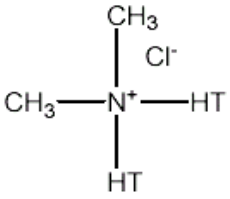

Figure 3.1 Chemical structure of the organic modifier of Cloisite® 15A.

Table 3.2 Properties of Cloisite® 15A [104].

Properties	Unit	Values
Modifier Concentration	meq/100g clay	125
Moisture	%	< 2
Weight Loss on Ignition	%	43
d-spacing	Å	31.5
Dry Particle Sizes		
10 %	μ, by volume	< 2
50 %	μ, by volume	< 6
90 %	μ, by volume	< 13
Density		
Loose Bulk	lbs/ft^3	10.79
Packed Bulk	lbs/ft^3	18.64
Specific Gravity	g/cc	1.66

3.1.2.2 Cloisite® 25A

Dimethyl, hydrogenated tallow, 2-ethylhexyl quaternary ammonium cation with methyl sulfate anion constitutes the chemical structure of the organic modifier of Cloisite® 25A where hydrogenated tallow contains mostly chains with 18 carbons (~65 %), to a lesser degree chains with 16 carbons (~30 %) and 14 carbons (~5 %). Chemical structure of the organic modifier and physical properties of Cloisite® 25A are given in Figure 3.2 and Table 3.3, respectively.

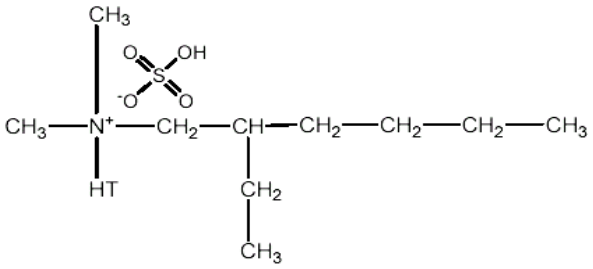

Figure 3.2 Chemical structure of the organic modifier of Cloisite® 25A.

Table 3.3 Properties of Cloisite® 25A [104].

Properties	Unit	Values
Modifier Concentration	meq/100g clay	95
Moisture	%	< 2
Weight Loss on Ignition	%	34
d-spacing	Å	18.6
Dry Particle Sizes		
10 %	μ, by volume	< 2
50 %	μ, by volume	< 6
90 %	μ, by volume	< 13
Density		
Loose Bulk	lbs/ft^3	12.08
Packed Bulk	lbs/ft^3	20.48
Specific Gravity	g/cc	1.87

3.1.2.3 Cloisite® 30B

Quaternary ammonium salt cation and anion of the organic modifier of Cloisite® 30B are methyl, tallow, bis-2-hydroxyethyl quaternary ammonium and chloride, respectively. Almost 65 % of the carbon chains have 18 carbons, 30 % has 16 carbons and 5 % has 14 carbons in the tallow structure like the other organoclays. Chemical structure of the organic modifier can be seen in Figure 3.3 and the physical properties of Cloisite® 30B are given in Table 3.4.

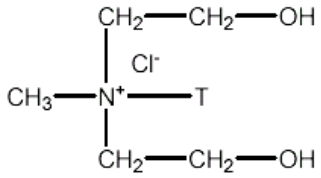

Figure 3.3 Chemical structure of the organic modifier of Cloisite® 30B.

Table 3.4 Properties of Cloisite® 30B [104].

Properties	Unit	Values
Modifier Concentration	meq/100g clay	90
Moisture	%	< 2
Weight Loss on Ignition	%	30
d-spacing	Å	18.5
Dry Particle Sizes		
10 %	μ, by volume	< 2
50 %	μ, by volume	< 6
90 %	μ, by volume	< 13
Density		
Loose Bulk	lbs/ft^3	14.25
Packed Bulk	lbs/ft^3	22.71
Specific Gravity	g/cc	1.98

3.1.3 Impact modifiers

Three impact modifiers including Lotader® AX8840 resin (a random copolymer of ethylene (E) and glycidyl methacrylate (GMA)), Lotader® AX8900 resin (a random terpolymer of ethylene (E), methyl acrylate (MA) and glycidyl methacrylate (GMA)) and Lotader® 2210 resin (a random terpolymer of (E), butyl acrylate (BA) and maleic anhydride (MAH)) were purchased from Arkema Inc., France. They were supplied in pellet form in 25 kg waterproof bags. All of them have high flexibility and reactivity with certain groups. The elastomers containing GMA groups are capable of reacting with acid; amine and hydroxyl groups and the one containing MAH group can react with the amine ends [105]. Chemical structures of Lotader® AX8840, Lotader® AX8900 and Lotader® 2210 are given in Figures 3.4, 3.5 and 3.6, respectively. Product specifications can be seen in Table 3.5.

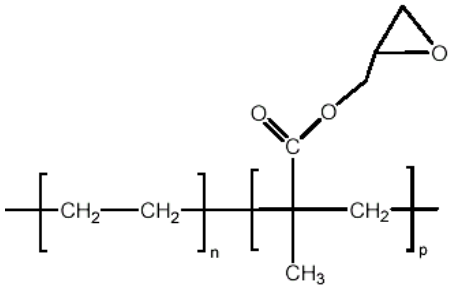

Figure 3.4 Chemical structure of Lotader® AX8840.

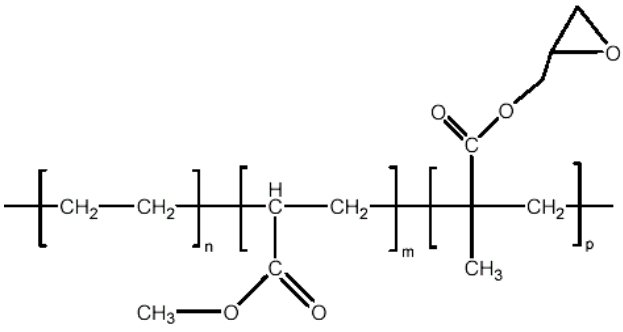

Figure 3.5 Chemical structure of Lotader® AX8900.

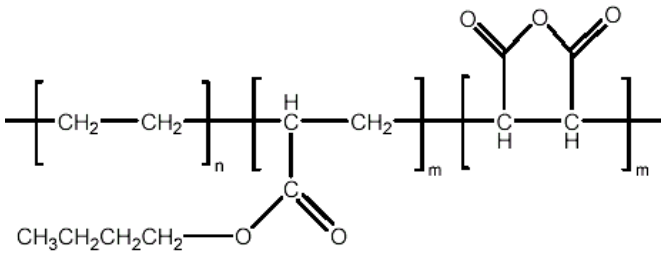

Figure 3.6 Chemical structure of Lotader® 2210.

Table 3.5 Properties of impact modifiers [105].

Impact Modifier Type			Lotader® AX8840	Lotader® AX8900	Lotader® 2210
Polymer Name			E-GMA	E-MA-GMA	E-BA-MAH
Properties	Unit	Test Method	Values		
Ester Content	%	FTIR	0	25	6
GMA Content	%	FTIR	8	8	0
MAH Content	%	FTIR	0	0	2.6
Melt Index	g/10 min	ISO 1133	5	6	3
Vicat Point	°C	ISO 306	87	< 40	80
Melting Point	°C	DSC	105	60	107
Tensile Strength	MPa	ISO 527	8	4	12
Young's Modulus	MPa	ISO 527	104	8	-
Elongation at Break	%	ISO 527	420	1100	600
Density	g/cm^3	ISO 1183	0.94	0.95	-
Hardness	Shore D	ISO 868	92	64	46

3.2 Experimental Procedure

3.2.1 Melt Compounding

The experiments were carried out in air atmosphere by Thermoprism TSE 16 TC, fully intermeshing, co-rotating twin-screw extruder with an L/D ratio of 24. The picture of the extruder by which the experiments were performed is given in Figure 3.7. Length of the extruder barrel and diameter of the screws are 384 and 16 mm, respectively. Maximum torque and screw speed that can be achieved during compounding are 12 Nm and 500 rpm, respectively.

The barrel temperatures were set to 260-275-275-275-280°C from hopper to die and the screw speed was fixed at 200 rpm for a feed rate of 25 g/min. Pure PA 66, PA 66 blends, binary and ternary PA 66 nanocomposites were extruded twice to increase the effect of shear intensity on the organoclay dispersion. After the first extrusion step, the extrudate was cooled in a cooling bath and pelletized in a grinder. The pellets of PA 66 containing compounds obtained at the end of the process were stored in polyethylene bags and were all dried at 100°C under vacuum for 24 hours before the next extrusion step or injection molding. Only impact modifier / clay combination was dried at 40°C for 12 hours prior to processing, because of the low melting temperature of the elastomers. Drying was performed in vacuo for 12 hours at 80°C for the organoclays and at 40°C for the elastomers, since elimination of physiabsorbed water is required before processing to obtain materials with improved properties. Drying step was repeated before each processing step.

Figure 3.7 Thermoprism TSE 16 TC twin-screw extruder.

3.2.2 Injection Molding

The specimens were simultaneously injection molded during the second extrusion step by DSM Xplore laboratory scale micro injection molding equipment shown in Figure 3.8. The barrel temperature was adjusted to 275°C and the mold temperature was set to 60°C.

Pressure profile of the molding cycle is one of the critical parameters affecting the alignment of the polymer chains, crystallinity and filling of the mold cavities to prevent short shots. Filling step of the molding cycle was 5 seconds at 10 bar and it was increased to 15 bar during the packing cycle to offset shrinkage. The pressure was relaxed during the cooling cycle. Molding cycle of the specimen took 25 seconds and the duration of having a specimen injection molded in continuous processing where injection molding was performed soon after the extrusion was only 60 seconds. A representation of continuous processing applied for the production of PA 66 nanocomposites and the equipments used in this study are shown in Figures 3.9-3.11.

Figure 3.8 DSM Xplore injection molding machine.

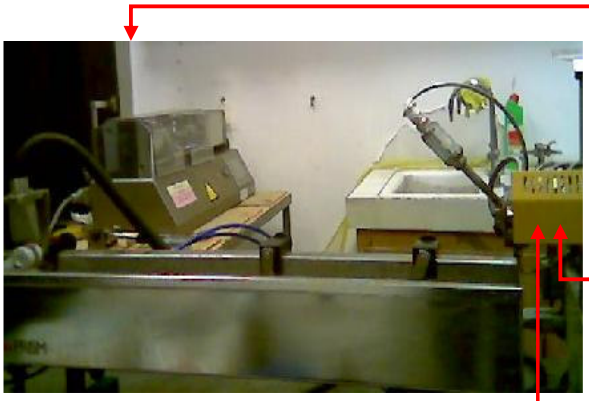

Figure 3.9 Extrusion and injection molding.

Figure 3.11 Polymer grinder.

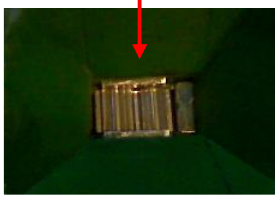

Figure 3.10 Top view of the blades of polymer grinder.

High melt flow index of PA 66 makes the use of a grinder in Figures 3.10-3.11 inevitable because of the insufficient drawing speed of the pelletizer of the laboratory scale extruder. Therefore, a polymer grinder that functions as a pelletizer and cuts the cooled polymer into 2-3 mm pellets, was designed and manufactured. After the grinding cycle, the extrusion process was repeated once more in combination with the injection molding of the specimens. Flowchart of the processing route and testing methods of the specimens are given below in Figure 3.12.

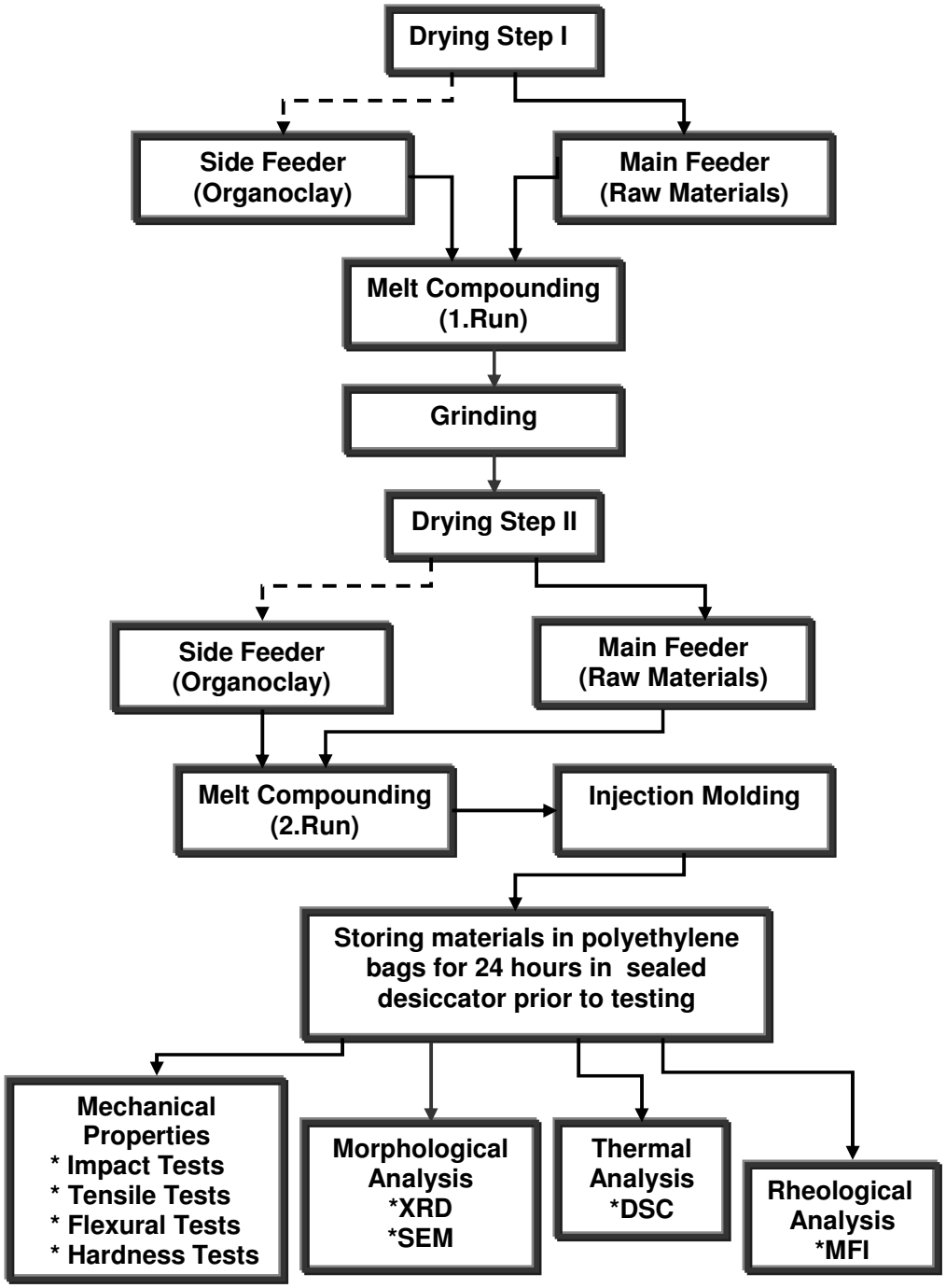

Figure 3.12 Flowchart of the processing route.

The second feeder was not utilized in both of the melt compounding steps. It was only used in one of the melt compounding steps when the organoclays were mixed with the polymer matrix, elastomers or blends during preparation of binary or ternary nanocomposites in different mixing sequences.

3.2.3 Mixing sequences of PA 66 Nanocomposites

When the mixing sequences of the nanocomposites with the same composition are varied, different microstructure and mechanical properties are exhibited. The aim is to obtain the best organoclay dispersion coupled with improved mechanical properties. Positive effect of the impact modifier type on the mechanical properties and the organoclay dispersion were also taken into account while deciding on the mixing sequences of ternary nanocomposites.

The screw speed was always kept constant at 200 rpm although the feed rate of the feeders was varied according to the composition and type of the components that were processed at a total feed rate of 25 g/min. All the components were dried under vacuum before each extrusion step, at temperatures given in section 3.2.1.

3.2.3.1 Mixing sequence (All-S)-(All simultaneous feeding)

1. Run: PA 66 and elastomer were fed to the extruder barrel from the first feeder and mixed with the organoclay coming from the second feeder. Blending of all the components was accomplished in the first step and they were all fed to the extruder barrel simultaneously. The feed rate of polymer / impact modifier blend was adjusted to 24.5 g/min while the organoclay feed rate was kept constant at 0.5 g/min so that its weight concentration could be 2 %.

2. Run: Only the main feeder was utilized in the second run for the extrusion, after melt mixing of all the components in the first step. The total feed rate was 25 g/min.

3.2.3.2 Mixing sequence (PC-I)-(Polymer / Clay - Impact modifier)

1. Run: PA 66 was reinforced with the organoclay at the first step. Therefore, both the main feeder and the side feeder were utilized. 0.5 g/min of the feed rate belonged to the organoclay, whereas the polymer matrix constituted most of the feed rate that was equal to 24.5 g/min.

2. Run: PA 66 / organoclay combination was blended with the elastomers in the second run. They were all fed to the extruder from the main feeder. The total feed rate was set to 25 g/min.

3.2.3.3 Mixing sequence (PI-C)-(Polymer / Impact modifier - Clay)

1. Run: PA 66 was blended with the elastomers first and they were both added to the extruder from the main feeder at a feed rate of 25 g/min.

2. Run: PA 66 / impact modifier blend was mixed with the organoclay in the second run. The feed rate of the components in the main feeder was set to 24.5 g/min, in order to have a feed rate of 0.5 g/min for the organoclay.

3.2.3.4 Mixing sequence (CI-P)-(Clay / Impact modifier - Polymer)

1. Run: The organoclay was blended at a rate of 0.5 g/min with the elastomer that was added to the extruder from the main feeder at a feed rate of 24.5 g/min.

2. Run: Organoclay / impact modifier compound and PA 66 were all fed to the extruder from the main feeder. The feed rate of the main feeder bearing all the components was adjusted to 25 g/min.

Only the main feeder was used in the extrusion of PA 66 blends (PI - Polymer / Impact modifier) containing 5, 10 and 15 wt% elastomer and pure PA 66 matrix. The total feed rate was maintained at 25 g/min for all the compositions. They were all extruded twice.

PA 66 was also mixed with the organoclay in the first step to produce binary ınanocomposites (PC - Polymer / Clay) and the materials were fed to the extruder from the main feeder at a feed rate of 25 g/min in all the extrusion steps as in the other mixing sequences. Compositions of all the experiments are given in Table 3.6.

Table 3.6 Compositions of the experiments.

Experiment Number	Components	Compounding Abbreviation	Concentration (wt%)		
			PA 66	Clay	Impact Modifier
1	PA 66	P	100	-	-
PA 66 – Impact Modifier Blends					
2	PA 66-2210	PI	95	-	5
3	PA 66-2210	PI	90	-	10
4	PA 66-2210	PI	85	-	15
5	PA 66-8840	PI	95	-	5
6	PA 66-8840	PI	90	-	10
7	PA 66-8840	PI	85	-	15
8	PA 66-8900	PI	95	-	5
9	PA 66-8900	PI	90	-	10
10	PA 66-8900	PI	85	-	15
PA 66 Binary Nanocomposites					
11	PA 66-15A	PC	98	2	-
12	PA 66-25A	PC	98	2	-
13	PA 66-30B	PC	98	2	-
PA 66 Ternary Nanocomposites					
14	(PA 66-15A-2210)	All-S	93	2	5
15	(PA 66-15A-8840)	All-S	93	2	5
16	(PA 66-15A-8900)	All-S	93	2	5
17	(PA 66-25A-2210)	All-S	93	2	5
18	(PA 66-25A-8840)	All-S	93	2	5
19	(PA 66-25A-8900)	All-S	93	2	5
20	(PA 66-30B-2210)	All-S	93	2	5
21	(PA 66-30B-8840)	All-S	93	2	5
22	(PA 66-30B-8900)	All-S	93	2	5
Mixing sequences of PA 66 Ternary Nanocomposites					
23	(15A / 2210)-PA 66	CI-P	93	2	5
24	(PA 66 / 15A)-2210	PC-I	93	2	5
24	(PA 66 / 2210)-15A	PI-C	93	2	5
26	(15A / 8840)-PA 66	CI-P	93	2	5
27	(PA 66 / 15A)-8840	PC-I	93	2	5
28	(PA 66 / 8840)-15A	PI-C	93	2	5

Table 3.6 Compositions of the experiments. (Cont'd)

Experiment Number	Components	Compounding Abbreviation	Concentration (wt%)		
			PA 66	Clay	Impact Modifier
Mixing sequences of PA 66 Ternary Nanocomposites					
29	(15A / 8900)-PA 66	CI-P	93	2	5
30	(PA 66 / 15A)-8900	PC-I	93	2	5
31	(PA 66 / 8900)-15A	PI-C	93	2	5
32	(25A / 8840)-PA 66	CI-P	93	2	5
33	(PA 66 / 25A)-8840	PC-I	93	2	5
34	(PA 66 / 8840)-25A	PI-C	93	2	5
35	(25A / 8900)-PA 66	CI-P	93	2	5
36	(PA 66 / 25A)-8900	PC-I	93	2	5
37	(PA 66 / 8900)-25A	PI-C	93	2	5

3.2.4 Morphological Analysis

XRD and SEM analyses were conducted to determine the morphological properties in this study. Increases in the basal spacings of the organoclays were calculated by the help of XRD patterns and a good vision of the dispersion of elastomeric phase in the polymer matrix was observed by SEM. However, TEM analyses are required for observing the materials at higher magnifications to decide on the degree of the organoclay dispersion in the polymer matrix.

3.2.4.1 X-Ray Diffraction Analysis

X-ray diffraction patterns were recorded by a RIGAKU D/MAX 2200/PC X-ray diffractometer at 40 kV and 40 mA, using a monochromatic Cu Kα radiation source (λ=1.5418). Each sample was scanned from 2θ =1 to 8° at a scan rate of 1° / min. The step size was 0.01°. Peak positions (d_{001} reflection) in XRD patterns were used to derive the basal spacings of the organoclays according to Bragg's equation.

3.2.4.2 Scanning Electron Microscopy Analysis

Phase structure was observed and the morphology of the impact-fractured surfaces of the specimens was examined to study the failure mechanisms by SEM (JEOL JSM-6400) after gold coating of the specimen surfaces. Samples were etched with boiling xylene for 6 hours to extract the elastomeric phases. SEM photographs of the impact-fractured surfaces were taken at x250 and x3500 magnifications.

3.2.5 Thermal Analysis

DSC that is one of the most common methods was conducted in this study for determination of the melting temperature and crystallinity, since changes in the properties of nanocomposites are also thought to be related with crystallinity.

3.2.5.1 Differential Scanning Calorimetry Analysis

DSC measurements were carried out under nitrogen atmosphere by using General V4.1.C DuPont 2000. Indium was used as a calibration standard. Samples of about 10 mg were cut from dry tensile bars and were placed in the DSC cells. They were heated from 25 to 280°C at a heating rate of 5°C/min. Percent crystallinity was calculated using the heat of fusion of the specimen and the heat of fusion of 100 % crystalline PA 66 that was taken as 206 J/g from the literature [91].

3.2.6 Mechanical Properties

Mechanical analyses utilized in this study include tensile, flexural, impact and hardness tests. The results obtained from tensile, flexural and hardness tests are useful in determining stiffness of the materials while impact test is an informative method for measuring toughness. The improvements in the mechanical properties are expected to be a direct reflection of the degree of dispersion of the organoclays and compatibility of the elastomeric materials with the polymer matrix.

3.2.6.1 Tensile Tests

Tensile tests were conducted using Lloyd LR 5K Universal Testing Machine at a strain rate 0.1 mm^{-1} at 23 ± 2°C according to ISO 527 [79]. Tensile strength (σ), Young's modulus and percent elongation at break (ε_b) were determined from the stress-strain curves. These properties were evaluated on five specimens. Tensile test specimen and its dimensions are given in Figure 3.13 and Table 3.7, respectively.

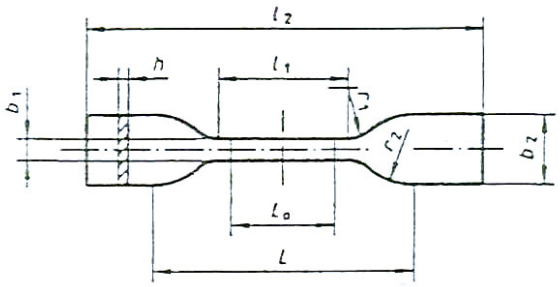

Figure 3.13 Tensile test specimen [79].

Table 3.7 Properties of the test specimen [79].

Type of the Test Specimen	ISO 527-2 / 5A
l_2 - Length of overall (mm)	75
b_2 - Width of overall (mm)	12.5
l_1 - Length of the narrow section (mm)	25
b_1 - Width of the narrow section (mm)	4
L - Distance between the grips (mm)	50
L_0 - Gauge length (mm)	20
h- Thickness (mm)	2
r_1 - Radius of fillet (mm)	8
r_2 - Outer radius (mm)	12.5

3.2.6.2 Flexural Tests

Three point bending tests were carried out according to ISO 178 [84] by Lloyd LR 5K Universal Testing Machine. The support span of 80x10x4 mm specimen was 60 mm in all the tests. The crosshead speed was calculated as 15 mm/min according to 0.1 min^{-1} strain rate. All the tests were conducted at ambient temperature and the average of five repeated tests was reported for each composition.

3.2.6.3 Impact Tests

Charpy impact strength of one sided notched specimens with the dimensions of 80x10x4 mm was measured by pendulum Ceast Resil Impactor according to ISO 179 [82]. All the tests were performed at room temperature and the results are the averages of five tests carried out for all the compositions.

3.2.6.4 Hardness Tests

Hardness measurements were accomplished by making use of a 5 kg mass positioned on top of a durameter stand and D type durameter of Bowers Metrology according to ISO 868 [86]. Five hardness measurements were taken from each specimen at ambient temperature.

3.2.7 Rheological Analysis

It has been demonstrated that melt compounding of nanocomposites is directly interrelated with molecular weight of the polymer, viscosity of the polymer melt, type of the extruder, screw design and chemical treatment of the clay. Shear intensity increases as a result of increased viscosity. Therefore, the changes in the morphology of all the compositions may also be attributed to the variations in MFI results.

3.2.7.1 Melt Flow Index Tests

Melt flow index tests were carried out according to ISO 1133 [90] by Omega Melt Flow Indexer shown in Figure 3.14. Five measurements were taken from all the compositions at 275°C under a load of 0.325 kg. The amount of polymer melt flowing through the capillary of the instrument in 10 minutes was reported as the melt index.

Figure 3.14 Omega melt flow index equipment.

CHAPTER 4

RESULTS AND DISCUSSION

4.1 Morphological Analysis

4.1.1 X-Ray Diffraction Analysis

X-ray diffraction is one of the most common and simplest methods for the morphological analysis of nanocomposites. The results obtained from X-ray patterns can be supported with TEM analysis since X-ray beams may hit a non-uniformly dispersed region in a sample due to low concentration of the organoclay or immiscibility and disorder in the sample may lead to elimination of a Bragg's reflection [106].

The changes in the interlayer spacings of the organoclays are calculated using Bragg's law in order to determine the extent of exfoliation or intercalation in the nanocomposites. A shift in the clay peak is associated with the formation of an intercalated structure, while disappearance of d_{001} peak is indicative of an exfoliated structure in nanocomposites [107]. Reduction in the intensity of the peak results from the decrease in the amount of intercalated clay; it suggests breakdown of platelet agglomerates or partial exfoliation. As the viscosity or other shear elements like screw configuration and screw speed increase, the shear intensity and dispersive forces become more effective. Consequently, the clay platelets are uniformly dispersed in the polymer matrix rather than be agglomerated as tactoids [108]. d-spacings of binary nanocomposites having 2 wt% organoclay and ternary nanocomposites having 2 wt% organoclay and 5 wt% impact modifier are given in Table 4.1. XRD patterns of each combination are shown in Appendix B, separately.

Table 4.1 XRD results.

Components	Peak I		Peak II	
	d-spacing (Å)	2θ (°)	d-spacing (Å)	2θ (°)
PA 66	-	-	-	-
Organoclays				
Cloisite ®15A	32.0	2.76	12.8	6.90
Cloisite ®25A	18.0	4.90	-	-
Cloisite ® 30B	18.0	4.92	-	-
PA 66 Binary Nanocomposites				
PA 66-15A	46.3	1.91	18.8	4.71
PA 66-25A	63.1	1.40	18.6	4.74
PA 66-30B	18.6	4.75	-	-
PA 66 Ternary Nanocomposites				
(PA 66-15A-2210) - (All-S)	44.8	1.97	18.6	4.74
(PA 66-15A-8840) - (All-S)	44.2	2.00	19.3	4.57
(PA 66-15A-8900) - (All-S)	33.2	2.66	21.7	4.08
(PA 66-25A-2210) - (All-S)	18.7	4.72	-	-
(PA 66-25A-8840) - (All-S)	52.9	1.67	18.7	4.73
(PA 66-25A-8900) - (All-S)	44.4	1.99	19.0	4.64
(PA 66-30B-2210) - (All-S)	44.4	1.99	18.8	4.70
(PA 66-30B-8840) - (All-S)	40.5	2.18	18.6	4.74
(PA 66-30B-8900) - (All-S)	45.8	1.93	18.7	4.72
Mixing sequences of PA 66 Ternary Nanocomposites				
(15A / 2210)-PA 66 - (CI-P)	59.3	1.49	18.0	4.92
(PA 66 / 15A)-2210 - (PC-I)	-	-	18.6	4.75
(PA 66 / 2210)-15A - (PI-C)	31.6	2.80	17.2	5.14
(15A / 8840)-PA 66 - (CI-P)	33.3	2.65	-	-
(PA 66 / 15A)-8840 - (PC-I)	-	-	18.9	4.68
(PA 66 / 8840)-15A - (PI-C)	31.7	2.79	16.0	5.51
(15A / 8900)-PA 66 - (CI-P)	34.8	2.54	19.8	4.46
(PA 66 / 15A)-8900 - (PC-I)	46.0	1.92	19.2	4.61
(PA 66 / 8900)-15A - (PI-C)	31.0	2.85	18.3	4.83
(25A / 8840)-PA 66 - (CI-P)	-	-	-	-
(PA 66 / 25A)-8840 - (PC-I)	53.2	1.66	18.8	4.70
(PA 66 / 8840)-25A - (PI-C)	43.7	2.02	18.6	4.74
(25A / 8900)-PA 66 - (CI-P)	39.1	2.26	-	-
(PA 66 / 25A)-8900 - (PC-I)	18.7	4.72	-	-
(PA 66 / 8900)-25A - (PI-C)	18.8	4.71	-	-

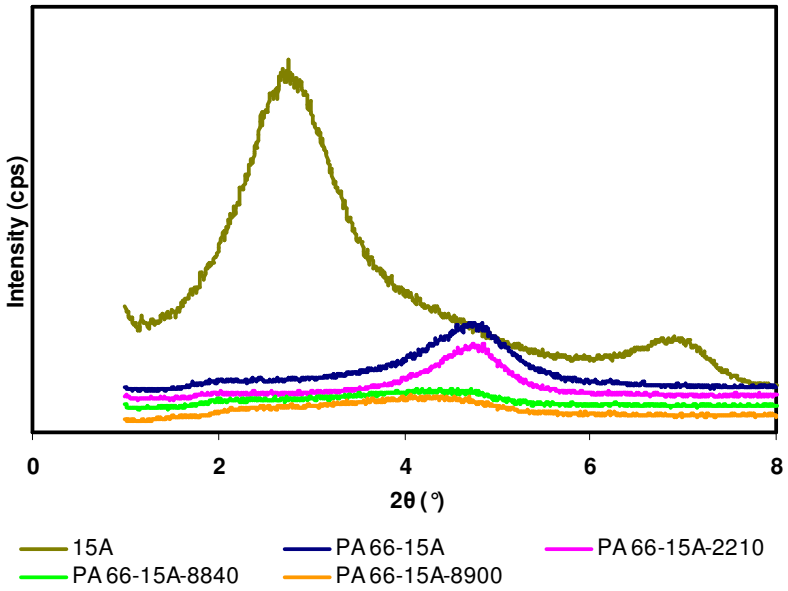

Figure 4.1 XRD patterns of PA 66-Cloisite® 15A-Impact modifier - (All-S) ternary nanocomposites.

XRD patterns of Cloisite® 15A and (PA 66-Cloisite® 15A-Impact modifier) - (All-S) nanocomposites are shown in Figure 4.1. Delamination of the organoclay was determined from the first basal reflection of montmorillonite (d_{001} peak) in Cloisite® 15A. The second peak can result from a second silicate layer if 2θ is about double the value of the first characteristic peak of the clay or it may be due to a reflection from a portion of the clay where the inorganic cations of the smectite clay were not fully replaced by the organic ions if 2θ is about 2θ for unmodified clay [67, 97, 109, 110]. The basal spacings of all the organoclays are consistent with the ones provided by Southern Clay Products that are 31.5, 18.6 and 18.5 Å for Cloisite® 15A, Cloisite® 25A and Cloisite® 30B, respectively.

Dispersive forces are more effective in delamination of Cloisite® 15A because of the absence of functional groups in its organic modifier that can form hydrogen bonds with either the matrix or the impact modifiers despite its relatively high initial d-spacing compared to the other organoclays. A tremendous decrease is observed in X-ray diffraction intensity of both the first and second peak that is an indication of transformation of large silicate agglomerates into small tactoids as a

result of increased viscosity and shear intensity. Extrusion of the polymer matrix twice helped overcome the cohesive forces between the clay layers by the hydrodynamic separation forces of the polymer matrix and provided easier diffusion of polymer chains into the organoclay gallery. Decrease in intensity can be associated with the decrease in the number of layers of individual clay particles [111]. Enlarged gallery height and decreased intensity of the characteristic peaks show that Cloisite® 15A was nearly delaminated in PA 66 matrix in All-S mixing sequences. XRD patterns of all CI-P and PC-I mixing sequences shown in Figures 4.2-4.4 indicate partially intercalated/exfoliated structures considering the presence of the first peak in CI-P mixing sequence and the second peak in both of CI-P and PC-I mixing sequences except (15A / 8840)-PA 66 - (CI-P) and (PA 66 / 15A)-8900 - (PC-I) mixing sequences at very low intensities and enlarged d-spacing.

GMA groups are capable of reacting with both the acid and amine ends present in the chemical structure of PA 66 [73]. Functional groups of the impact modifiers may increase compatibility or lead to crosslinking because of the existence of some fraction of chains having two amine or acid end groups [69]. However, it is more likely here that GMA group containing impact modifiers (Lotader® AX8840 and Lotader® AX8900) aided dispersion of the organoclay by their interaction with the polymer matrix like impact modifiers (Lotader® 2210) containing MAH group which can only react with the amine ends of PA 66 [72]. Ester groups of acrylates in Lotader® 2210 and Lotader® AX8900 can also contribute to the reactions at the interface by reacting with the terminal amino groups of PA 66 matrix [112].

The first characteristic peak almost completely disappeared in PC-I and CI-P mixing sequences of Cloisite 15A. Both of the peaks are obviously visible in PI-C mixing sequences in spite of quiet low intensities which indicate that the organoclay was well dispersed in the polymer matrix. It is expected to obtain better organoclay dispersion in CI-P and PI-C mixing sequences because of higher matrix viscosity. Since the clay undergoes a single extrusion step, the shear intensity was not capable of dispersing the clay platelets in PI-C mixing sequences.

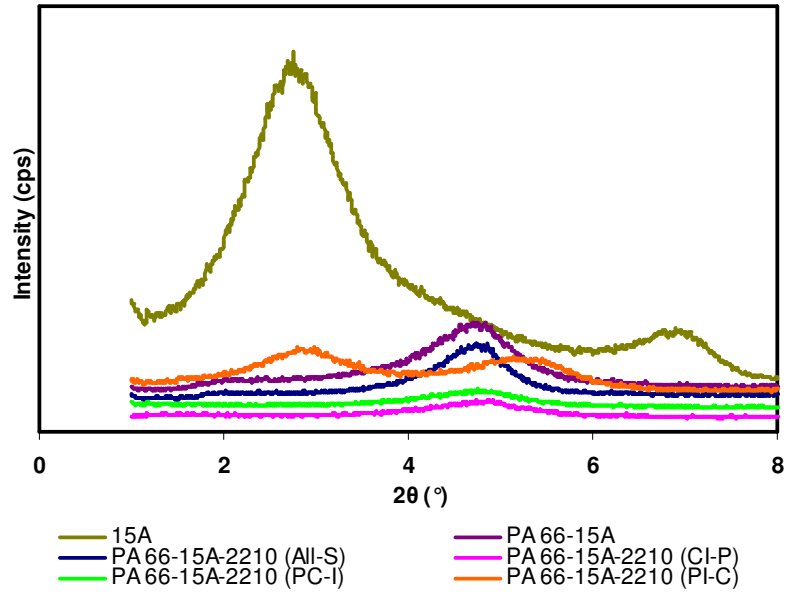

Figure 4.2 XRD patterns of PA 66-Cloisite® 15A-Lotader® 2210 mixing sequences.

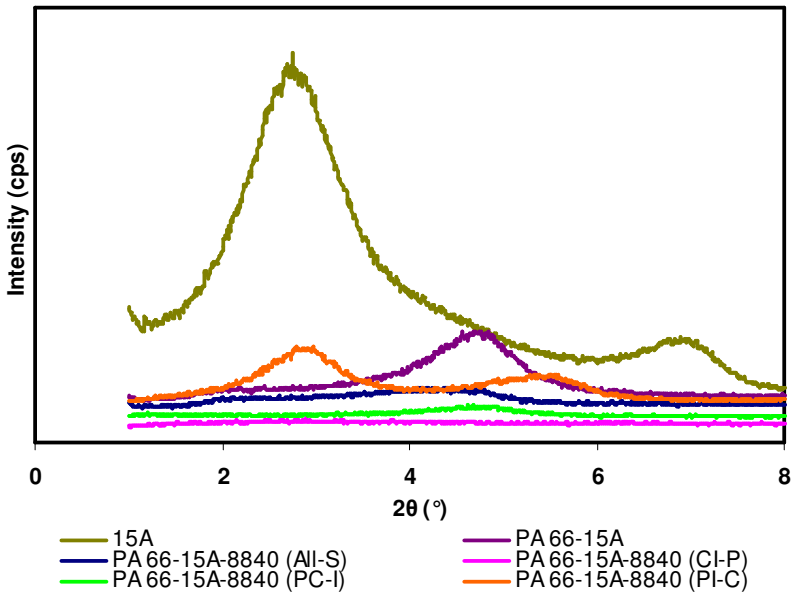

Figure 4.3 XRD patterns of PA 66-Cloisite® 15A-Lotader® AX8840 mixing sequences.

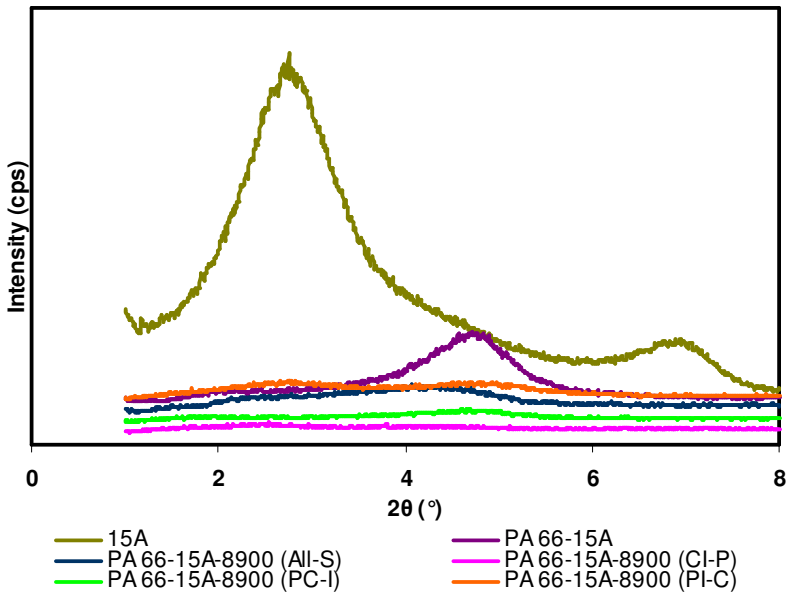

Figure 4.4 XRD patterns of PA 66-Cloisite® 15A-Lotader® AX8900 mixing sequences.

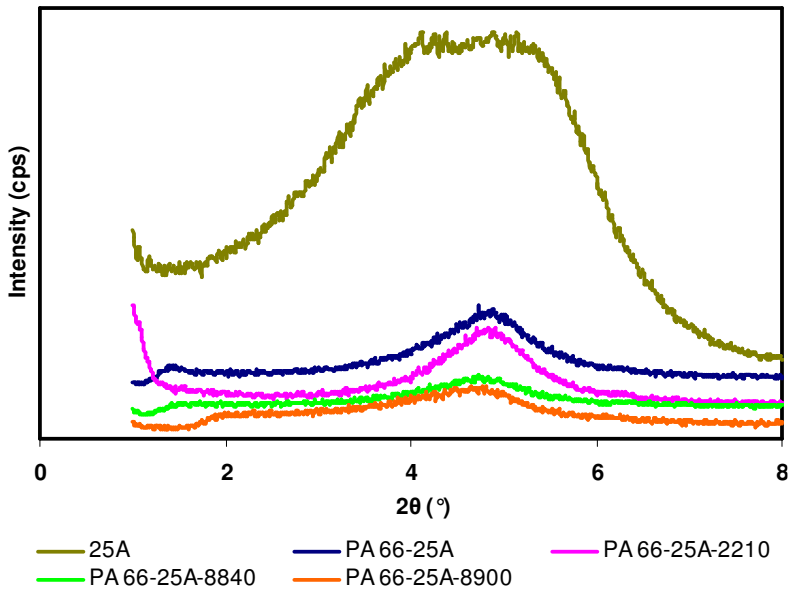

Figure 4.5 XRD patterns of PA 66-Cloisite® 25A-Impact modifier - (All-S) ternary nanocomposites.

Cloisite® 25A exhibited the best dispersion with Lotader® AX8840 and Lotader® AX 8900 as it can be seen in Figure 4.5. Therefore, the mixing sequences were varied for the ternary nanocomposites containing these impact modifiers considering both the organoclay dispersion and the mechanical properties. XRD patterns of the mixing sequences of PA 66-Cloisite® 25A-Lotader® AX8840 and PA 66-Cloisite® 25A-Lotader® AX8900 are given in Figures 4.6-4.7. Delamination of the organoclay occurred in the polymer matrix in (25A / 8840)-PA 66 - (CI-P) mixing sequence. The gallery height of the main peak also increased for the nanocomposite that has Lotader® AX8900 as impact modifier in CI-P mixing sequence and most of the organoclay was intercalated in the polymer matrix. Only a small portion of the organoclay was intercalated in (PA 66 / 8840)-25A - (PI-C) mixing sequence. However, the substantial reduction in the intensity of the peaks in all XRD patterns cannot be ignored since a good dispersion was obtained and the silicate aggregates were broken down into smaller tactoids. Although the main peak is visible in both of PC-I sequences, there is also a shoulder indicating the presence of an intercalated region in (PA 66 / 25A)-8840 - (PC-I) mixing sequence. In spite of the low intensities of PI-C mixing sequences resulting from high viscosity that helps dispersing the clay platelets, the increase in d-spacings of PI-C mixing sequences were found to be lower or similar with PC-I mixing sequences.

It has been demonstrated that the main peak of the organoclay might be visible in XRD patterns although a diffraction peak that is shifted to lower 2θ values can also be observed [52]. The presence of the second peak in XRD patterns of Cloisite® 25A containing nanocomposites can be related with the unintercalated organoclay or d_{002} of the interlayer distance of d_{001} [107]. The intensities of the intercalated regions are smaller than the intensity of the main peak in some of the mixing sequences of Cloisite® 25A nanocomposites. It corroborates that one or more polymer chains could succeed in getting inserted within the silicate galleries without achieving complete separation. Most of the organoclay is intercalated or in the form of tactoids in these types of nanocomposites but there are also a few exfoliated structures [63].

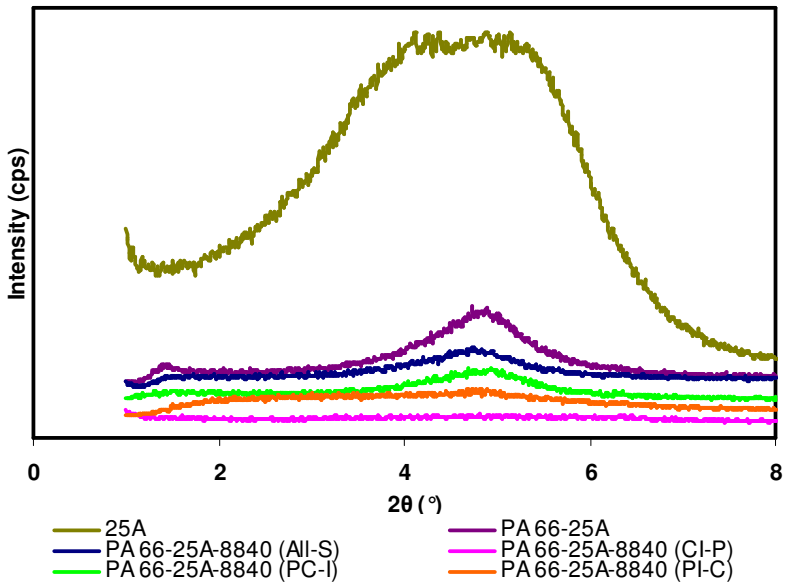

Figure 4.6 XRD patterns of PA 66-Cloisite® 25A-Lotader® AX8840 mixing sequences.

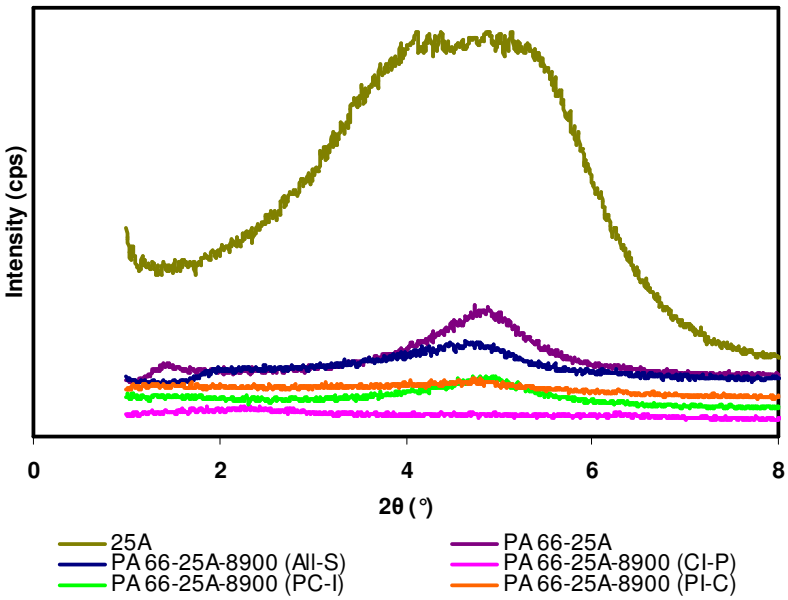

Figure 4.7 XRD patterns of PA 66-Cloisite® 25A-Lotader® AX8900 mixing sequences.

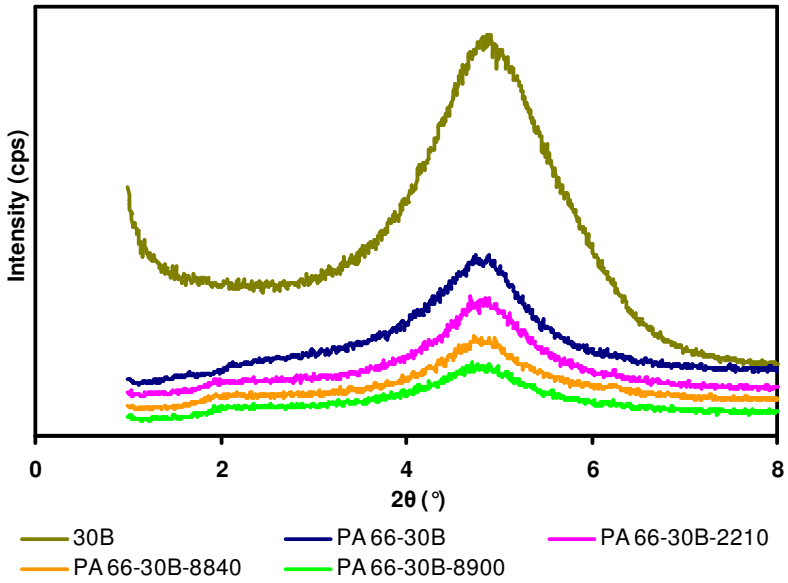

Figure 4.8 XRD patterns of PA 66-Cloisite® 30B-Impact modifier - (All-S) ternary nanocomposites.

Figure 4.8 shows XRD patterns of (PA 66-Cloisite® 30B-Impact modifier) - (All-S) nanocomposites. The organoclay is intercalated or in the form of tactoids in the polymer matrix. It is expected to obtain better organoclay dispersion for Cloisite® 30B because of the polar hydroxyl groups of the organic modifier that can form hydrogen bonds with either the matrix or the impact modifier functional groups. Cloisite® 30B was dispersed better in the presence of Lotader® AX8840 and Lotader® AX8900.

It was stated that substitution of polar groups on ammonium ions tends to increase the binding energies with nylon. The level of exfoliation is largely affected by the amount of platelet-platelet separation, platelet-modifier and modifier-polymer interactions, stability of the organic modifier and packing density. If a larger percentage of the silicate surface is covered by alkyl ammonium ions, polar polyamide and polar clay interactions are hindered leading to less delamination. Hence, organic modification is solely required to overcome the cohesive forces between the neighboring platelets at the initial step. Hydroxyethyl groups occupy more space than methyl groups and the

organoclays whose modifiers contain hydroxyethyl groups result in a denser molecular packing compared to the others without these units [57]. This may be due to the hydrogen bonding between the hydroxyl groups and the oxygen of the clay surface and between the hydroxyl groups of the surfactant. It is revealed that the packing is disordered in nature and the organic modifier adopts a high proportion of trans and gauche conformations between the clay platelets [113].

High packing density, the interactions within the clay modifier and the interactions between the clay and the modifier may have restricted penetration of the polymer chains between the clay platelets eliminating dispersion of Cloisite® 30B in the polymer matrix. Although the probability of reactions that can take place between the polymer, the organic modifier and the impact modifier is really high in PA 66 nanocomposites, it is emphasized that the interactions between the clay and the polymer are more favorable than the interactions between the modifier and the polymer since the binding forces at the interface of the clay and the polymer matrix are more effective in the separation of clay platelets [56].

Penetration of the polymer chains into the clay layers might also have been impeded by the hydrogenated tallows of Cloisite® 15A surrounding the surface of the clay since the nonpolar interactions between the surfactant and the polymer are undesirable. Nevertheless, extrusion of the polymer matrix twice and increasing the viscosity by adding elastomeric phase to the matrix increased the shear intensity and thereby facilitated the diffusion of the polymer chains into the van der Waals gallery of the clay. Additionally, d-spacing of Cloisite® 15A was already higher than the others in the beginning. Yet, it is proven that the interaction between the clay and the polymers are more favorable than larger initial d-spacing values of the organoclay [56, 57].

d-spacings of Cloisite® 30B nanocomposites increase upon addition of the impact modifier. That can be ascribed to the presence of polar groups in the organoclay surfactant to interact with the impact modifier. On the other hand, the decreases in the intensity of the peaks can be attributed to viscosity changes as the polymer matrix was mixed with the elastomeric material in all the ternary nanocomposites.

Regarding the results, it can be concluded that organoclay delamination is affected by the structural and thermal properties of the organic modifier, shear intensity and the interactions between clay layers, polymer matrix, impact modifier and organic modifier. Organic modifier polarity is highly effective in forming interactions with the polymer chains at the first step. However, packing density of the organic modifier resulting from the interactions of the polar groups within its own structure and with the clay must allow passage of the polymer chains to interact with the clay surface for further separation of the clay layers and the shear intensity has to be sufficient to yield higher dispersive forces for homogeneous dispersion of the organoclay.

4.1.2 Scanning Electron Microscopy Analysis

SEM analyses were conducted to examine the morphological structure of PA 66 blends, binary and ternary PA 66 nanocomposites at x250 and x3500 magnifications. The specimens were etched in boiling xylene to dissolve the elastomeric phase before SEM analysis was carried out. Sizes of 100-250 domains were analyzed by Image J program and they are given in Table 4.2. The number of analyzed domains had to be kept at small values for especially All-S mixing sequences since the amount of domains and the surface roughness did not enable use of large areas. Calculation of the average domain size was carried out by using the area (A_i) obtained by the program for a number of the domains (n_i) in Equations 4.1 and 4.2.

$$\bar{A} = \sum n_i A_i / \sum n_i \tag{4.1}$$

$$\bar{d} = \sqrt{\frac{\bar{A} \times 4}{\pi}} \tag{4.2}$$

Table 4.2 Average domain sizes.

Components	PA 66 Concentration (wt%)	$\bar{d}$ (nm)
PA 66 – Impact Modifier Blends		
PA 66-2210	95	81.3
PA 66-2210	90	148.4
PA 66-2210	85	309.1
PA 66-8840	95	93.6
PA 66-8840	90	123.1
PA 66-8840	85	292.8
PA 66-8900	95	181.6
PA 66-8900	90	200.2
PA 66-8900	85	228.5
PA 66 Ternary Nanocomposites		
(PA 66-15A-2210) - (All-S)	93	52.4
(PA 66-15A-8840) - (All-S)	93	55.1
(PA 66-15A-8900) - (All-S)	93	63.7
(PA 66-25A-2210) - (All-S)	93	92.5
(PA 66-25A-8840) - (All-S)	93	97.1
(PA 66-25A-8900) - (All-S)	93	83.0
(PA 66-30B-2210) - (All-S)	93	80.6
(PA 66-30B-8840) - (All-S)	93	-
(PA 66-30B-8900) - (All-S)	93	58.2
Mixing sequences of PA 66 Ternary Nanocomposites		
(15A-2210) / PA 66 - (CI-P)	93	91.6
(PA 66-15A) / 2210 - (PC-I)	93	97.8
(PA 66-2210) / 15A - (PI-C)	93	103.5
(15A-8840) / PA 66 - (CI-P)	93	202.7
(PA 66-15A) / 8840 - (PC-I)	93	119.8
(PA 66-8840) / 15A - (PI-C)	93	129.5
(15A-8900) / PA 66 - (CI-P)	93	155.5
(PA 66-15A) / 8900 - (PC-I)	93	205.2
(PA 66-8900) / 15A - (PI-C)	93	116.9
(25A-8840) / PA 66 - (CI-P)	93	161.4
(PA 66-25A) / 8840 - (PC-I)	93	191.8
(PA 66-8840) / 25A - (PI-C)	93	124.6
(25A-8900) / PA 66 - (CI-P)	93	148.3
(PA 66-25A) / 8900 - (PC-I)	93	134.0
(PA 66-8900) / 25A - (PI-C)	93	156.3

It is shown in Figures 4.9-4.12 that relatively smooth structure of the material is transformed into a porous structure because of the cavitation effect caused by the compatibilizers. The compatibilizers also function as impact modifiers and compensate for the decrease in toughness upon incorporation of the organoclay into the polymer matrix in nanocomposites.

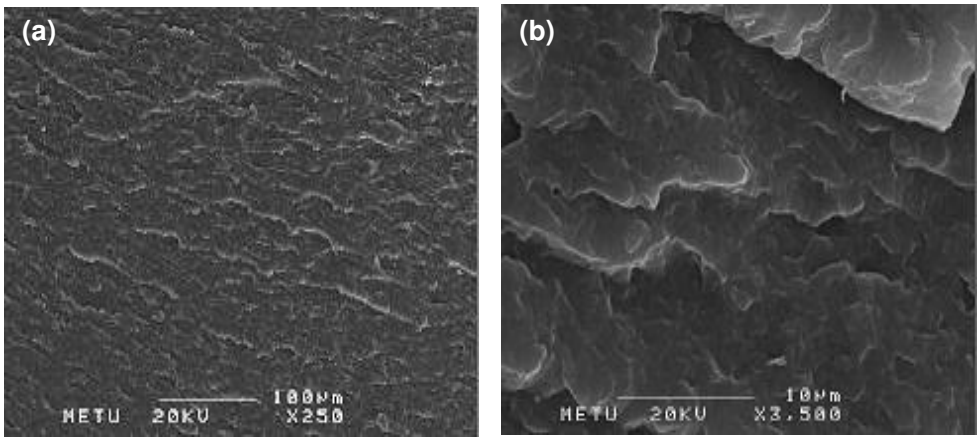

Figure 4.9 SEM micrographs of PA 66: (a) (x250); (b) (x3500).

The presence of GMA and MAH functional groups on the impact modifiers are expected to increase the interaction between the polymer matrix, the organoclay and the elastomeric phase. If no adhesion occurs between the phases, stress transfer cannot be achieved at the interface resulting in early failure of the material as soon as the strain where the physical union formed during blending is overcome. Once a chemical reaction is formed at the interface, the surface tension is lowered and the interface is immobilized. Thus, the coalescence rate of the domains is reduced since a lower tension promotes a very fine morphology with smaller drops [63].

Crack propagation is stopped by the bonding at the interface by which good adhesion, an optimum domain size, a specific interparticulate distance and uniform distribution of the elastomeric domains are accomplished. The modulus ratio between the elastomer and the polymer matrix has to be low and there has

to be a good balance between the melt viscosity and melt elasticity ratios of the components. Shear stresses and rates are also significant in the homogeneous dispersion of the elastomeric domains [63]. The presence of elastomer in the matrix results in an increase in the viscosity and the shear stress. Therefore, the elastomer content and the shear rate have to be determined accordingly. As the screw speed is fixed at a specified value, the shear intensity may not be enough for uniform dispersion of the elastomeric domains as their content is increased. Yet, extrusion of the polymer twice helped break up of the elastomeric domains and reduction in domain sizes. SEM micrographs of PA 66 blends are presented in Figures 4.10-4.12. The domain sizes of the blends increased with the increase in the elastomer content. The probability of coalescence increases as the weight average of the elastomeric phase present in the matrix becomes higher. The shear intensity may not also be enough for distributing the impact modifiers homogeneously at high concentrations since it is evident from SEM micrographs that a few large domains deviate from the common domain sizes.

Organoclay also plays an important role in the dispersion of the elastomeric domains. When the organoclay is well dispersed in the polymer matrix, the clay platelets suppress the agglomeration of the elastomeric domains [62]. Thus, the domains of All-S mixing sequences were found to be smaller compared to the blends that contain the same amount of impact modifier except the slight difference in Cloisite® 25A - (All-S) nanocomposites of PA 66 compounded with Lotader® 2210 and Lotader® AX8840 and the blends of the same impact modifiers at 5 wt% concentration. This difference can arise from the interaction between the impact modifier and the organoclay which can inhibit the dispersion of the domains and the decrease in their sizes [61].

The toughness values of the blends given in section 4.2.2 are not negatively affected from the increase in the domain sizes of the elastomers. The toughness difference is higher for Lotader® AX8840 blends although the toughness of the other blends does not differ much from each other at different concentrations especially for the ones containing Lotader® AX8900 like the slight changes in its domain sizes.

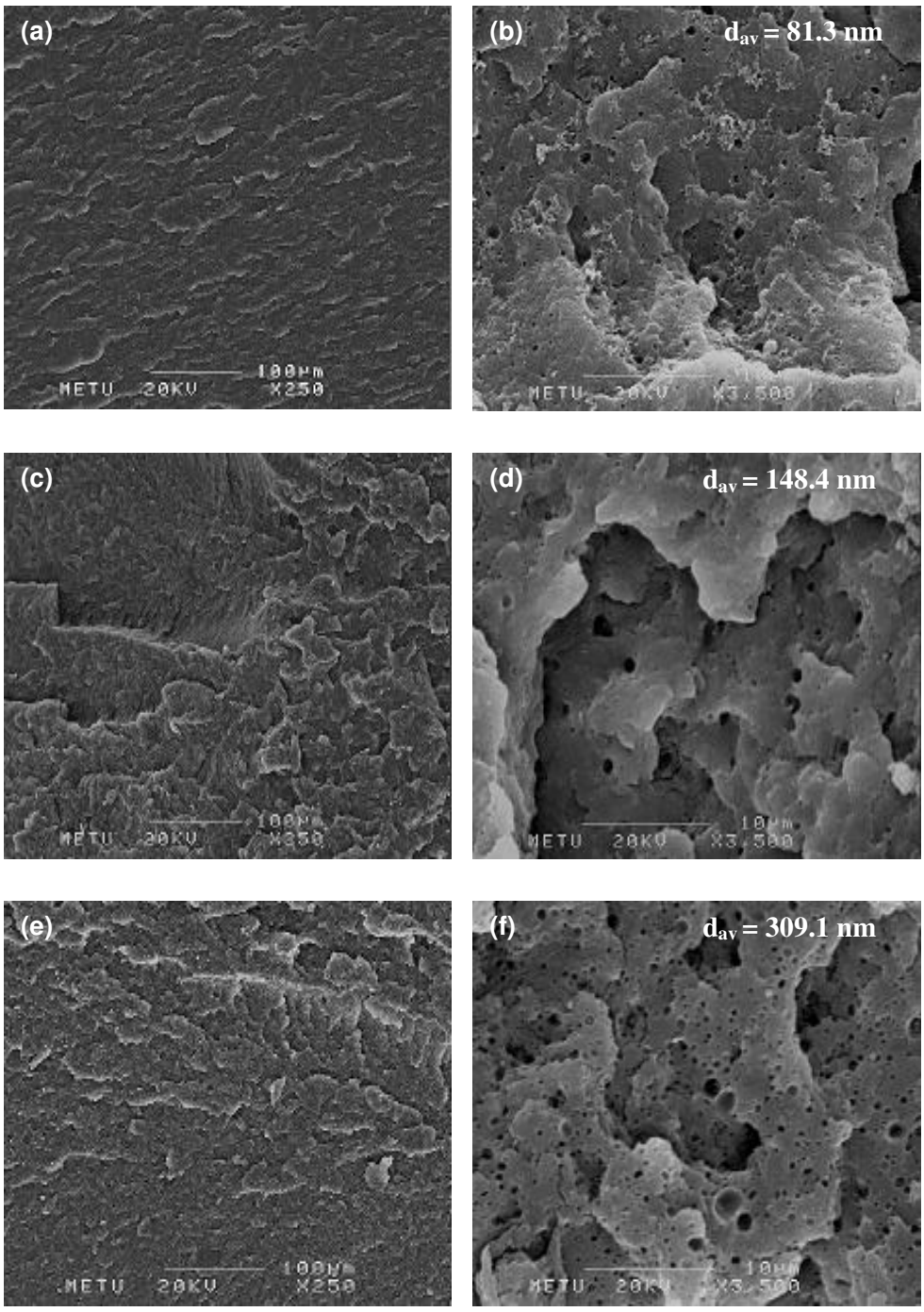

Figure 4.10 SEM micrographs of PA 66-Lotader® 2210 blends: (a) 5 wt% (x250); (b) 5 wt% (x3500); (c) 10 wt% (x250); (d) 10 wt% (x3500); (e) 15 wt% (x250); (f) 15 wt% (x3500).

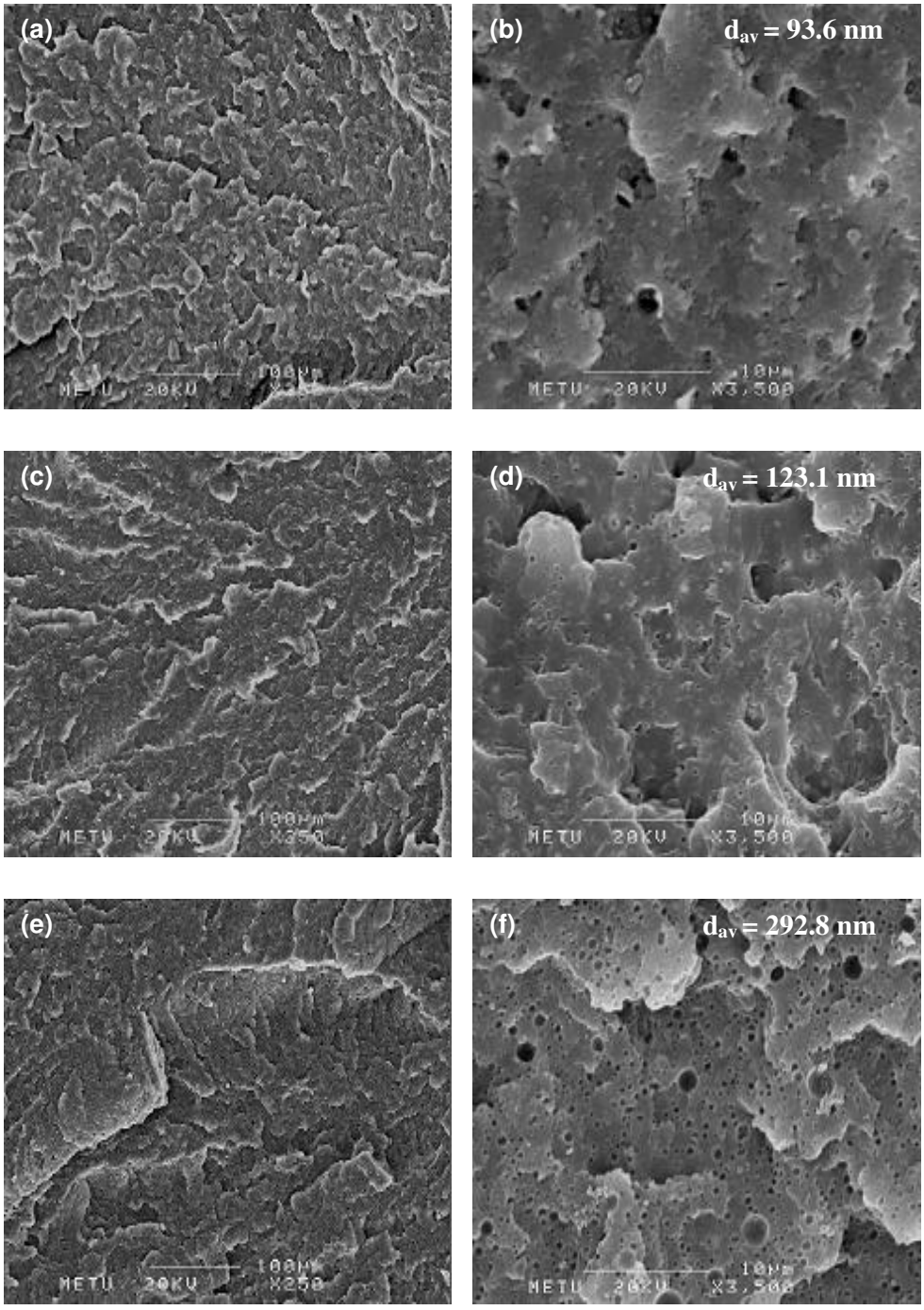

Figure 4.11 SEM micrographs of PA 66-Lotader® AX8840 blends: (a) 5 wt% (x250); (b) 5 wt% (x3500); (c) 10 wt% (x250); (d) 10 wt% (x3500); (e) 15 wt% (x250); (f) 15 wt% (x3500).

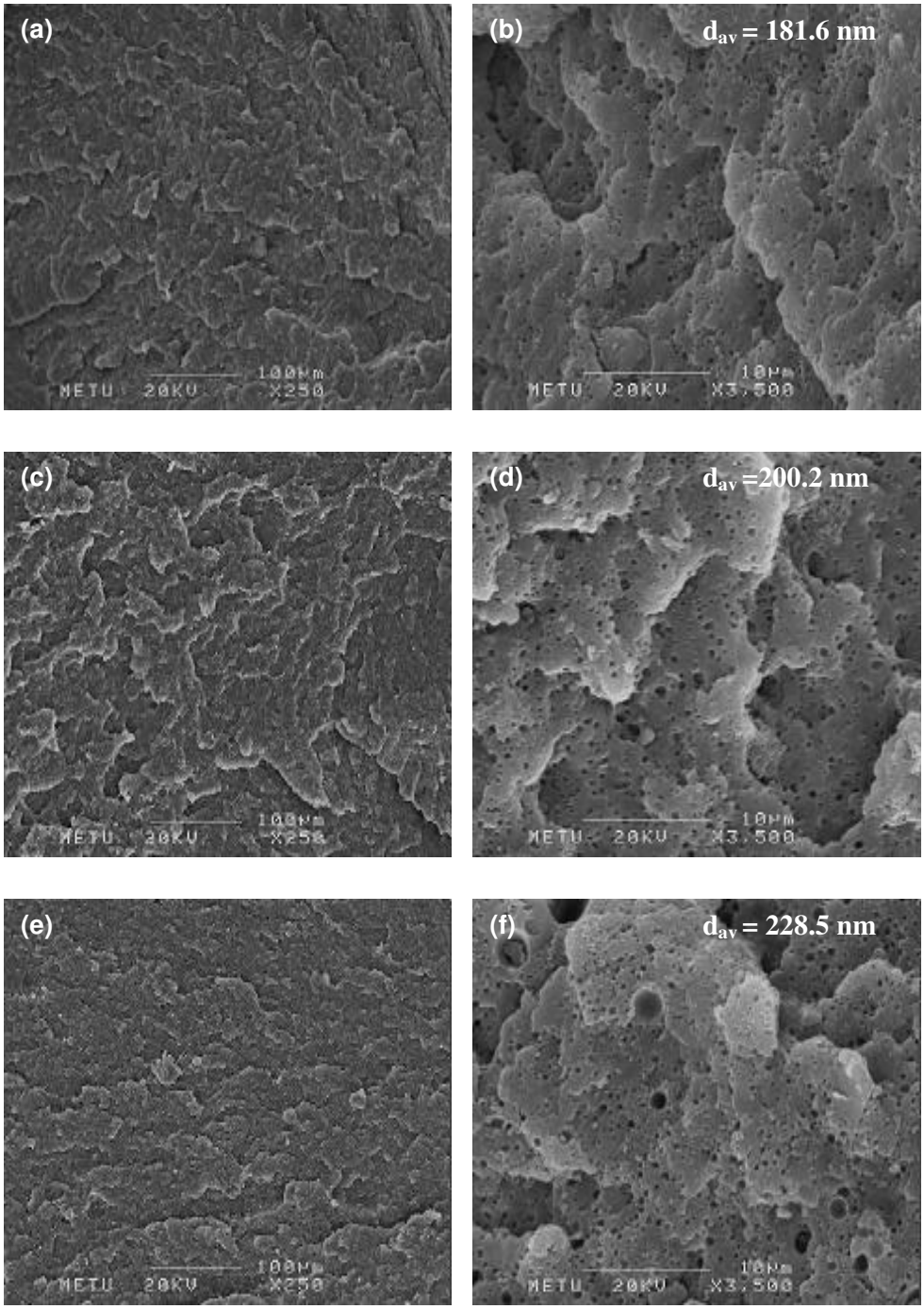

Figure 4.12 SEM micrographs of PA 66-Lotader® AX8900 blends: (a) 5 wt% (x250); (b) 5 wt% (x3500); (c) 10 wt% (x250); (d) 10 wt% (x3500); (e) 15 wt% (x250); (f) 15 wt% (x3500).

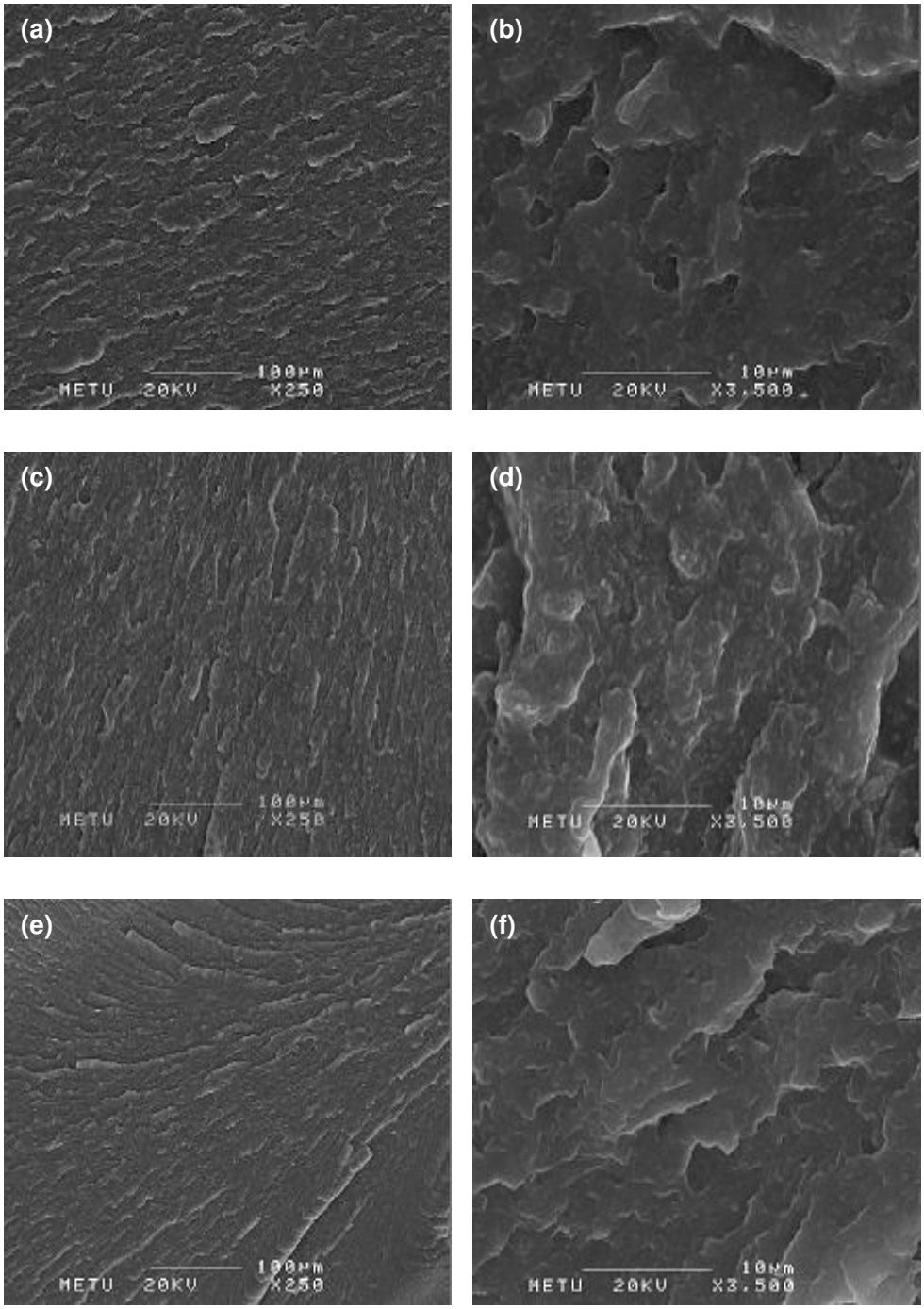

Figure 4.13 SEM micrographs of PA 66-Organoclay binary nanocomposites: (a) Cloisite® 15A (x250); (b) Cloisite® 15A (x3500); (c) Cloisite® 25A (x250); (d) Cloisite® 25A (x3500); (e) Cloisite® 30B (x250); (f) Cloisite® 30B (x3500).

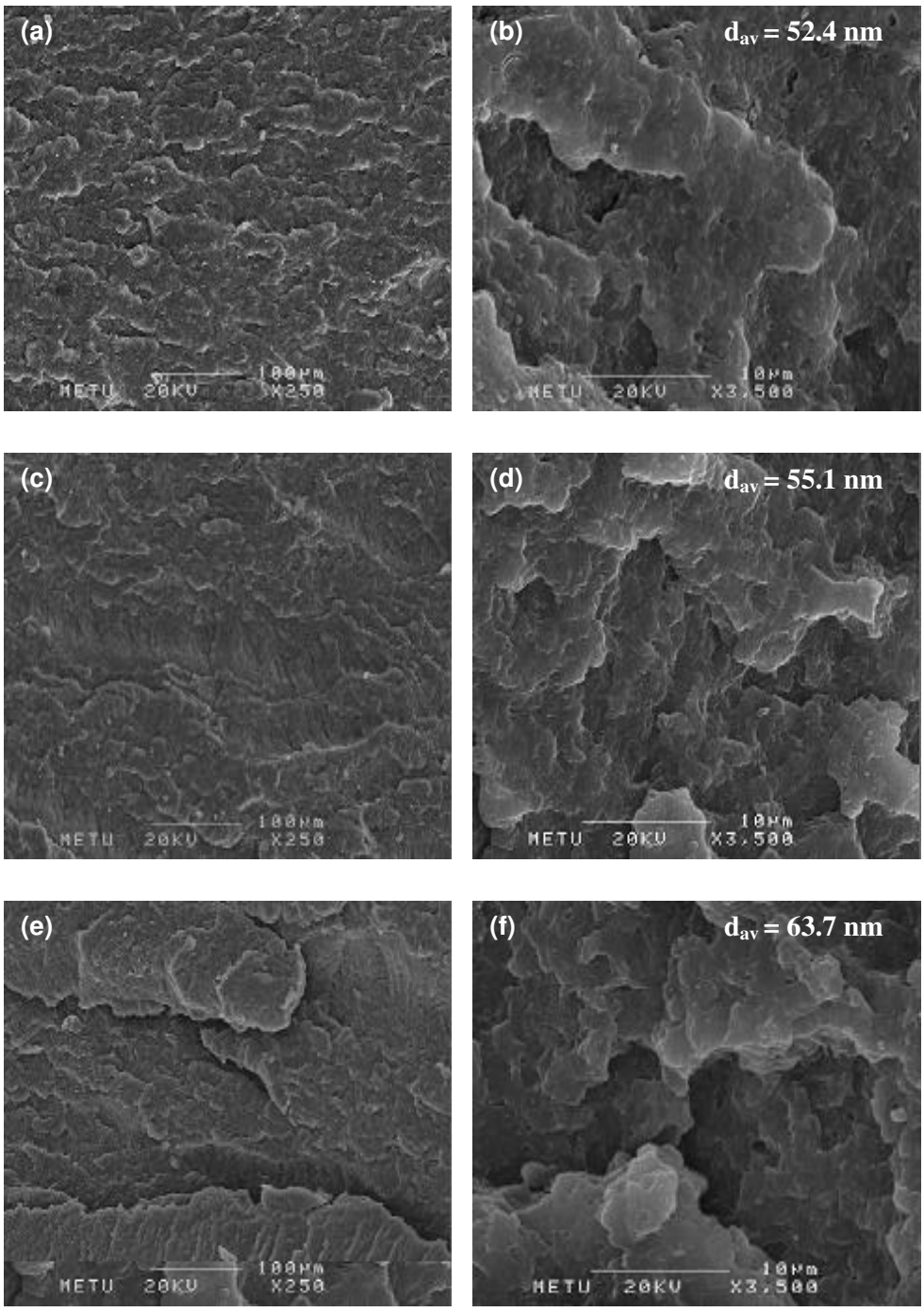

Figure 4.14 SEM micrographs of PA 66-Cloisite® 15A-Impact modifier - (All-S) ternary nanocomposites: (a) Lotader® 2210 (x250); (b) Lotader® 2210 (x3500); (c) Lotader® AX8840 (x250); (d) Lotader® AX8840 (x3500); (e) Lotader® AX8900 (x250); (f) Lotader® AX8900 (x3500).

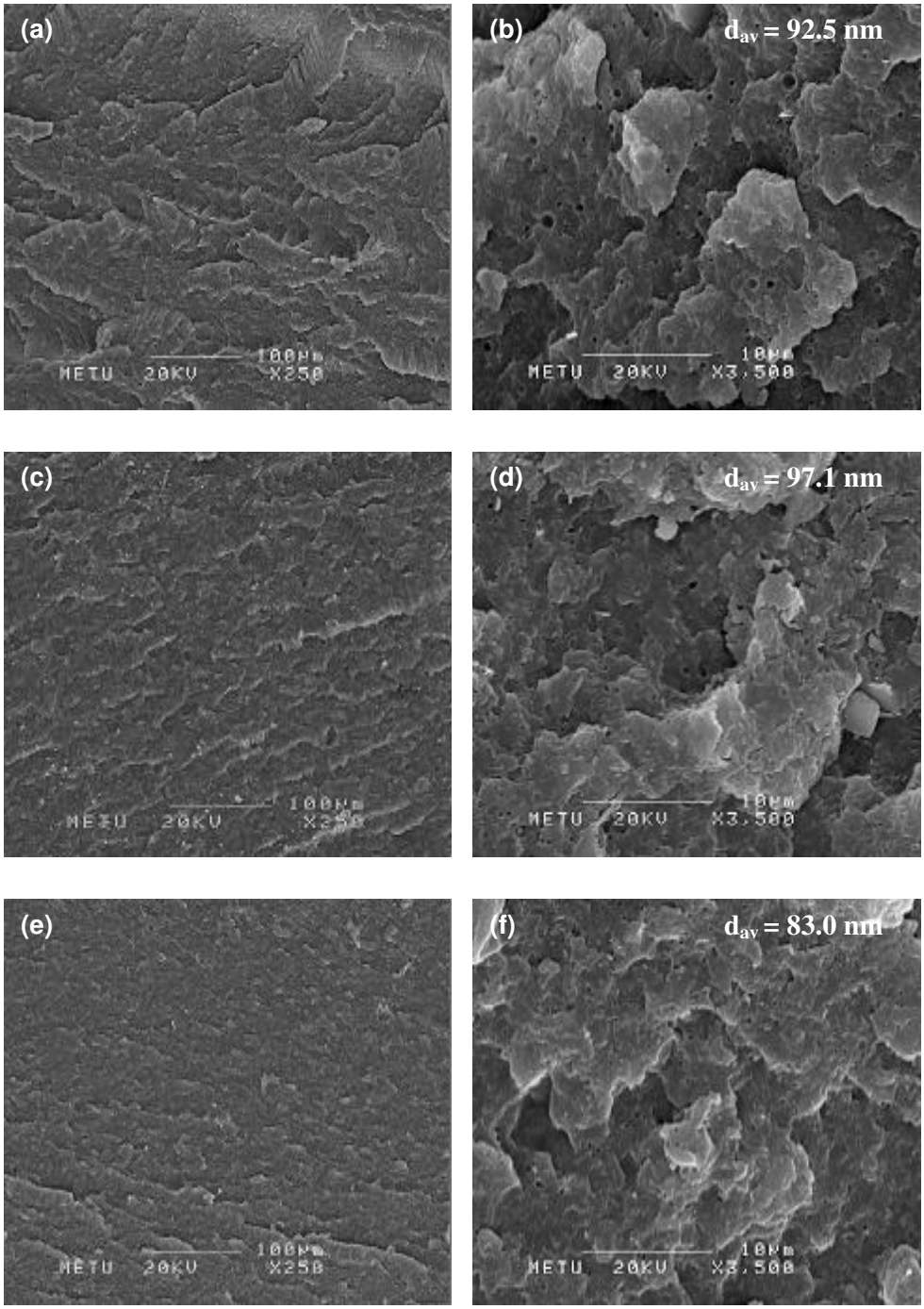

Figure 4.15 SEM micrographs of PA 66-Cloisite® 25A-Impact modifier - (All-S) ternary nanocomposites: (a) Lotader® 2210 (x250); (b) Lotader® 2210 (x3500); (c) Lotader® AX8840 (x250); (d) Lotader® AX8840 (x3500); (e) Lotader® AX8900 (x250); (f) Lotader® AX8900 (x3500).

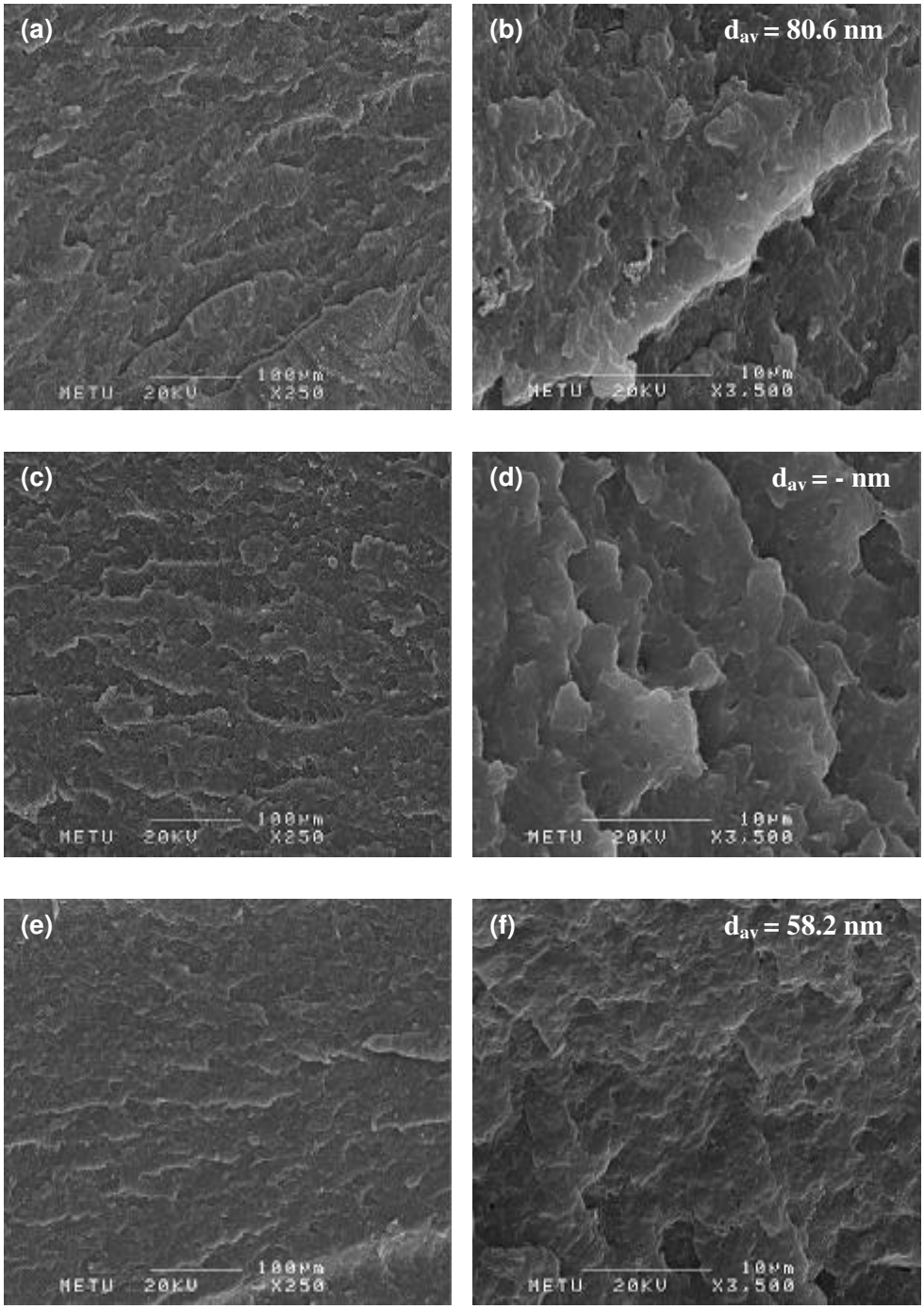

Figure 4.16 SEM micrographs of PA 66-Cloisite® 30B-Impact modifier - (All-S) ternary nanocomposites: (a) Lotader® 2210 (x250); (b) Lotader® 2210 (x3500); (c) Lotader® AX8840 (x250); (d) Lotader® AX8840 (x3500); (e) Lotader® AX8900 (x250); (f) Lotader® AX8900 (x3500).

Binary and ternary PA 66 nanocomposites are shown in Figures 4.13-4.16. No clay agglomeration can be observed that is an indication of improved mechanical properties in all of the nanocomposites. Average domain size and interdomain distance are really significant factors affecting the changes in toughness of the materials. The size of the domains must neither be too small nor too big. Lower toughness values can be acquired for ultrafine domains of elastomers because of the reduced deformability caused by crosslinking or lower adhesion that arises from the absence of compatibilization [114]. Larger elastomeric domains influence the toughness results negatively since they form large cavities. High aspect ratio of the clay platelets also contribute to the reduction in domain sizes since they can act as barriers to prevent coalescence of dispersed phase [62].

The domain sizes of PA 66 matrix were found to be larger because of its difunctionality that enables it to react twice per chain with MAH and more with GMA containing elastomers compared to monofunctional PA 6 [102]. Difunctionality can also lead to crosslinking type effects [69]. The domain sizes are expected to increase with increasing elastomer content and insufficient shear stress. Taking these factors into consideration, the elastomer content was kept constant at 5 wt% as well as the organoclay content that was 2 wt% in all the compositions to eliminate clay agglomerations and non-uniform distribution of elastomeric domains.

It can be observed from all SEM micrographs taken at x250 magnification that crack propagates along a tortuous path. The microstructure is also closely related with the toughness results. The domain sizes observed in Cloisite® 15A - (All-S) nanocomposites are almost the smallest ones among the domain sizes of all the nanocomposites. Higher values were obtained for Cloisite® 25A - (All-S) nanocomposites. Domain sizes of (PA 66-30B-8840) - (All-S) could not be evaluated because the elastomeric domains were almost invisible. It is apparent from SEM micrographs that the interdomain distance is larger in Cloisite® 30B nanocomposites except the one having Lotader® AX8900. It is a drawback for toughness since crack propagation is facilitated between two domains.

According to the impact test results given in section 4.2.2, the highest toughness is obtained for Cloisite® 15A - (All-S) nanocomposites and the lowest for Cloisite® 30B - (All-S) nanocomposites. Therefore, the domain sizes have to be at an optimum level and distance from each other to prevent crack propagation and increase the energy absorption during crack formation. The domain sizes of Cloisite® 25A - (All-S) nanocomposites are somewhat larger and more complex in shape than the domain sizes of the other All-S nanocomposites. Thus, it is expected to obtain lower toughness increase in Cloisite® 25A - (All-S) nanocomposites in comparison with Cloisite® 15A - (All-S) nanocomposites. Upon homogeneous dispersion of the clay platelets as in Cloisite® 15A - (All-S) and Cloisite® 25A - (All-S) nanocomposites, the dispersion of the elastomeric domains can also be more uniform in addition to the decreased domain sizes.

The toughness of Lotader® 2210 containing All-S nanocomposites was found to be similar with the ones having Lotader® AX8900 although it is slightly lower for Lotader® AX8840 containing All-S nanocomposites. The reaction possibility is higher between GMA group and PA 66 matrix and higher viscosity of ternary nanocomposites containing elastomers with GMA functional group resulted in fine dispersion of the elastomeric domains as well as the organoclay dispersion. The domain sizes of Lotader® 2210 - (All-S) nanocomposites are not much different from Lotader® AX8900 - (All-S) and Lotader® AX8840 - (All-S) nanocomposites except the ones containing Cloisite® 30B. The presence of MAH and GMA functional groups immobilized the interface and prevented the coalescence of elastomeric domains both in the nanocomposites and the blends by forming chemical bonds with difunctional PA 66 matrix. MAH group is capable of reacting with the amine ends while GMA group can react with both acid and amine ends [72,73]. Although the number of reactions to enhance compatibility between the matrix and GMA group is higher, the resultant domain sizes are close to Lotader® 2210 containing nanocomposites. The presence of ester groups in acrylates in Lotader® 2210 and Lotader® AX8900 can also increase the reaction possibilities by reacting with the terminal amino groups [112]. The reactions between GMA group and difunctional PA 66 matrix did not have a more positive or adverse effect on the dispersion of elastomeric domains compared to MAH group of Lotader® 2210. The presence of elastomeric domains of moderate

size in the polymer matrix is considered as an advantage since ultrafine and large domains are not really effective in hindering the crack propagation and increasing the toughness in nanocomposites.

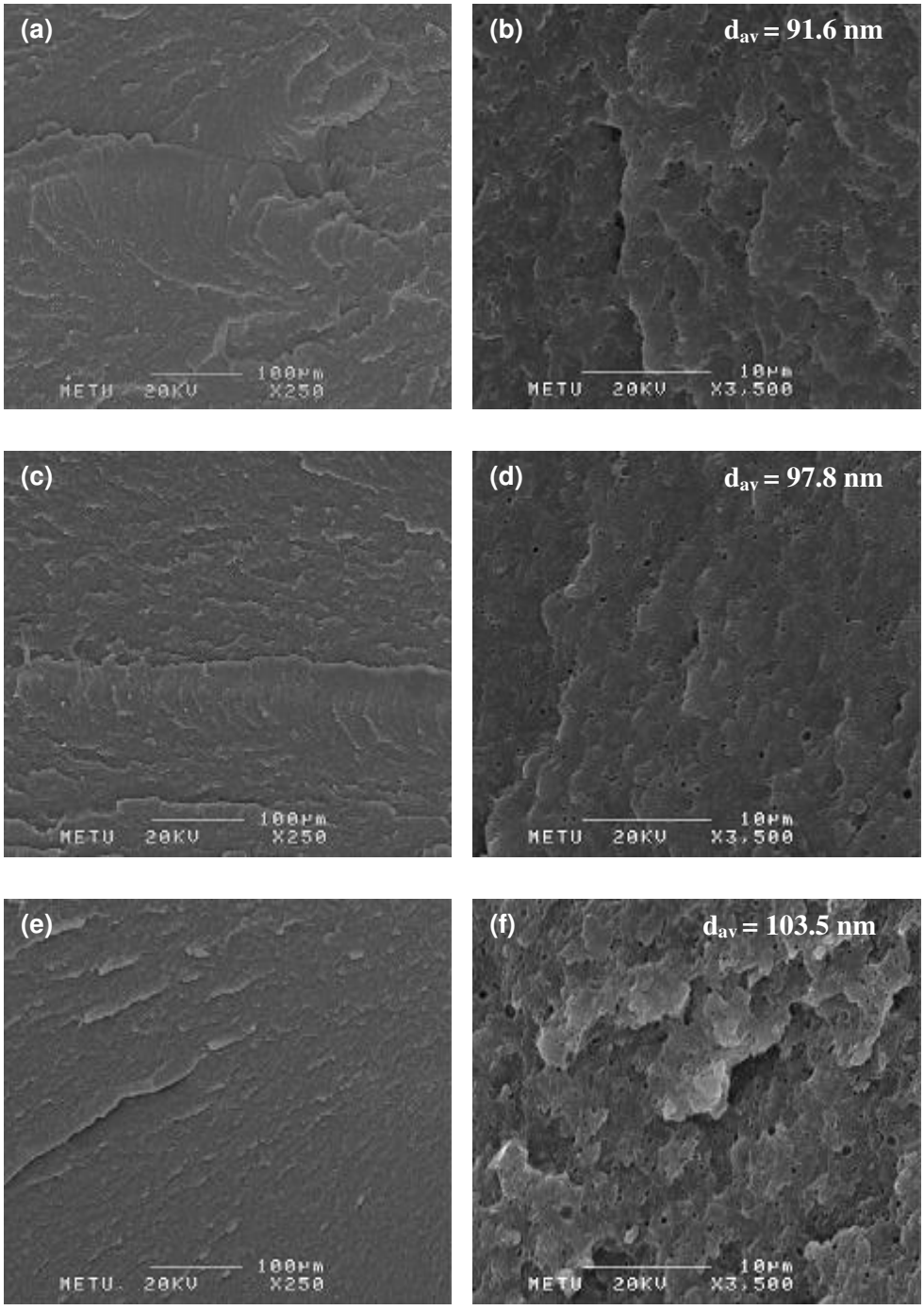

Figure 4.17 SEM micrographs of PA 66-Cloisite® 15A-Lotader® 2210 mixing sequences: (a) CI-P (x250); (b) CI-P (x3500); (c) PC-I (x250); (d) PC-I (x3500); (e) PI-C (x250); (f) PI-C (x3500).

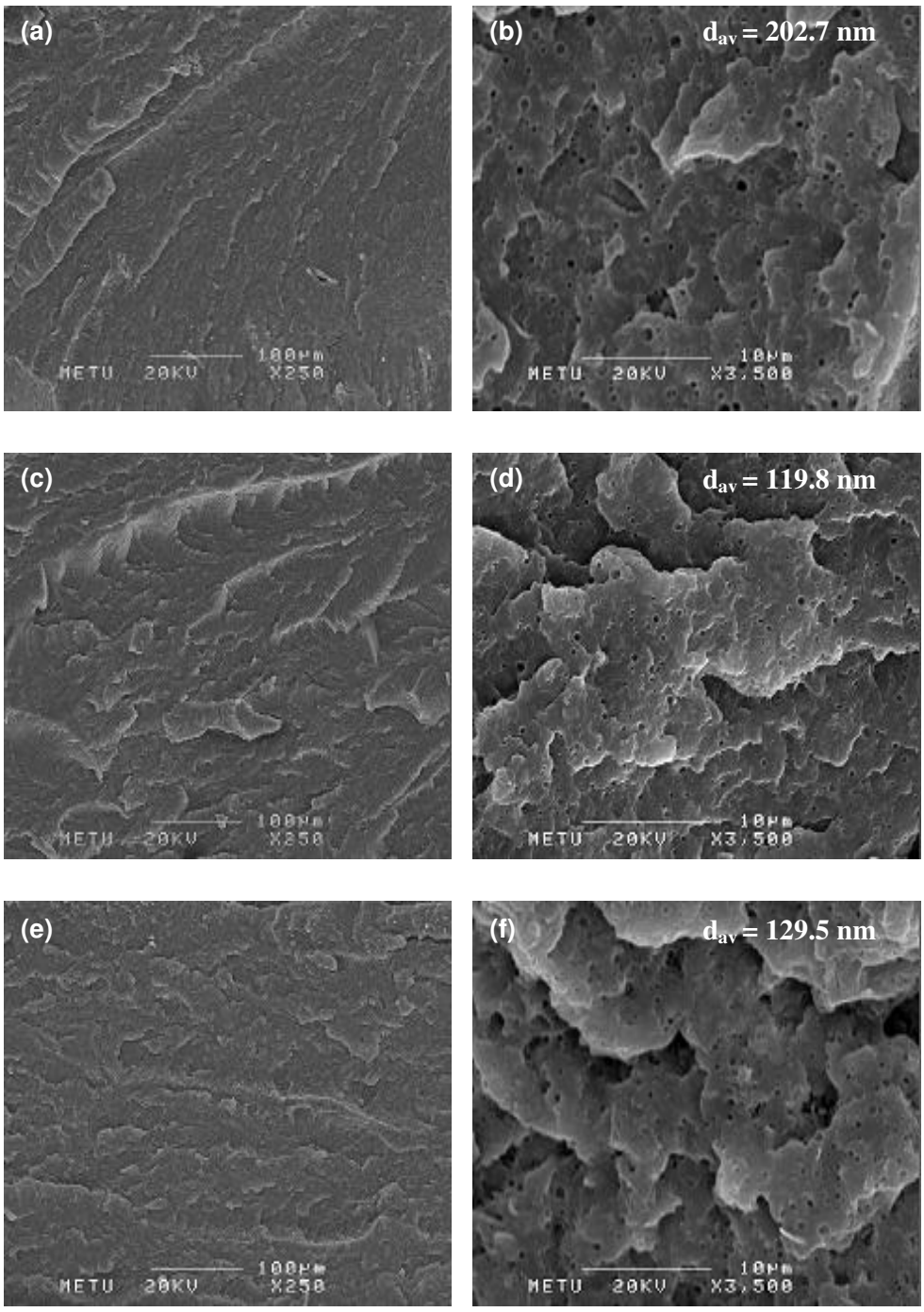

Figure 4.18 SEM micrographs of PA 66-Cloisite® 15A-Lotader® AX8840 mixing sequences: (a) CI-P (x250); (b) CI-P (x3500); (c) PC-I (x250); (d) PC-I (x3500); (e) PI-C (x250); (f) PI-C (x3500).

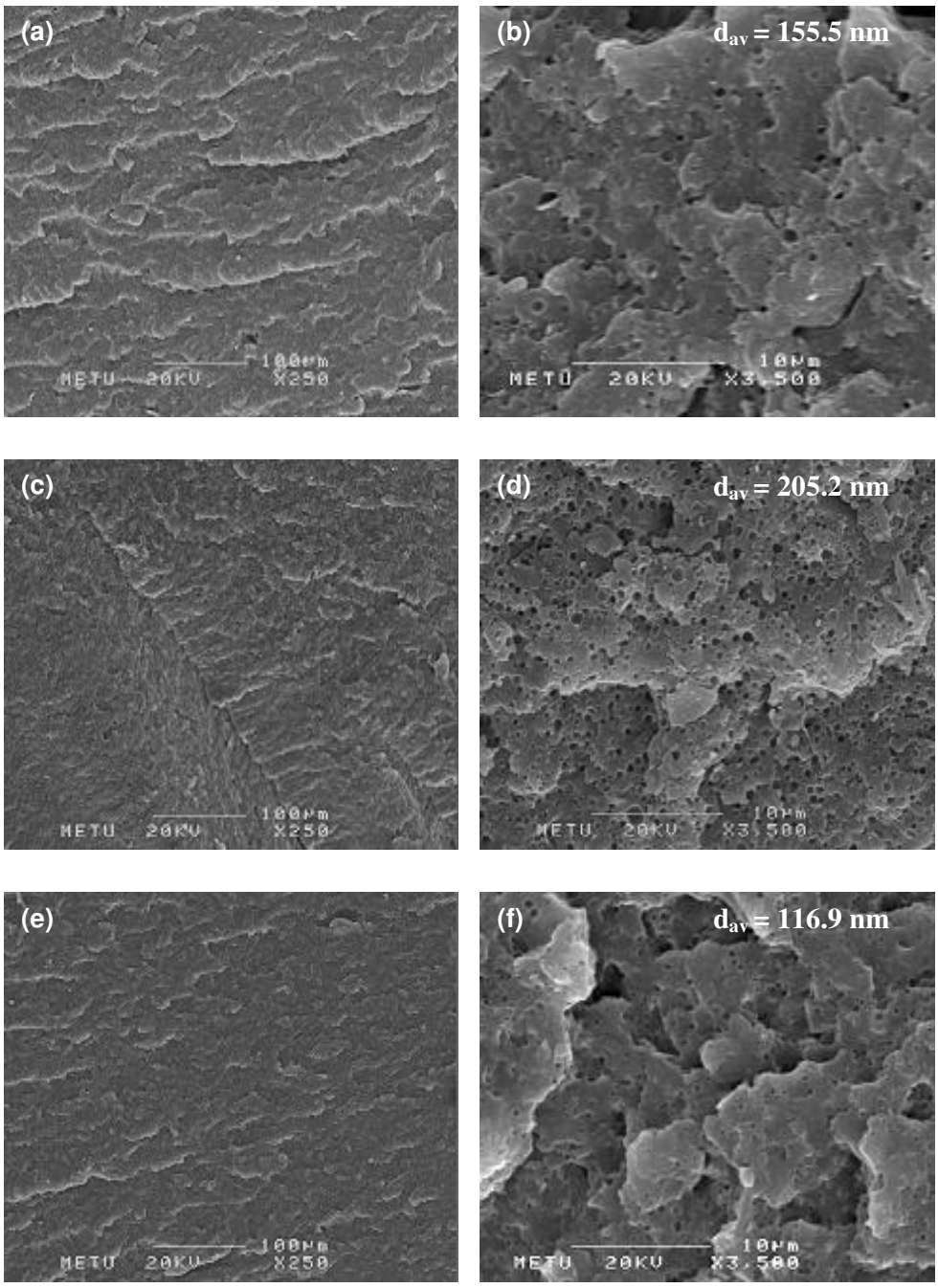

Figure 4.19 SEM micrographs of PA 66-Cloisite® 15A-Lotader® AX8900 mixing sequences: (a) CI-P (x250); (b) CI-P (x3500); (c) PC-I (x250); (d) PC-I (x3500); (e) PI-C (x250); (f) PI-C (x3500).

Mixing sequences of Cloisite® 15A with different types of impact modifiers can be seen in Figures 4.17-4.19. The domain sizes of PI-C mixing sequence are generally close to the domain sizes of CI-P and PC-I mixing sequences despite the fact that the elastomer was extruded twice with the polymer matrix in PI-C mixing sequence. The toughness results of CI-P mixing sequence are higher than PI-C mixing sequence's toughness results because the organoclay meets the impact modifiers in the first extrusion step and the lack of shear which leads to clay agglomerations and decrease in toughness was eliminated by extruding the matrix containing the organoclay twice. The clay platelets were further separated during the second extrusion in CI-P mixing sequence whose domain sizes are slightly larger or similar with PC-I sequences. It results from the fact that clay-impact modifier interactions are more intense and combination of the elastomer, clay and polymer in the second extrusion step did not cause a reduction in the domain sizes of the elastomeric phase of CI-P mixing sequence.

The same results are also valid for the mixing sequences of Cloisite® 25A nanocomposites whose SEM micrographs are shown in Figures 4.20-4.21. The domain sizes of PI-C mixing sequence do not differ drastically from the domain sizes of CI-P and PC-I mixing sequences. The elastomeric phase was not subjected to the second extrusion step in PC-I mixing sequence of all the nanocomposites. This is why the cavitations caused by the impact modifiers are large in this mixing sequence. The largest toughness value belongs to the nanocomposites of PC-I mixing sequence, followed by CI-P and PI-C mixing sequences.

Large increases in the domain sizes is an indication of the interaction of the elastomeric phase with the organoclay for CI-P mixing sequence and insufficient shear intensity to decrease the domain sizes for PC-I mixing sequence. These increases in domain sizes are unfavorable since they retard the improvements in toughness values. However, the toughness of both CI-P and PC-I mixing sequences is larger than PI-C because of the aforementioned effect of poorly dispersed clay platelets.

On the other hand, the toughness of All-S mixing sequence is the largest among all the mixing sequences since the elastomeric phase is uniformly dispersed and the domain sizes are moderate. The presence of the organoclay in the elastomeric phase and the large domain sizes may eliminate the enhancements in toughness in CI-P mixing sequence. Although the toughness of PC-I mixing sequence is higher than PI-C and CI-P mixing sequences, it is also lower than All-S mixing sequence except the slightly higher toughness values of (PA 66 / 15A)-8900 - (PC-I) and (PA 66 / 25A)-8900 - (PC-I). This is due to the difference in the domain sizes and interdomain distances between the two mixing sequences.

The domain sizes of All-S mixing sequences are smaller than the domain sizes of PI-C mixing sequences. The difference in the domain sizes can be ascribed to extrusion of the polymer matrix without the organoclay in the first step in PI-C mixing sequence. Polymer-elastomer combination was melt compounded without the organoclay that interacts with both the polymer matrix and the elastomers and has a barrier effect on coalescence of the elastomeric domains in PI-C mixing sequence. Interactions were already formed between the elastomer and the polymer matrix in the first step and incorporation of the organoclay in the second step eliminated break up of clay agglomerations besides the increases in the viscosity. The large domain sizes and poor mechanical properties of PI-C mixing sequences also indicate that the compatibilization and impact toughening effect of the elastomer diminished in the first extrusion step compared with the other mixing sequences before it was mixed with the organoclay.

Consequently, increasing the interfacial interaction by blending three of the components simultaneously and melt mixing the polymer matrix containing all the components twice aided dispersion of both the elastomeric phase and the organoclay in all All-S mixing sequences.

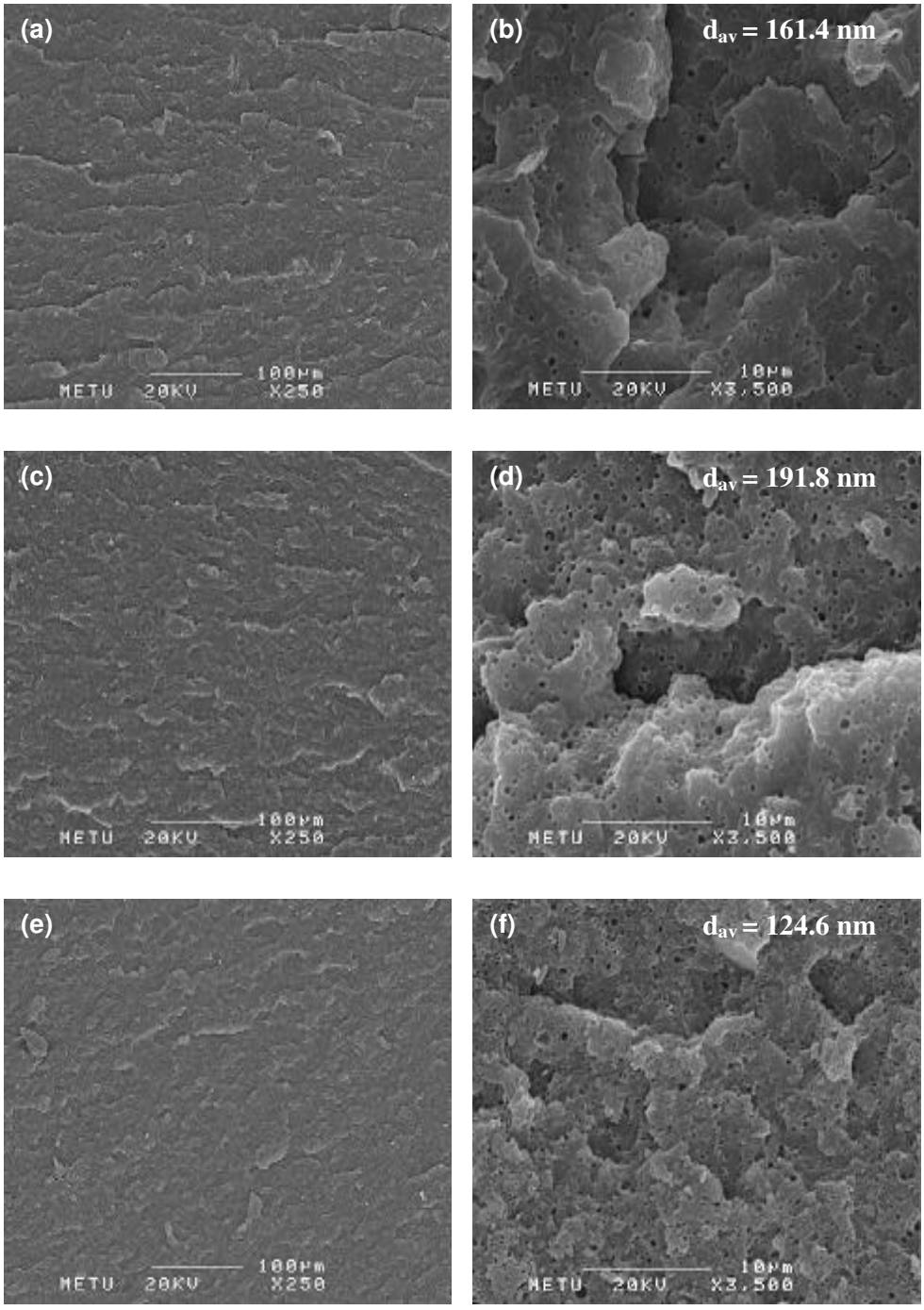

Figure 4.20 SEM micrographs of PA 66-Cloisite® 25A-Lotader® AX8840 mixing sequences: (a) CI-P (x250); (b) CI-P (x3500); (c) PC-I (x250); (d) PC-I (x3500); (e) PI-C (x250); (f) PI-C (x3500).

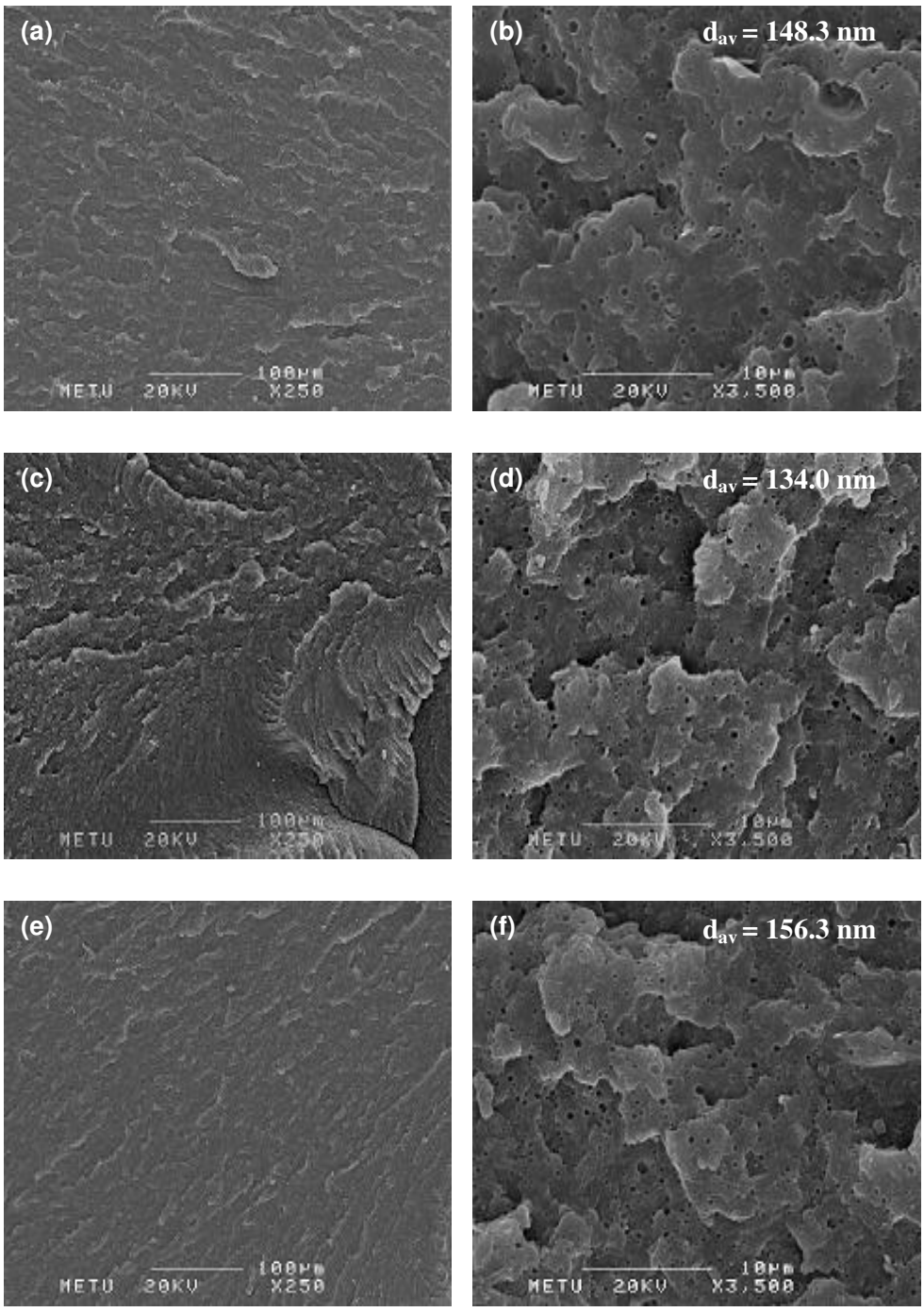

Figure 4.21 SEM micrographs of PA 66-Cloisite® 25A-Lotader® AX8900 mixing sequences: (a) CI-P (x250); (b) CI-P (x3500); (c) PC-I (x250); (d) PC-I (x3500); (e) PI-C (x250); (f) PI-C (x3500).

4.2 Mechanical Properties

Mechanical properties are prominent in determining the endurance of a material to various types of deformation mechanisms. Tensile, impact, flexural and hardness tests were performed in this study to analyze the degree of improvement in the strength and toughness of nanocomposites upon addition of the organoclay and compatibilizers which also serve as impact modifiers. The results of these tests given in Appendix A are interrelated with the stiffness of PA 66 nanocomposites, dispersion of the organoclay and the impact modifier in PA 66 matrix. The effect of the type of the impact modifiers, the organoclays and mixing sequences on the mechanical properties is demonstrated by the help of the graphs.

4.2.1 Tensile Tests

Tensile strength, Young's modulus and elongation at break (%) values were determined by tensile tests. Stress-strain curves of PA 66 binary nanocomposites and PA 66 blends are shown in Figures 4.22-4.25.

It is obvious from stress-strain curves that the organoclay stiffens the matrix and results in an increase in the tensile strength and Young's modulus. High aspect ratio of the organoclay that creates a large contact area with the polymer matrix contributes to the reinforcement effect [62]. The interfacial adhesion between PA 66 and the organoclay is also significant in dispersing the clay homogeneously in the polymer matrix and increasing the strength of the material. However, high elongation at break values diminish upon addition of the reinforcement phase since inorganic silicate particles cannot be strained by external stresses [63]. The tie chain amount between the crystalline areas is reduced and the stress cannot be transferred through the sample causing early failure. The sphereulite size also decreases in PA 66, upon addition of the organoclay, leading to brittle structure [20]. Elastomeric materials enhance the bonding between the polymer and the organoclay and compensate for the decrease in toughness caused by reinforcements. Elastomeric phase has a lower Young's modulus compared to the matrix and it acts as stress concentrator during the elongation. Thus, yielding or crazing occurs around the elastomeric domains and a higher amount of energy

is absorbed by the polymer. As the strain at break values become higher, yield strength decreases because of the plastic deformation mechanism that involves dilatational strain [63]. An optimum amount of 5 wt% elastomeric phase and 2 wt% organoclay was added into the polymer matrix in all the combinations to balance the stiffness and toughness of the materials.

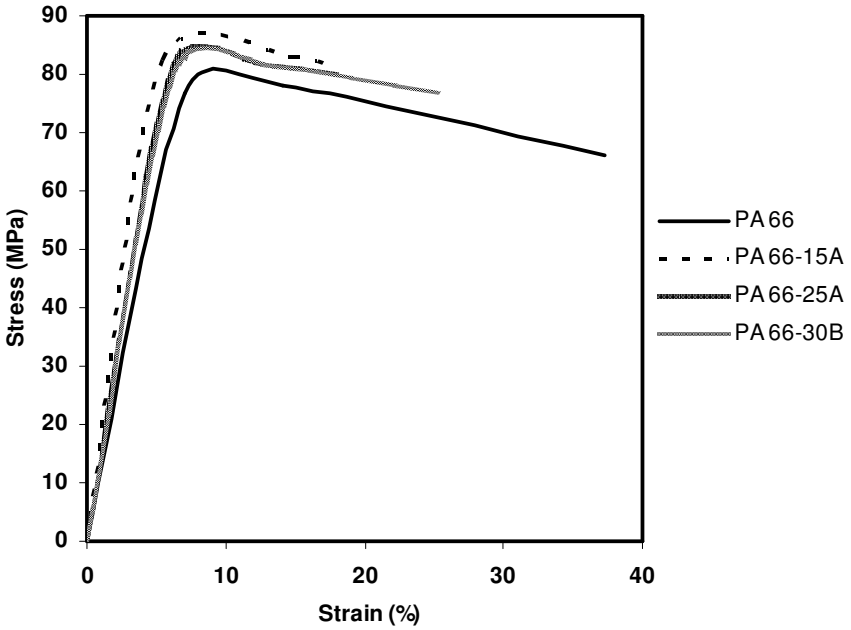

Figure 4.22 Stress-strain curves of PA 66-Organoclay binary nanocomposites.

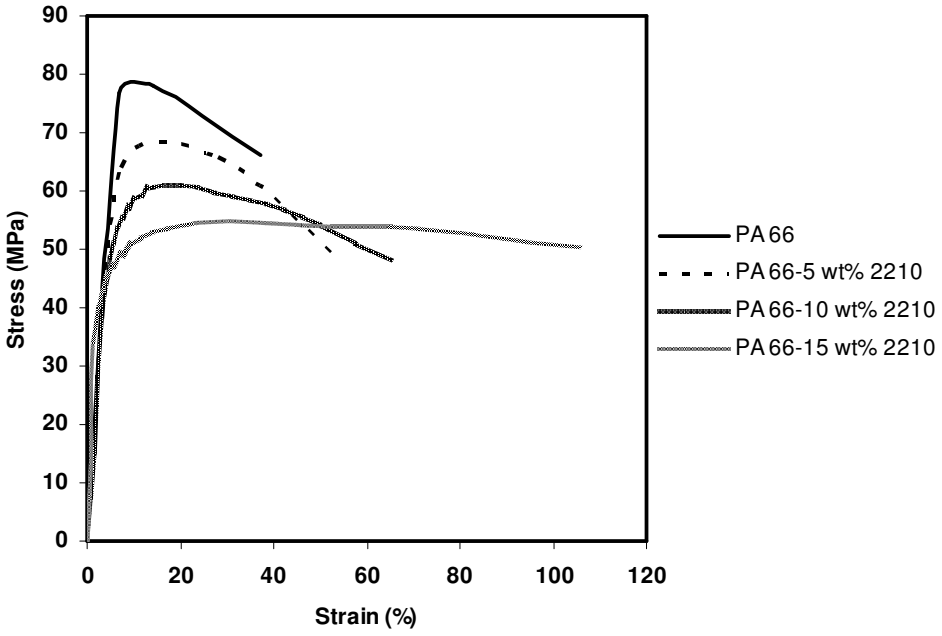

Figure 4.23 Stress-strain curves of PA 66-Lotader® 2210 blends.

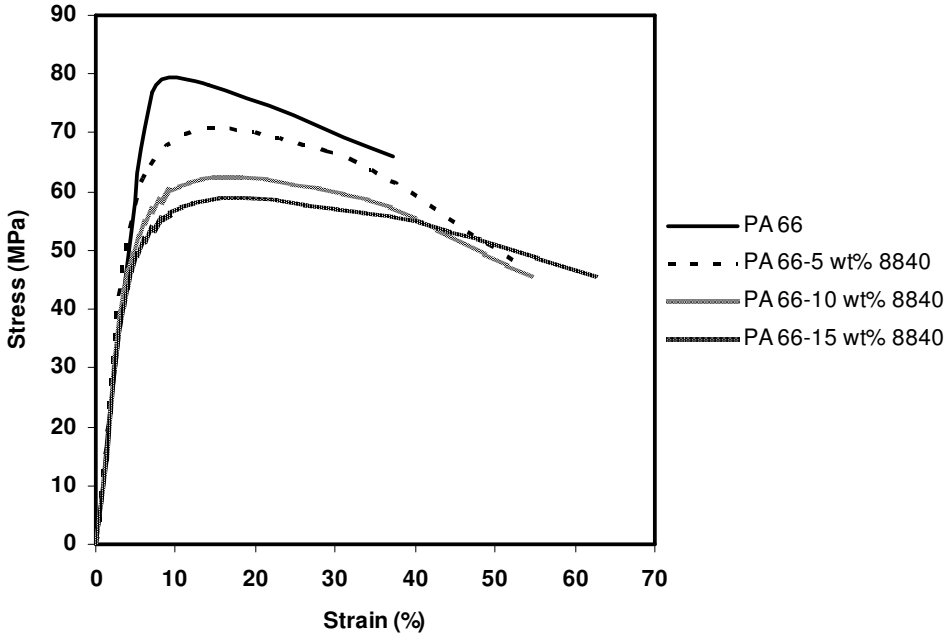

Figure 4.24 Stress-strain curves of PA 66-Lotader® AX8840 blends.

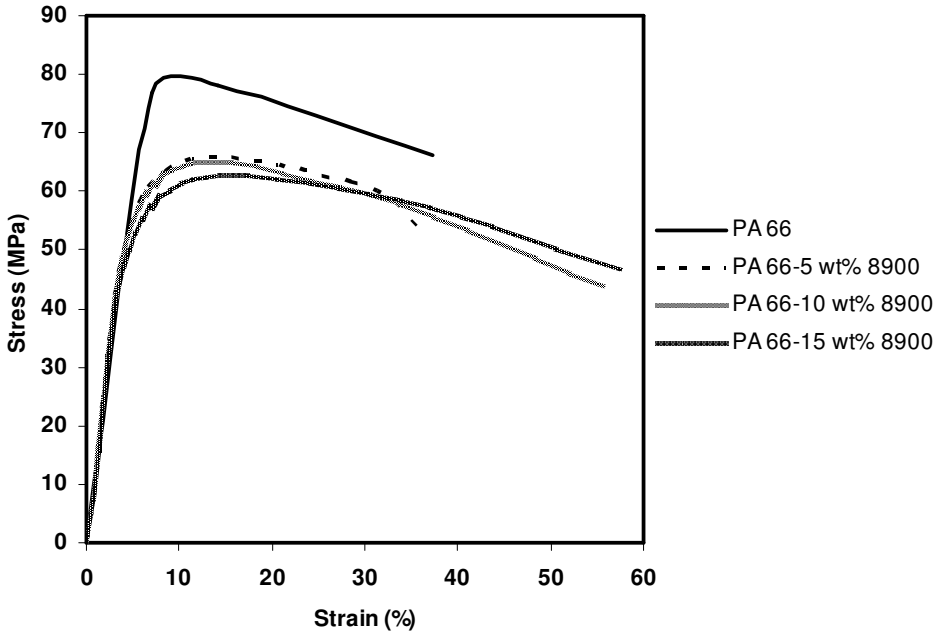

Figure 4.25 Stress-strain curves of PA 66-Lotader® AX8900 blends.

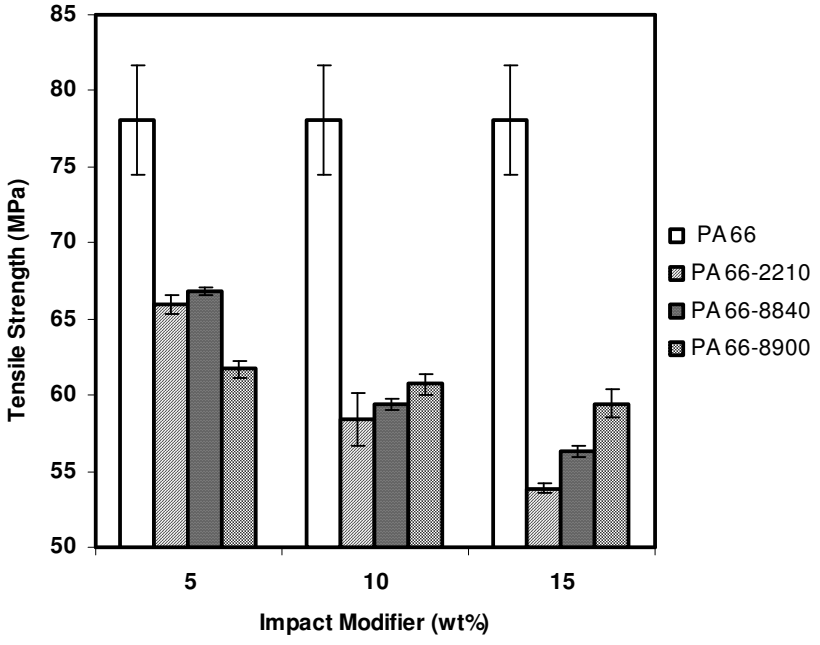

Figure 4.26 Tensile strength of PA 66-Impact modifier blends.

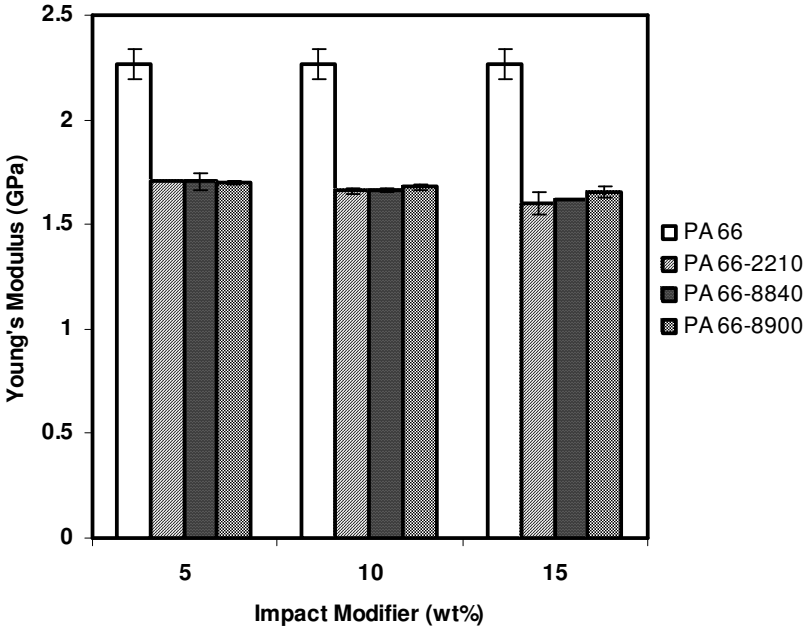

Figure 4.27 Young's modulus of PA 66-Impact modifier blends.

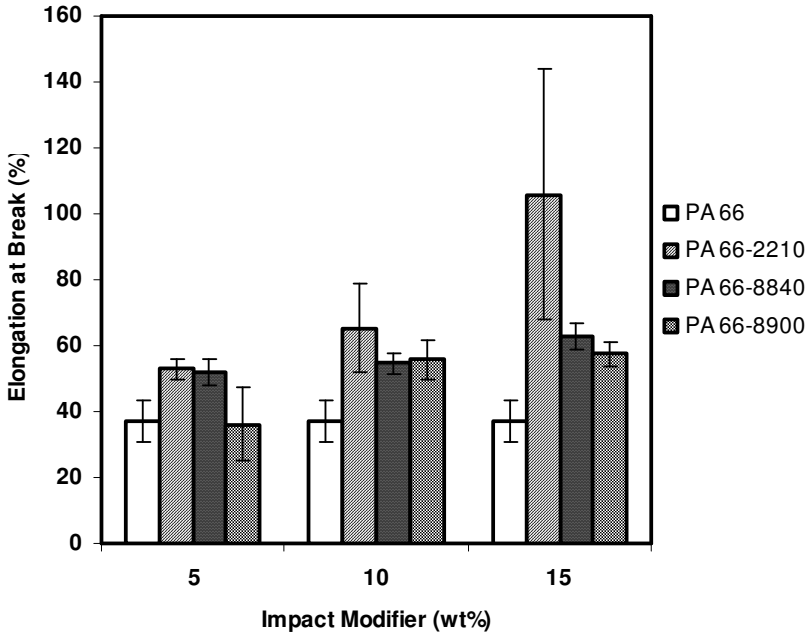

Figure 4.28 Elongation at break (%) of PA 66-Impact modifier blends.

Tensile strength, Young's modulus and elongation at break of PA 66 that was twice extruded were found to be 78.1 MPa, 2.3 GPa and 37.3 %, respectively. These values are within the range given by Polyone Company for wet and dry as moulded PA 66. Although all the samples were conditioned as dry as moulded, it is expected to observe a slight decrease in the values because of being subjected to extrusion twice.

As it is seen from Figures 4.26-4.28, Lotader® 2210 caused the greatest increase in elongation at break values as well as the greatest decrease in tensile strength and Young's modulus from 5 wt% content up to 15 wt% in comparison with Lotader® AX8840 and Lotader® AX8900. The least reduction in tensile strength at 5 wt% elastomer content is caused by Lotader® AX8840. Although the lowest strength and modulus values are observed for the blends having Lotader® AX8900 at 5 wt% composition, the decrease in these values is not as pronounced as the other impact modifiers at the other compositions. As the ductility of the blends increased, severe decreases occurred in the tensile strength and Young's modulus.

Increase in the elastomer content can have adverse effects on the ductility of the material since the shear intensity may not be sufficient to disperse the elastomeric domains resulting in retarded adhesion of the elastomer to the polymer matrix and increase in the domain sizes. However, such a case is not observed in the mechanical properties here. Even though all the impact modifiers seem to have fair interaction with the polymer matrix regarding their mechanical properties in the blends, the objective is to obtain the best impact modification of PA 66 nanocomposites and the least reduction in the strength and modulus values.

Stress-strain curves of PA 66 ternary nanocomposites can be seen in Figures 4.29-4.31 and the values obtained from stress-strain curves are compared in Figures 4.32-4.34. "IM" notation used in the graphs denotes the impact modifier type. It is seen that Cloisite® 15A binary nanocomposites has the highest tensile strength (82.8 MPa) and Young's modulus (2.5 GPa) that is one of the prior results indicating good dispersion of the organoclay in PA 66 matrix while the

lowest tensile strength (81.2 MPa) and Young's modulus (2.4 GPa) values of the binary nanocomposites belong to the ones containing Cloisite® 30B. Despite the fact that the organic modifier of Cloisite® 30B is more polar, the interactions of the organic modifier with the clay and hydroxyl groups within its own chemical structure may have prevented diffusion of the polymer chains between the clay platelets while the dispersive forces managed to overcome the nonpolar interactions between the hydrogenated tallows of the organic modifier and the polymer for Cloisite® 15A and Cloisite® 25A [113]. The differences between the tensile strength and Young's modulus of nanocomposites containing Cloisite® 15A and Cloisite® 30B are not too high in spite of the fact that Cloisite® 15A was almost delaminated in the polymer matrix. This can be attributed to the good dispersion of all the organoclays in the polymer matrix and the presence of an intercalated region in all the nanocomposites as it can be seen from XRD patterns in section 4.1.1.

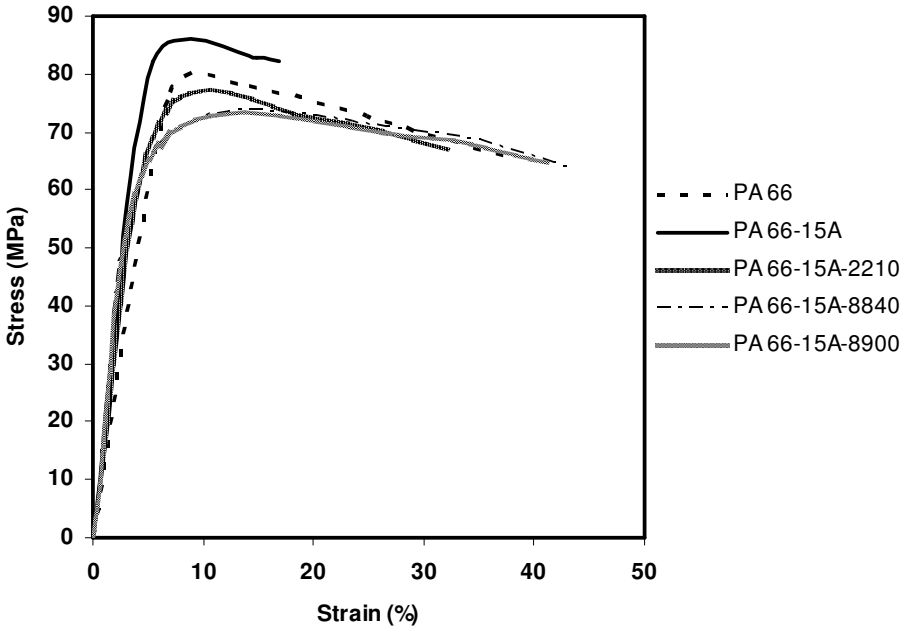

Figure 4.29 Stress-strain curves of PA 66-Cloisite® 15A-Impact modifier - (All-S) ternary nanocomposites.

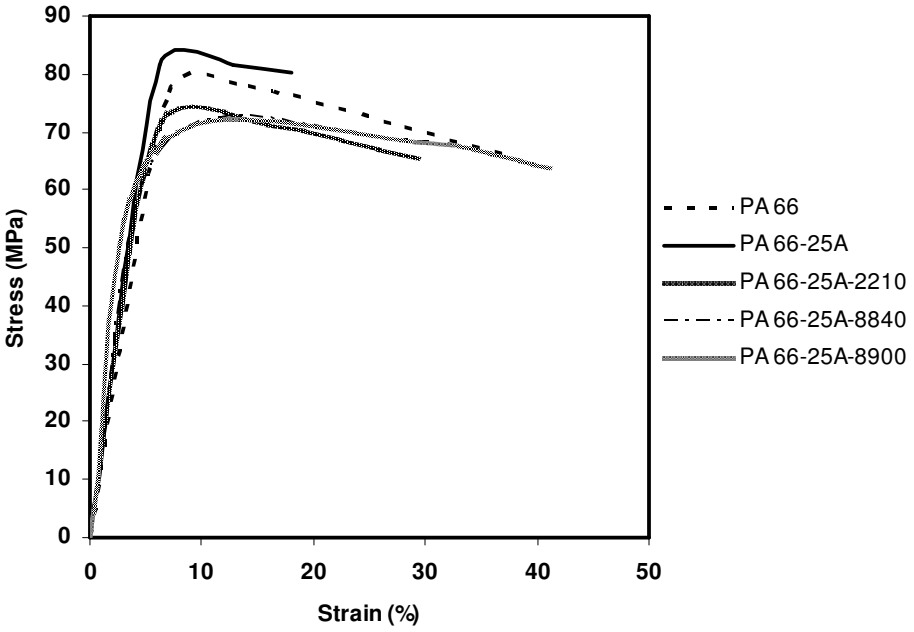

Figure 4.30 Stress-strain curves of PA 66-Cloisite® 25A-Impact modifier - (All-S) ternary nanocomposites.

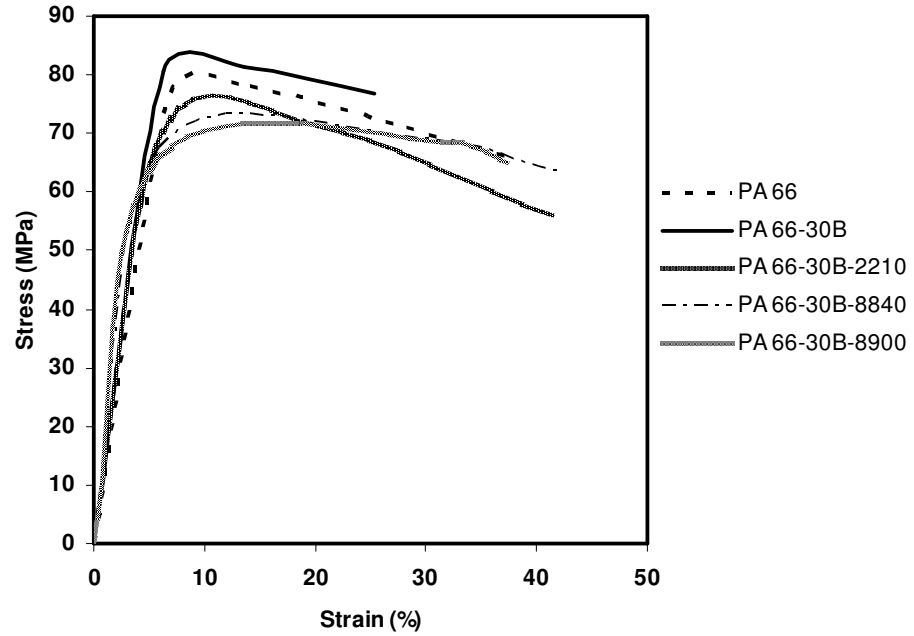

Figure 4.31 Stress-strain curves of PA 66-Cloisite® 30B-Impact modifier - (All-S) ternary nanocomposites.

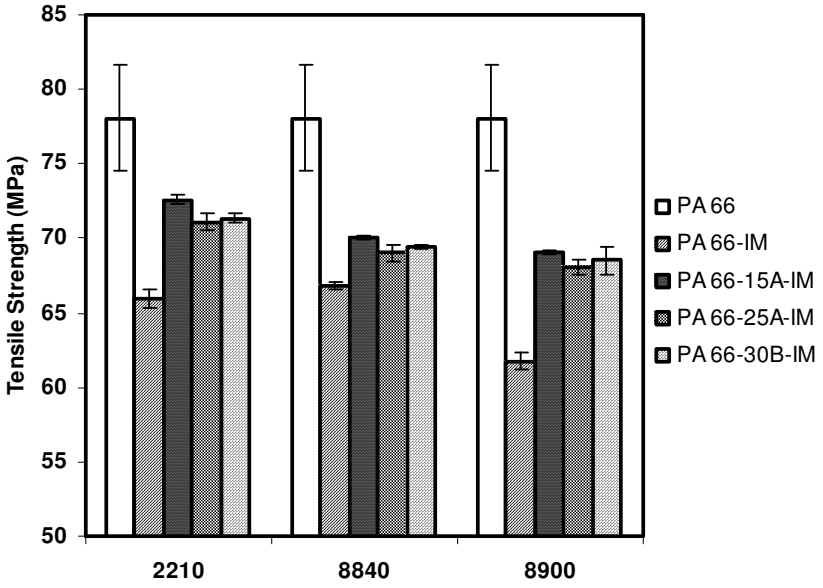

Figure 4.32 Tensile strength of PA 66-Organoclay-Impact modifier - (All-S) ternary nanocomposites.

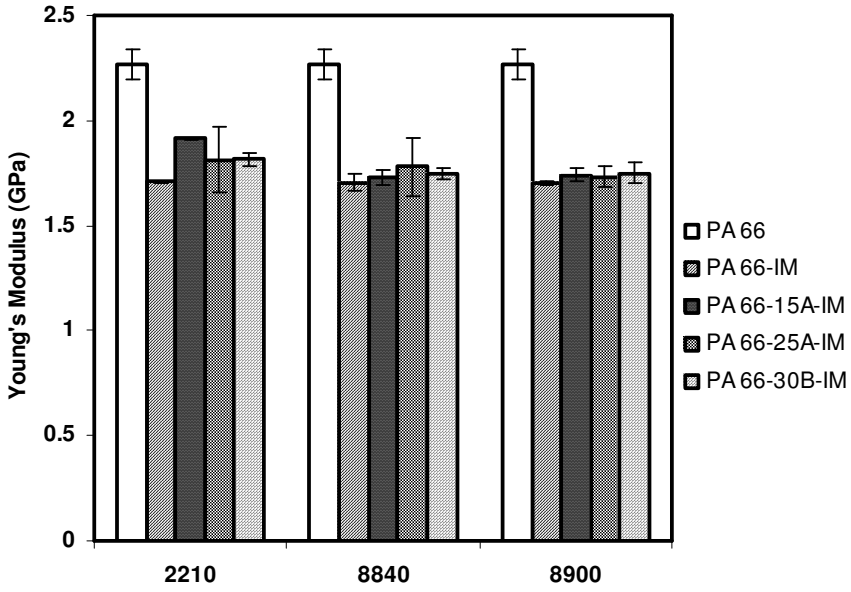

Figure 4.33 Young's modulus of PA 66-Organoclay-Impact modifier - (All-S) ternary nanocomposites.

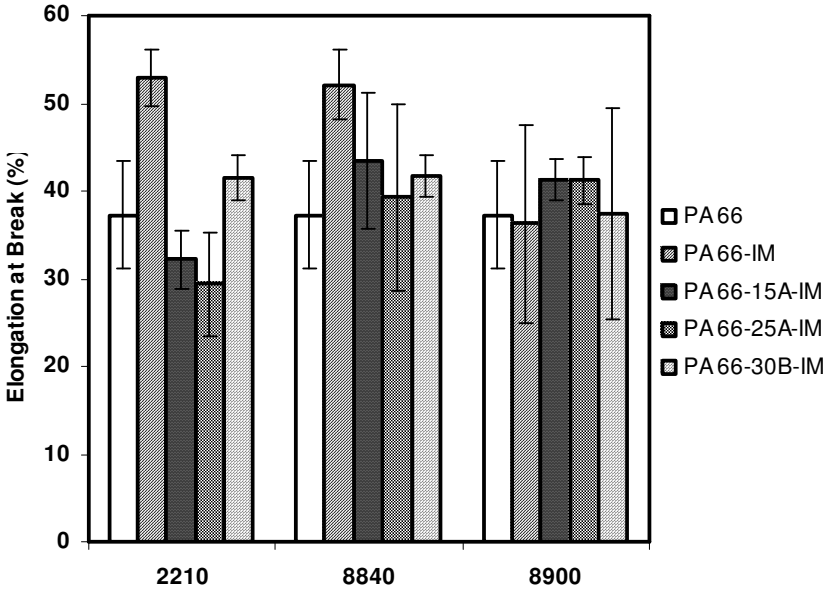

Figure 4.34 Elongation at break (%) of PA 66-Organoclay-Impact modifier - (All-S) ternary nanocomposites.

The same behavior is exhibited in the tensile test results of PA 66 ternary nanocomposites as in PA 66 binary nanocomposites. Average tensile strength and Young's modulus of All-S nanocomposites containing Lotader® 2210 are higher than the others. The highest mechanical test results belong to (PA 66-15A-2210) - (All-S) mixing sequence. Toughness of (PA 66-Organoclay-2210) - (All-S) mixing sequences is more improved compared to the other mixing sequences. The increase in the elongation at break values of All-S nanocomposites containing the other impact modifiers generally resulted in a lower increase in the toughness because of the small differences in tensile strength values between them and All-S nanocomposites having Lotader® 2210 except Cloisite® 25A - (All-S) nanocomposites.

It is desired to obtain high toughness results coupled with high tensile strength and Young's modulus in most applications of the materials. The reductions in elongation at break have to be compensated by the addition of elastomeric phase without significantly decreasing the tensile strength values too much. Therefore, the mixing sequences were varied for All-S sequences with high tensile strength,

Young's modulus, moderate elongation at break and toughness values. Increased d-spacing and low intensity of the peaks in XRD patterns is also taken into consideration since it is a sign of the uniform dispersion of the organoclay in the polymer matrix promoting enhanced mechanical properties. The mixing sequences were varied for all PA 66-15A-Impact modifier ternary nanocomposites, PA 66-25A-8840 and PA 66-25A-8900 ternary nanocomposites.

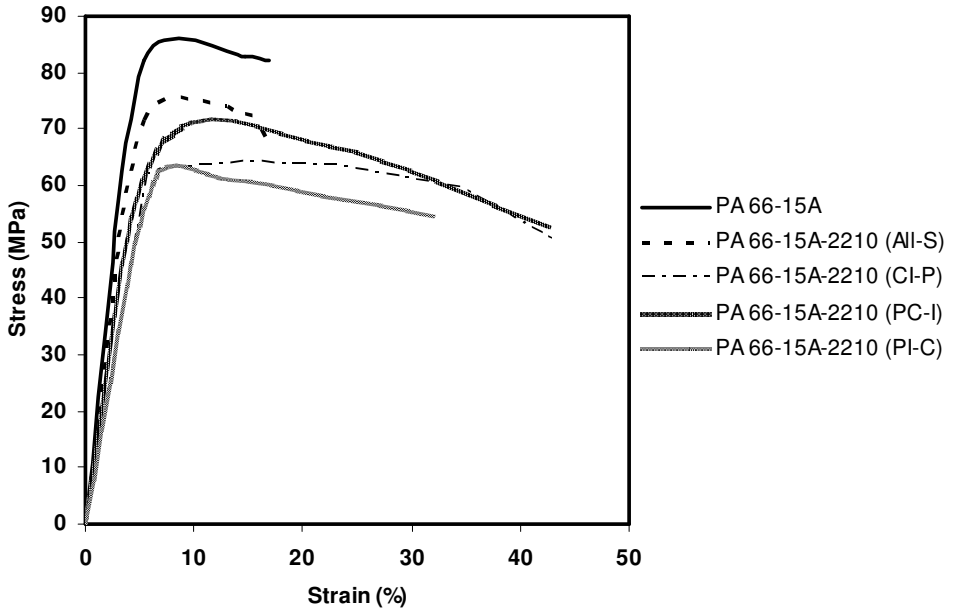

Figure 4.35 Stress-strain curves of PA 66-Cloisite® 15A-Lotader® 2210 mixing sequences.

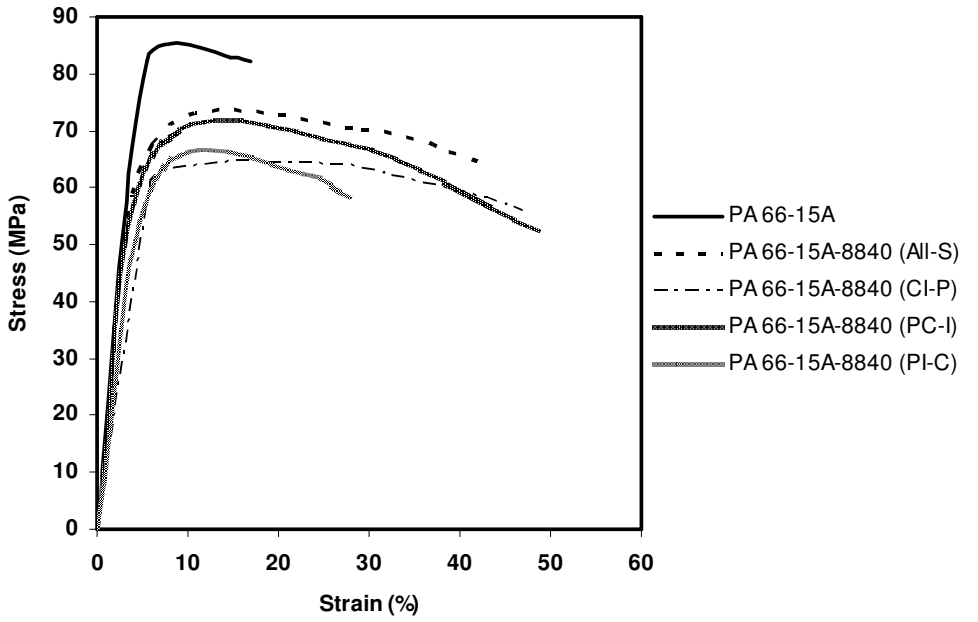

Figure 4.36 Stress-strain curves of PA 66-Cloisite® 15A-Lotader® AX8840 mixing sequences.

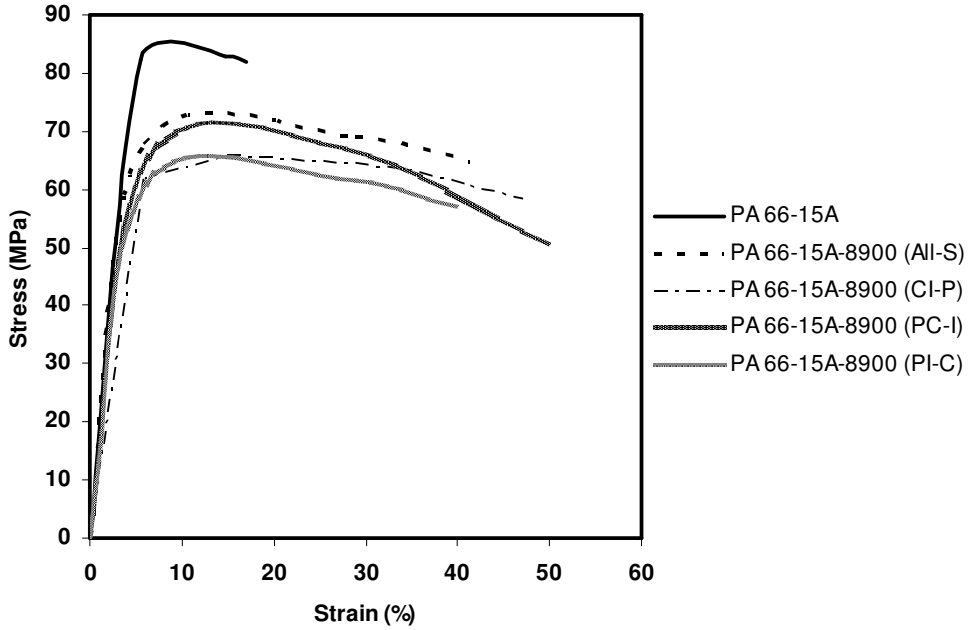

Figure 4.37 Stress-strain curves of PA 66-Cloisite® 15A-Lotader® AX8900 mixing sequences.

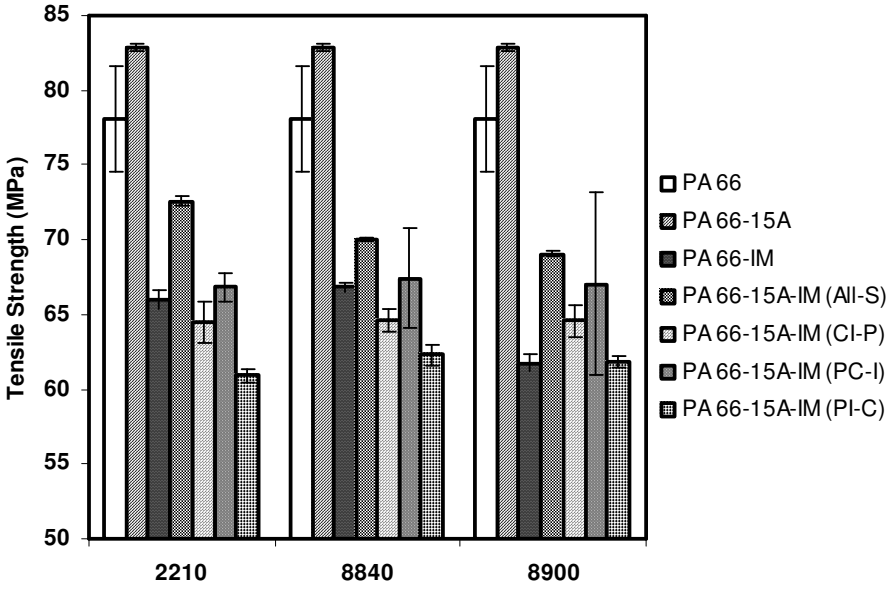

Figure 4.38 Tensile strength of PA 66-Cloisite® 15A-Impact modifier mixing sequences.

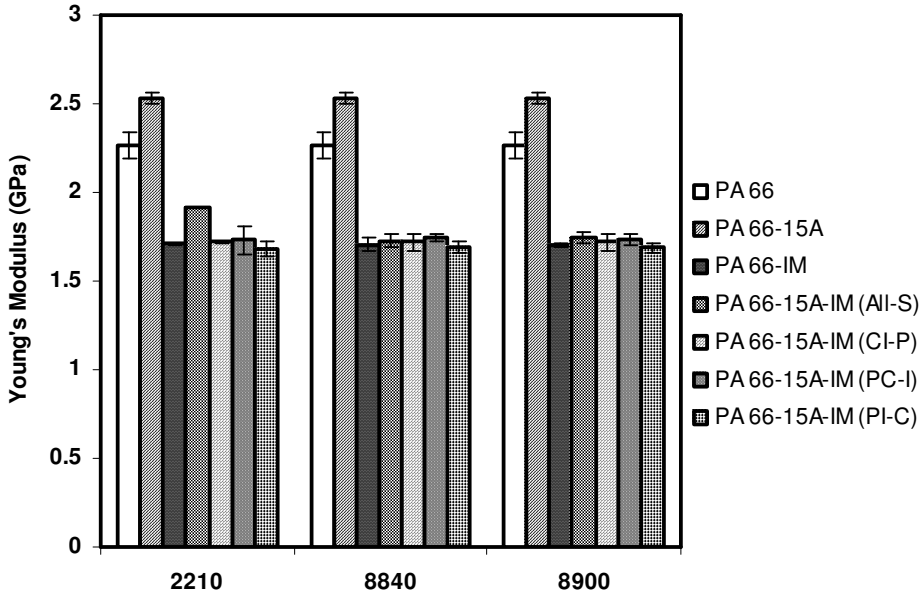

Figure 4.39 Young's modulus of PA 66-Cloisite® 15A-Impact modifier mixing sequences.

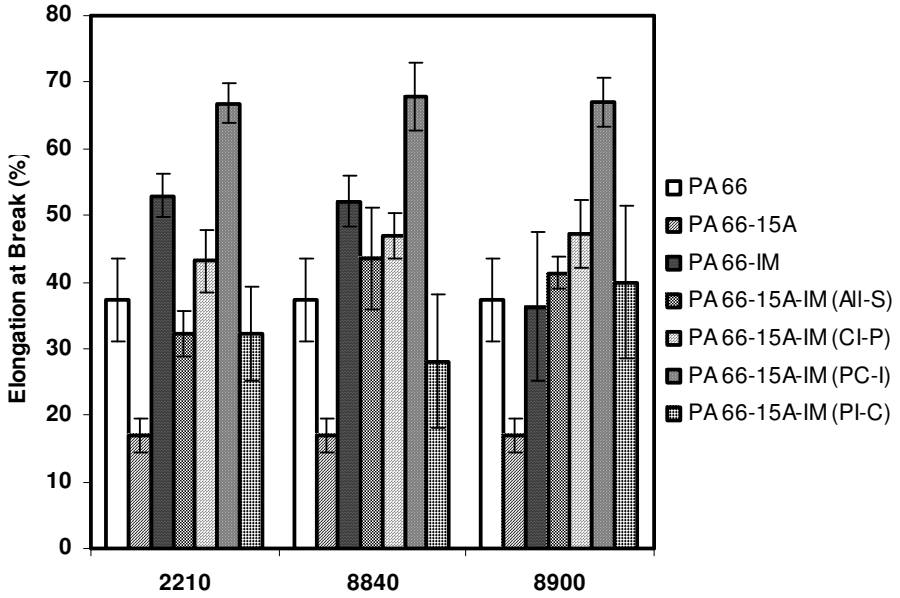

Figure 4.40 Elongation at break (%) of PA 66-Cloisite® 15A-Impact modifier mixing sequences.

The tensile test results of Cloisite® 15A mixing sequences are analyzed by the stress-strain curves given in Figures 4.35-4.37. Tensile strength, Young's modulus and elongation at break values are illustrated in Figures 4.38-4.40.

Varying the mixing sequences helps disperse the organoclay by the increases in viscosity and better interaction of two of the components. However, all the components were not treated in the same way since one of the components was extruded only once. This is why the mechanical properties of the mixing sequences differ from each other. The highest tensile strength values mostly belong to PC-I after All-S mixing sequence and it is followed by CI-P and PI-C mixing sequences of Cloisite® 15A ternary nanocomposites. In PC-I mixing sequence, the same shear intensity was applied on the organoclay in both of the extrusion steps and a better dispersion was obtained as well as high tensile strength, modulus and elongation at break values. In fact, the mechanical properties of PI-C mixing sequence are expected to be close to the mechanical properties of All-S mixing sequence. Yet, it was also mentioned in section 4.1 that mixing the organoclay with the polymer matrix in the second extrusion step

limited its dispersion in PI-C mixing sequence. It is better to mix all the components simultaneously rather than adding the organoclay in the second step considering the interactions between the components and the shear intensity in both of the extrusion steps. The organoclay was almost partially delaminated in PA 66 matrix in the mixing sequences of Cloisite® 15A ternary nanocomposites. The dispersion degree was better in CI-P and PC-I mixing sequences. High viscosity of CI-P mixing sequence is supposed to peel the clay platelets apart and the second extrusion step was helpful in uniform dispersion of the organoclay. In PI-C mixing sequence, high viscosity dispersed the clay platelets throughout the matrix but it was not as effective as the case in CI-P mixing sequence resulting from the extrusion of the organoclay with the polymer matrix only once. Better mechanical properties were obtained for PC-I mixing sequence in comparison with CI-P mixing sequence since the interactions between the organoclay and the elastomeric phase may hinder the dispersion of the domains and the reductions in their sizes.

Tensile test results of the mixing sequences of Cloisite® 25A containing ternary nanocomposites were evaluated according to stress-strain curves in Figures 4.41-4.42 and the graphs indicating the values of tensile strength, Young's modulus and percent elongation at break in Figures 4.43-4.45.

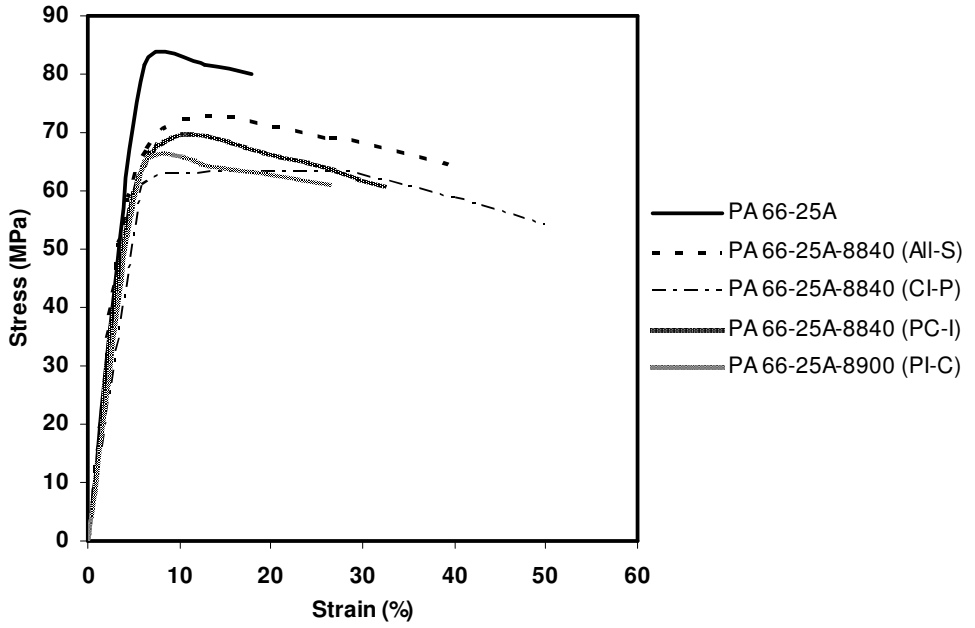

Figure 4.41 Stress-strain curves of PA 66-Cloisite® 25A-Lotader® AX8840 mixing sequences.

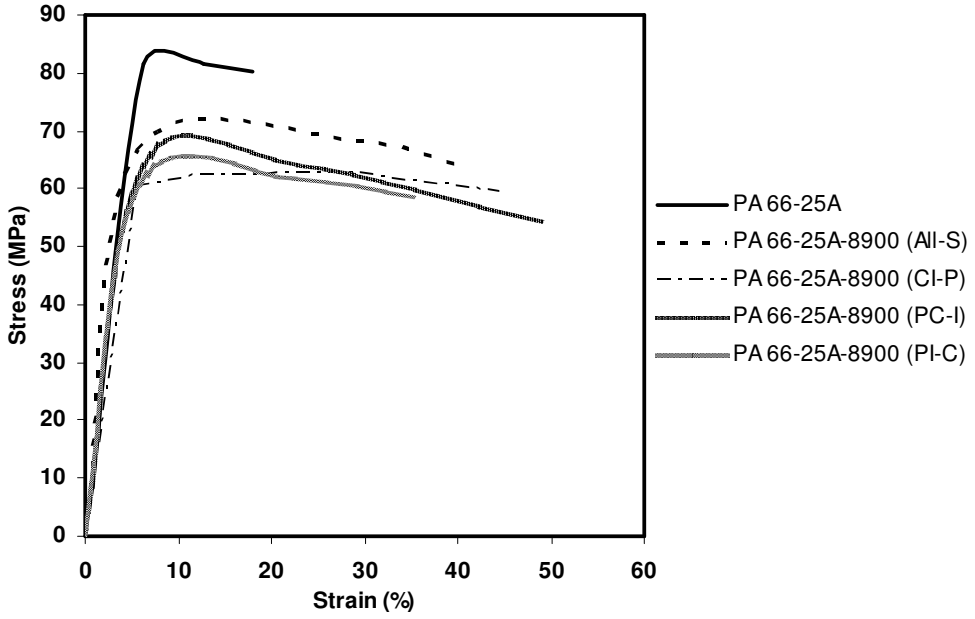

Figure 4.42 Stress-strain curves of PA 66-Cloisite® 25A-Lotader® AX8900 mixing sequences.

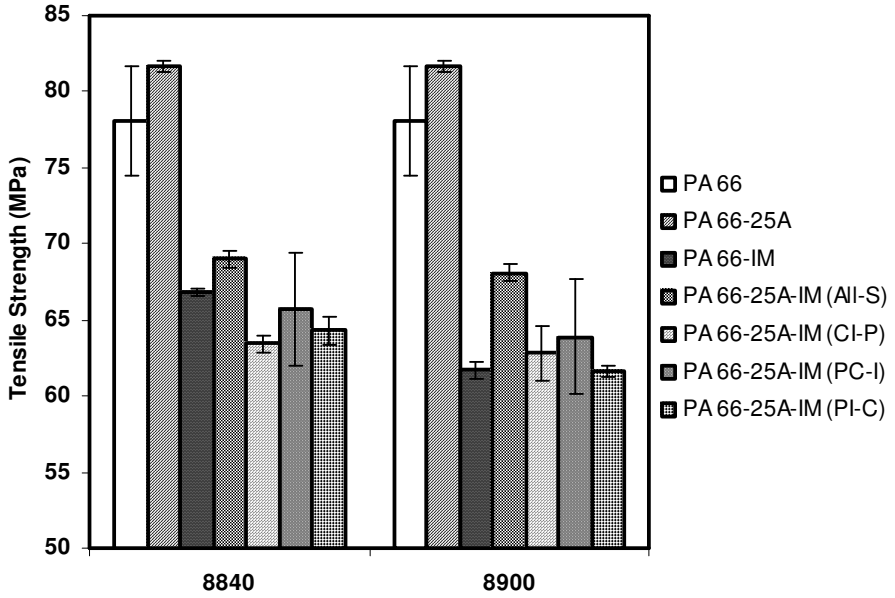

Figure 4.43 Tensile strength of PA 66-Cloisite® 25A-Impact modifier mixing sequences.

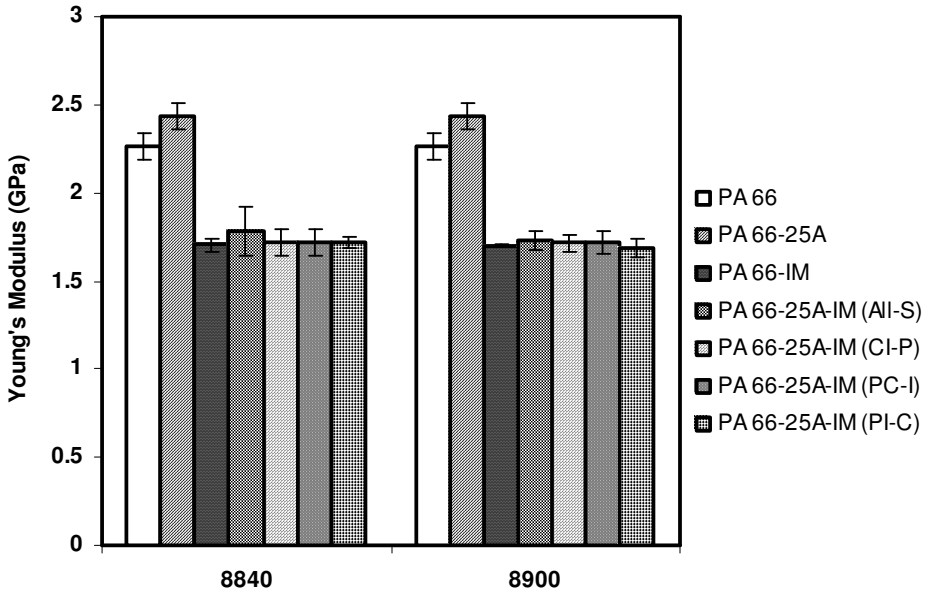

Figure 4.44 Young's modulus of PA 66-Cloisite® 25A-Impact modifier mixing sequences.

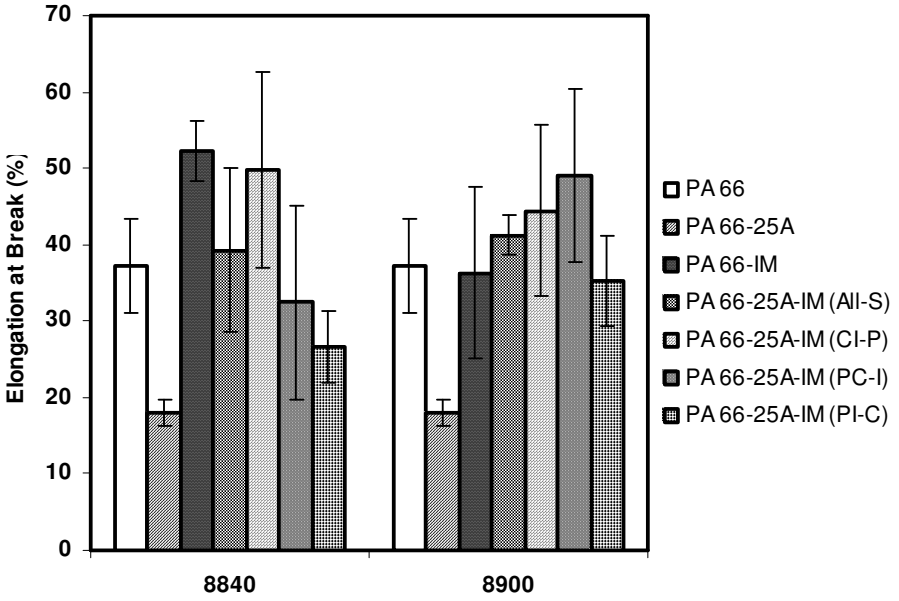

Figure 4.45 Elongation at break (%) of PA 66-Cloisite® 25A-Impact modifier mixing sequences.

The tensile test results of CI-P, PC-I and PI-C mixing sequences of Cloisite® 25A ternary nanocomposites are not also as high as All-S mixing sequence. The highest tensile strength is typically observed for PC-I mixing sequence followed by CI-P and PI-C mixing sequences and generally the highest increases in the elongation at break values are exhibited by PI-C, PC-I and CI-P mixing sequences in increasing order. Young's modulus values of the mixing sequences which do not differ much from each other happened to increase in order of PI-C, CI-P and PC-I mixing sequences.

(PA 66-15A-2210) - (All-S) mixing sequence gave the best results in terms of high Young's modulus, tensile strength and moderate ductility. The tensile test results of All-S mixing sequences of Cloisite® 15A are better than all of the other mixing sequences. It is more favorable to mix all of the components simultaneously since the same shear intensity is applied on all of them and the interactions that can take place between the components are not minimized. The worst results are given by PI-C mixing sequence because the shear intensity

applied on clay in only one extrusion step was not sufficient to disperse the clay platelets uniformly.

4.2.2 Impact Tests

Charpy notched impact strength tests were carried out to measure the toughness of PA 66 nanocomposites and blends.

PA 66 is a tough plastic and has been preferred in many applications requiring impact resistance. Fillets and generous radii are utilized to prevent any notch effect in the design of parts since nylons are notch sensitive and a rapid increase occurs in impact strength upon an increase of larger than 2.5 mm in notch radius [46].

In the case of PA 66 nanocomposites, toughness decreases to a great extent when the organoclay is added into the polymer matrix. Organoclay makes the polymer matrix stiffer by decreasing the molecular mobility as a consequence of its interaction with the polymer matrix and the dispersed volume in the large interface area [64]. Therefore, in this study an elastomeric phase was incorporated into PA 66 matrix both for impact modification and increasing the compatibility between the organoclay and the polymer matrix to aid delamination of the organoclay.

There are lots of factors affecting the toughness including the interactions between the polymer and the elastomer, dispersion and size of the elastomeric domains, interdomain distances and modulus ratio of the matrix and dispersed phase (E_m/E_d). The size of the elastomeric domains is also influenced by the mobility of the interface, melt viscosity of the matrix, shear stresses and surface tension. High shear stresses and melt viscosity are efficient in uniform dispersion of the elastomeric domains and promoting the formation of finer elastomeric domains. In addition to it, the domain size decrease is also dependent upon the stabilization of surface mobility and decrease of interfacial tension by the interactions between the elastomers and PA 66. The domain sizes and interdomain distances must not exceed a certain range to obtain toughness increases [63]. Interdomain distance is affected both by intrinsic parameters

(interfacial adhesion, modulus of the matrix, modulus of the matrix/modulus of the rubber ratio) and extrinsic parameters (impact speed, test temperature and mode of deformation). The critical interdomain distance becomes lower with an increase in the modulus of the matrix and increases as the modulus of the elastomeric phase decreases [67]. The intrinsic parameters are more predominant in determining the toughness of the nanocomposites and blends in this study since the extrinsic parameters were kept constant for all the compositions. Exfoliation of the organoclay also plays an important role in hindering the coalescence of the elastomeric domains by acting as barriers to decrease the matrix mobility and enhance the interfacial adhesion between the elastomeric domains and the polymer matrix [62]. Thus, toughness of the nanocomposites with the exfoliated organoclay is expected to be higher compared to the ones that contain organoclay agglomerations for the same amount of loading.

Impact strength of PA 66 blends is shown in Figure 4.46. Toughness of the blends containing Lotader® AX8900 is higher than the others up to 10 wt% loading. At 15 wt% elastomer content, toughness of Lotader® AX8840 blends exceed the toughness of Lotader® AX8900 blends. The lowest toughness values are mostly obtained for Lotader® 2210 blends at all the compositions. The probability of the reactions that can take place between the matrix and the elastomeric phase is higher for the GMA group in Lotader® AX8840 and Lotader® AX8900 rather than MAH group in Lotader® 2210, although the ester groups of the acrylates in Lotader® AX8900 and Lotader® 2210 structures also contribute to the interfacial adhesion [112]. However, the mechanical test results do not show much difference according to the type of the functional groups of the impact modifiers.

As it can be understood from Figures 4.47-4.48, the toughness values rely on the degree of organoclay and elastomer dispersion in the polymer matrix. The high toughness values obtained for Cloisite® 15A binary nanocomposites are followed by Cloisite® 25A and Cloisite® 30B binary nanocomposites. The organoclay dispersion is better in All-S ternary nanocomposites containing Lotader® AX8900 and Lotader® AX8840 because of increased viscosity as a result of the

interactions at the interface although the domain sizes of all the elastomers are not much different from each other. The highest toughness results are observed for All-S nanocomposites that contain Lotader® 2210 and Lotader® AX8900 as impact modifiers. In spite of the higher possibility of reactions with GMA group in Lotader® AX8840 and Lotader® AX8900, drastic changes did not occur in either the domain size of the elastomeric phase or the toughness values in All-S mixing sequences of PA 66 ternary nanocomposites. There is an intercalated region and the characteristic peaks of the organoclays are almost eliminated in XRD patterns which show that the clay agglomerates were broken down and the polymer chains could penetrate between the clay platelets although they were not completely separated in all All-S mixing sequences. Thus, the toughness of All-S ternary nanocomposites is improved with respect to the binary nanocomposites and it is generally close to the toughness of the blends which contain 5 wt% impact modifier especially for Cloisite® 15A - (All-S) and Cloisite® 25A - (All-S) nanocomposites.

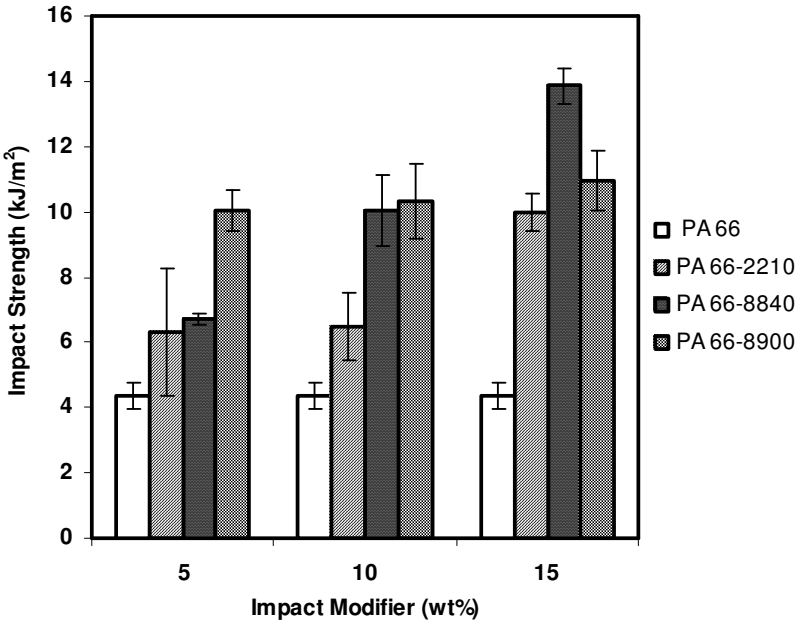

Figure 4.46 Impact strength of PA 66-Impact modifier blends.

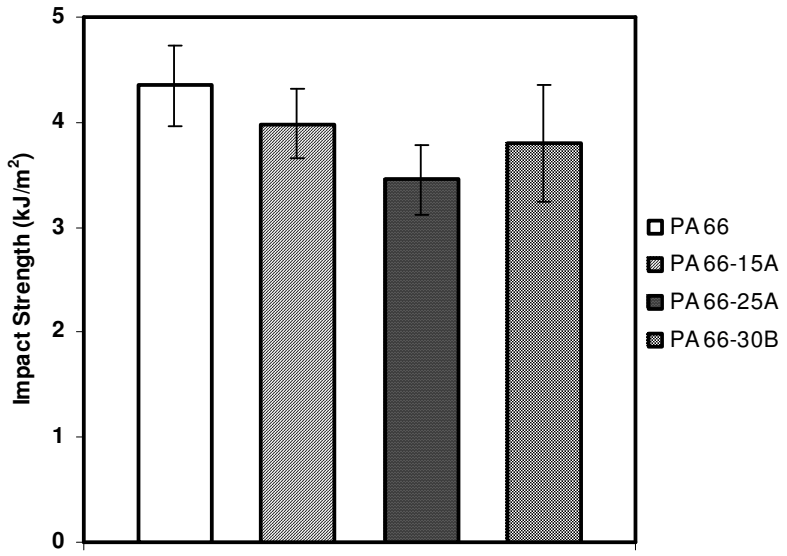

Figure 4.47 Impact strength of PA 66-Organoclay binary nanocomposites.

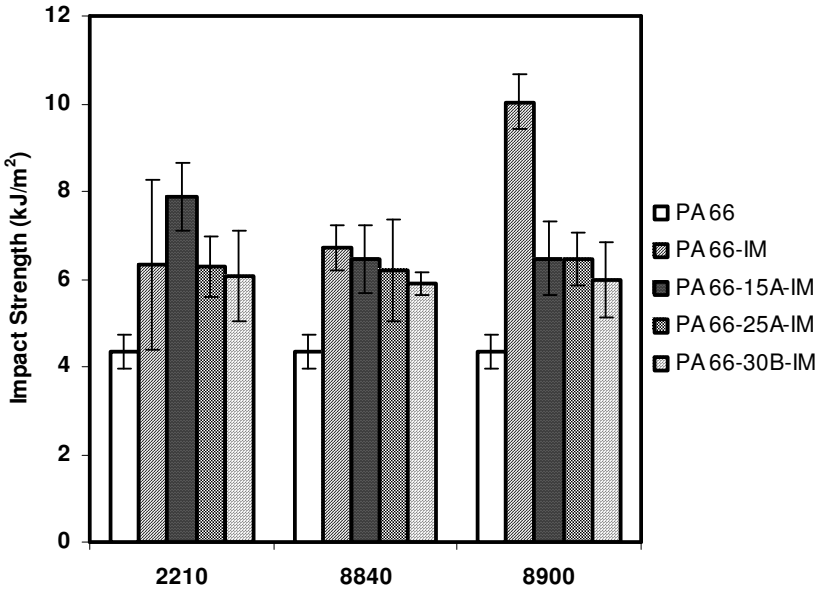

Figure 4.48 Impact strength of PA 66-Organoclay-Impact modifier - (All-S) ternary nanocomposites.

It is obvious from Figures 4.49-4.50 that the average toughness values generally increase in the following order of PI-C, CI-P, PC-I and All-S for the mixing sequences of the ternary nanocomposites. The high viscosity of PI-C mixing sequence did not aid dispersion of the organoclay and increase of the toughness. The sizes of the elastomeric domains are also greater than the domain sizes of All-S mixing sequence although the elastomeric phase was also extruded twice in this mixing sequence. Low impact strength for PI-C mixing sequence arises from the insufficient shear applied on the clay platelets in a single extrusion step. On the other hand, the toughness of PC-I mixing sequence is higher than both PI-C and CI-P mixing sequences. In CI-P mixing sequence, the interactions of the organoclay with the elastomeric phase may retard the improvements in the toughness as the organoclay was first mixed with the elastomer.

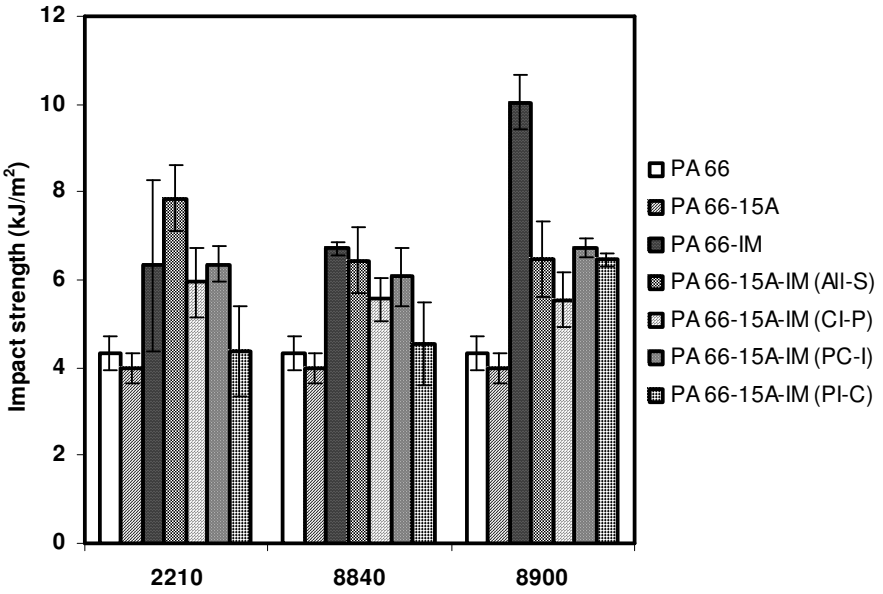

Figure 4.49 Impact strength of PA 66-Cloisite® 15A-Impact modifier mixing sequences.

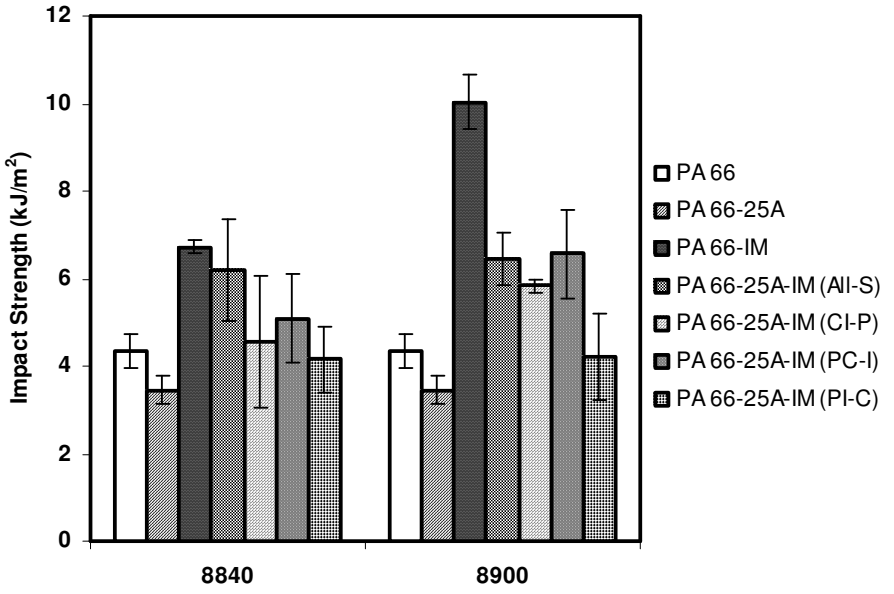

Figure 4.50 Impact strength of PA 66-Cloisite® 25A-Impact modifier mixing sequences.

The organoclay was almost delaminated in All-S mixing sequences of Cloisite® 15A ternary nanocomposites and intercalation of the organoclay occurred in All-S mixing sequences of Cloisite® 25A ternary nanocomposites coupled with a fairly good dispersion. However, changing the addition order lowered the mechanical test results with respect to All-S ternary nanocomposites. This can be associated with the differences in the elastomeric domain sizes, dispersion level of the elastomer and the organoclay and the interactions between the organoclay, elastomeric phase and polymer matrix.

4.2.3 Flexural Tests

Three point bending test was employed to calculate the flexural strength and flexural modulus in this study.

A rod specimen of rectangular cross section is bent until fracture occurs in flexural tests. The top of the specimen is kept in compression as the bottom surface is in tension. The specimen thickness, the bending moment and the

moment of inertia are effective in determining the flexural strength. Flexural strength decreases upon an increase in the volume of the specimen because a crack producing flaw is more probable to occur. Flexural strength and modulus were generally found to be greater than the tensile strength and Young's modulus because the specimen is subjected to both compressive and tensile stresses in three-point bending tests. Maximum tensile stress is applied at the bottom of the specimen surface just below the load application point where fracture occurs [2].

No fracture occurred in the specimens of PA 66 blends, binary and ternary nanocomposites. The test was stopped after the maximum degree of bending was reached for the specimen fixed between two supports. Both flexural strength and modulus are significantly higher than the tensile strength and Young's modulus. This is attributed to the presence of two types of stresses by which the specimen is bent in flexural tests.

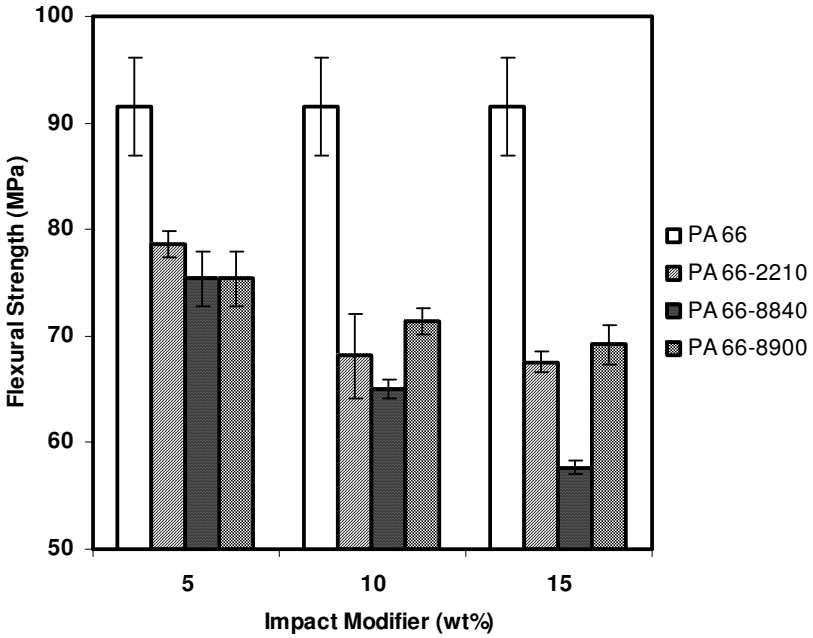

Figure 4.51 Flexural strength of PA 66-Impact modifier blends.

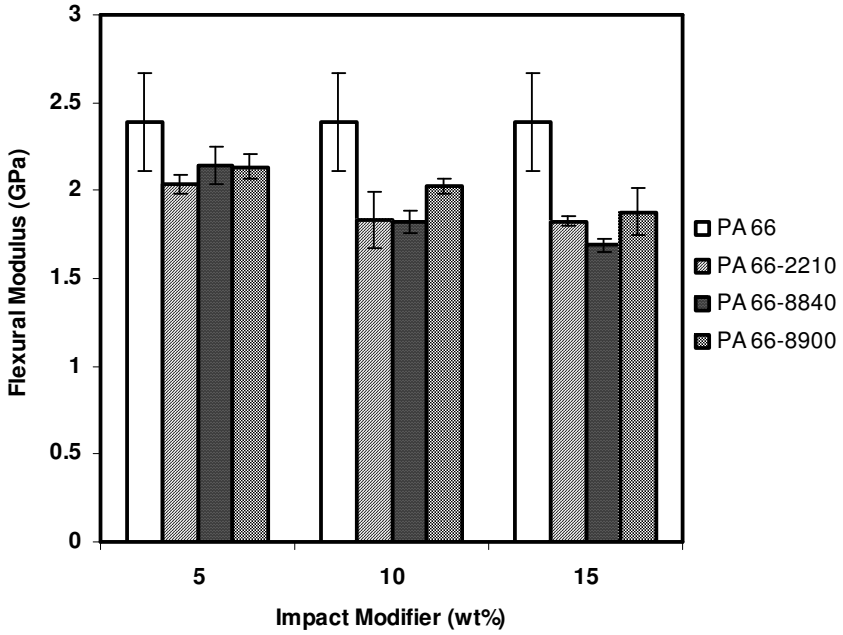

Figure 4.52 Flexural modulus of PA 66-Impact modifier blends.

Flexural strength and modulus values of PA 66 blends and binary nanocomposites are shown in Figures 4.51-4.54. Increases in the elastomer content decreased the flexural strength and modulus as in the tensile tests. The increase in the flexural strength and modulus values is almost similar with the tensile test results. It is observed here once more that the elastomers resulted in a decrease in the strength and modulus values with their increasing content. Flexural test results are also higher for Cloisite® 15A - (All-S) and Cloisite® 25A - (All-S) nanocomposites compared to Cloisite® 30B - (All-S) because of their better degree of organoclay dispersion which stiffens the matrix. Flexural strength and modulus of All-S nanocomposites containing Lotader® 2210 are higher than the ones that have Lotader® AX8840 and Lotader® AX8900 except Cloisite® 30B - (All-S) nanocomposites.

The flexural test results of the addition orders are relevant with the tensile test results in terms of increasing strength and modulus as it can be seen in Figures 4.55-4.60. Flexural strength is mostly higher for CI-P and PC-I mixing sequences with respect to PI-C mixing sequence for Cloisite® 15A ternary nanocomposites

as well as for Cloisite® 25A ternary nanocomposites. The differences between the flexural test results of the mixing sequences of the ternary nanocomposites are not as pronounced as the tensile test results.

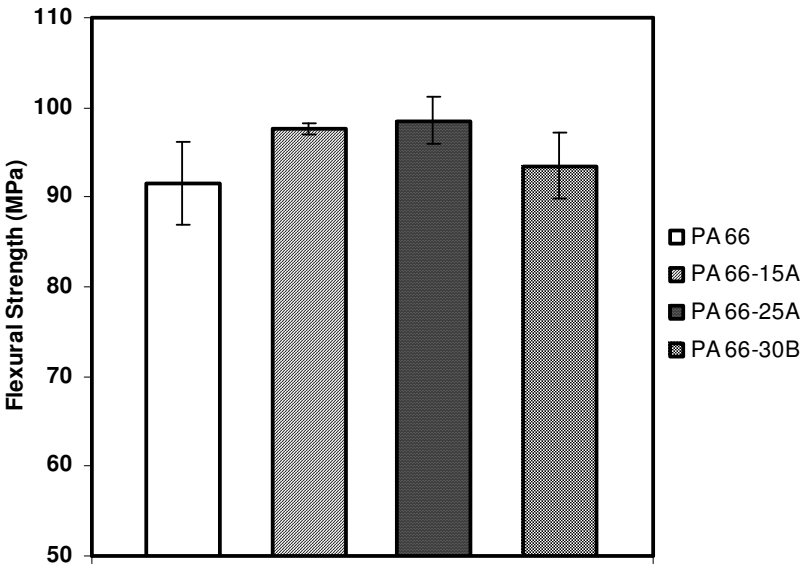

Figure 4.53 Flexural strength of PA 66-Organoclay binary nanocomposites.

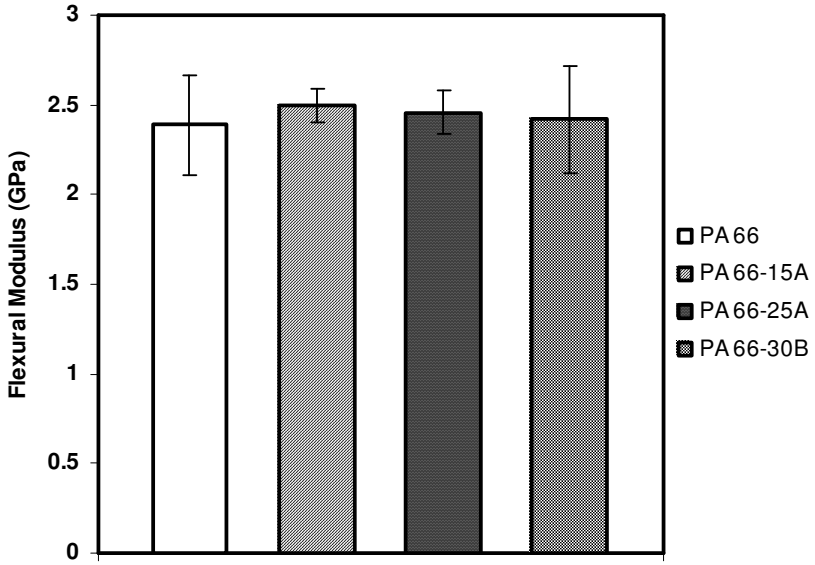

Figure 4.54 Flexural modulus of PA 66-Organoclay binary nanocomposites.

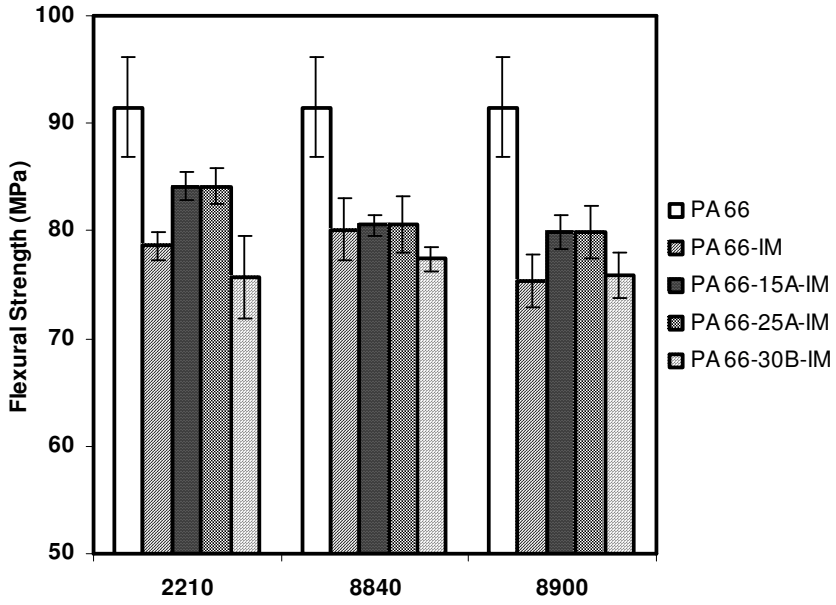

Figure 4.55 Flexural strength of PA 66-Organoclay-Impact modifier - (All-S) ternary nanocomposites.

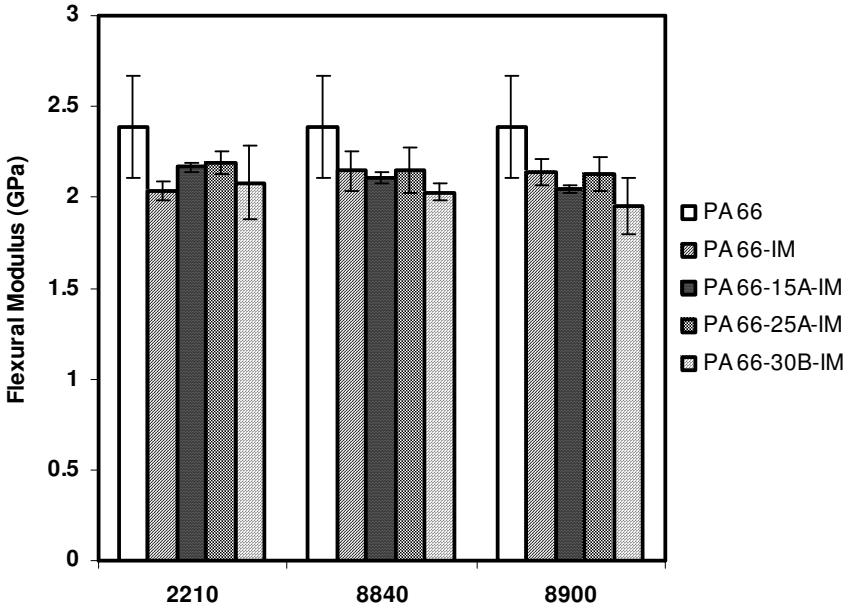

Figure 4.56 Flexural modulus of PA 66-Organoclay-Impact modifier - (All-S) ternary nanocomposites.

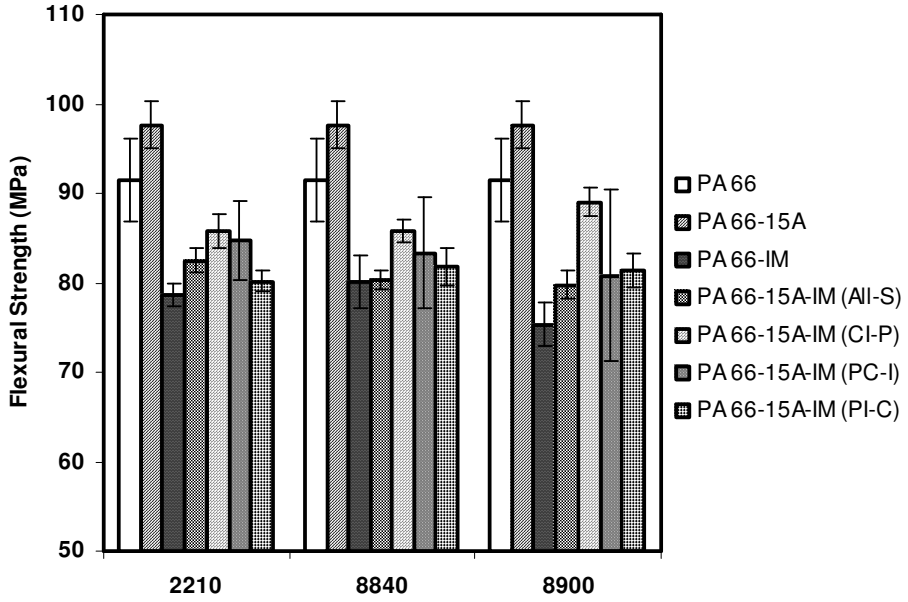

Figure 4.57 Flexural strength of PA 66-Cloisite® 15A-Impact modifier mixing sequences.

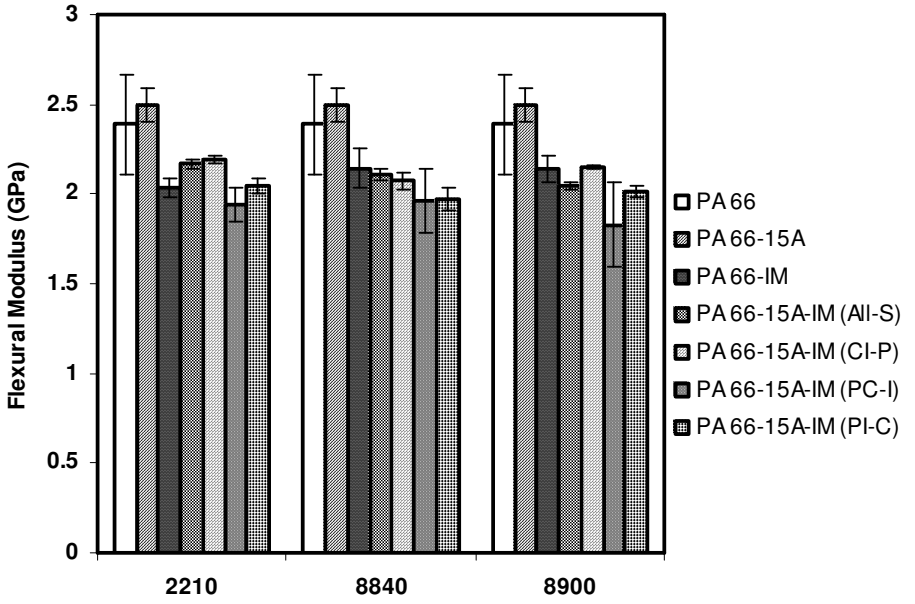

Figure 4.58 Flexural modulus of PA 66-Cloisite® 15A-Impact modifier mixing sequences.

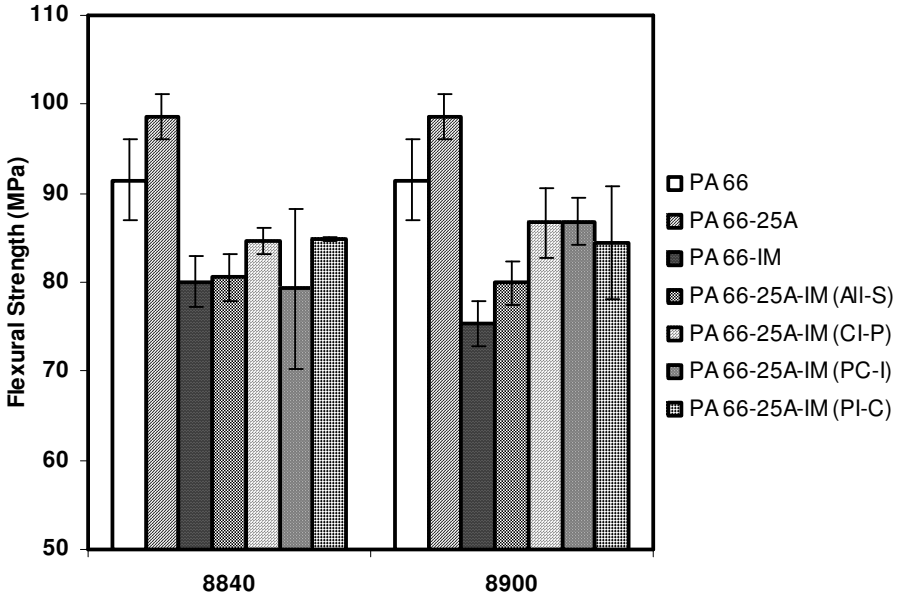

Figure 4.59 Flexural strength of PA 66-Cloisite® 25A-Impact modifier mixing sequences.

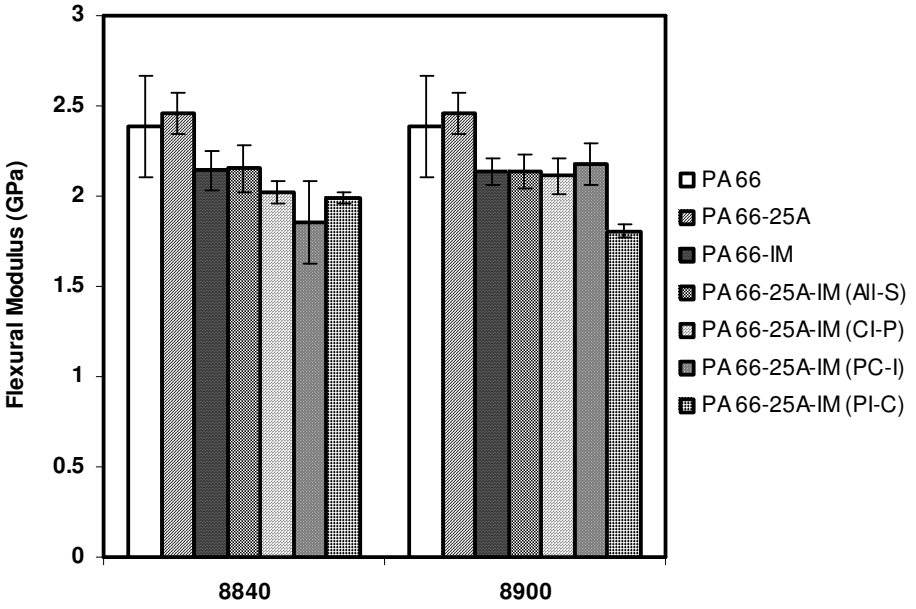

Figure 4.60 Flexural modulus of PA 66-Cloisite® 25A-Impact modifier mixing sequences.

4.3 Hardness Tests

Hardness is a measure of the stiffness of the material [46]. Hardness measurements were carried out by a D shore durameter on an operating stand with a 5 kg load positioned on top of it.

It is obvious from the results in Table 4.3 that addition of the elastomeric material into the polymer matrix decreases the hardness of the nanocomposites whereas the opposite behavior is exhibited upon the increase in the organoclay content. The increase in the hardness mostly indicates the reduction in the ductility of the materials. However, the decrease in the hardness is not so severe in the blends except for the one that has Lotader® 2210 in it. The same trend is encountered in the tensile test results. Blending PA 66 with Lotader® 2210 decreases the tensile strength and the modulus more than the other impact modifiers do.

Table 4.3 Hardness results.

Components	PA 66 Concentration (wt%)	Hardness (D shore)	Standard Deviation
PA 66	100	74.2	1.4
PA 66 – Impact Modifier Blends			
PA 66-2210	95	70.2	1.9
PA 66-2210	90	66.3	0.6
PA 66-2210	85	65.9	0.5
PA 66-8840	95	71.2	4.3
PA 66-8840	90	70.8	3.8
PA 66-8840	85	70.4	0.6
PA 66-8900	95	72.0	5.9
PA 66-8900	90	71.7	2.9
PA 66-8900	85	70.8	3.8
PA 66 Binary Nanocomposites			
PA 66-15A	98	77.3	2.2
PA 66-25A	98	75.7	1.2
PA 66-30B	98	74.7	1.9
PA 66 Ternary Nanocomposites			
(PA 66-15A-2210) - (All-S)	93	74.1	1.1
(PA 66-15A-8840) - (All-S)	93	72.5	1.4
(PA 66-15A-8900) - (All-S)	93	70.8	2.5
(PA 66-25A-2210) - (All-S)	93	73.5	3.0
(PA 66-25A-8840) - (All-S)	93	72.8	4.2
(PA 66-25A-8900) - (All-S)	93	70.6	1.0
(PA 66-30B-2210) - (All-S)	93	72.5	0.9
(PA 66-30B-8840) - (All-S)	93	71.4	0.3
(PA 66-30B-8900) - (All-S)	93	70.3	3.1
Mixing sequences of PA 66 Ternary Nanocomposites			
(15A / 2210)-PA 66 - (CI-P)	93	72.9	2.5
(PA 66 / 15A)-2210 - (PC-I)	93	71.2	0.5
(PA 66 / 2210)-15A - (PI-C)	93	71.0	1.0
(15A / 8840)-PA 66 - (CI-P)	93	71.7	1.3
(PA 66 / 15A)-8840 - (PC-I)	93	73.1	1.5
(PA 66 / 8840)-15A - (PI-C)	93	71.8	1.2
(15A / 8900)-PA 66 - (CI-P)	93	73.7	1.3
(PA 66 / 15A)-8900 - (PC-I)	93	72.7	1.9
(PA 66 / 8900)-15A - (PI-C)	93	72.8	0.4
(25A / 8840)-PA 66 - (CI-P)	93	74.1	1.1
(PA 66 / 25A)-8840 - (PC-I)	93	72.0	2.1
(PA 66 / 8840)-25A - (PI-C)	93	73.5	1.2
(25A / 8900)-PA 66 - (CI-P)	93	72.6	1.8
(PA 66 / 25A)-8900 - (PC-I)	93	72.8	0.9
(PA 66 / 8900)-25A - (PI-C)	93	72.2	1.8

The increase in the hardness results of the nanocomposites is relevant with the dispersion level of the clay platelets in PA 66. Agglomerations of organoclay in certain regions of the specimens lead to decreases in the hardness results, in both binary and ternary nanocomposites of Cloisite® 30B. On the other hand, higher hardness values are obtained for Cloisite® 15A and Cloisite® 25A containing nanocomposites. This stems from uniform dispersion of the organoclay in the polymer matrix in contrast to Cloisite® 30B nanocomposites. The hardness trend observed for binary nanocomposites does not vanish upon addition of the impact modifiers in ternary nanocomposites. The differences between the hardness results of ternary nanocomposites are not large. In fact, the variations are subtle for all the compositions since hardness is susceptible to the amount of additives present in the matrix and it was not affected drastically by delamination of the organoclay especially at low loadings.

Likewise, the differences in the hardness results of different mixing sequences of the nanocomposites of either Cloisite® 15A or Cloisite® 25A are not crucial. Hardness values of the specimens with poor clay dispersion are lower than the specimens wherein the clay was exfoliated. Hardness increases are generally in accordance with the increases in the stiffness of the materials.

4.4 Melt Flow Index Tests

Melt flow index measurements were performed under a load of 0.325 kg at 275°C. Melt flow index is inversely proportional to the melt viscosity and it is affected by the molecular weight of the polymer matrix, the presence of additives and the processing methods. Melt flow index results of all the compositions can be seen in Table 4.4.

Table 4.4 MFI results of all the compositions.

Components	PA 66 Concentration (wt%)	MFI (g/10min)	Standard Deviation
PA 66 (not extruded)	100	16.4	1.6
PA 66 (twice extruded)	100	16.3	1.0
Impact Modifiers			
Lotader® 2210	-	4.8	0.2
Lotader® AX8840	-	5.4	0.2
Lotader® AX8900	-	3.8	0.2
PA 66 – Impact Modifier Blends			
PA 66-2210	95	13.3	0.6
PA 66-2210	90	7.2	1.1
PA 66-2210	85	0.5	0.2
PA 66-8840	95	11.6	3.0
PA 66-8840	90	8.1	0.4
PA 66-8840	85	5.4	0.3
PA 66-8900	95	11.8	1.6
PA 66-8900	90	8.1	0.4
PA 66-8900	85	5.5	0.2
PA 66 Binary Nanocomposites			
PA 66-15A	98	17.7	2.6
PA 66-25A	98	18.7	1.4
PA 66-30B	98	16.6	0.4
PA 66 Ternary Nanocomposites			
(PA 66-15A-2210) - (All-S)	93	11.3	1.0
(PA 66-15A-8840) - (All-S)	93	8.1	0.2
(PA 66-15A-8900) - (All-S)	93	7.0	0.2
(PA 66-25A-2210) - (All-S)	93	11.8	1.0
(PA 66-25A-8840) - (All-S)	93	8.5	0.3
(PA 66-25A-8900) - (All-S)	93	8.5	0.2
(PA 66-30B-2210) - (All-S)	93	16.3	1.9
(PA 66-30B-8840) - (All-S)	93	9.4	0.7
(PA 66-30B-8900) - (All-S)	93	9.3	0.7
Mixing sequences of PA 66 Ternary Nanocomposites			
(15A / 2210)-PA 66 - (CI-P)	93	13.5	1.2
(PA 66 / 15A)-2210 - (PC-I)	93	13.8	0.5
(PA 66 / 2210)-15A - (PI-C)	93	13.7	1.1
(15A / 8840)-PA 66 - (CI-P)	93	11.5	0.9
(PA 66 / 15A)-8840 - (PC-I)	93	13.2	0.7
(PA 66 / 8840)-15A - (PI-C)	93	12.6	1.3
(15A / 8900)-PA 66 - (CI-P)	93	10.2	0.6
(PA 66 / 15A)-8900 - (PC-I)	93	12.7	0.6
(PA 66 / 8900)-15A - (PI-C)	93	10.4	0.5
(25A / 8840)-PA 66 - (CI-P)	93	11.9	0.5
(PA 66 / 25A)-8840 - (PC-I)	93	12.3	0.7
(PA 66 / 8840)-25A - (PI-C)	93	11.8	0.5

Table 4.4 MFI results of all the compositions. (Cont'd)

Components	PA 66 Concentration (wt%)	MFI (g/10min)	Standard Deviation
Mixing sequences of PA 66 Ternary Nanocomposites			
(25A / 8900)-PA 66 - (CI-P)	93	11.1	1.6
(PA 66 / 25A)-8900 - (PC-I)	93	12.3	0.4
(PA 66 / 8900)-25A - (PI-C)	93	11.1	0.4

As it can be seen from MFI results, the melt viscosity of extruded PA 66 is nearly the same as the one that is not extruded. A dramatic decrease did not occur in the molecular weight of the polymer matrix because of being subjected to high shear intensity twice at high processing temperatures. On the other hand, the presence of impact modifiers in the matrix increased the viscosity substantially. The expected trend is observed in the results because an increase in the weight percent of the elastomeric material would inevitably cause an increase in the viscosity values due to their higher viscosity compared to the polymer in the beginning.

The clays are thought to impart resistance to flow at low shear rates and impede the flow of the molten polymer. As a result, viscosity increases with the increase in filler concentration depending on the size and shape of the filler. However, incorporation of the organoclay into the polymer matrix increased the melt flow index values in binary nanocomposites. The reduction in viscosity may have been caused by the slip between PA 66 matrix and the dispersed clay platelets during high shear flow [8,115]. Molecular weight decreases could not have caused any substantial change in the viscosity because the melt viscosity of polyamide that was not extruded and the one that was twice extruded is almost the same. In spite of the decrease in shear intensity resulting from low viscosity that is critical on clay dispersion, a wide range of processibility options can be provided by the low melt viscosity of the polymer matrix containing fillers [8].

In all the mixing sequences, melt viscosity was found to be higher for the nanocomposites containing Lotader® AX8840 and Lotader® AX8900 compared to the ones with Lotader® 2210. Increases in the melt viscosity can be

interrelated with the results of XRD analysis. It is observed that the dispersion of the organoclay is better when PA 66 is mixed with Lotader® AX8840 and Lotader® AX8900. The profound effect of melt viscosity on the uniform dispersion of clay is noteworthy here in terms of increasing the shear intensity applied on the clay platelets.

Melt flow index values are lower for all the compositions of PI-C and CI-P mixing sequences. High melt viscosities of PI-C mixing sequences did not give rise to homogeneous dispersion of the organoclay in contrast to CI-P mixing sequences that displayed almost exfoliated structure. Melt flow index values of PC-I mixing sequences are slightly larger than the other mixing sequences. However, the melt viscosities are close to each other for all the mixing sequences. Impact modifier effect is more pronounced on the melt viscosity of all the mixing sequences since their melt viscosity is higher than the extruded PA 66 and binary PA 66 nanocomposites.

4.5 Differential Scanning Calorimetry Analysis

Crystallization of PA 66 nanocomposites is composed of two nucleation mechanisms that are called as homogeneous and heterogeneous nucleation. Low temperatures are required to form stable nucleation by chain aggregation below the melting point for homogeneous nucleation whereas heterogeneous nucleation begins as soon as the crystallization temperature is reached. Crystallization proceeds through heterogeneous nucleation in PA 66 nanocomposites because of the presence of many montmorillonite layers which act as active sites for nucleation [99]. Therefore, the temperature to reach the maximum crystallization rate is lower for pure PA 66 than for PA 66 nanocomposites. Increasing the degree of supercooling promotes the nucleation effect while it is counteracted by the increases in the viscosity. Nucleation is followed by the diffusion by which a polymer segment is transported to a growing crystal [61]. Crystallinity of the polyamide phase in all the combinations was determined by DSC analysis and the results are given below in Table 4.5. DSC thermograms are presented in Appendix C.

Table 4.5 Thermal properties of all the compositions.

Components	PA 66 Concentration (wt%)	T_m (°C)	ΔH_f (J/g)	Crystallinity (%)
PA 66	100	262.96	52.7	25.6
PA 66 – Impact Modifier Blends				
PA 66-2210	95	262.55	44.5	21.6
PA 66-2210	90	262.05	47.9	23.2
PA 66-2210	85	261.11	49.1	23.8
PA 66-8840	95	261.92	47.2	22.9
PA 66-8840	90	261.22	47.3	23.0
PA 66-8840	85	262.01	44.9	21.8
PA 66-8900	95	262.38	47.8	23.2
PA 66-8900	90	262.85	48.1	23.4
PA 66-8900	85	261.83	47.9	23.3
PA 66 Binary Nanocomposites				
PA 66-15A	98	263.41	50.9	24.7
PA 66-25A	98	261.78	48.4	23.5
PA 66-30B	98	261.51	49.1	23.9
PA 66 Ternary Nanocomposites				
(PA 66-15A-2210) - (All-S)	93	262.26	47.7	23.2
(PA 66-15A-8840) - (All-S)	93	262.16	48.8	23.7
(PA 66-15A-8900) - (All-S)	93	262.45	46.0	22.3
(PA 66-25A-2210) - (All-S)	93	261.93	46.6	22.6
(PA 66-25A-8840) - (All-S)	93	262.74	44.6	21.7
(PA 66-25A-8900) - (All-S)	93	261.94	52.1	25.3
(PA 66-30B-2210) - (All-S)	93	261.74	51.9	25.2
(PA 66-30B-8840) - (All-S)	93	262.14	48.4	23.5
(PA 66-30B-8900) - (All-S)	93	261.75	52.0	25.3
Mixing sequences of PA 66 Ternary Nanocomposites				
(15A / 2210)-PA 66 - (CI-P)	93	262.72	43.7	21.2
(PA 66 / 15A)-2210 - (PC-I)	93	262.14	45.2	21.9
(PA 66 / 2210)-15A - (PI-C)	93	261.71	47.6	23.1
(15A / 8840)-PA 66 - (CI-P)	93	262.33	46.0	22.3
(PA 66 / 15A)-8840 - (PC-I)	93	262.00	53.7	26.1
(PA 66 / 8840)-15A - (PI-C)	93	261.56	46.0	22.3
(15A / 8900)-PA 66 - (CI-P)	93	263.72	52.4	25.5
(PA 66 / 15A)-8900 - (PC-I)	93	262.80	56.3	27.3
(PA 66 / 8900)-15A - (PI-C)	93	262.57	45.3	22.0
(25A / 8840)-PA 66 - (CI-P)	93	262.08	49.5	24.0
(PA 66 / 25A)-8840 - (PC-I)	93	263.03	55.7	27.0
(PA 66 / 8840)-25A - (PI-C)	93	261.82	47.2	22.9
(25A / 8900)-PA 66 - (CI-P)	93	263.15	51.2	24.8
(PA 66 / 25A)-8900 - (PC-I)	93	262.46	47.6	23.1
(PA 66 / 8900)-25A - (PI-C)	93	261.89	59.0	28.7

Degree of crystallinity was found to be neither dependent on the organoclay content nor on the elastomer content in PA 66 nanocomposites. Significant variations are not observed in the crystallinity results. Although the organoclay content was kept constant in this study, increasing it could have caused agglomeration that retards the catalyst effect of the organoclay for nucleation. The effect of the organoclay content on the crystallinity has been investigated previously and it was seen that clay contributed only to the rise of the crystallization temperature and reduction of the crystallite sizes [7,96,98]. Processing factors, the orientation of silicate layers, their effect on polymer conformation and morphology and dispersion of fillers in the matrix are all the factors that influence the correlation between property and structure of nanocomposites predominantly [61]. However, no correlation could be made between the mechanical properties of PA 66 nanocomposites and crystallinity here. Variations in the mixing sequences did not also significantly contribute to any increase in crystallinity. The changes in the properties are probably due to the presence of the organoclay and the impact modifier in the polymer matrix rather than the subtle changes that occur in the crystallinity upon addition of these materials.

CHAPTER 5

CONCLUSIONS

Binary PA 66 nanocomposites, ternary PA 66 nanocomposites and PA 66 blends were produced by melt compounding method in this study. The concentration of the components including the impact modifiers and organoclays, their types and addition orders are related with the morphology, mechanical, thermal and rheological properties of the nanocomposites.

The profound effect of the uniform organoclay dispersion on the mechanical properties is obviously observed in the nanocomposites containing Cloisite® 15A in comparison with the other binary nanocomposites at 2 wt% organoclay loading. Incorporation of the elastomers aided dispersion of the organoclay despite the fact that the degree of intercalation varied slightly. High viscosity of the elastomers resulted in an increase in the shear intensity and broke the clay agglomerates down into smaller tactoids, but the characteristic peak of the organoclay is also visible in XRD patterns as well as the small shoulders that are shifted to smaller angles which is an indication of the presence of the clay platelets that were not completely separated by the polymer chains especially in Cloisite® 30B - (All-S) nanocomposites. The mechanical test results of the binary nanocomposites are close to each other. This is also valid for the ternary nanocomposites of the same mixing sequence because of the fact that the organoclays were mostly well dispersed in almost all the nanocomposites. The mixing sequences were varied using the results obtained from XRD patterns and the mechanical tests including tensile, flexural, impact and hardness tests. Higher tensile, impact and flexural test results are obtained for the nanocomposites wherein the organoclay dispersion was better. Thus, the organoclay content was determined as 2 wt% and the impact modifier content as 5 wt% not to cause any clay agglomerates or result in decreases in the mechanical test results. Flexural test results were found to be in harmony with the tensile test results. Delamination of the organoclay also aided the increases in the impact strength of the nanocomposites. Hardness increased in a regular fashion with the increase in

the stiffness, but hardness results are not as sensitive to the variation of the addition orders as the other mechanical test results.

(PA 66-15A-2210) - (All-S) mixing sequence exhibits the most improved mechanical properties among all the mixing sequences. This arises from the difference in the addition order of the components which affects the dispersion of the elastomeric phase, the domain sizes and the interactions between the constituents.

The elastomeric domain sizes of All-S mixing sequences are smaller than the others. It can be ascribed to the extrusion of all the components twice together. On the other hand, both the mechanical properties and delamination of the organoclay is poor in PI-C mixing sequences besides their high viscosity. The domain size of the elastomers in PI-C mixing sequence is close to CI-P and PC-I mixing sequences in spite of being extruded twice. The shear intensity applied in a single extrusion step was insufficient to tear the clay platelets apart in this mixing sequence. The coalescence of the domains could not be prevented without the organoclay which functions as barrier to impede the coalescence of elastomeric domains by immobilizing the matrix. The mechanical test results are higher for PC-I mixing sequence since some of the organoclay may have been retained in the elastomeric phase in CI-P mixing sequence and the impact toughening function of the elastomers can diminish. Interactions between the elastomeric phase and the organoclay may inhibit the break up of the elastomeric domains. Therefore, the domain sizes of PC-I and CI-P mixing sequences are close to each other.

MFI test results indicate that melt flow index values are lower in the presence of Lotader® AX8840 and Lotader® AX8900 like the decreases in the intensities of the characteristic clay peaks in their XRD patterns. Neither the increases in d-spacings of the organoclay nor the increases in their mechanical properties are higher than the nanocomposites containing Lotader® 2210. The domain sizes formed by all of these impact modifiers are not also much different from each other. The presence of GMA functional group in Lotader® AX8840 and Lotader® AX8900 that is capable of reacting with the acid and the amine ends did not

improve the interactions at the interface any further compared to MAH group in Lotader® 2210 that can react with the amine ends of PA 66. The acrylates in Lotader® 2210 and Lotader® AX8900 may have contributed to the reactions between the functional groups of the polymer matrix, the impact modifier and the organic modifier. Even though there are too many possible reactions that can occur between the polymer matrix and the elastomers, crosslinking effects were not faced with.

Melting points and crystallinities were not affected much upon addition of the organoclay and the elastomers. Thus, the changes in the crystallinity did not play an important role in the changes of the mechanical properties of PA 66 nanocomposites.

REFERENCES

1. Chawla K., "Composite Materials Science and Engineering", 2nd Ed., Springer - Verlag, New York, 1998.

2. Callister Jr., William D., "Materials Science and Engineering: An Introduction", 6th Ed., John Wiley & Sons, New York, 2003.

3. Rosen S.L., "Fundamental Principles of Polymeric Materials", John Wiley & Sons, New York, 1982.

4. Kroschwitz J.I., Mark H.F., "Encyclopedia of Polymer Science and Technology", 3rd Ed., Wiley Interscience, Hoboken, N.J., 2003.

5. Fornes T.D., Yoon P.J., Keskkula H., Paul D.R., Polymer, 42, 9929-9940, 2001.

6. Jang B.N., Wang D., Wilkie C.A., Macromolecules, 38, 6533-6543, 2005.

7. Liu X., Wu Q., Berglund L. A., Polymer, 43, 4967-4972, 2002.

8. Cho J.W., Paul D.R., Polymer, 42, 1083-1094, 2001.

9. Fornes T.D., Yoon P.J., Paul D.R., Polymer, 44, 7545-7556, 2003.

10. Matthews F.L., Rowlings R.D., "Composite Materials, Engineering & Science", Chapman & Hall, London, New York, 1994.

11. Rodriguez F., Cohen C., Ober C., Archer A.L., "Principles of Polymer Systems", Taylor & Francis, New York, 2003.

12. Strong A.B., "Fundamentals of Composites Manufacturing: Materials, Methods and Applications", Society of Manufacturing Engineers, Publications Development Dept., Reference Publications Division, Dearborn, Michigan, 1989.

13. Mazumdar S.K., "Composites Manufacturing", CRC Press, Boca Raton, Fla., 2002.

14. S.Deutsch 23rd National SAMPE Symposium, 34, 1978.

15. Schier J.F, Juergens R.J., “Astronautics and Aeronautics”, 44, 1983.

16. Daniel I., Ishai O., “Engineering Mechanics of Composite Materials”, Oxford University Press, New York, 1994.

17. Strong A B., “High Performance and Engineering Thermoplastic Composites”, Technomic Pub. Co., Lancaster, Pennsylvannia, 1993.

18. Alexandre M., Dubois P., Materials Science and Engineering, 28, 1-63, 2000.

19. Giannelis E.P., Advanced Materials, 8, 29-35, 1996.

20. Vlasveld D.P.N, Vaidya S.G., Bersee H.E.N, Picken S.J, Polymer, 46, 3452-3461, 2005.

21. Mark J.E., Polymer Engineering and Science, 36, 2905-2920, 1996.

22. Reynaud E., Gauthier C., Perez J., Revue De Metallurgie-Cahiers D Informations Techniques, 96, 169-176, 1999.

23. von Werne T., Patten T.E., Journal of the American Chemical Society, 121, 7409-7410, 1999.

24. Herron N., Thorn D.L., Advanced Materials, 10, 1173-1184, 1998.

25. Calvert P., “Potential Applications of Nanotubes, in: T.W. Ebbesen (Ed.), Carbon Nanotubes, CRC Press, Boca Raton, FL, 1997.

26. Favier V., Canova G.R., Shrivastava S.C., Cavaille J.Y., Polymer Engineering and Science, 37, 1732-1739, 1997.

27. Chazeau L., Cavaille J.Y., Canova G., Dendievel R., Boutherin B., Journal of Applied Polymer Science, 71, 1797-1808,1999.

28. Xie W., Gao Z., Hunter D., Singh A., Vaia R., Chemistry of Materials, 13, 2979-2990, 2001.

29. Aranda P., Ruiz-Hitzky E., Chemistry of Materials, 4, 1395-1403, 1992.

30. Ray S.S., Okamoto M., Progress in Polymer Science, 28, 1539-1641, 2003.

31. Greenland D.J., Journal of Colloid and Interface Science, 18, 647-664, 1963.

32. Blumstein A., Journal of Polymer Science. Part A, Polymer Chemistry, 3, 2665-2673, 1965.

33. Krishnamoorti R., Vaia R.A, Giannelis E.P., Chemistry of Materials, 8, 1728-1734, 1996.

34. Lebaron P.C., Wang Z., Pinnavaia T., Journal of Applied Clay Science, 15, 11-29, 1999.

35. Lagaly G., Solid State Ionics, 22, 43-51, 1986.

36. Dennis H.R., Hunter D.L., Chang D., Kim S., White J.L., Cho J.W., Paul D.R., Polymer, 42, 9513-9522, 2001.

37. Sinha R.S., Okamoto K., Okamoto M., Macromolecules, 36, 2355-2367, 2003.

38. Vaia R.A, Giannelis E.P., Macromolecules 30, 7990-7999, 1997.

39. Burnside S.D., Giannelis E.P., Chemistry of Materials, 7, 1597-1600, 1995.

40. Usuki A., Kojima Y., Kawasumi M., Okada A., Fukushima Y., Kurauchi T., Kamigaito O., Journal of Materials Research, 8, 1179-1183, 1993.

41. Vlasveld D.P.N., Parlevliet P.P., Bersee H.E.N., Picken S.J., Composites. Part A, Applied Science and Manufacturing, 36, 1-11, 2005.

42. Lee D.C., Jang L.W., Journal of Applied Polymer Science, 61, 1117-1122, 1996.

43. Noh M.W., Lee D.C., Polymer Bulletin, 42, 619-626, 1999.

44. Lee D.C., Jang L.W., Journal of Applied Polymer Science, 68, 1997-2005, 1998.

45. Won J.C., Fulchıron R., Douillard A., Chabert B., Varlet J., Chomier D., Journal of Applied Polymer Science, 80, 1021-1029, 2001.

46. Kohan M.I., "Nylon Plastics", John Wiley & Sons, New York, 1973.

47. Elzein T., Brogly M., Castelein G., Schultz J., Journal of Polymer Science. Part B, Polymer Physics, 40, 1464-1476, 2002.

48. Seymour B.S., Carraher C.E., "Structure and Property Relationships in Polymers", Plenum Press, New York, 1984.

49. Vasanthan N., Kotek R., Jung D.W., Shin D., Tonelli A.E., Salem D.R., Polymer, 43, 4077-4085, 2004.

50. Kang X., He S., Zhu C., Lu L.W.L., Guo J., Journal of Applied Polymer Science, 95, 756-763, 2005.

51. Lu Y., Zhang Y., Zhang G., Yang M., Yan S., Shen D., Polymer, 45, 8999-9009, 2004.

52. Yu Z.Z., Yang M., Zhang Q., Zhao C., Mai Y.W., Journal of Polymer Science. Part B, Polymer Physics, 41, 1234-1243, 2003.

53. Chavarria F., Paul D.R., Polymer, 45, 8501-8515, 2004.

54. Karabulut M., "Production and Characterization of Nanocomposite Materials from Recycled Thermoplastics", MS Thesis, METU, 2003.

55. Liu X., Wu Q., Berglund L.A., Polymer, 43, 4967-4972, 2002.

56. Fornes T.D., Hunter D.L., Paul D.R., Macromolecules, 37, 1793-1798, 2004.

57. Fornes T.D., Yoon P.J., Hunter D.L., Keskkula H., Paul D.R., Polymer, 43, 5915-5933, 2002.

58. Vanderhart D.L., Asano A., Gilman J.W., Macromolecules, 34, 3819-3822, 2001.

59. Tanaka G., Goettler L.A., Polymer, 43, 541-553, 2002.

60. Okada A., Usuki A., Materials Science & Engineering. C, Biomimetic Materials, Sensors and Systems, 3, 109-115, 1995.

61. Dasari A., Yu Z.Z., Yang M., Zhang Q.X., Xie X.L., Mai Y.W, Composites Science and Technology, 66, 3097-3114, 2006.

62. Hassan A., Othman N., Wahit M.U., Wei L.J., Rahmat A.R., Ishak Z.A.M., Macromolecular Symposia, 239, 182-191, 2006.

63. Contreras V., Cafiero M., Da Silva S., Rosales C., Perera R., Matos M., Polymer Engineering and Science, 46, 1111-1120, 2006.

64. Tjong S.C., Bao S.P., Journal of Polymer Science. Part B, Polymer Physics, 43, 585-595, 2005.

65. Okada O., Keskkula H., Paul D.R., Polymer, 41, 8061-8074, 2000.

66. Baldi F., Bignotti F., Tieghi G., Riccó T., Journal of Applied Polymer Science, 99, 3406-3416, 2006.

67. Gonzáles I., Eguiazábal J.I., Nazábal J., Composites Science and Technology, 66, 1833-1843, 2006.

68. Chiu F.C., Lai S.M., Chen Y.L., Lee T.H., Polymer, 46, 11600-11609, 2005.

69. Huang J.J., Keskkula H., Paul D.R., Polymer 47, 624-638, 2006.

70. Huang J.J., Keskkula H., Paul D.R., Polymer 47, 639-651, 2006.

71. Karayannidis G.P., Bikiaris D.N., Papageorgiou G.Z., Advances in Polymer Technology, 21,153-163, 2002.

72. Thomas S., Groeninckx G., Polymer, 40, 5799-5819, 1999.

73. Tedesco A., Krey P. F., Barbosa R. V., Mauler R.S., Polymer International, 51, 105-110, 2001.

74. SFSU-Extrusion, "online.sfsu.edu/~jge/html/topofchachapter5.html", last accessed; October 2006.

75. Middleman S., "Fundamentals of Polymer Processing", McGraw- Hill, 1977.

76. Salamone J.C., "Polymeric Material Encyclopedia", CRC Press, New York, 1996.

77. Shah A., Gupta M., "Comparison of the Flow in Co-rotating and Counter rotating Twin- Screw Extruders", Antec, 443-447, 2004.

78. Anderson P., "Twin-Screw Extruders", 83-87, Society of Plastics Engineers.

79. ISO 527, International Organization for Standardization - Plastics, "Determination of Tensile Properties" & "Test Conditions for Moulding and Extrusion Plastics".

80. Seymour R.B., "Polymer Chemistry: An Introduction", 4th ed., Marrel Dekker, New York, 1996.

81. The Ohio State University, MSE 205 Directory, Lecture Notes, "http://www.matsceng.ohio-state.edu/mse205/mse_205/", (Chapter 14 & 15), last accessed; January 2007.

82. ISO 179, International Organization for Standardization - Plastics, "Determination of Charpy Impact Properties".

83. Billmeyer F.W., "Textbook of Polymer Science", John Wiley & Sons, New York, 1984.

84. ISO 178, International Organization for Standardization - Plastics, “Determination of Flexural Properties”.

85. MatWeb, Material Property Data, “http://www.matweb.com/reference/flexuralstrength.asp”, last accessed; January 2007.

86. ISO 868, International Organization for Standardization - Plastics & Ebonite, ”Determination of Indentation Hardness by means of a Durometer (Shore Hardness)”.

87. Danmarks Tekniske Universitet, Institut for Kemiteknik, DSC, “http://hekabe.kt.dtu.dk/~vigild/2005_04_melitek/index.html”, last accessed; March 2006.

88. Alyamac E., “Impact Modified PET-Organoclay Nanocomposites”, MS thesis, METU, 2004.

89. Greg Beaucage & Research Group Page, Chemical and Materials Engineering University of Cincinah, Polymer Analysis, X-ray diffraction, “http://www.eng.uc.edu/~gb.eaucag/Classes/Analysis/Chapter7.html”,last accessed; January 2007.

90. ISO 1133, International Organization for Standardization-Plastics, ”Determination of Melt Volume Flow Rate (MVR) - Melt Mass Flow Rate (MFR) of Thermoplastics Materials.

91. Yu Z.Z., Yan C., Yang M., Mai Yiu W., Polymer International, 53, 1093-1098, 2004.

92. Liu X., Wu Q., Macromolecular Materials and Engineering, 287, 180-186, 2002.

93. Shen L., Phang I.Y., Chen L., Liu T., Zeng K., Polymer, 45, 3341-3349, 2004.

94. Gyoo P.M., Venkataramani S., Kim S.C., Journal of Applied Polymer Science, 101, 1711-1722, 2006.

95. Dasari A., Yu Z.Z., Mai Y.W., Polymer, 46, 5986-5991, 2005.

96. Qin H., Su Q., Zhang S., Zhao B., Yang M., Polymer, 44, 7533-7538, 2003.

97. Mehrabzadeh M., Kamal M., Polymer Engineering and Science, 44, 1151-1161, 2004.

98. Liu X., Wu Q., Zhang Q., Mo Z., Journal of Polymer Science. Part B, Polymer Physics, 41, 63-67, 2003.

99. Zhang Q.X., Yu Z.Z., Yang M., Ma J., Mai Y.W., Journal of Polymer Science. Part B, Polymer Physics, 41, 2861-2869, 2003.

100. Hedicke K., Wittich H., Mehler C., Gruber F., Altstädt V., Composites Science and Technology, Article in Press, 2005.

101. Nair S.V., Goettler L.A., Lysek B.A., Polymer Engineering and Science, 42, 1872-1882, 2002.

102. Tomova D., Radusch H.J., Polymers for Advanced Technologies, 14, 19-26, 2003.

103. PolyOne Company, “http://www.polyone.com”, last accessed; January 2007.

104. Southern Clay Products, “http://www.scprod.com”, last accessed; January 2007.

105. Arkema Chemicals, “http://www.atofinachemicals.com”, last accessed; January 2007.

106. Morgan A., Gilman J., Journal of Applied Polymer Science, 87, 1329-1338, 2003.

107. Xu W., Liang G., Wang W., Tang S., He P., Pan W.P., Journal of Applied Polymer Science, 88, 3225-3231, 2003.

108. Chang J., An Y.U., Journal of Polymer Science. Part B, Polymer Physics, 40, 670-677, 2002.

109. Finnigan B., Martin D., Halley P., Truss R., Campell K., Journal of Applied Polymer Science, 97, 300-309, 2005.

110. Borse K.N., Kamal M.R., Polymer Engineering and Science, 46, 1094-1103, 2006.

111. Lee M.H., Dan C.H., Kim J.H., Cha J., Kim S., Hwang Y., Lee C.H., Polymer, 47, 4359-4369, 2005.

112. Raval H., Devi S., Singh Y.P., Mehta M.H., Polymer, 32, 493-500, 1991.

113. Paul D.R., Zeng Q.H., Yu A.B., Lu G.Q., Journal of Colloid and Interface Science, 292, 462-468, 2005.

114. Kelnar I., Kotek J., Kaprálková L., Munteanu B.S., Journal of Applied Polymer Science, 96, 288-293, 2005.

115. Gonzáles I., Eguiazábal J.I., Nazábal J., Polymer, 46, 2978-2985, 2005.

APPENDIX A

Mechanical Test Results

Table A.1 Tensile strength data and standard deviations for all the compositions.

Components	PA 66 Concentration (wt%)	Tensile Strength (MPa)	Standard Deviation
PA 66	100	78.1	3.6
PA 66 – Impact Modifier Blends			
PA 66-2210	95	66.0	0.6
PA 66-2210	90	58.4	1.7
PA 66-2210	85	53.9	0.4
PA 66-8840	95	66.8	0.3
PA 66-8840	90	59.4	0.4
PA 66-8840	85	56.3	0.4
PA 66-8900	95	61.7	0.6
PA 66-8900	90	60.7	0.7
PA 66-8900	85	59.4	0.9
PA 66 Binary Nanocomposites			
PA 66-15A	98	82.8	0.3
PA 66-25A	98	81.7	0.4
PA 66-30B	98	81.2	0.5
PA 66 Ternary Nanocomposites			
(PA 66-15A-2210) - (All-S)	93	72.6	0.3
(PA 66-15A-8840) - (All-S)	93	70.0	0.1
(PA 66-15A-8900) - (All-S)	93	69.1	0.2
(PA 66-25A-2210) - (All-S)	93	71.1	0.6
(PA 66-25A-8840) - (All-S)	93	69.0	0.6
(PA 66-25A-8900) - (All-S)	93	68.1	0.5
(PA 66-30B-2210) - (All-S)	93	71.4	0.3
(PA 66-30B-8840) - (All-S)	93	69.4	0.2
(PA 66-30B-8900) - (All-S)	93	68.5	0.9
Mixing sequences of PA 66 Ternary Nanocomposites			
(15A / 2210)-PA 66 - (CI-P)	93	64.5	1.4
(PA 66 / 15A)-2210 - (PC-I)	93	66.8	1.1
(PA 66 / 2210)-15A - (PI-C)	93	60.9	0.5
(15A / 8840)-PA 66 - (CI-P)	93	64.6	0.8
(PA 66 / 15A)-8840 - (PC-I)	93	67.8	3.7
(PA 66 / 8840)-15A - (PI-C)	93	62.3	0.8
(15A / 8900)-PA 66 - (CI-P)	93	64.6	1.0
(PA 66 / 15A)-8900 - (PC-I)	93	67.0	6.7
(PA 66 / 8900)-15A - (PI-C)	93	61.8	0.4

Table A.1 Tensile strength data and standard deviations for all the compositions. (Cont'd)

Components	PA 66 Concentration (wt%)	Tensile Strength (MPa)	Standard Deviation
Mixing sequences of PA 66 Ternary Nanocomposites			
(25A / 8840)-PA 66 - (CI-P)	93	63.4	0.5
(PA 66 / 25A)-8840 - (PC-I)	93	65.7	3.7
(PA 66 / 8840)-25A - (PI-C)	93	64.3	0.9
(25A / 8900)-PA 66 - (CI-P)	93	62.8	1.8
(PA 66 / 25A)-8900 - (PC-I)	93	63.9	3.8
(PA 66 / 8900)-25A - (PI-C)	93	61.6	0.4

Table A.2 Young's modulus data and standard deviations for all the compositions.

Components	PA 66 Concentration (wt%)	Young's Modulus (GPa)	Standard Deviation
PA 66	100	2.266	0.074
PA 66 – Impact Modifier Blends			
PA 66-2210	95	1.708	0.002
PA 66-2210	90	1.659	0.017
PA 66-2210	85	1.601	0.058
PA 66-8840	95	1.705	0.038
PA 66-8840	90	1.662	0.011
PA 66-8840	85	1.618	0.004
PA 66-8900	95	1.703	0.010
PA 66-8900	90	1.679	0.012
PA 66-8900	85	1.658	0.027
PA 66 Binary Nanocomposites			
PA 66-15A	98	2.533	0.035
PA 66-25A	98	2.434	0.078
PA 66-30B	98	2.406	0.090
PA 66 Ternary Nanocomposites			
(PA 66-15A-2210) - (All-S)	93	1.914	0.001
(PA 66-15A-8840) - (All-S)	93	1.728	0.034
(PA 66-15A-8900) - (All-S)	93	1.742	0.032
(PA 66-25A-2210) - (All-S)	93	1.813	0.158
(PA 66-25A-8840) - (All-S)	93	1.782	0.139
(PA 66-25A-8900) - (All-S)	93	1.730	0.050
(PA 66-30B-2210) - (All-S)	93	1.816	0.031
(PA 66-30B-8840) - (All-S)	93	1.748	0.028
(PA 66-30B-8900) - (All-S)	93	1.750	0.050

Table A.2 Young's modulus data and standard deviations for all the compositions. (Cont'd)

Components	PA 66 Concentration (wt%)	Young's Modulus (GPa)	Standard Deviation
Mixing Sequences of PA 66 Ternary Nanocomposites			
(15A / 2210)-PA 66 - (CI-P)	93	1.719	0.009
(PA 66 / 15A)-2210 - (PC-I)	93	1.732	0.078
(PA 66 / 2210)-15A - (PI-C)	93	1.684	0.043
(15A / 8840)-PA 66 - (CI-P)	93	1.721	0.050
(PA 66 / 15A)-8840 - (PC-I)	93	1.742	0.022
(PA 66 / 8840)-15A - (PI-C)	93	1.690	0.035
(15A / 8900)-PA 66 - (CI-P)	93	1.720	0.049
(PA 66 / 15A)-8900 - (PC-I)	93	1.730	0.031
(PA 66 / 8900)-15A - (PI-C)	93	1.687	0.026
(25A / 8840)-PA 66 - (CI-P)	93	1.716	0.074
(PA 66 / 25A)-8840 - (PC-I)	93	1.722	0.074
(PA 66 / 8840)-25A - (PI-C)	93	1.720	0.034
(25A / 8900)-PA 66 - (CI-P)	93	1.715	0.046
(PA 66 / 25A)-8900 - (PC-I)	93	1.717	0.067
(PA 66 / 8900)-25A - (PI-C)	93	1.685	0.057

Table A.3 Elongation at break (%) data and standard deviations for all the compositions.

Components	PA 66 Concentration (wt%)	Elongation at Break (%)	Standard Deviation
PA 66	100	37.3	6.1
PA 66 – Impact Modifier Blends			
PA 66-2210	95	53.0	3.2
PA 66-2210	90	65.3	13.3
PA 66-2210	85	106.0	38.1
PA 66-8840	95	52.1	3.9
PA 66-8840	90	54.6	3.2
PA 66-8840	85	62.6	4.0
PA 66-8900	95	36.3	11.2
PA 66-8900	90	55.7	5.8
PA 66-8900	85	57.6	3.7
PA 66 Binary Nanocomposites			
PA 66-15A	98	17.0	2.6
PA 66-25A	98	18.0	1.8
PA 66-30B	98	25.3	6.8

Table A.3 Elongation at break (%) data and standard deviations for all the compositions. (Cont'd)

Components	PA 66 Concentration (wt%)	Elongation at Break (%)	Standard Deviation
PA 66 Ternary Nanocomposites			
(PA 66-15A-2210) - (All-S)	93	32.2	3.3
(PA 66-15A-8840) - (All-S)	93	43.5	7.6
(PA 66-15A-8900) - (All-S)	93	41.3	2.4
(PA 66-25A-2210) - (All-S)	93	29.4	6.0
(PA 66-25A-8840) - (All-S)	93	39.3	10.7
(PA 66-25A-8900) - (All-S)	93	41.3	2.7
(PA 66-30B-2210) - (All-S)	93	41.5	2.5
(PA 66-30B-8840) - (All-S)	93	41.8	2.3
(PA 66-30B-8900) - (All-S)	93	37.5	12.0
Mixing sequences of PA 66 Ternary Nanocomposites			
(15A / 2210)-PA 66 - (CI-P)	93	43.1	4.6
(PA 66 / 15A)-2210 - (PC-I)	93	42.8	3.0
(PA 66 / 2210)-15A - (PI-C)	93	32.1	7.1
(15A / 8840)-PA 66 - (CI-P)	93	46.9	3.5
(PA 66 / 15A)-8840 - (PC-I)	93	48.8	5.2
(PA 66 / 8840)-15A - (PI-C)	93	28.1	9.0
(15A / 8900)-PA 66 - (CI-P)	93	47.1	5.0
(PA 66 / 15A)-8900 - (PC-I)	93	50.0	3.3
(PA 66 / 8900)-15A - (PI-C)	93	40.0	10.1
(25A / 8840)-PA 66 - (CI-P)	93	49.8	1.8
(PA 66 / 25A)-8840 - (PC-I)	93	32.4	12.8
(PA 66 / 8840)-25A - (PI-C)	93	26.6	5.2
(25A / 8900)-PA 66 - (CI-P)	93	44.4	4.6
(PA 66 / 25A)-8900 - (PC-I)	93	49.1	11.2
(PA 66 / 8900)-25A - (PI-C)	93	35.3	6.7

Table A.4 Impact strength data and standard deviations for all the compositions.

Components	PA 66 Concentration (wt%)	Impact Strength (kJ/m^2)	Standard Deviation
PA 66	100	4.4	0.4
PA 66 – Impact Modifier Blends			
PA 66-2210	95	6.3	2.0
PA 66-2210	90	6.5	1.0
PA 66-2210	85	10.0	0.6
PA 66-8840	95	6.7	0.5
PA 66-8840	90	7.2	0.2
PA 66-8840	85	13.9	1.1

Table A.4 Impact strength data and standard deviations for all the compositions. (Cont'd)

Components	PA 66 Concentration (wt%)	Impact Strength (kJ/m^2)	Standard Deviation
PA 66 – Impact Modifier Blends			
PA 66-8900	95	10.0	0.6
PA 66-8900	90	10.3	1.2
PA 66-8900	85	11.0	0.9
PA 66 Binary Nanocomposites			
PA 66-15A	98	4.0	0.3
PA 66-25A	98	3.5	0.3
PA 66-30B	98	3.8	0.6
PA 66 Ternary Nanocomposites			
(PA 66-15A-2210) - (All-S)	93	7.9	0.8
(PA 66-15A-8840) - (All-S)	93	6.4	0.8
(PA 66-15A-8900) - (All-S)	93	6.5	0.8
(PA 66-25A-2210) - (All-S)	93	6.3	0.7
(PA 66-25A-8840) - (All-S)	93	6.2	1.2
(PA 66-25A-8900) - (All-S)	93	6.5	0.6
(PA 66-30B-2210) - (All-S)	93	6.1	1.0
(PA 66-30B-8840) - (All-S)	93	5.9	0.3
(PA 66-30B-8900) - (All-S)	93	6.0	0.9
Mixing sequences of PA 66 Ternary Nanocomposites			
(15A / 2210)-PA 66 - (CI-P)	93	5.9	0.8
(PA 66 / 15A)-2210 - (PC-I)	93	6.4	0.4
(PA 66 / 2210)-15A - (PI-C)	93	4.4	1.0
(15A / 8840)-PA 66 - (CI-P)	93	5.6	0.5
(PA 66 / 15A)-8840 - (PC-I)	93	6.1	0.7
(PA 66 / 8840)-15A - (PI-C)	93	4.5	1.0
(15A / 8900)-PA 66 - (CI-P)	93	5.6	0.6
(PA 66 / 15A)-8900 - (PC-I)	93	6.7	0.2
(PA 66 / 8900)-15A - (PI-C)	93	6.5	0.2
(25A / 8840)-PA 66 - (CI-P)	93	4.6	1.5
(PA 66 / 25A)-8840 - (PC-I)	93	5.1	1.0
(PA 66 / 8840)-25A - (PI-C)	93	4.2	0.8
(25A / 8900)-PA 66 - (CI-P)	93	5.8	0.1
(PA 66 / 25A)-8900 - (PC-I)	93	6.6	1.0
(PA 66 / 8900)-25A - (PI-C)	93	4.2	1.0

Table A.5 Flexural strength data and standard deviations for all the compositions.

Components	PA 66 Concentration (wt%)	Flexural Strength (MPa)	Standard Deviation
PA 66	100	91.5	4.6
PA 66 – Impact Modifier Blends			
PA 66-2210	95	78.6	1.3
PA 66-2210	90	68.1	4.0
PA 66-2210	85	67.6	1.0
PA 66-8840	95	80.1	2.9
PA 66-8840	90	65.0	1.0
PA 66-8840	85	57.7	0.7
PA 66-8900	95	75.4	2.5
PA 66-8900	90	71.4	1.2
PA 66-8900	85	69.2	1.9
PA 66 Binary Nanocomposites			
PA 66-15A	98	97.6	0.6
PA 66-25A	98	98.6	2.6
PA 66-30B	98	93.5	3.7
PA 66 Ternary Nanocomposites			
(PA 66-15A-2210) - (All-S)	93	82.5	1.4
(PA 66-15A-8840) - (All-S)	93	80.3	1.0
(PA 66-15A-8900) - (All-S)	93	79.8	1.6
(PA 66-25A-2210) - (All-S)	93	84.2	1.6
(PA 66-25A-8840) - (All-S)	93	80.6	2.6
(PA 66-25A-8900) - (All-S)	93	79.9	2.4
(PA 66-30B-2210) - (All-S)	93	75.7	3.8
(PA 66-30B-8840) - (All-S)	93	77.4	1.1
(PA 66-30B-8900) - (All-S)	93	75.9	2.0
Mixing sequences of PA 66 Ternary Nanocomposites			
(15A / 2210)-PA 66 - (CI-P)	93	85.7	1.9
(PA 66 / 15A)-2210 - (PC-I)	93	84.8	4.4
(PA 66 / 2210)-15A - (PI-C)	93	80.2	1.2
(15A / 8840)-PA 66 - (CI-P)	93	85.7	1.2
(PA 66 / 15A)-8840 - (PC-I)	93	83.3	6.2
(PA 66 / 8840)-15A - (PI-C)	93	81.8	2.1
(15A / 8900)-PA 66 - (CI-P)	93	89.0	1.6
(PA 66 / 15A)-8900 - (PC-I)	93	80.8	9.6
(PA 66 / 8900)-15A - (PI-C)	93	81.5	1.9
(25A / 8840)-PA 66 - (CI-P)	93	84.7	1.4
(PA 66 / 25A)-8840 - (PC-I)	93	79.3	9.0
(PA 66 / 8840)-25A - (PI-C)	93	84.9	0.2
(25A / 8900)-PA 66 - (CI-P)	93	86.7	4.0
(PA 66 / 25A)-8900 - (PC-I)	93	86.8	2.7
(PA 66 / 8900)-25A - (PI-C)	93	84.5	6.3

Table A.6 Flexural modulus data and standard deviations for all the compositions.

Components	PA 66 Concentration (wt%)	Flexural Modulus (GPa)	Standard Deviation
PA 66	100	2.388	0.280
PA 66 – Impact Modifier Blends			
PA 66-2210	95	2.035	0.053
PA 66-2210	90	1.837	0.160
PA 66-2210	85	1.825	0.030
PA 66-8840	95	2.144	0.110
PA 66-8840	90	1.822	0.067
PA 66-8840	85	1.689	0.039
PA 66-8900	95	2.136	0.074
PA 66-8900	90	2.026	0.039
PA 66-8900	85	1.877	0.134
PA 66 Binary Nanocomposites			
PA 66-15A	98	2.497	0.096
PA 66-25A	98	2.458	0.117
PA 66-30B	98	2.419	0.303
PA 66 Ternary Nanocomposites			
(PA 66-15A-2210) - (All-S)	93	2.167	0.028
(PA 66-15A-8840) - (All-S)	93	2.109	0.034
(PA 66-15A-8900) - (All-S)	93	2.048	0.020
(PA 66-25A-2210) - (All-S)	93	2.189	0.065
(PA 66-25A-8840) - (All-S)	93	2.152	0.127
(PA 66-25A-8900) - (All-S)	93	2.132	0.093
(PA 66-30B-2210) - (All-S)	93	2.079	0.201
(PA 66-30B-8840) - (All-S)	93	2.028	0.050
(PA 66-30B-8900) - (All-S)	93	1.954	0.154
Mixing sequences of PA 66 Ternary Nanocomposites			
(15A / 2210)-PA 66 - (CI-P)	93	2.195	0.024
(PA 66 / 15A)-2210 - (PC-I)	93	1.942	0.097
(PA 66 / 2210)-15A - (PI-C)	93	2.044	0.045
(15A / 8840)-PA 66 - (CI-P)	93	2.073	0.044
(PA 66 / 15A)-8840 - (PC-I)	93	1.966	0.178
(PA 66 / 8840)-15A - (PI-C)	93	1.971	0.060
(15A / 8900)-PA 66 - (CI-P)	93	2.146	0.011
(PA 66 / 15A)-8900 - (PC-I)	93	1.830	0.234
(PA 66 / 8900)-15A - (PI-C)	93	2.016	0.028
(25A / 8840)-PA 66 - (CI-P)	93	2.022	0.066
(PA 66 / 25A)-8840 - (PC-I)	93	1.852	0.228
(PA 66 / 8840)-25A - (PI-C)	93	1.992	0.032
(25A / 8900)-PA 66 - (CI-P)	93	2.110	0.100
(PA 66 / 25A)-8900 - (PC-I)	93	2.175	0.115
(PA 66 / 8900)-25A - (PI-C)	93	1.804	0.038

APPENDIX B

X-Ray Diffraction Patterns

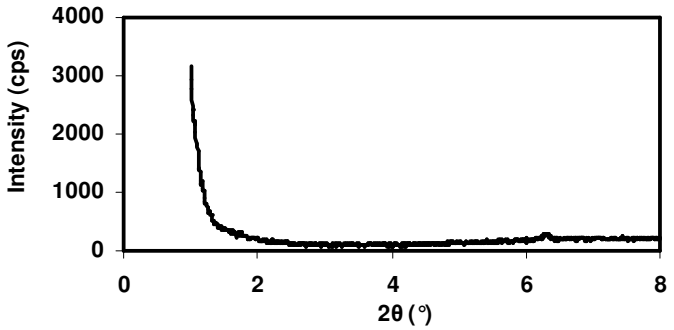

Figure B.1 XRD pattern of PA 66.

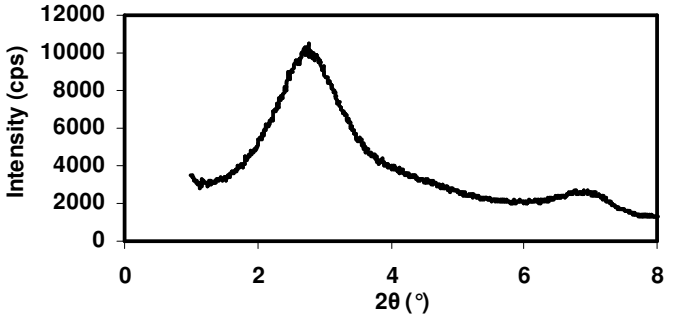

Figure B.2 XRD pattern of Cloisite® 15A.

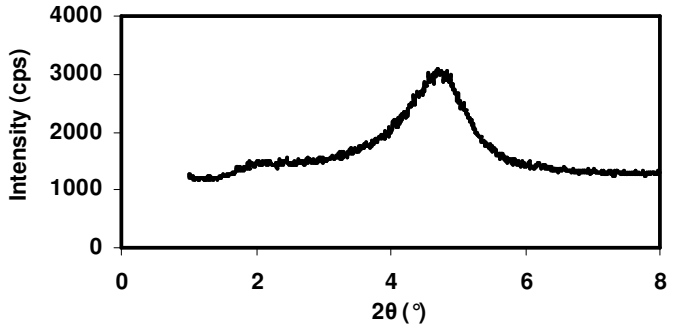

Figure B.3 XRD pattern of PA 66-Cloisite® 15A binary nanocomposite.

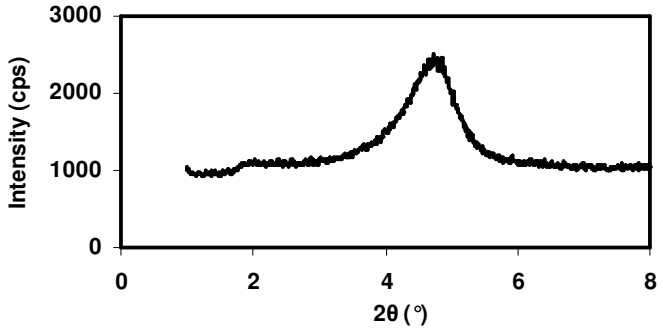

Figure B.4 XRD pattern of PA 66-Cloisite® 15A-Lotader® 2210 - (All-S) ternary nanocomposite.

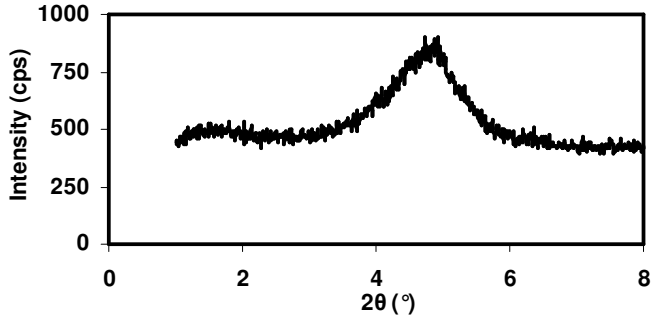

Figure B.5 XRD pattern of PA 66-Cloisite® 15A-Lotader® 2210 - (CI-P) ternary nanocomposite.

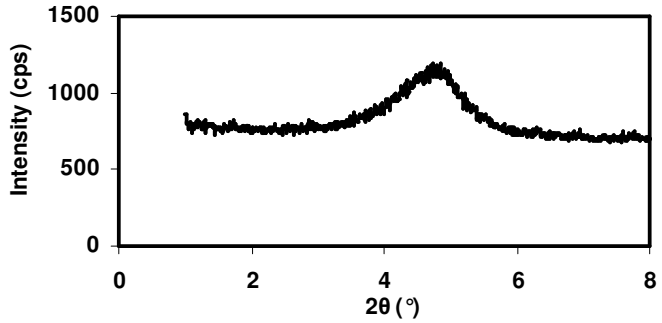

Figure B.6 XRD pattern of PA 66-Cloisite® 15A-Lotader® 2210 - (PC-I) ternary nanocomposite.

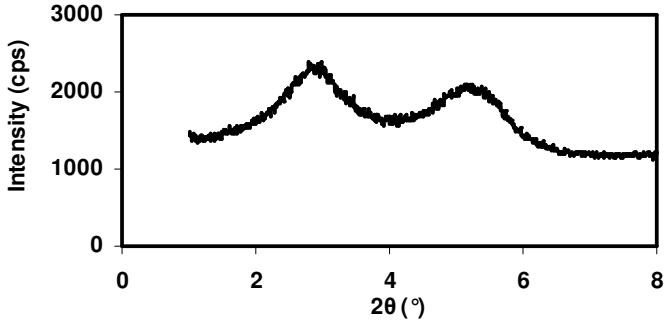

Figure B.7 XRD pattern of PA 66-Cloisite® 15A-Lotader® 2210 - (PI-C) ternary nanocomposite.

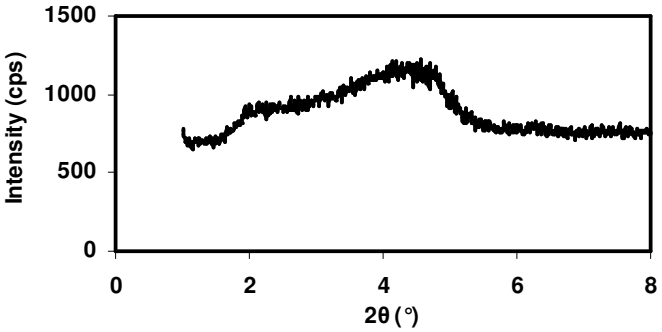

Figure B.8 XRD pattern of PA 66-Cloisite® 15A-Lotader® AX8840 - (All-S) ternary nanocomposite.

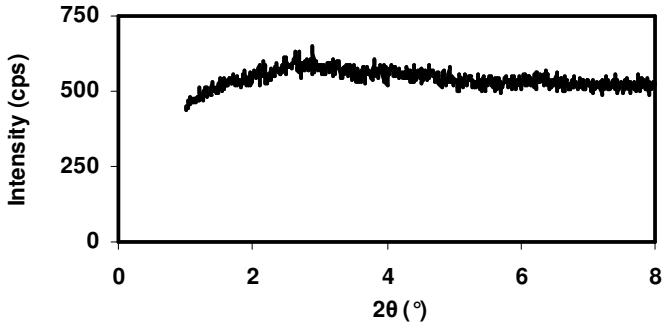

Figure B.9 XRD pattern of PA 66-Cloisite® 15A-Lotader® AX8840 - (CI-P) ternary nanocomposite.

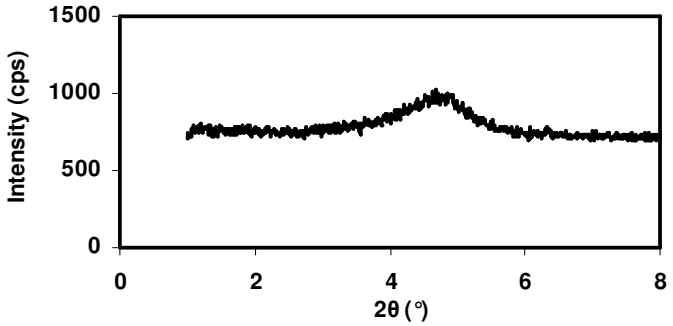

Figure B.10 XRD pattern of PA 66-Cloisite® 15A-Lotader® AX8840 - (PC-I) ternary nanocomposite.

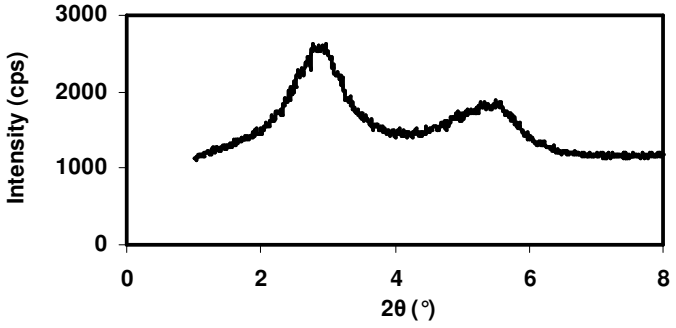

Figure B.11 XRD pattern of PA 66-Cloisite® 15A-Lotader® AX8840 - (PI-C) ternary nanocomposite.

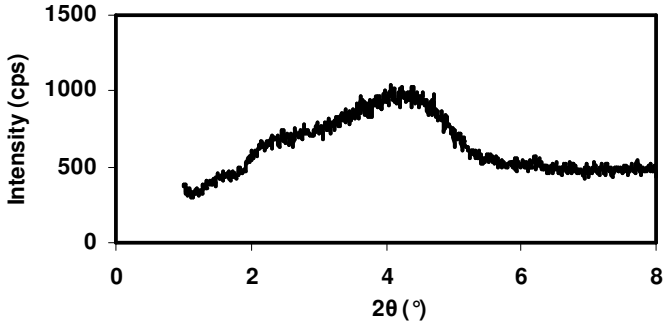

Figure B.12 XRD pattern of PA 66-Cloisite® 15A-Lotader® AX8900 - (All-S) ternary nanocomposite.

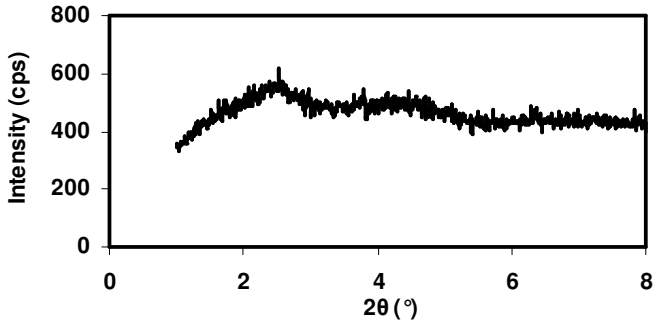

Figure B.13 XRD pattern of PA 66-Cloisite® 15A-Lotader® AX8900 - (CI-P) ternary nanocomposite.

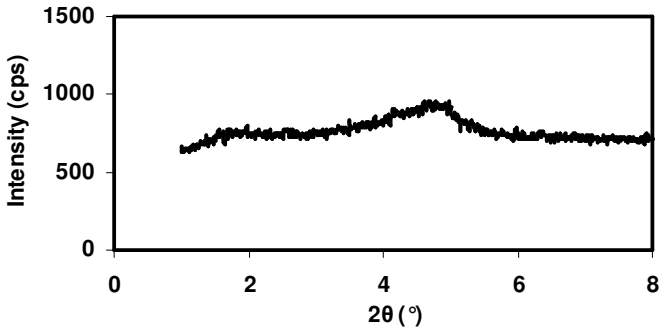

Figure B.14 XRD pattern of PA 66-Cloisite® 15A-Lotader® AX8900 - (PC-I) ternary nanocomposite.

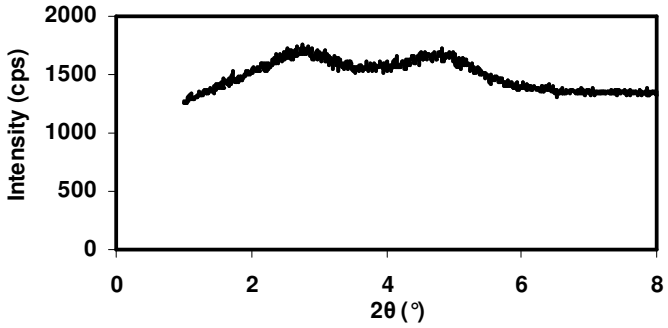

Figure B.15 XRD pattern of PA 66-Cloisite® 15A-Lotader® AX8900 - (PI-C) ternary nanocomposite.

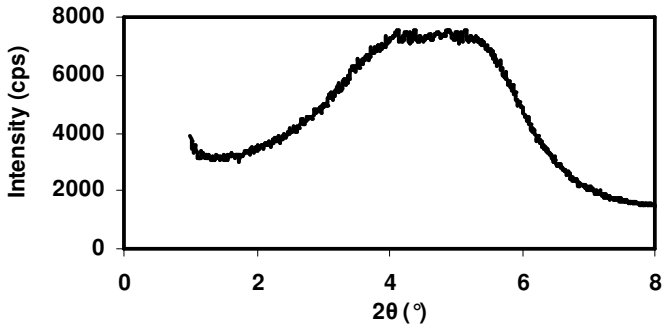

Figure B.16 XRD pattern of Cloisite® 25A.

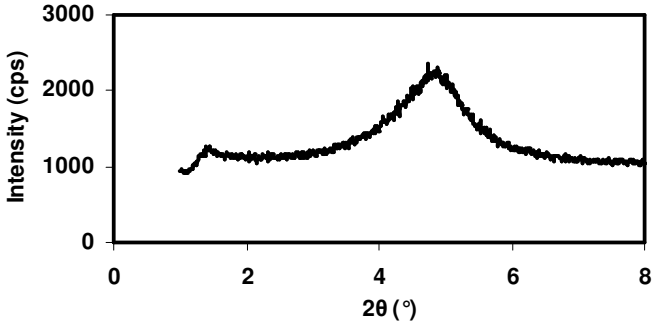

Figure B.17 XRD pattern of PA 66-Cloisite® 25A binary nanocomposite.

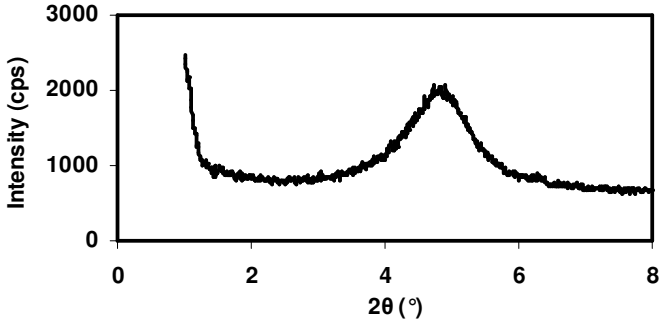

Figure B.18 XRD pattern of PA 66-Cloisite® 25A-Lotader® 2210 - (All-S) ternary nanocomposite.

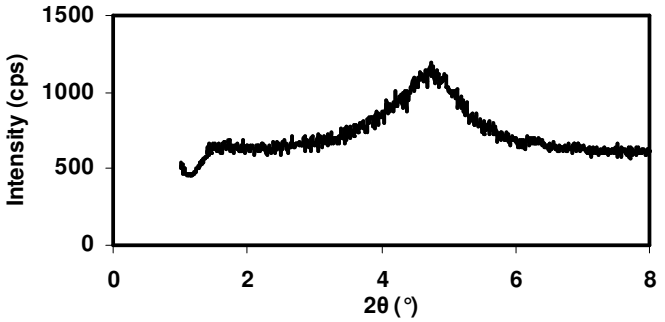

Figure B.19 XRD pattern of PA 66-Cloisite® 25A-Lotader® AX8840 - (All-S) ternary nanocomposite.

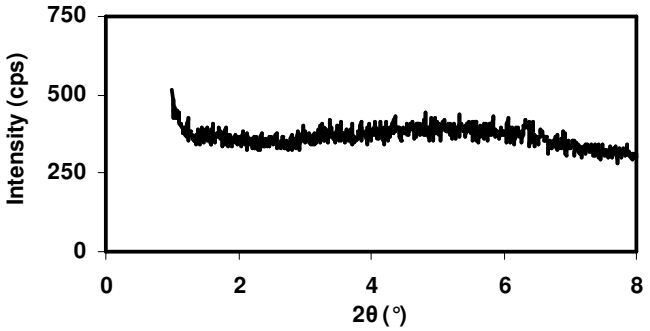

Figure B.20 XRD pattern of PA 66-Cloisite® 25A-Lotader® AX8840 - (CI-P) ternary nanocomposite.

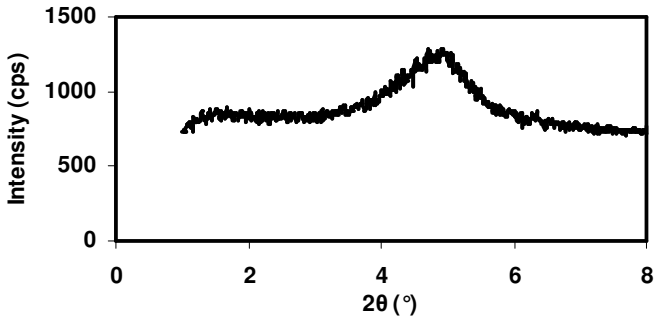

Figure B.21 XRD pattern of PA 66-Cloisite® 25A-Lotader® AX8840 - (PC-I) ternary nanocomposite.

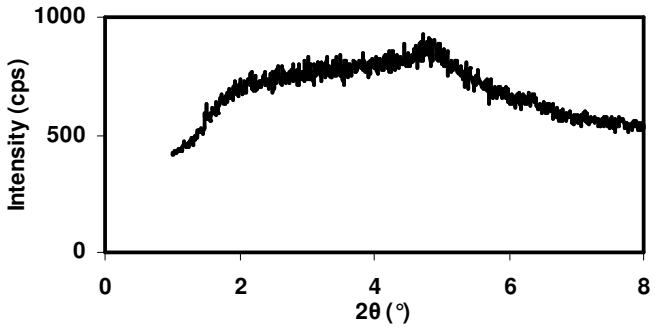

Figure B.22 XRD pattern of PA 66-Cloisite® 25A-Lotader® AX8840 - (PI-C) ternary nanocomposite.

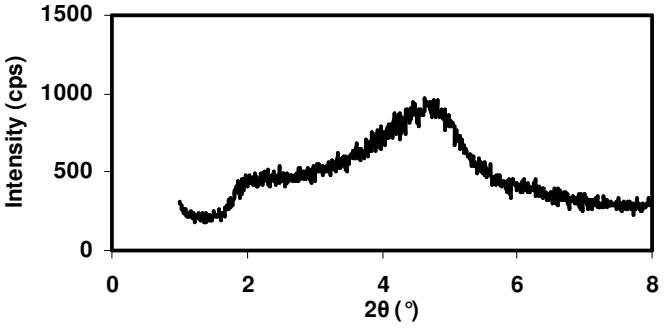

Figure B.23 XRD pattern of PA 66-Cloisite® 25A-Lotader® AX8900 - (All-S) ternary nanocomposite.

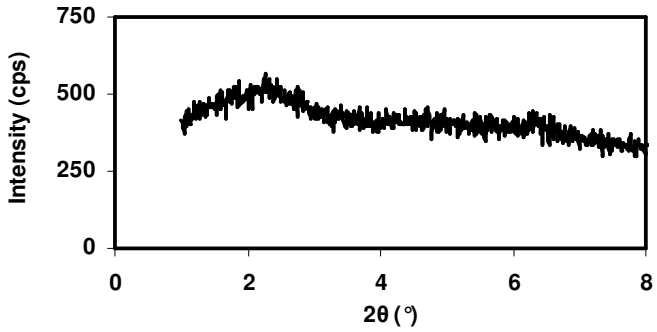

Figure B.24 XRD pattern of PA 66-Cloisite® 25A-Lotader® AX8900 - (CI-P) ternary nanocomposite.

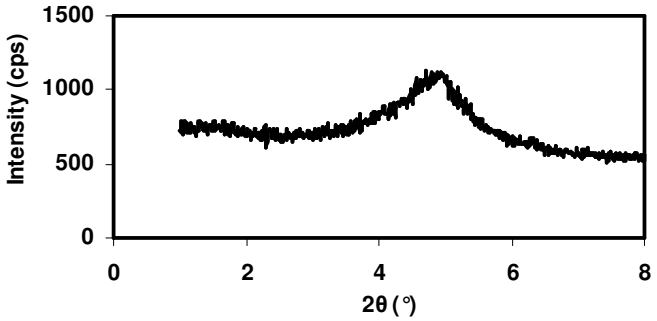

Figure B.25 XRD pattern of PA 66-Cloisite® 25A-Lotader® AX8900 - (PC-I) ternary nanocomposite.

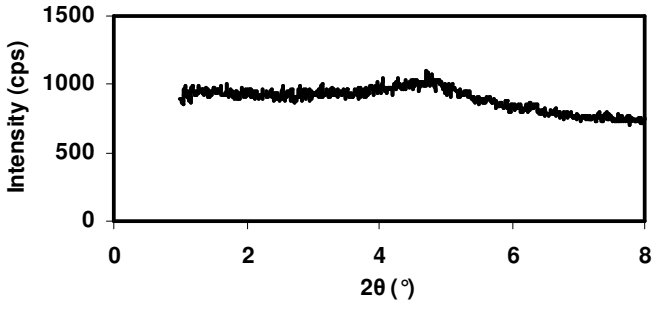

Figure B.26 XRD pattern of PA 66-Cloisite® 25A-Lotader® AX8900 - (PI-C) ternary nanocomposite.

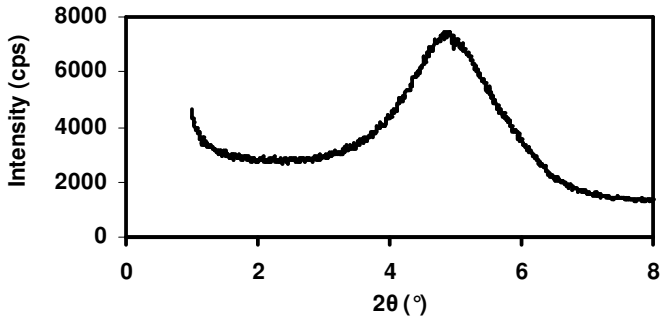

Figure B.27 XRD pattern of Cloisite® 30B.

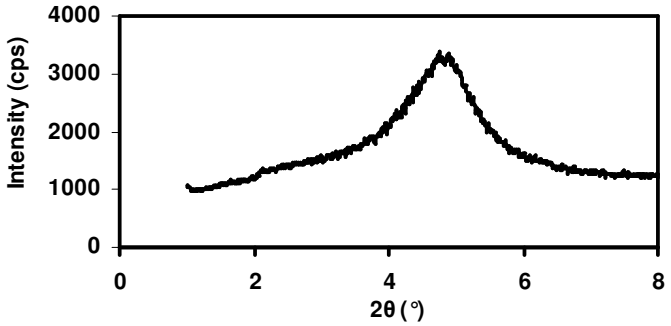

Figure B.28 XRD pattern of PA 66-Cloisite® 30B binary nanocomposite.

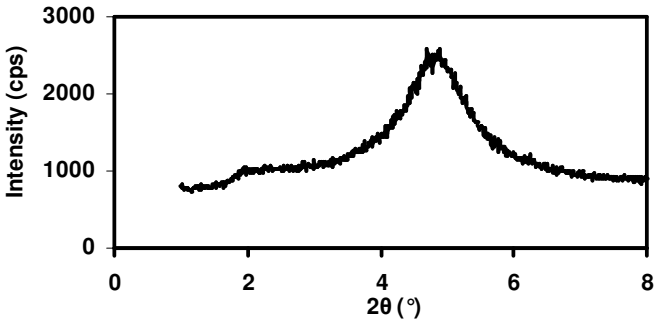

Figure B.29 XRD pattern of PA 66-Cloisite® 30B-Lotader® 2210 - (All-S) ternary nanocomposite.

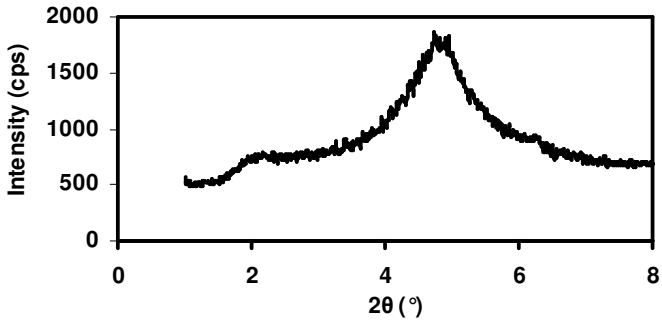

Figure B.30 XRD pattern of PA 66-Cloisite® 30B-Lotader® AX8840 - (All-S) ternary nanocomposite.

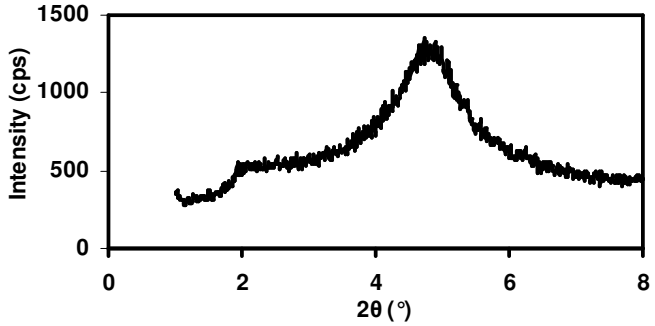

Figure B.31 XRD pattern of PA 66-Cloisite® 30B-Lotader® AX8900 - (All-S) ternary nanocomposite.

APPENDIX C

Differential Scanning Calorimetry Analysis

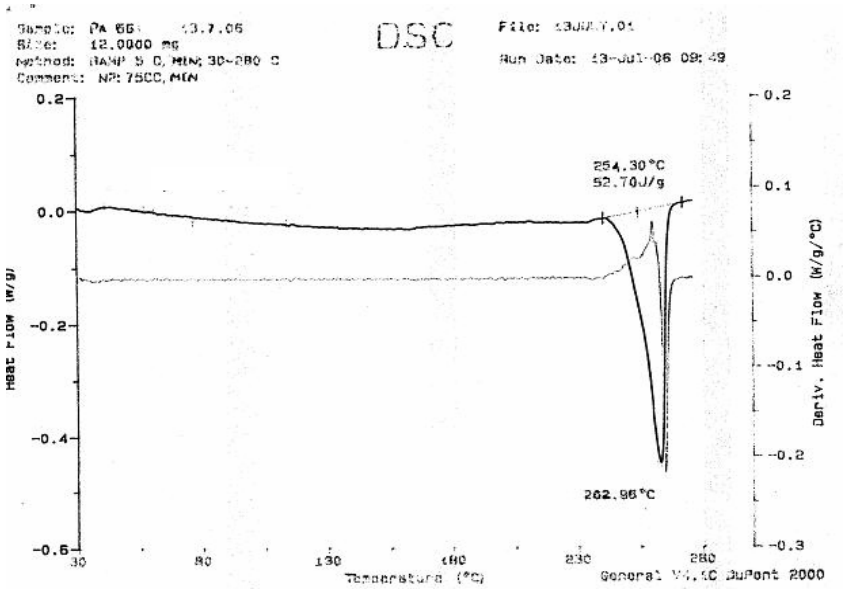

Figure C.1 DSC thermogram of PA 66.

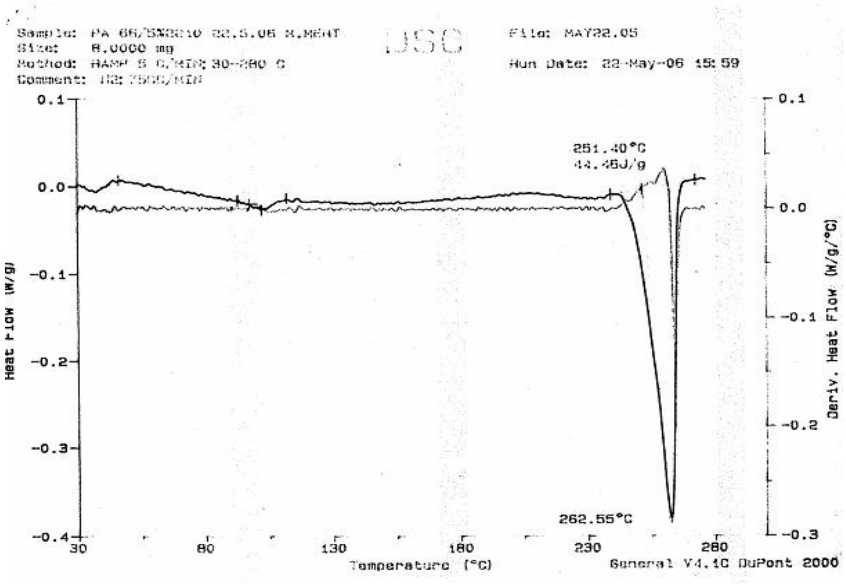

Figure C.2 DSC thermogram of PA 66-Lotader® 2210 (5 wt%) blend.

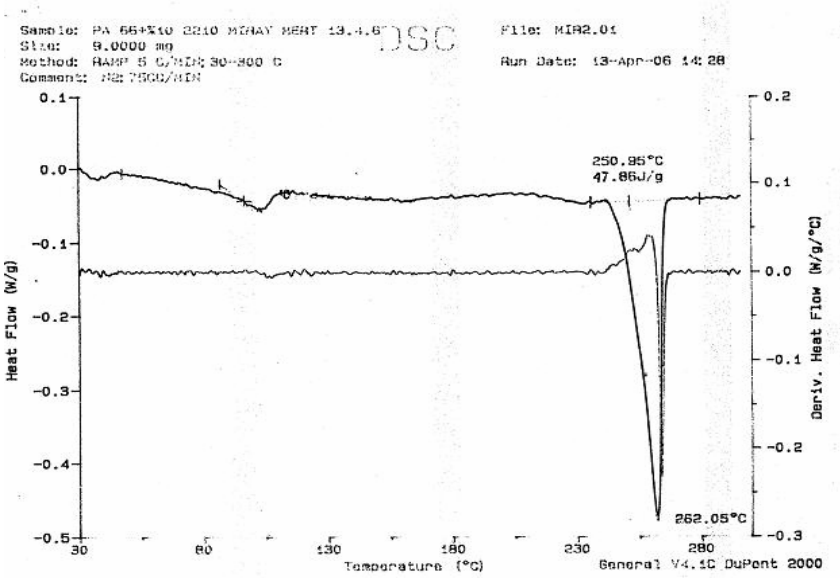

Figure C.3 DSC thermogram of PA 66-Lotader® 2210 (10 wt%) blend.

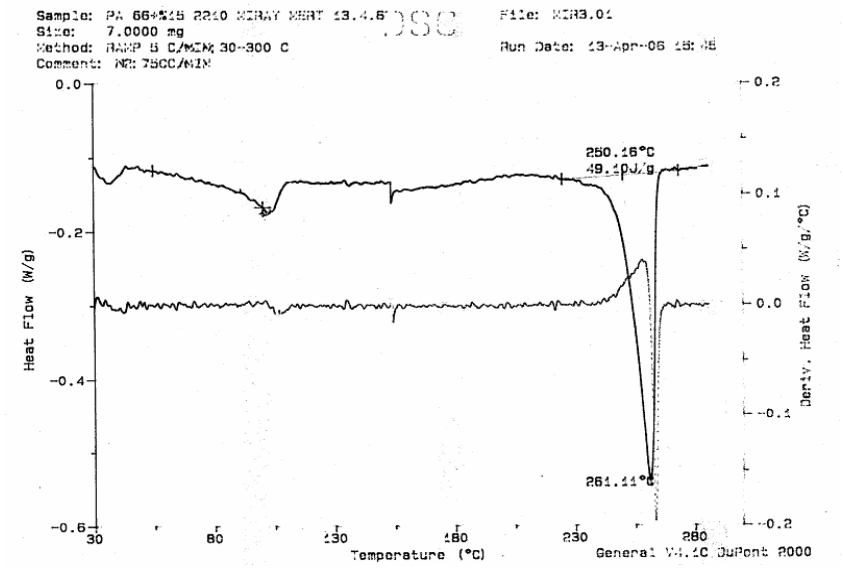

Figure C.4 DSC thermogram of PA 66-Lotader® 2210 (15 wt%) blend.

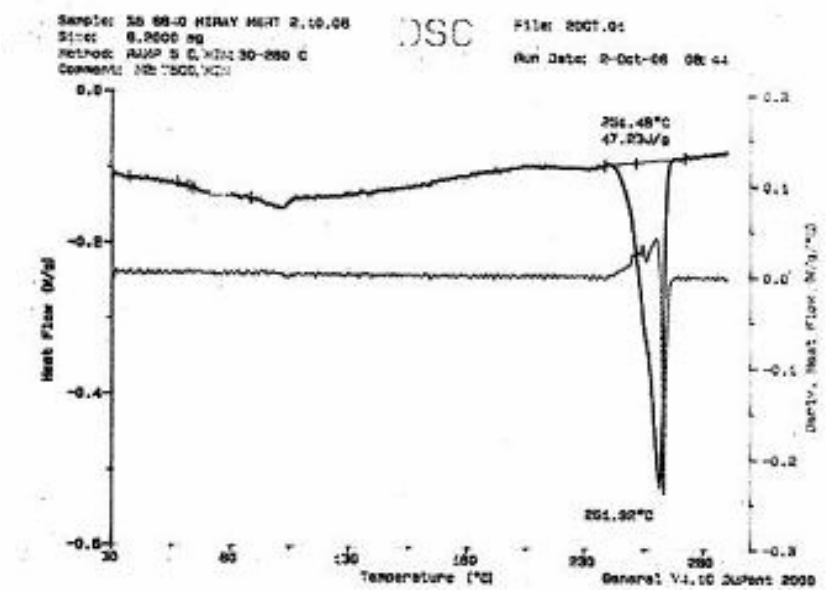

Figure C.5 DSC thermogram of PA 66-Lotader® AX8840 (5 wt%) blend.

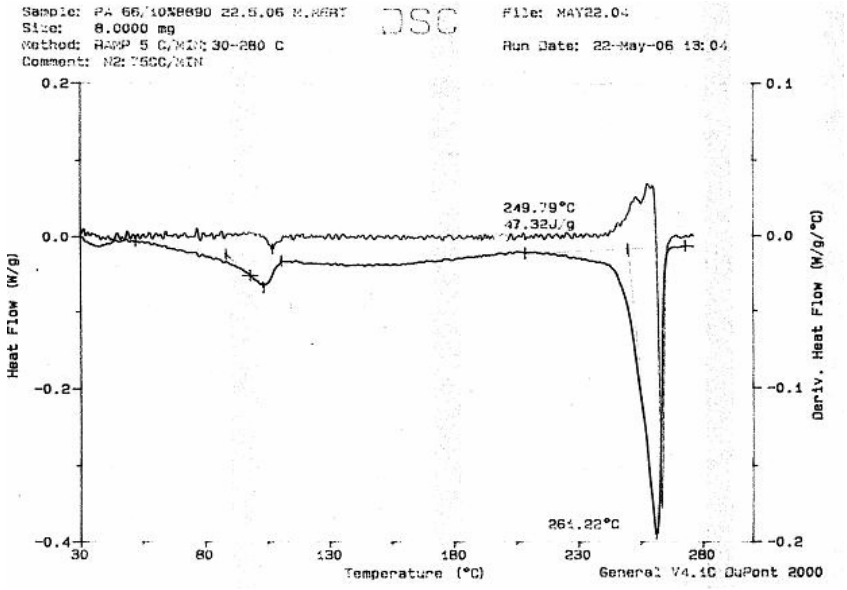

Figure C.6 DSC thermogram of PA 66-Lotader® AX8840 (10 wt%) blend.

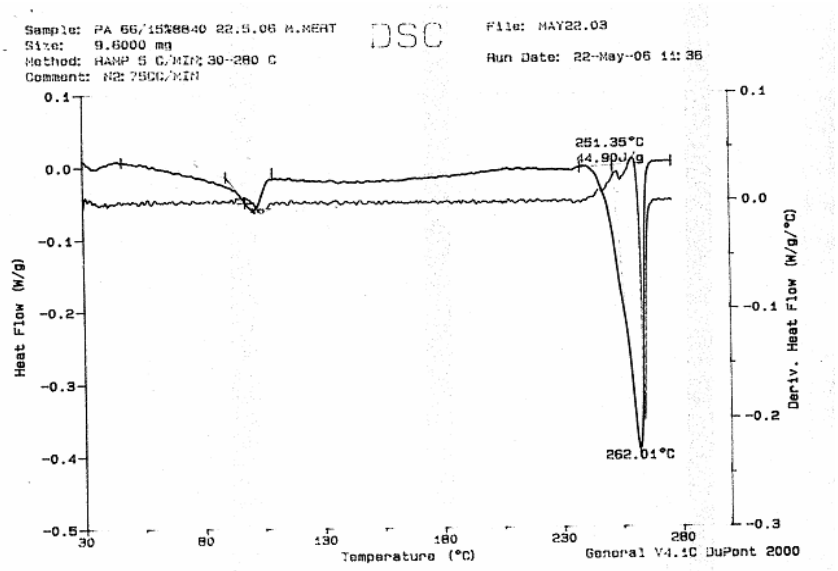

Figure C.7 DSC thermogram of PA 66-Lotader® AX8840 (15 wt%) blend.

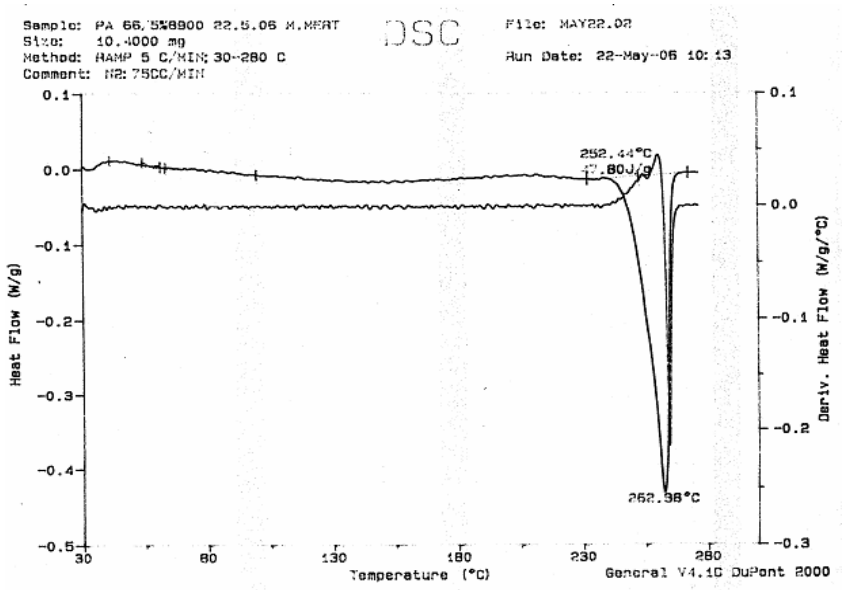

Figure C.8 DSC thermogram of PA 66-Lotader® AX8900 (5 wt%) blend.

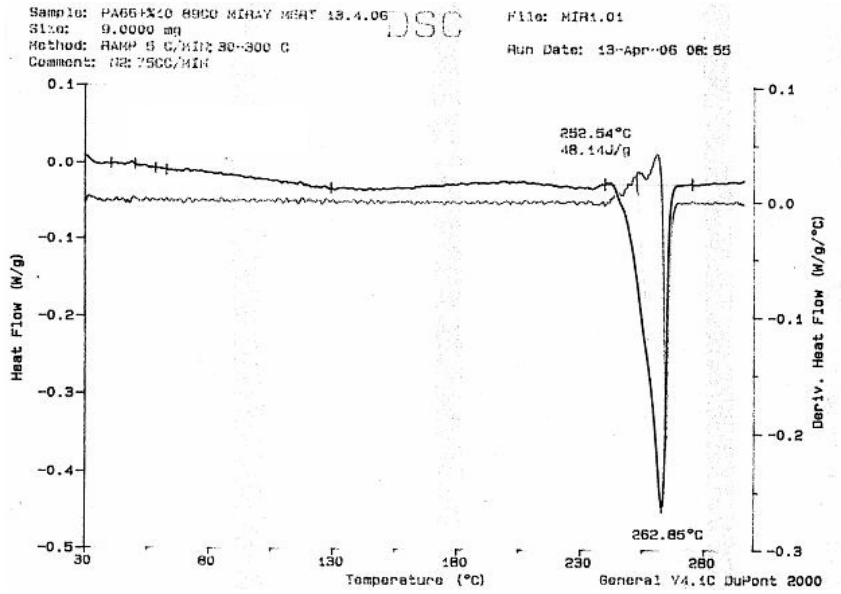

Figure C.9 DSC thermogram of PA 66-Lotader® AX8900 (10 wt%) blend.

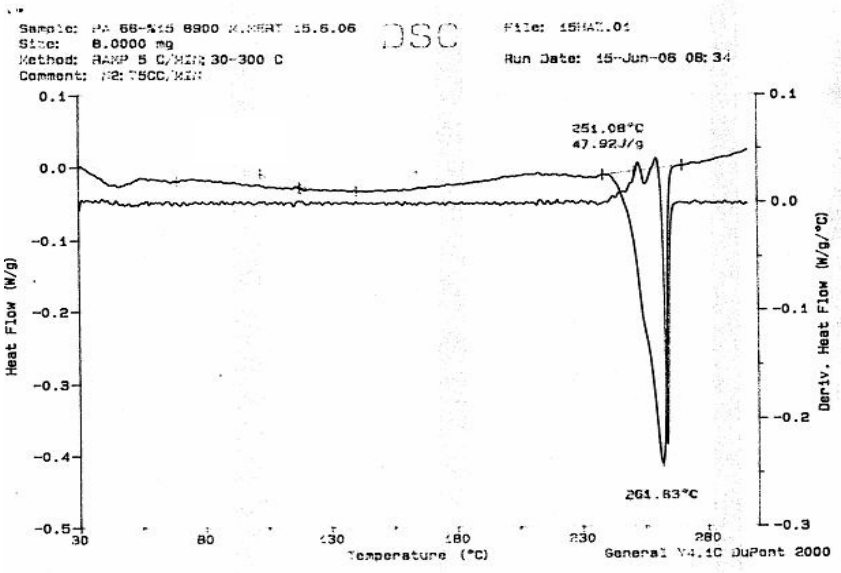

Figure C.10 DSC thermogram of PA 66-Lotader® AX8900 (15 wt%) blend.

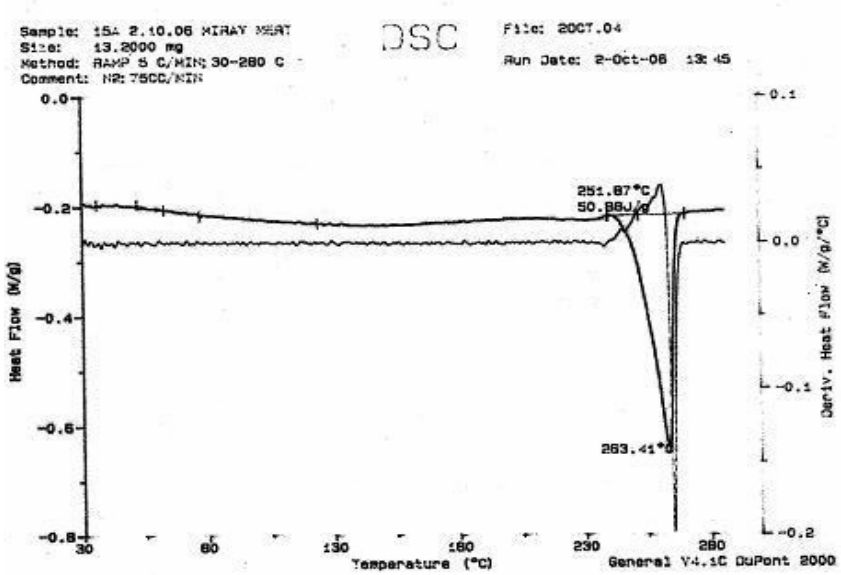

Figure C.11 DSC thermogram of PA 66-Cloisite® 15A binary nanocomposite.

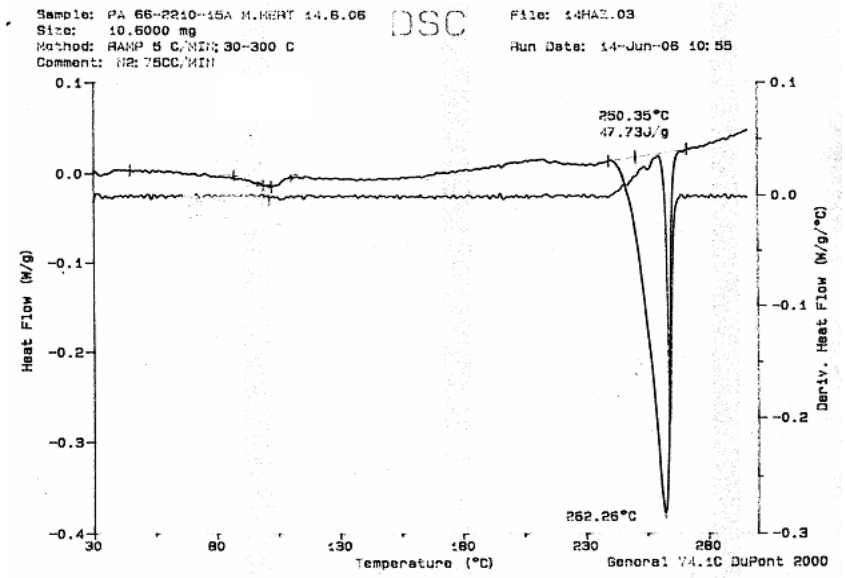

Figure C.12 DSC thermogram of PA 66-Cloisite® 15A-Lotader® 2210 - (All-S) ternary nanocomposite.

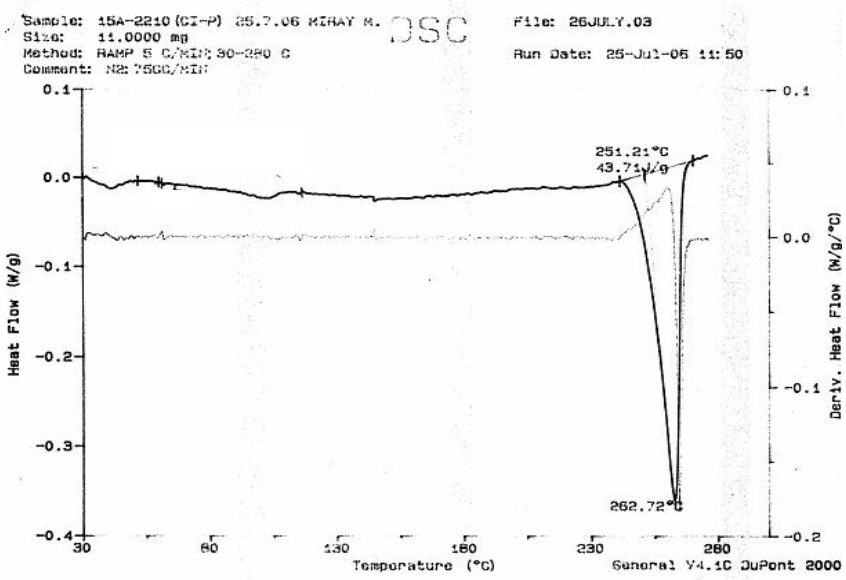

Figure C.13 DSC thermogram of PA 66-Cloisite® 15A-Lotader® 2210 - (CI-P) ternary nanocomposite.

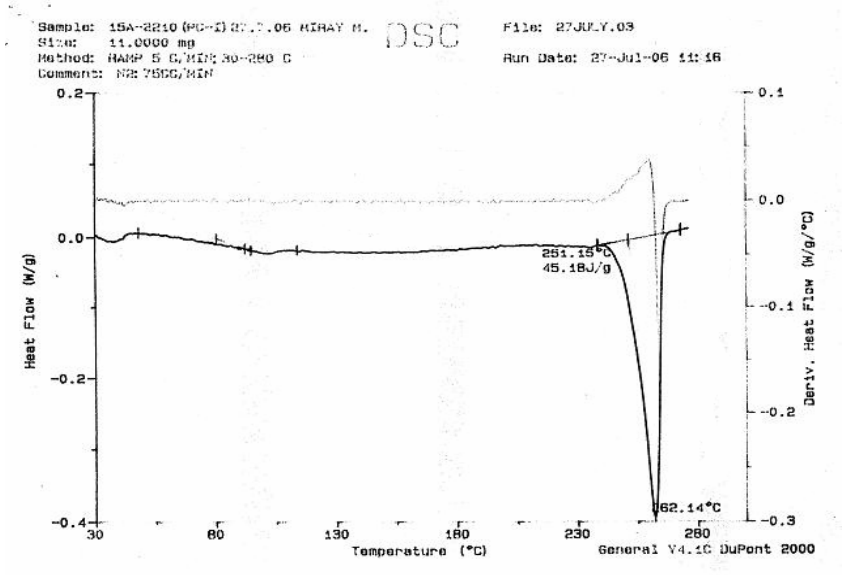

Figure C.14 DSC thermogram of PA 66-Cloisite® 15A-Lotader® 2210 - (PC-I) ternary nanocomposite.

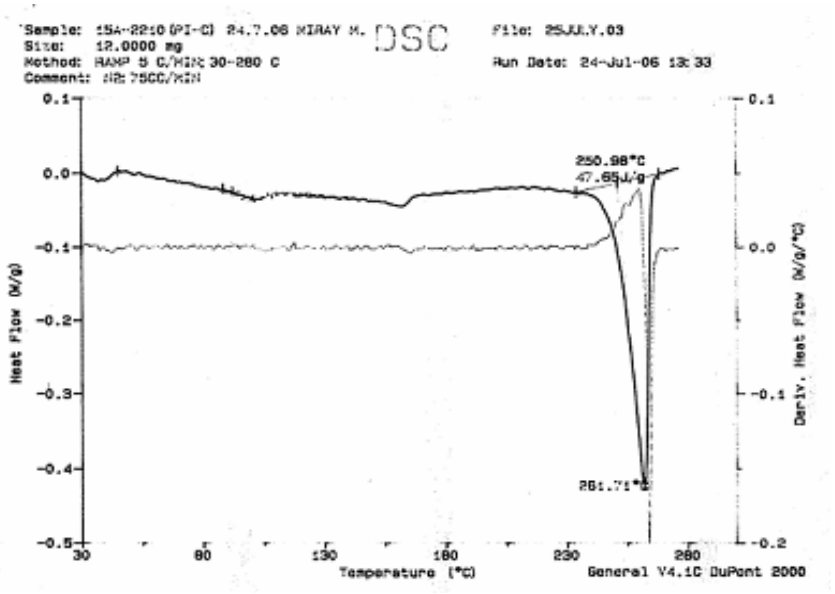

Figure C.15 DSC thermogram of PA 66-Cloisite® 15A-Lotader® 2210 - (PI-C) ternary nanocomposite.

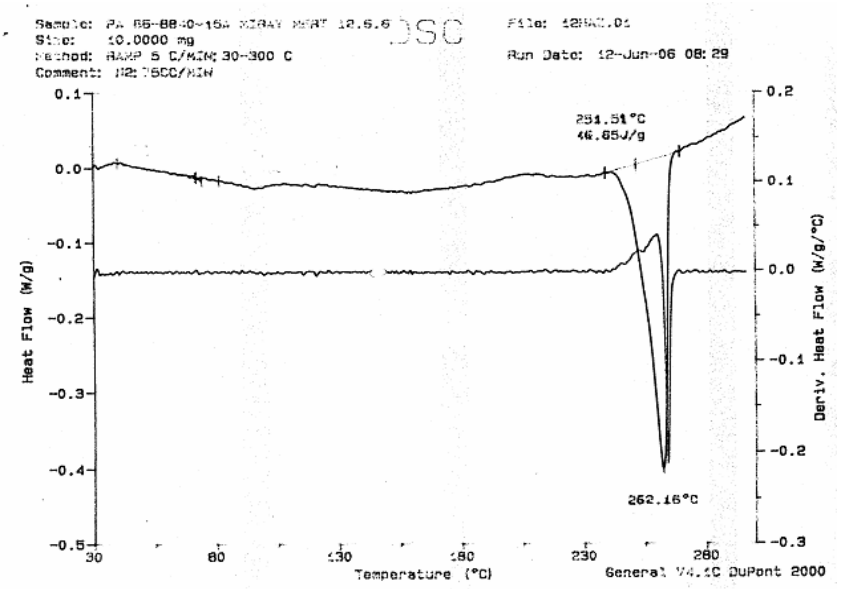

Figure C.16 DSC thermogram of PA 66-Cloisite® 15A-Lotader® AX8840 - (All-S) ternary nanocomposite.

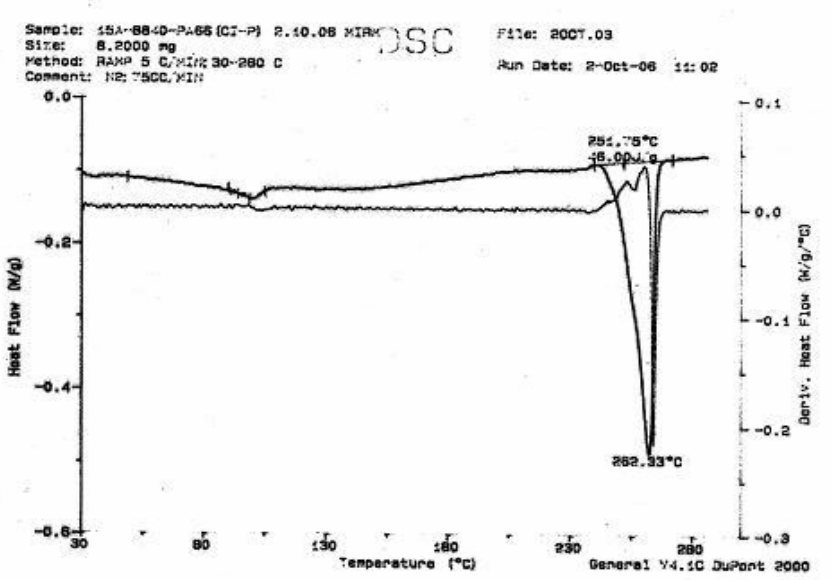

Figure C.17 DSC thermogram of PA 66-Cloisite® 15A-Lotader® AX8840 - (CI-P) ternary nanocomposite.

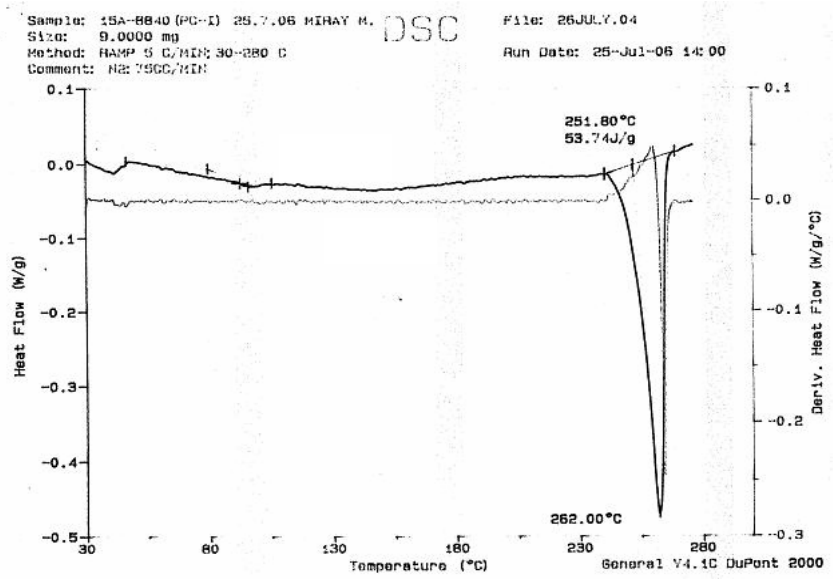

Figure C.18 DSC thermogram of PA 66-Cloisite® 15A-Lotader® AX8840 - (PC-I) ternary nanocomposite.

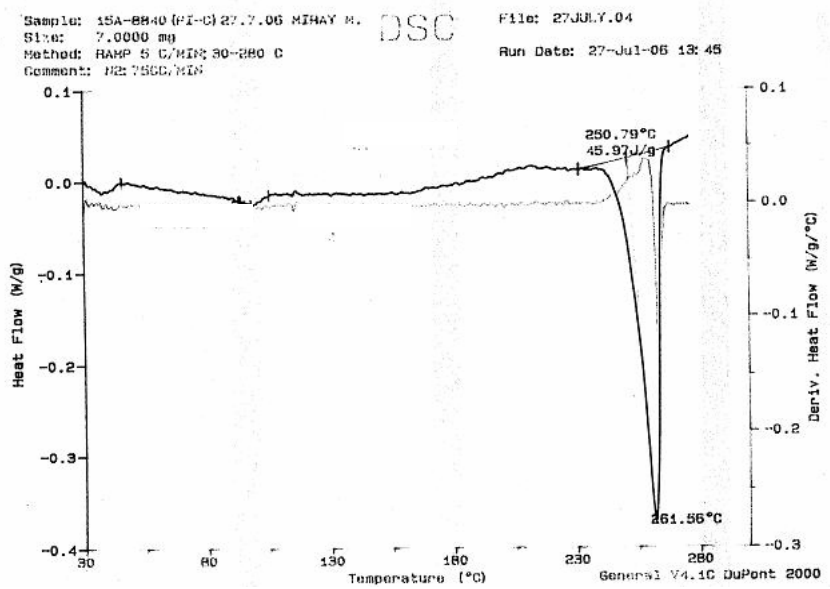

Figure C.19 DSC thermogram of PA 66-Cloisite® 15A-Lotader® AX8840 - (PI-C) ternary nanocomposite.

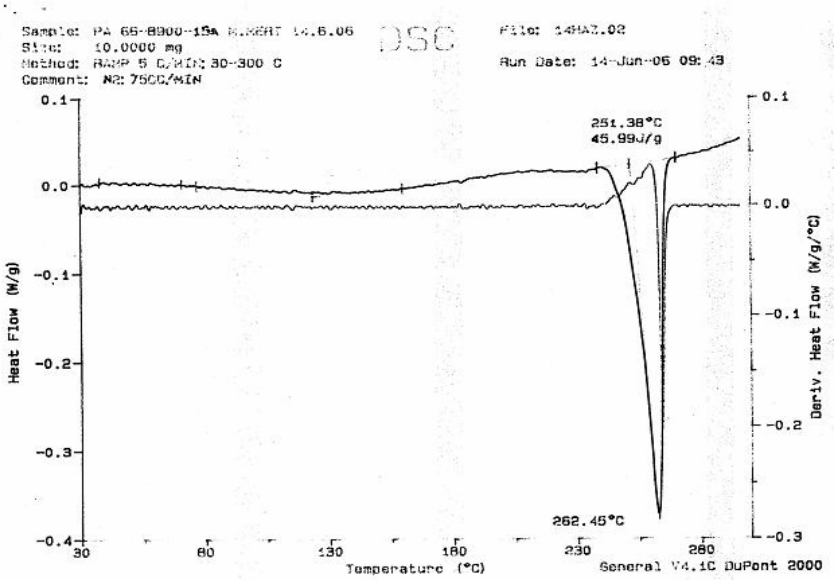

Figure C.20 DSC thermogram of PA 66-Cloisite® 15A-Lotader® AX8900 - (All-S) ternary nanocomposite.

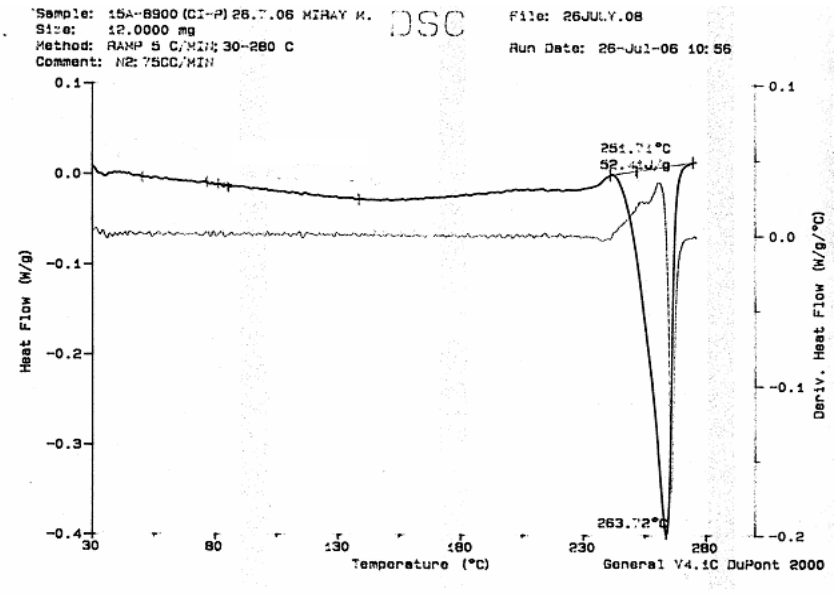

Figure C.21 DSC thermogram of PA 66-Cloisite® 15A-Lotader® AX8900 - (CI-P) ternary nanocomposite.

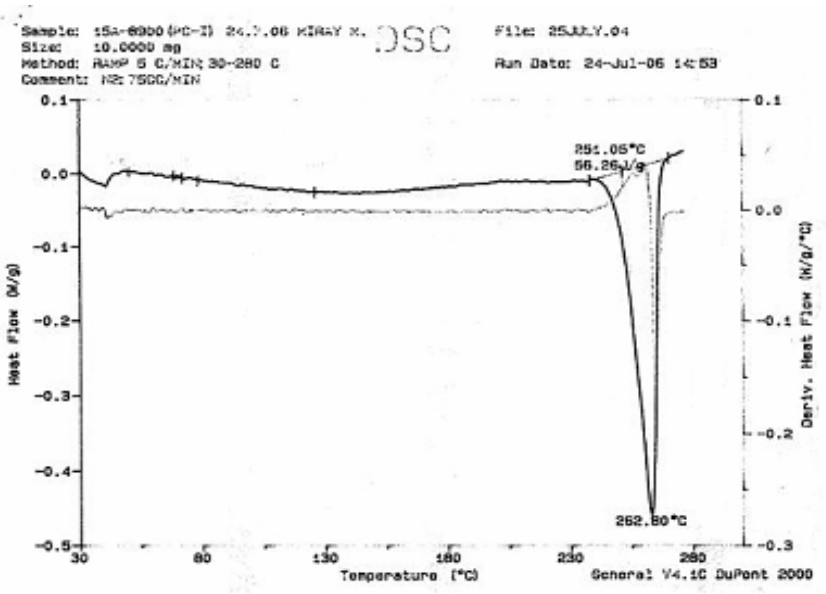

Figure C.22 DSC thermogram of PA 66-Cloisite® 15A-Lotader® AX8900 - (PC-I) ternary nanocomposite.

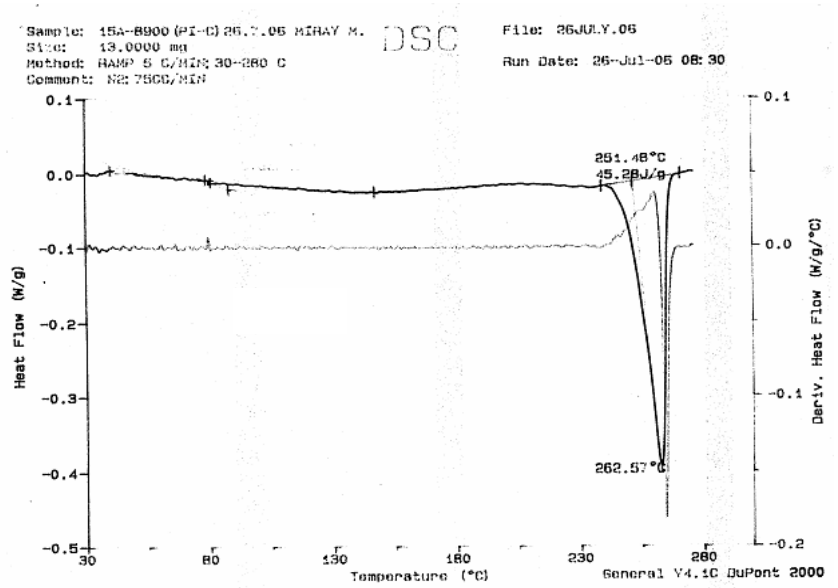

Figure C.23 DSC thermogram of PA 66-Cloisite® 15A-Lotader® AX8900 - (PI-C) ternary nanocomposite.

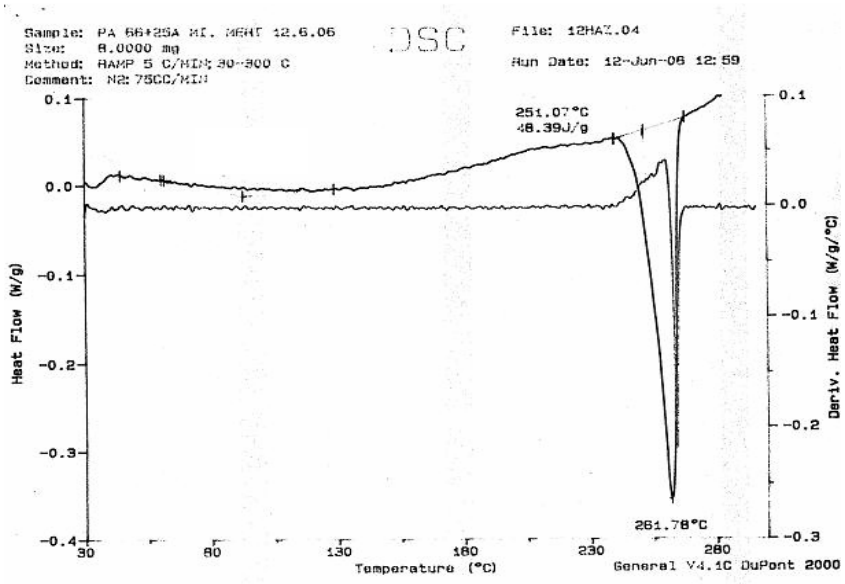

Figure C.24 DSC thermogram of PA 66-Cloisite® 25A binary nanocomposite.

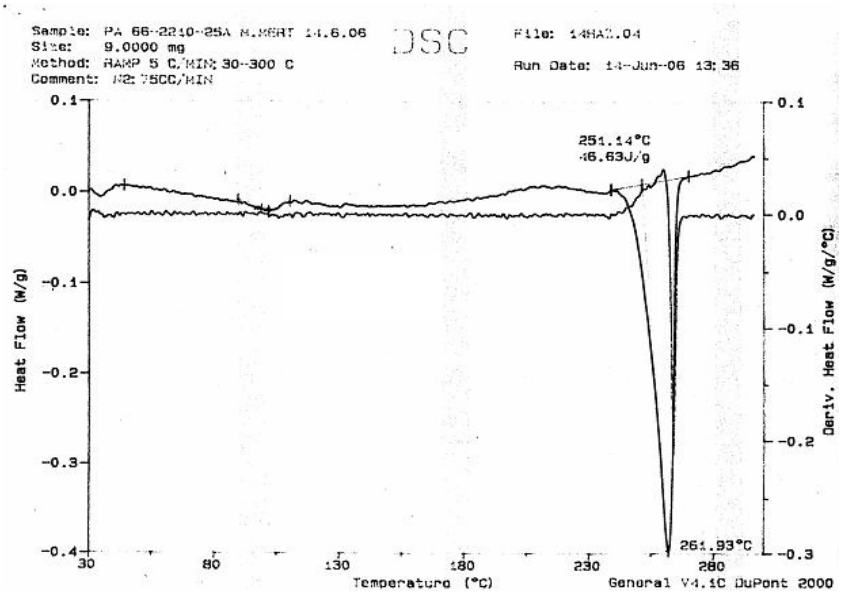

Figure C.25 DSC thermogram of PA 66-Cloisite® 25A-Lotader® 2210 - (All-S) ternary nanocomposite.

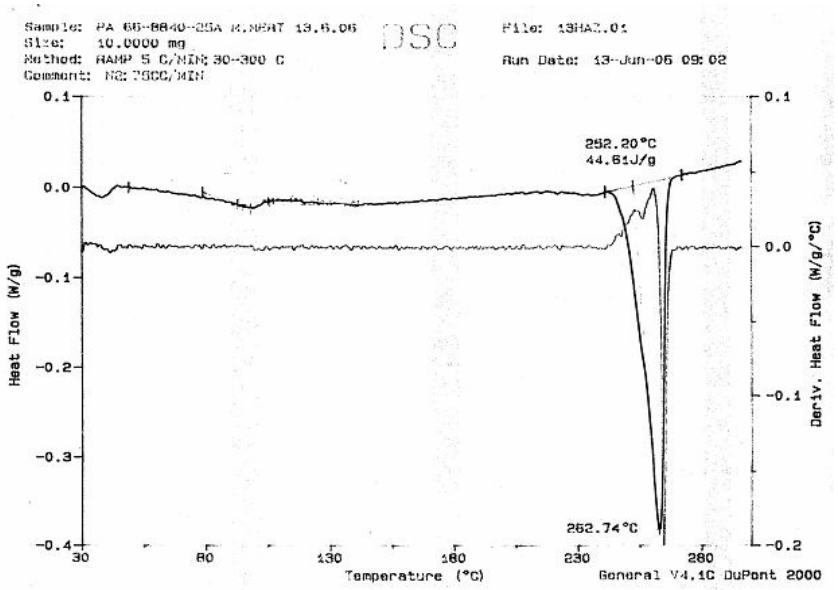

Figure C.26 DSC thermogram of PA 66-Cloisite® 25A-Lotader® AX8840 - (All-S) ternary nanocomposite.

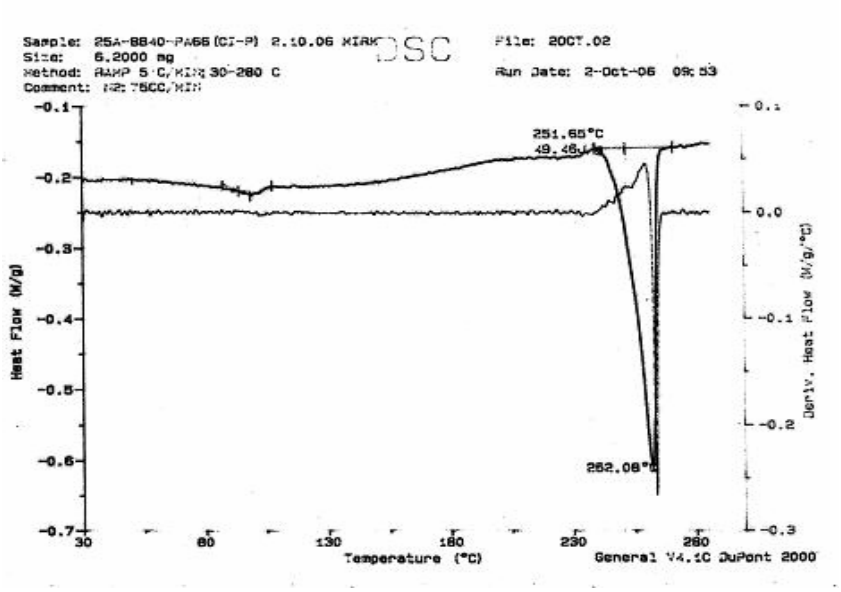

Figure C.27 DSC thermogram of PA 66-Cloisite® 25A-Lotader® AX8840 - (CI-P) ternary nanocomposite.

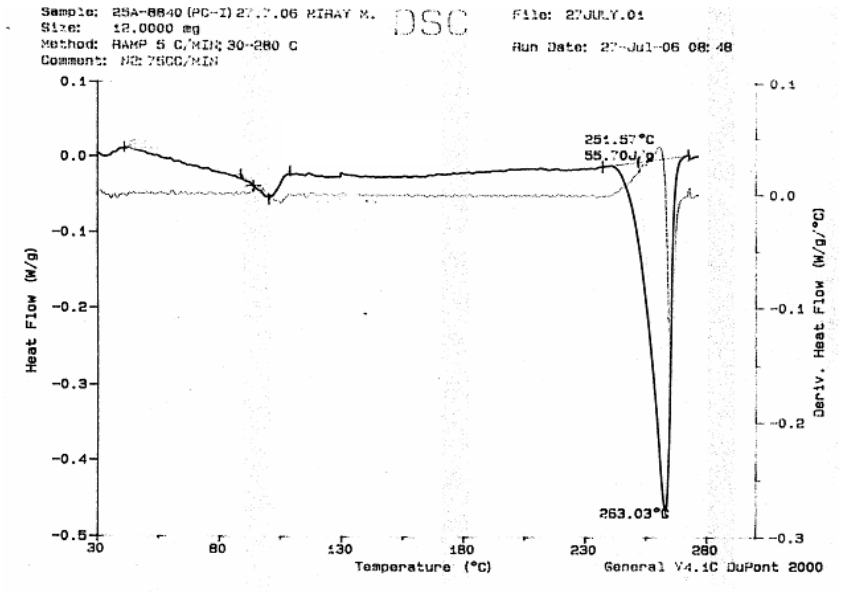

Figure C.28 DSC thermogram of PA 66-Cloisite® 25A-Lotader® AX8840 - (PC-I) ternary nanocomposite.

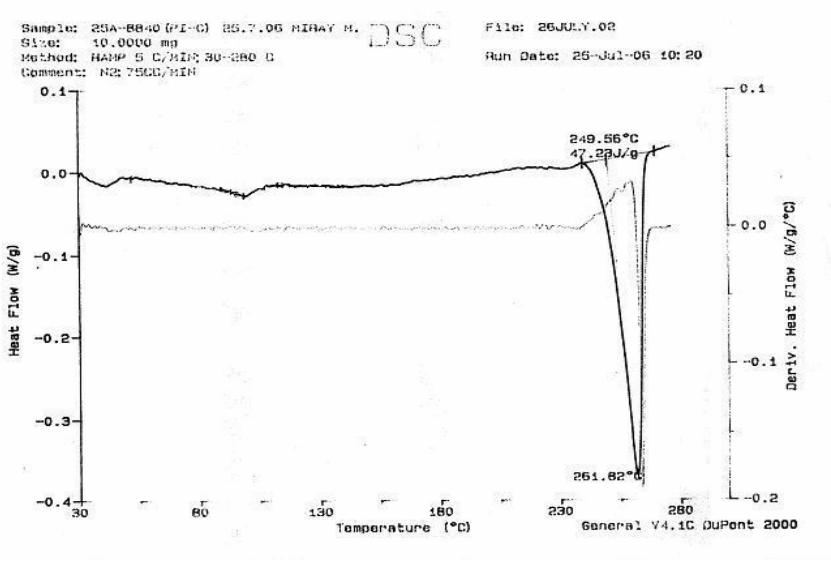

Figure C.29 DSC thermogram of PA 66-Cloisite® 25A-Lotader® AX8840 - (PI-C) ternary nanocomposite.

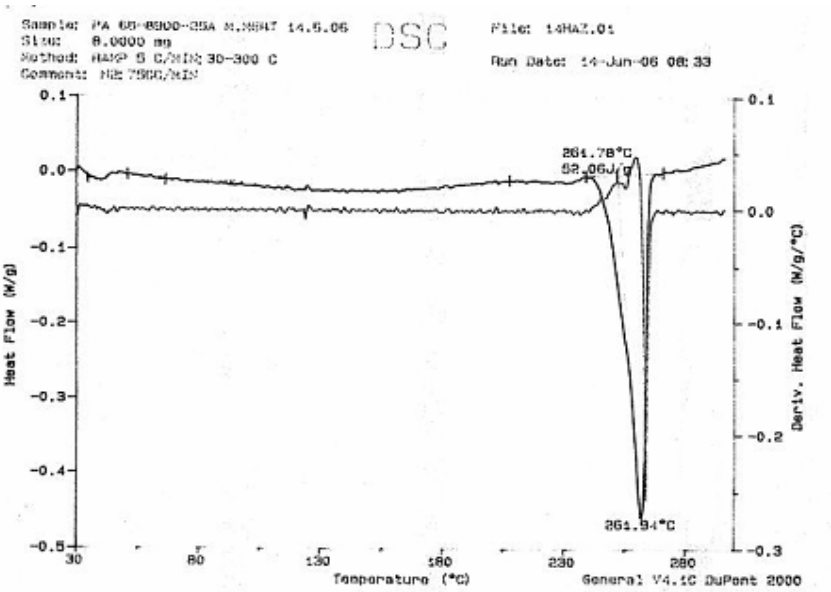

Figure C.30 DSC thermogram of PA 66-Cloisite® 25A-Lotader® AX8900 - (All-S) ternary nanocomposite.

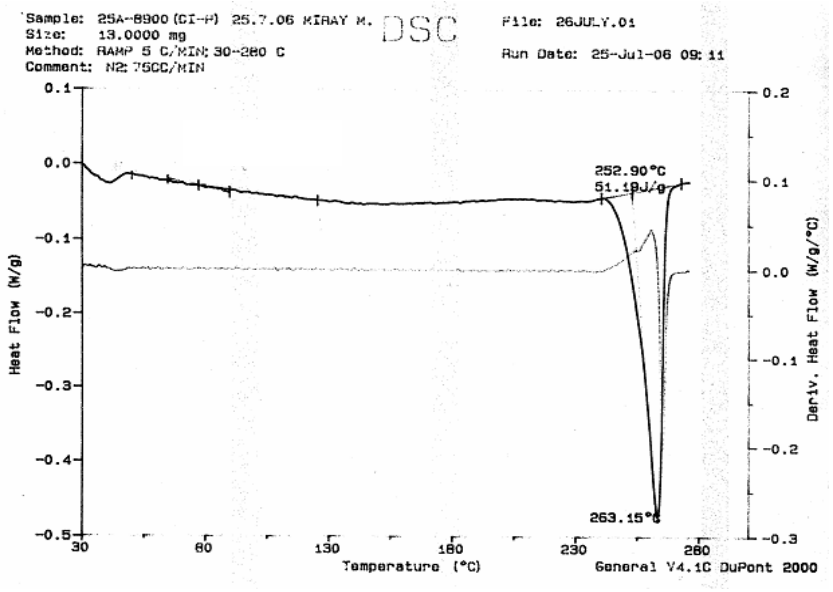

Figure C.31 DSC thermogram of PA 66-Cloisite® 25A-Lotader® AX8900 - (CI-P) ternary nanocomposite.

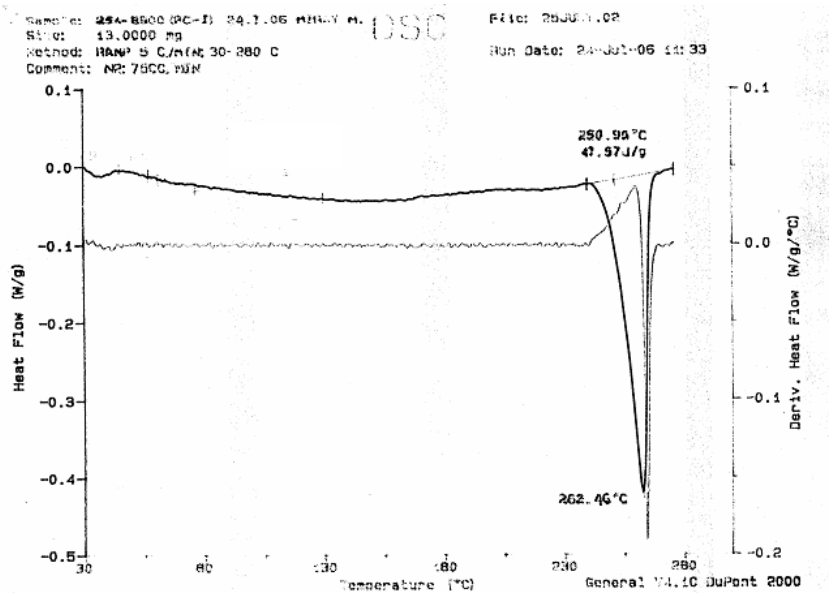

Figure C.32 DSC thermogram of PA 66-Cloisite® 25A-Lotader® AX8900 - (PC-I) ternary nanocomposite.

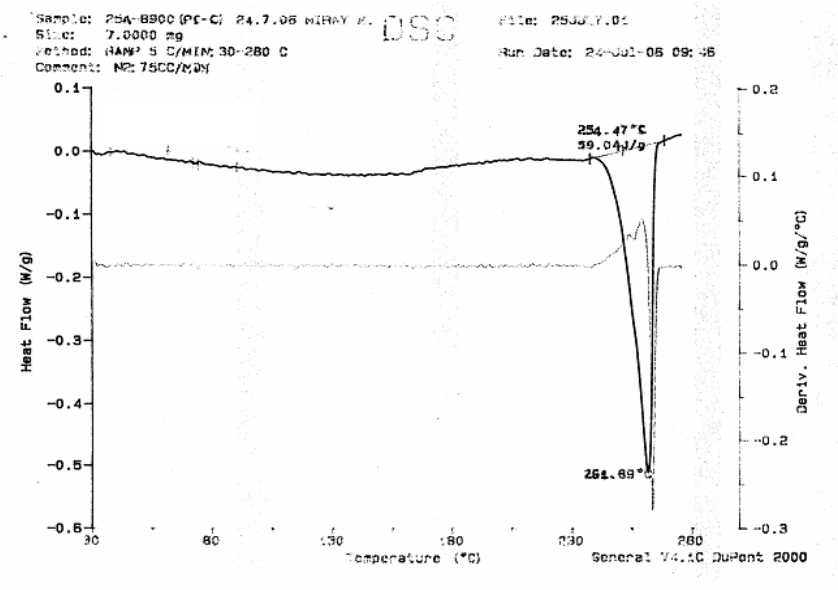

Figure C.33 DSC thermogram of PA 66-Cloisite® 25A-Lotader® AX8900 - (PI-C) ternary nanocomposite.

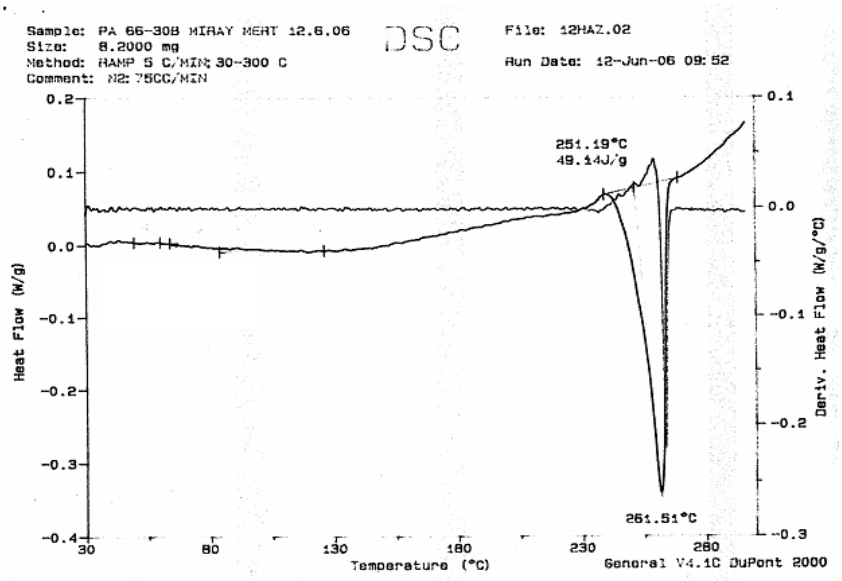

Figure C.34 DSC thermogram of PA 66-Cloisite® 30B binary nanocomposite.

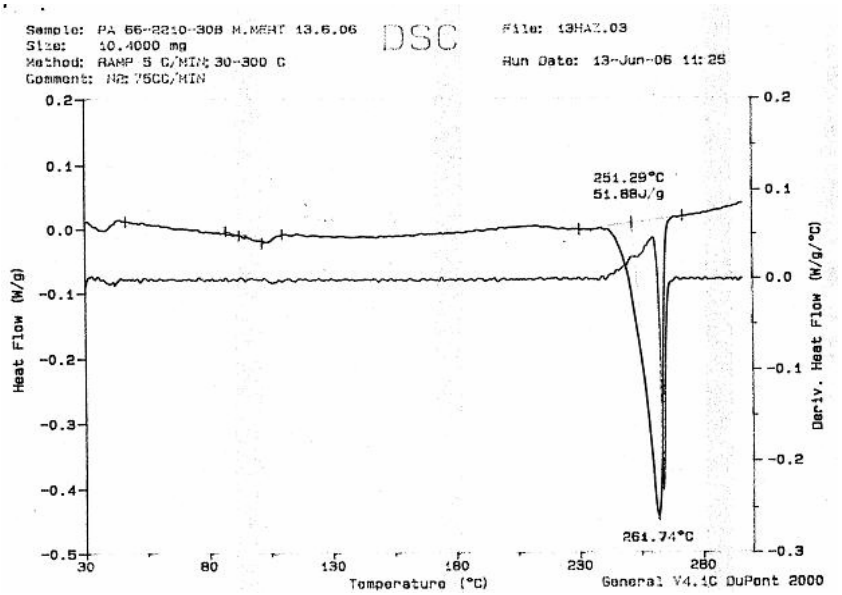

Figure C.35 DSC thermogram of PA 66-Cloisite® 30B-Lotader® 2210 - (All-S) ternary nanocomposite.

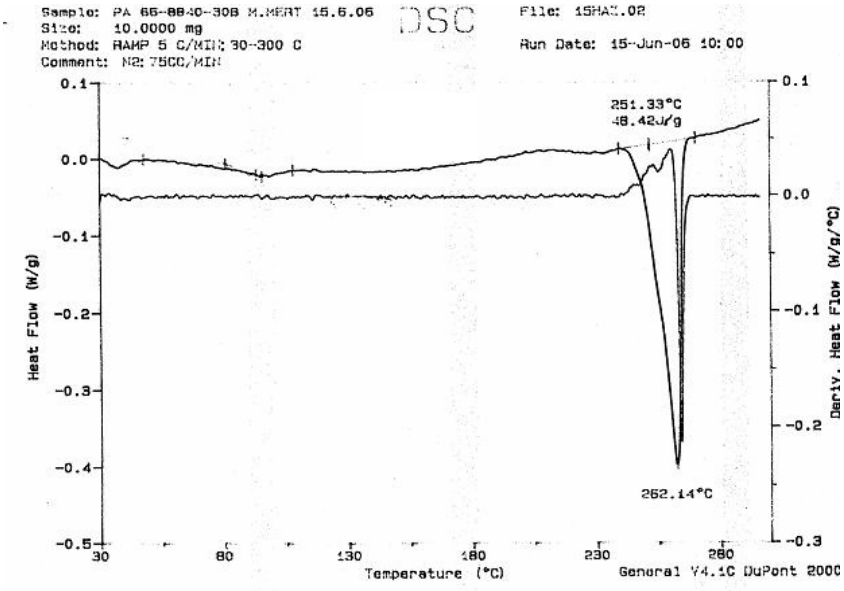

Figure C.36 DSC thermogram of PA 66-Cloisite® 30B-Lotader® AX8840 - (All-S) ternary nanocomposite.

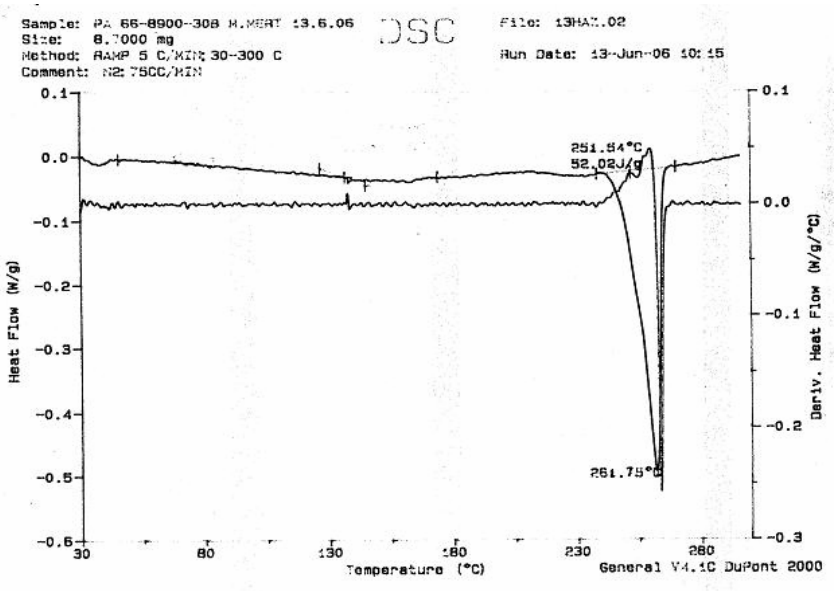

Figure C.37 DSC thermogram of PA 66-Cloisite® 30B-Lotader® AX8900 - (All-S) ternary nanocomposite.

APPENDIX D

Thermal Gravimetric Analysis

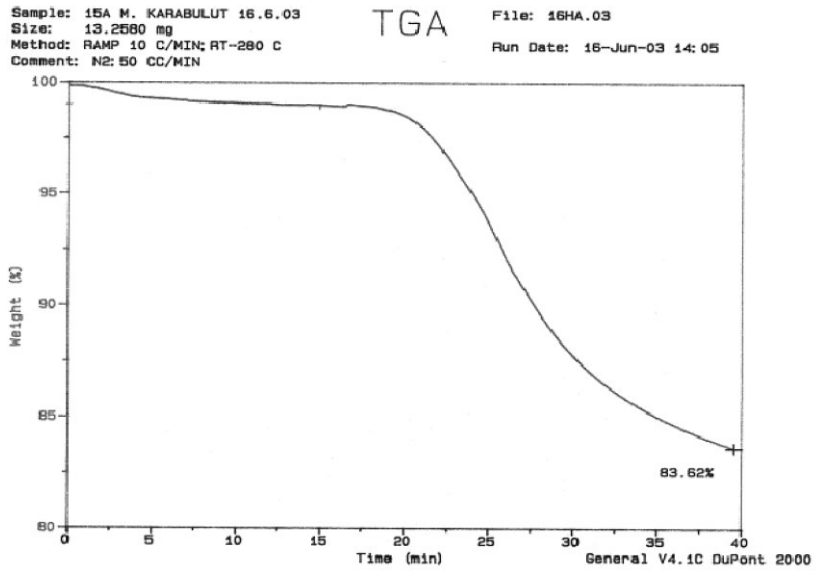

Figure D.1 TGA of Cloisite® 15A.

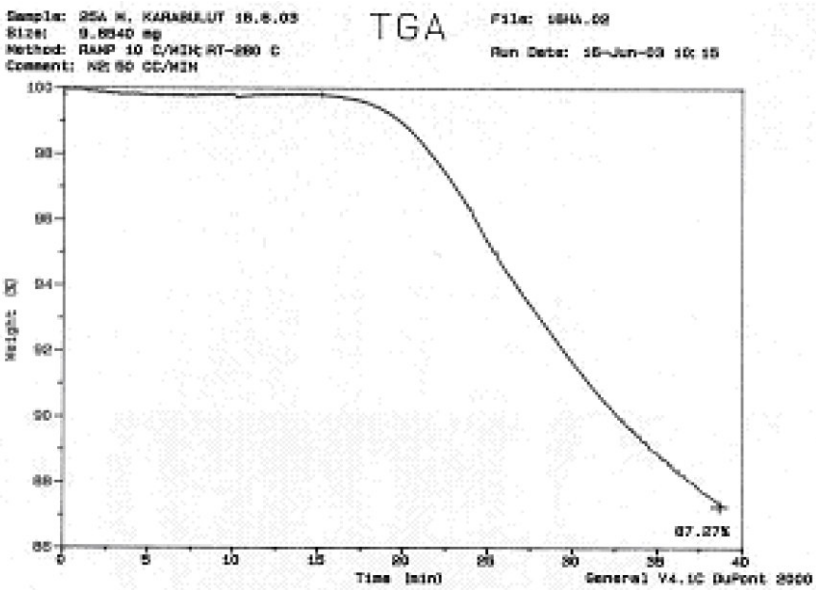

Figure D.2 TGA of Cloisite® 25A.

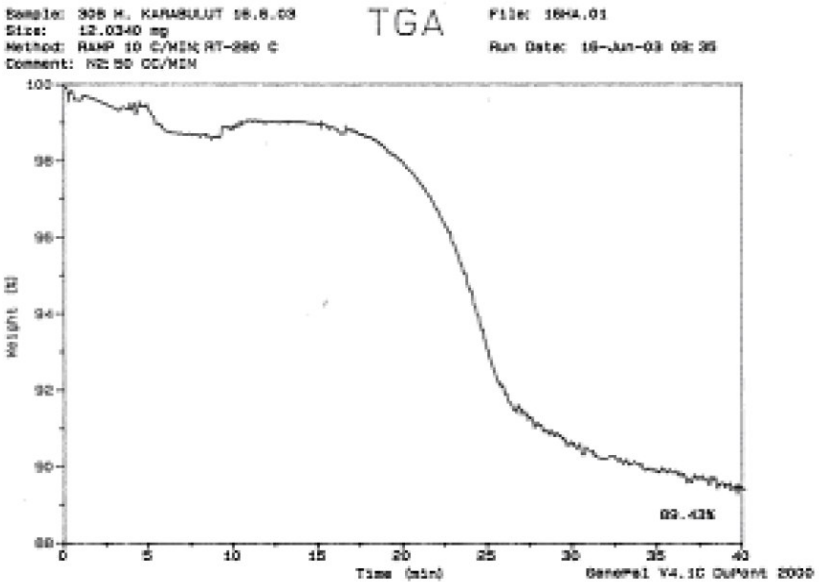

Figure D.3 TGA of Cloisite® 30B.